

Electronic Thesis and Dissertation Repository

9-23-2016 12:00 AM

Enhancing the Seismic Performance of Steel Structures Utilizing Superelastic Shape Memory Alloys

Papia Sultana
The University of Western Ontario

Supervisor
Maged A. Youssef
The University of Western Ontario

Graduate Program in Civil and Environmental Engineering
A thesis submitted in partial fulfillment of the requirements for the degree in Doctor of Philosophy
© Papia Sultana 2016

Follow this and additional works at: <https://ir.lib.uwo.ca/etd>



Part of the [Structural Engineering Commons](#)

Recommended Citation

Sultana, Papia, "Enhancing the Seismic Performance of Steel Structures Utilizing Superelastic Shape Memory Alloys" (2016). *Electronic Thesis and Dissertation Repository*. 4171.
<https://ir.lib.uwo.ca/etd/4171>

This Dissertation/Thesis is brought to you for free and open access by Scholarship@Western. It has been accepted for inclusion in Electronic Thesis and Dissertation Repository by an authorized administrator of Scholarship@Western. For more information, please contact wlsadmin@uwo.ca.

ABSTRACT

Although conventional earthquake-resisting structural systems provide the life safety level during earthquakes, they experience significant structural damage when exposed to strong ground shaking that render structural retrofitting as uneconomical. Superelastic shape memory alloys (SMAs) can be used in steel structures to reduce the residual deformations due to their recentering capability, which can facilitate post-seismic retrofitting. The primary aim of this thesis is to enhance the seismic performance of both regular and modular steel structures using certain amount of superelastic SMAs material in terms of maximum inter-storey drift, residual drift, and damage scheme.

First, a simplified method based on pushover analysis is proposed to identify the severely damaged floor of a typical SMRF. It was validated with the studies by other researchers. Three and ten-storey SMRFs are considered to further validate the method. The predicted location of damage for the SMRFs using this method is compared to the results of static pushover and nonlinear dynamic analyses. The method accurately identified the severely damaged floors of SMRFs.

The proposed simplified method as well as incremental dynamic analysis is then utilized to determine the best locations of SMA connections to improve the seismic performance of SMRFs. Six different SMA frames are examined using nonlinear dynamic analyses. Among all SMA frames, the frame using SMA connections at the critical first and fourth floors showed very good seismic performance compared with the steel frame.

The seismic performance of modular steel braced frames (MSBFs) is significantly different from regular steel braced frames because of their unique detailing and construction procedure. An analytical model that can accurately predict the seismic behaviour of MSBFs equipped with buckling restrained SMA braces is first developed. This model is then implemented to identify the locations of SMA braces to improve the seismic performance of MSBFs. The study highlighted the need to use SMA braces at all floors.

The study also examines the seismic performance of MSBFs utilizing superelastic SMA bolts at the vertical connections between the modules. It was observed that the seismic performance of a MSBF can be improved by using SMA connections at the right locations.

Keywords: Seismic performance, Steel moment resisting frames, Maximum inter-storey drift, Maximum residual inter-storey drift, Incremental dynamic analysis. Shape memory alloy, Modular steel building, Bolted connection, Dynamic analysis.

COPYRIGHT AND CO-AUTHORSHIP

This doctoral thesis is prepared according to the regulations for an integrated-article format thesis stipulated by the faculty of Graduate and Post Doctoral Studies at the Western University. All the design and analytical works were conducted by the author of this thesis under the supervision of Dr. Maged A. Youssef. Major portions of the work outlined in this thesis have been published or are under review for possible publication in peer-reviewed technical journals and conferences. The author wrote the initial drafts of the manuscripts, while her research advisors, Maged A. Youssef, contributed to the final versions of the manuscripts. The publications are as follow:

REFERRED JOURNAL PUBLICATIONS

P.Sultana, M.A. Youssef, “Seismic performance of steel moment resisting frames utilizing superelastic shape memory alloys”, *Journal of Constructional Steel Research*, 2016, Vol.125, 2016 pp. 239–251

P.Sultana, M.A. Youssef, “Prediction of local seismic damage in steel moment resisting frames”, *Journal of Constructional Steel Research*, 2016, Vol.122, pp.122–137

P.Sultana, M.A. Youssef, “Seismic performance of modular steel frames equipped with shape memory alloy braces”, in review, *Journal of Constructional Steel Research*, 2016.

P.Sultana, M.A. Youssef, “Seismic performance of modular steel braced frames utilizing superelastic shape memory alloy bolts in the vertical module connections”, in review, *Journal of Earthquake Engineering*, 2016.

REFERRED CONFERENCE PROCEEDINGS

P.Sultana, M.A.Youssef, “ Seismic performance of modular steel frames equipped with shape memory alloy braces”, Proceedings of 5th International Structural Specialty Conference, CSCE, London, ON, 2016, paper no-834.

P. Sultana, M.A. Youssef, “Variations of maximum inter-storey drift for steel moment resisting frames considering the horizontal and vertical seismic components”, Proceedings of 5th International Conference on Performance, Protection and Strengthening of Structures under Extreme Loading, East Lansing, Michigan, USA, 2015, pp. 463-470.

DEDICATION

I dedicate this thesis to my parents, Mosleh Uddin Ahmed and Hasna Banu who have always been a great encouragement for this great achievement, and to my husband for his constant support and inspiration.

ACKNOWLEDGEMENT

First and foremost, I would like to thank my supervisor Dr. Maged A. Youssef. It has been an honor to be his Ph.D student. I admire his wealth of knowledge, professionalism and dedication to the excellence. I appreciate all his continuous advice, guidance and encouragement throughout this research. Without his help, the thesis could not be completed.

I gratefully acknowledge the funding from the Western University, Natural Science and Engineering Research Council of Canada (NSERC), Ontario Ministry of Training, Colleges and Universities through OGS scholarships, Julie Lassonde Scholarship that made my Ph.D. work possible.

Lastly, I would like to thank my parents who supported me in all my pursuits, my sister who is always there for me when I need her the most. Finally, to my husband, Sufian, and lovely children Arita and Ahyan, words can not just describe how valuable your love, encouragement, prayers, and patience have been to my completion of this work.

TABLE OF CONTENTS

ABSTRACT	II
COPYRIGHT AND CO-AUTHORSHIP	IV
DEDICATION	VI
ACKNOWLEDGEMENT	VII
TABLE OF CONTENTS	VIII
LIST OF TABLES	XII
LIST OF FIGURES	XIII
LIST OF NOTATIONS	XVIII
CHAPTER 1 INTRODUCTION	1
1.1 INTRODUCTION	1
1.2 LITERATURE REVIEW	2
1.2.1 Design philosophy of steel moment resisting frames	3
1.2.2 Design philosophy of braced frames	4
1.2.3 Modular construction	5
1.2.4 Drawbacks of current design philosophy	6
1.2.5 Shape memory alloys	8
1.3 OBJECTIVES AND SCOPES	15
1.4 ORGANIZATION AND OUTLINE	17
1.4.1 Prediction of local seismic damage in steel moment resisting frames	17
1.4.2 Seismic performance of steel moment resisting frames utilizing superelastic shape memory alloys	18
1.4.3 Seismic performance of modular steel frames equipped with shape memory alloy braces	18
1.4.4 Seismic performance of modular steel braced frames utilizing superelastic shape memory alloy bolts in the vertical module connections	19

1.5	REFERENCES	20
CHAPTER 2 PREDICTION OF LOCAL SEISMIC DAMAGE IN STEEL MOMENT RESISTING FRAMES		25
2.1	INTRODUCTION	25
2.2	Proposed Method	26
2.2.1	Lateral drift (Δm) based on P- Δ effect	26
2.2.2	Lateral drift (Δm) based on storey-pushover analysis	28
2.2.3	Application of the proposed method	29
2.2.4	Vertical seismic component	30
2.3	ASPECTS OF MODELING	31
2.3.1	Failure criteria	31
2.4	VALIDATION OF THE PROPOSED METHOD	33
2.5	CASE STUDY	35
2.6	PUSHOVER ANALYSIS	37
2.7	DYNAMIC ANALYSIS	40
2.7.1	Building damage considering the horizontal components	42
2.7.2	Inter-storey drift limit at yield	48
2.7.3	Building damage considering the seismic vertical components	50
2.7.4	Deflection of beams	51
2.8	SUMMARY AND CONCLUSIONS	56
2.9	REFERENCES	58
CHAPTER 3 SEISMIC PERFORMANCE OF STEEL MOMENT RESISTING FRAMES UTILIZING SUPERELASTIC SHAPE MEMORY ALLOYS		60
3.1	INTRODUCTION	60
3.2	STEEL MOMENT FRAME CHARACTERISTICS AND MODELING	64
3.3	PREDICTION OF THE SEVERELY DAMAGED FLOOR	65
3.4	DYNAMIC ANALYSIS OF THE SMRF	66

3.5	SMA- STEEL FRAME CHARACTERISTICS AND MODELING	69
3.5.1	SMA connections	70
3.6	DYNAMIC ANALYSIS OF SMA-STEEL FRAMES	73
3.7	CONCLUSION	85
3.8	REFERENCES	87

**CHAPTER 4 SEISMIC PERFORMANCE OF MODULAR STEEL FRAMES
EQUIPPED WITH SHAPE MEMORY ALLOY BRACES 90**

4.1	INTRODUCTION	90
4.2	MODULAR STEEL BRACED FRAME	93
4.3	FINITE ELEMENT MODELING OF MSBF	95
4.3.1	Validation of FE modeling technique	96
4.4	DYNAMIC ANALYSIS OF STEEL-MSBF (FRAME 1)	99
4.4.1	Results for Frame 1	100
4.5	SMA-MSBFs CHARACTERISTICS AND MODELING	102
4.6	RESULTS FOR SMA-MSBFs	106
4.7	CONCLUSION	117
4.8	REFERENCES	120

**CHAPTER 5 SEISMIC PERFORMANCE OF MODULAR STEEL BRACED
FRAMES UTILIZING SUPERELASTIC SHAPE MEMORY ALLOY BOLTS IN
THE VERTICAL MODULE CONNECTIONS 123**

5.1	INTRODUCTION	123
5.2	MODULAR STEEL BRACED FRAMES	126
5.3	FINITE ELEMENT MODELING OF MSBFs	129
5.3.1	Validation of FE modeling technique	130
5.4	MSBF WITH STEEL BOLTED VERTICAL CONNECTION (FRAME 1)	136

5.5 MSBF EQUIPPED WITH SMA BOLTED VERTICAL CONNECTIONS	139
5.6 CONCLUSIONS	154
5.7 REFERENCES	156
CHAPTER 6 CONCLUSIONS AND RECOMMENDATIONS	159
6.1 SUMMARY	159
6.1.1 Prediction of local seismic damage in steel moment resisting frames	159
6.1.2 Seismic performance of steel moment resisting frames utilizing superelastic shape memory alloys	160
6.1.3 Seismic performance of modular steel frames equipped with shape memory alloy braces	161
6.1.4 Seismic performance of Modular steel braced frame using superelastic shape memory alloy bolts	162
6.2 MAJOR RESEARCH CONTRIBUTIONS	164
6.3 RECOMMENDATIONS FOR FURTHER STUDIES	165
APPENDIX A	167
APPENDIX B	168
CURRICULUM VITAE	169

LIST OF TABLES

Table 2. 1: Modeling parameters for nonlinear procedures according to FEMA356 [1]	32
Table 2. 2: Section properties of Frame 3	35
Table 2. 3: Section properties of Frame 10	36
Table 2. 4: Limiting FID (%) for different floors of 3 storey frame	37
Table 2. 5: Limiting FID (%) for different floors of 10 storey frame	37
Table 2. 6: Characteristics of ground motions	41
Table 2. 7: MID at different ground motions	42
Table 3. 1: Limiting FID (%) for different floors of the 10 storey frame	65
Table 3. 2: Characteristics of ground motions	67
Table 3. 3: MID and MRID of steel frame (Frame 1)	67
Table 3. 4: Natural time period of different frames (Seconds)	74
Table 3. 5: Percentage change of MID and MRID of SMA frames	75
Table 4. 1: section properties of the MSBF	94
Table 4. 2: Material properties of SMA	96
Table 4. 3: Characteristics of the ground motions	99
Table 4. 4: MID and MRID of Frame 1 at collapse	101
Table 4. 5: Percentage change of MID and MRID of SMA frames	107
Table 5. 1: Section properties of the MSBF	127
Table 5. 2: Material properties of SMA	128
Table 5. 3: Characteristics of ground motions	136
Table 5. 4: MID and MRID of Frame 1 at different intensity of ground motions	138
Table 5. 5: Percentage change of MID and MRID of SMA frames	144

LIST OF FIGURES

Figure 2. 1: Fixed-end moments induced by lateral displacement Δm	27
Figure 2. 2: Isolated column and restraining beams	29
Figure 2. 3: Proposed method to estimate inter-storey drift limits for the second storey of a three storey building	30
Figure 2. 4: Moment-rotation behaviour for steel elements	32
Figure 2. 5: Estimated FID at collapse compared with the IDs measured by Suita et al. [17]	33
Figure 2. 6: Plan and elevation of selected 3-storey building [20]	36
Figure 2. 7: Plan and elevation of selected 10-storey building [21]	36
Figure 2. 8 :Pushover analysis results for Frame 3 (a) Relationship between base shear and roof drift, (b) ID obtained from pushover analysis as compared with the proposed collapse ID limits (c) Observed damage at collapse	39
Figure 2. 9: Pushover analysis results for Frame 10 (a) Relationship between base shear and roof drift, (b) ID obtained from pushover analysis as compared with the proposed collapse ID limits (c) Observed damage at collapse	40
Figure 2. 10: Elastic response spectral acceleration for horizontal seismic component	42
Figure 2. 11: Results of Frame 3 considering horizontal component of Imperial earthquake at $S_a(T1) = 10.10g$ (a) Distribution of yielding (b) ID compared with FID limits	44
Figure 2. 12: Results of Frame 3 considering horizontal component of Loma earthquake at $S_a(T1) = 32.71g$ (a) Distribution of yielding (b) ID compared with FID limits.	44
Figure 2. 13: Results of Frame 3 considering horizontal component of Northridge earthquake at $S_a(T1) = 13.92g$ (a) Distribution of yielding (b) ID compared with FID limits.	45
Figure 2. 14: Results of Frame-3 considering horizontal component of San Fernando earthquake at $S_a(T1) = 17.1g$ (a) Distribution of yielding (b) ID compared with FID limits.	45
Figure 2. 15: Results of Frame 3 considering horizontal component of Tabas earthquake at $S_a(T1) = 14.75g$ (a) Distribution of yielding (b) ID compared with FID limits.	45
Figure 2. 16: Results of Frame 10 considering horizontal component of Imperial earthquake at $S_a(T1) = 0.348g$ (a) Distribution of yielding (b) ID compared with FID limits.	46
Figure 2. 17: Results of Frame 10 considering horizontal component Northridge earthquake at $S_a(T1) = 0.424g$ (a) Distribution of yielding (b) ID compared with FID limits.	46

Figure 2. 18: Results of Frame 10 considering horizontal component of San Fernando Earthquake at $Sa(T1) = 0.339g$ (a) Distribution of yielding (b) ID compared with FID limits.	47
Figure 2. 19: Results of Frame 10 considering horizontal component of Tabas earthquake at $Sa(T1) = 0.351g$ (a) Distribution of yielding (b) ID compared with FID limits.	47
Figure 2. 20: Results of Frame 10 considering horizontal component of Loma earthquake at $Sa(T1) = 0.573g$ (a) Distribution of yielding (b) ID compared with FID limits.	48
Figure 2. 21: Comparison of YDL and ID for horizontal component of Northridge [$Sa(T1) = 0.424g$] and Loma Earthquake [$Sa(T1) = 0.573g$]	49
Figure 2. 22: Proposed Limiting FID considering horizontal and both horizontal and vertical components of ground motion.	50
Figure 2. 23: Results of Frame 3 considering horizontal and vertical component of Loma earthquake at $Sa(T1) = 31.87g$ (a) Yielding distribution (b) ID compared with FID	52
Figure 2. 24: Results of Frame 3 considering horizontal and vertical component of Northridge earthquake at $Sa(T1) = 13.67g$ (a) Yielding distribution (b) ID compared with FID	52
Figure 2. 25: Results of Frame 3 considering horizontal and vertical component of San Fernando earthquake at $Sa(T1) = 17.25g$ (a) Yielding distribution (b) ID compared with FID	52
Figure 2. 26: Results of Frame 3 considering horizontal and vertical component of Imperial earthquake at $Sa(T1) = 10.14g$ (a) Yielding distribution (b) ID compared with FID	53
Figure 2. 27: Results of Frame 3 considering horizontal and vertical component of Tabas earthquake at $Sa(T1) = 15.07g$ (a) Yielding distribution (b) ID compared with FID	53
Figure 2. 28: Results of Frame 10 considering horizontal and vertical component of Loma earthquake at $Sa(T1) = 0.325g$ (a) Yielding distribution (b) ID compared with FID	54
Figure 2. 29: Results of Frame 10 considering horizontal and vertical component of Imperial earthquake at $Sa(T1) = 0.271g$ (a) Distribution of yielding (b) ID compared with FID limit	54
Figure 2. 30: Results of Frame 10 considering horizontal and vertical component of Northridge earthquake at $Sa(T1) = 0.313g$ (a) Distribution of yielding (b) ID compared with FID limit.	55
Figure 2. 31: Results of Frame 10 considering horizontal and vertical component of Tabas earthquake at $Sa(T1) = 0.27g$ (a) Distribution of yielding (b) ID compared with FID limit.	55

Figure 2. 32: Results of Frame 10 considering horizontal and vertical component of San Fernando earthquake at $S_a(T_1) = 0.244g$ (a) Distribution of yielding (b) ID compared with FID limit.	56
Figure 3. 1: 10-storey building [23]	65
Figure 3. 2: Elastic response spectral acceleration for horizontal seismic component	67
Figure 3. 3: Damage distribution of the steel frame (Frame 1)	68
Figure 3. 4: Location of SMA connections	70
Figure 3. 5: Location of SMA connections	71
Figure 3. 6: Finite element model of martensite SMA connection	72
Figure 3. 7: Experimental and simulated moment rotation behaviour of the superelastic SMA connection	72
Figure 3. 8: Experimental and simulated moment rotation behaviour of martensite SMA connection	73
Figure 3. 9: Comparison of MID and MRID of different frames	75
Figure 3. 10: Imperial earthquake [$S_a(T_1, 5\%)=0.341g$]	76
Figure 3. 11: Damage distribution of the Frame 2	79
Figure 3. 12: Damage distribution of the Frame 3	80
Figure 3. 13: Damage distribution of the Frame 4	81
Figure 3. 14: Damage distribution of the Frame 5	82
Figure 3. 15: Damage distribution of the Frame 6	83
Figure 3. 16: Damage distribution of the Frame 7	84
Figure 4. 1: A typical plan and section of a modular steel building [1]	92
Figure 4. 2: Six-storey modular steel braced frames	94
Figure 4. 3: Comparison of numerical and experimental responses	97
Figure 4. 4: Geometry of MSBF tested by Annan et al. [2]	97
Figure 4. 5: Model of vertical connection of MSBF	98
Figure 4. 6: Comparison of experimental and numerical results	98
Figure 4. 7: Elastic response spectra	100
Figure 4. 8: ID and RID distribution for Frame 1 at collapse	101
Figure 4. 9: Damage distribution of Frame 1 at collapse	104
Figure 4. 10: Different configurations for the SMA braces	105
Figure 4. 11: Braced bay of SMA-MSBF	106
Figure 4. 12: Drift values at intensity causing collapse to Frame 1	108
Figure 4. 13: Storey drifts for Imperial earthquake [$S_a(T_1, 5\%)=3.84g$]	108
Figure 4. 14: Storey drifts for Tabas earthquake [$S_a(T_1, 5\%)=5.95g$]	109
Figure 4. 15: Storey drifts for Loma earthquake [$S_a(T_1, 5\%)=3.95g$]	109
Figure 4. 16: Storey drifts for Northridge earthquake [$S_a(T_1, 5\%)=2.81g$]	110
Figure 4. 17: Storey drifts for Superstation hill earthquake [$S_a(T_1, 5\%)=3.36g$]	110
Figure 4. 18: Damage distribution of Frame 2	112
Figure 4. 19: Damage distribution of Frame 3	113

Figure 4. 20: Damage distribution of Frame 4	114
Figure 4. 21: Damage distribution of Frame 5	115
Figure 4. 22: Damage distribution of Frame 6	116
Figure 4.23: Load- deformation curve of a first storey steel brace (Frame 1) due to Tabas earthquake, $S_a(T1) = 5.95g$	117
Figure 4.24 Load- deformation curve of a first storey SMA brace (Frame 2) due to Tabas earthquake, $S_a(T1) = 5.95g$	117
Figure 5. 1: Vertical connections between upper and lower modules	124
Figure 5. 2: Six-storey modular steel braced frames	127
Figure 5. 3: Locations of SMA connections	128
Figure 5. 4: Finite element model of MSBF	130
Figure 5. 5: Geometry of MSBF tested by Annan et al. [3]	131
Figure 5. 6: Model of vertical connection of MSBF	132
Figure 5. 7: Comparison of experimental and numerical results	132
Figure 5. 8: Bolted end-plate connection	134
Figure 5. 9: Comparison of experimental and simulated moment rotation behaviour of bolted connection	134
Figure 5. 10: Finite element model of superelastic SMA connection	135
Figure 5. 11: Moment rotation behaviour of the superelastic SMA connection	135
Figure 5. 12: Elastic response spectral acceleration	137
Figure 5. 13: Damage distribution of Frame 1	139
Figure 5. 14: Drifts considering Loma earthquake	141
Figure 5. 15: Drift considering Tabas earthquake	142
Figure 5. 16: Drifts considering Northridge earthquake	142
Figure 5. 17: Drifts considering Superstation Hill earthquake	143
Figure 5. 18: Drifts considering San Fernando earthquake	143
Figure 5. 19: ID and RID distribution considering Loma earthquake at $S_a(T1,5\%) = 1.2g$	145
Figure 5. 20: ID and RID distribution due to Tabas earthquake at $S_a(T1,5\%) = 1.2g$	145
Figure 5. 21: ID and RID distribution due to Northridge earthquake at $S_a(T1,5\%) = 1.2g$	146
Figure 5. 22: ID and RID distribution due to Superstation Hill earthquake at $S_a(T1,5\%) = 1.2g$	146
Figure 5. 23: ID and RID distribution due to San Fernando earthquake at $S_a(T1,5\%) = 1.2g$	147
Figure 5. 24: Damage distribution due to Loma earthquake $S_a(T1,5\%) = 1.3g$	149
Figure 5. 25: Damage distribution due to Tabas earthquake $S_a(T1,5\%) = 1.5g$	150
Figure 5. 26: Damage distribution due to Northridge earthquake $S_a(T1,5\%) = 1.3g$	151
Figure 5. 27: Damage distribution due to Superstation Hill earthquake $S_a(T1,5\%) = 1.5g$	152
Figure 5. 28: Damage distribution due to San Fernando earthquake $S_a(T1,5\%) = 1.5g$	153

Figure 5. 29: Rotation of vertical connection at first floor due to Tabas earthquake [Sa
(T1,5%) =1.5g]

153

LIST OF NOTATIONS

b_f	Flange width
d_{ct}	Moment distribution factor
E_s	Modulus of elasticity
F_{ye}	Expected yield strength of material
h	Web height
h_c	Column height
I_b	Beam moment of inertia
I_c	Column moment of inertia
K_b	Factor for moment at bottom of column
K_c	Stiffness of column
K_t	Factor for moment at top of column
$K_1, K_2, K_3 \text{ \& } K_4$	Stiffness of beam
L	Beam span
m	Drift magnification factor
m_{av}	Average drift magnification factor
M_{cb}	Moment acting at bottom of column
M_{ct}	Moment acting at top of column
P	Axial force
P_{CL}	Lower bound compression strength of column
t_f	Flange thickness
t_w	Web thickness
V_f	Shear force for fully restrained column
V_i	Shear force for partially restrained column
α	Reduction factor for lateral stiffness
Δ_m	Inter-storey drift
θ_y	Yield rotation
A_{SMA}	Area of SMA bars
BRB	Buckling restrained braces
BRBF	Buckling restrained braced frame
FE	Finite element

FID	Failure inter-storey drift
F_y	Yield stress of steel
$F_{y(SMA)}$	Stress at which SMA state changes from the austenite to stress-induced martensite
ID	Inter-storey drift
IDA	Incremental dynamic analysis
MID	Maximum inter-storey drift
M_{pb}	Plastic moment of beam
MRID	Maximum residual inter-storey drift
MSB	Modular steel building
MSBF	Modular steel braced frame
PGA	Peak ground acceleration
PR	Partially restrained
PT	Post tensioned
RC	Reinforced concrete
RID	Residual inter-storey drift
S_a	Spectral acceleration
SMA	Shape memory alloy
SMRF	Steel moment resisting frame
V/H	Vertical-to-horizontal peak ground acceleration
YDL	Inter-storey drift limit at yielding

CHAPTER 1

INTRODUCTION

1.1 INTRODUCTION

The recent earthquakes in Nepal and Japan have shown that seismic damage can be extensive. Every year, earthquakes take the lives of thousands of people, and destroy properties that worth billions of dollars. The seismic design philosophy allows structure to deform and dissipate the seismic energy while, experiencing inelastic deformations. The resulting seismic residual drifts complicate the repair of damaged structures or render them as irreparable which have forced researchers to innovate to find alternative design procedures.

Steel moment resisting frames (SMRFs) and steel braced frames are widely used as lateral load resisting systems for mid-to high-rise buildings. After 1994 Northridge earthquake, significant research was conducted to improve their seismic performance. Response parameters that assess the global seismic performance of steel structures include maximum roof drift, maximum inter-storey drift, and base shear force.

Nowadays, Modular steel structures are becoming very popular as an effective alternative to traditional on-site steel construction. In modular construction, units are built and finished under a controlled manufacturing environment. They are then transported to the building site, where they are connected horizontally and vertically. The lateral force on each floor level is transferred through the horizontal connections to the modular braced frames, and, then through the vertical connections to the foundation. Modular construction

is more advantageous over the regular construction because of their reduced construction duration and highly controlled quality.

Shape memory alloys (SMAs) have widely attracted the attention of researchers because of their unique material properties. Superelastic SMA has the ability to undergo large deformations and recover all the plastic deformations upon unloading. Their utilization in steel structures can significantly reduce seismic residual deformations, which can facilitate post-seismic retrofitting.

Although the existing literature provides few research data on using SMA in beam-column connections and bracing elements of steel frames, previous research did not address their minimum use. Also, the use of SMA in modular steel structures was not examined. This study examines the potential use of SMAs in steel moment resisting frames (SMRFs) and modular steel braced frames (MSBFs). The study also explores the possibility of using SMA material economically at certain locations to minimize the cost and optimize the seismic performance. The following sections present a brief background and literature review on the topic, the objectives and scope of this study and the organization of the thesis.

1.2 LITERATURE REVIEW

This section provides an overview of current design philosophy of earthquake resistant steel structures, modular construction, and published research on the application of SMA in civil structures.

1.2.1 Design philosophy of steel moment resisting frames

Seismic design of steel moment resisting frames (SMRFs) is based on the strong column and weak beam (SC-WB) concept, where ductility is provided by formation of flexural plastic hinges at the beam faces as shown in Figure 1.1. This concept is followed in many design standards [1-3]. Schneider et al. [4] showed that meeting the SC-WB requirement increases the seismic energy dissipation capacity through flexural yielding of the beams at multiple levels before yielding of columns. Besides ensuring this SC-WB criteria, the beam-to-column connections of special moment resisting frames should be designed to sustain a storey drift angle of at least 0.04 radian [3].

As an alternative to welded connections, partially restrained (PR) bolted connections have been recommended by many researchers [5-7]. These connections are designed to form the plastic hinges through yielding of their elements. Research has shown that properly detailed PR connections have good seismic performance and can be considered as a viable alternative to fully restrained connections [5-7]. The plastic moment capacity of these connections is typically a fraction of that of the connected framing elements, encouraging the inelastic behavior to occur within the connection.

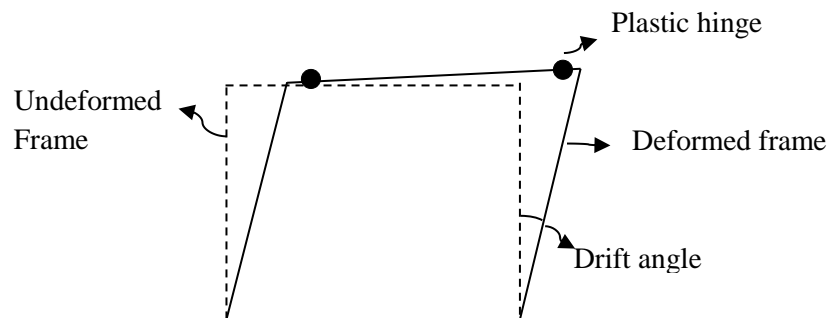


Figure 1. 1: Inelastic behaviour of frame with plastic hinges in the beam

1.2.2 Design philosophy of braced frames

The design philosophy of steel braced frames ensures that plastic deformations occur only in the braces, leaving the beams, columns and connections undamaged. Thus, the structure is expected to survive strong earthquakes without losing its stability for supporting gravity loads.

Conventional steel bracing elements show unsymmetrical behaviour under cyclic loading, Figure 1.2. It is characterized by high ductility in tension and buckling in compression. To overcome the limitations of brace buckling of conventional braces, buckling restrained braces (BRB) were proposed by a team of investigators in Japan [8-10]. A BRB has two basic components: a steel core element that supports the entire brace axial force, and a restraining exterior element that prevents the core from buckling in compression. BRBs have stable, predictable hysteretic behaviour and provide significant energy dissipation and large ductility, Figure 1.2.

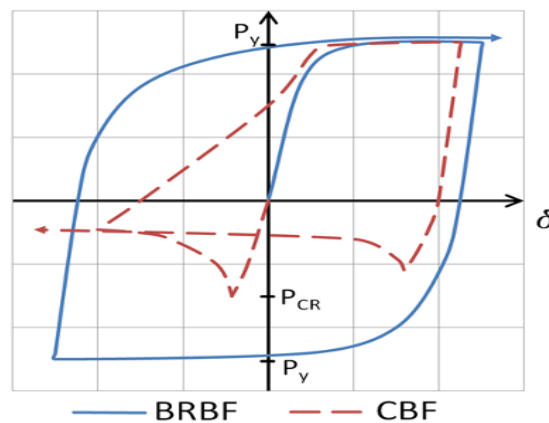


Figure 1. 2: Comparison of load-deformation behaviour of conventional brace and buckling restrained brace.

In Canada, CSA S16-09 [1] introduced provisions for the design of BRBFs in 2009. The beam-to column connections of BRBFs are typically non moment resisting connections. The code restricts the height of BRBFs to 40 meters in moderate and high seismic regions to eliminate the risk of a soft-storey response. For taller structures BRBs can be used if inelastic dynamic stability is demonstrated.

1.2.3 Modular construction

A modular building consists of multiple prefabricated units called “Modules”. These units are manufactured in a controlled manufacturing industry and transported to the construction site. They are then connected to form the building. Modular construction is mainly used where repetitive units are required, such as in hospitals, office buildings, student accommodation, apartments, etc. Their popularity is increasing because of their quality, fast on-site installation, and lower cost of construction. They are generally used in low-rise buildings (up to six storey). Lawson and Richards [11] reviewed recent modular technologies and proposed a design method for high-rise-modular buildings that accounts for the installation and construction tolerance. Lawson et al. [12] considered case studies of 12, 17 and 25 storey modular buildings. They recommended the use of steel or concrete frames to achieve structural stability for high-rise modular buildings. Annan et al. [13-15] investigated the seismic performance of modular steel braced frames (MSBFs). They emphasized that the seismic performance of MSBFs is significantly different from regular steel braced frames. Such difference is attributed to the existence of ceiling beams, the eccentricity developed at the joints as the braces do not intersect at a single working point, the semi-rigid connections between the columns of a module and the ones above or below it. MSBFs possess significant overstrength when compared to the regular braced frame

due to the intrinsic redundancies in the frame system [14]. Fathieh and Mercan [16] analytically studied the seismic performance of MSBF using two and three-dimensional(3D) models of a four storey modular steel building. They concluded that the MSBFs can resist higher base shear than that of the regular traditional steel buildings.

Although, modular steel building systems differ significantly from traditional on-site buildings in terms of behaviour, detailing requirements and method of construction, there is no guidelines for their design in CAN/CSA S16-09 [1] or in the National Building Code of Canada [17].

1.2.4 Drawbacks of current design philosophy

Although the current design philosophy guarantees the life safety level during earthquakes, it allows severe damage to form in the beams, connections, or braces. Such damage leads to residual drifts [18-23] that render structural retrofitting as uneconomical.

Researchers are trying to find alternative design procedures to overcome the residual deformations of structures after a seismic event. Special types of post-tensioned (PT) PR connections were proposed [21-23] due to their recentering capability as shown in Figure 1.3. The posttensioning contributed to the moment capacity of the connections and provided an elastic restoring force that returned the frame to its pre-earthquake position. Six full- scale interior PT connections were tested by Garlock et al. [22] under cyclic loading. The seismic energy was dissipated by the inelastic deformations of top and bottom seat angles while the beams and columns remained elastic up to 4% drift. Ricles et al. [21] conducted dynamic analysis of a six-storey SMRF equipped with PT connections. The frame showed good self-centering capability, adequate strength, and ductility.

Christopoulos et al. [23] proposed a PT energy dissipating connection for steel frames. This connection incorporates post-tensioned high strength steel bars to provide self-centering response and energy dissipating bars to dissipate the seismic energy. The proposed connection was able to undergo large inelastic deformation without any damage in the beam or column, and no residual drifts were observed.

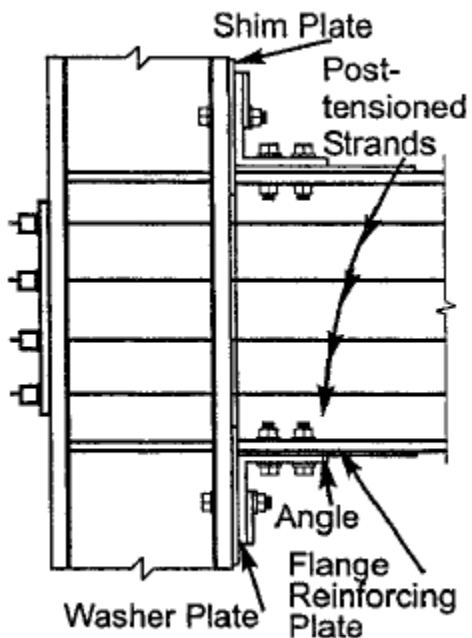


Figure 1. 3: Post-tensioned connection [21]

Shape memory alloy (SMA) material has also attracted the attention of researchers because of its self-centering and energy dissipation capability. Several studies have been conducted in the past twenty years to explore the use of SMA in new civil structures as well as for retrofitting purposes.

1.2.5 Shape memory alloys

Shape memory alloys based on Nickel and Titanium (NiTi) are found to be the most suitable alloy for construction applications [24]. NiTi alloy has two stable phases: austenite, which is stable at high temperatures and low stresses; and martensite, which is stable at low temperatures and high stresses. The martensite start temperature (M_s), martensite finish temperature (M_f), austenite start temperature (A_s) and austenite finish temperature (A_f), define the temperatures of phase transformations. Figure 1.4 shows the hysteric behaviour of NiTi SMA during cooling and heating. When the stress is induced to a twinned martensite SMA at a temperature below M_f , the twinned martensite transforms to detwinned martensite showing large deformation (6%-8%). By heating the detwinned martensite to a temperature above A_f , the martensite SMA transforms to austenite phase and regains undeformed shape. This characteristic is called the shape memory effect. If the SMA is in the austenite phase at a temperature greater than A_f , stress-induced large deformation occurs due to phase transformation from austenite to stressed detwinned martensite. By removal of the load, the material returns back to austenite, and, thus regain the residual deformation. without the application of heat. This effect is known as superelasticity.

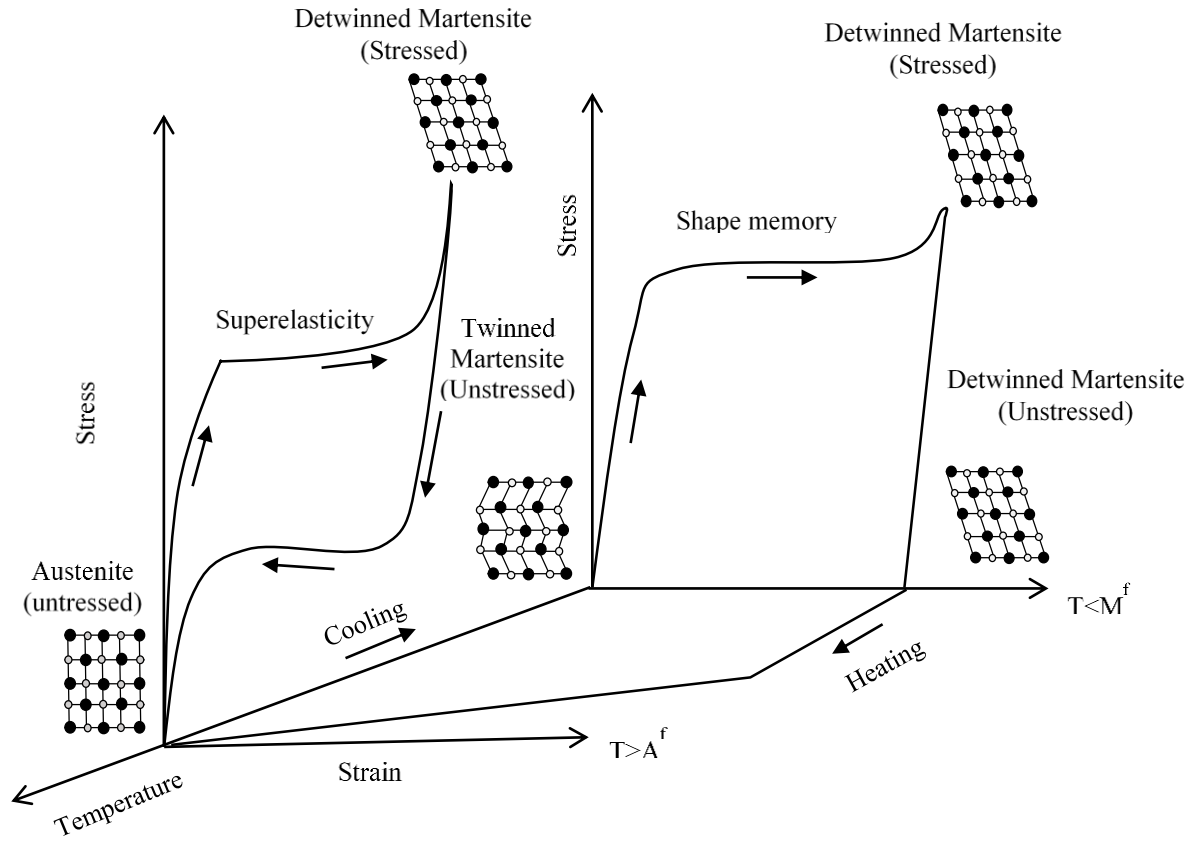


Figure 1. 4: Three-dimensional stress-strain-temperature diagram of NiTi shape memory alloy [25]

Different types of material models of SMAs are proposed in the literature. Among them, one-dimensional uniaxial material models were proposed to model superelastic SMA [26-29]. Different commercial software packages including ANSYS, ABAQUS, OPENSEES and SEISMOSTRUCT implemented the superelastic SMA material model proposed by Auricchio et al. [27], Auricchio and Taylor [28], and Auricchio and Sacco [29], respectively. The parameters used to define the material are: 1) austenite to martensite starting stress, 2) austenite to martensite finishing stress, 3) martensite to austenite starting

stress, 4) martensite to austenite finishing stress, 5) length of superelastic plateau strain or maximum residual strain, and 6) modulus of elasticity.

1.2.5.1 Application of SMA in reinforced concrete structures

Several studies have been conducted to improve the seismic performance of reinforced concrete structures by utilizing SMA in columns, beams, beam-column connections, and shear walls. Wang [30] conducted a shake table test to investigate the seismic performance of reinforced concrete (RC) columns. SMA longitudinal reinforcement was used in the plastic hinge area and steel reinforcement was used in other areas. Using SMA reduced the residual displacements of the tested columns. Billah and Alam [31] incorporated SMA and fiber reinforced polymer bars in RC columns to reduce seismic residual deformations as well as enhance corrosion resistance. Superleastic SMA was used in plastic hinge region to reduce the permanent damage and FRP was used in remaining regions to enhance its corrosion resistance. The corrosion-resistant hybrid- column had significantly reduced seismic residual deformations. RC beams utilizing SMA bars were tested under cyclic loading by Ayoub et al. [32]. The results showed that SMA bars reduce residual deformations of the beams by more than 75% and minimize the permanent width of cracks. Abdulridha et al. [33] investigated the structural performance of RC beams utilizing superelastic SMA bars. The tested SMA beams showed higher ductility and strength capacity, and were able to recover the inelastic deformations. The structural performance of a RC shear wall utilizing SMA bars was assessed analytically by Ghassemieh et al. [34]. They conducted parametric studies using different percentage of SMA bars along with regular steel bars. The study revealed that replacing more than 50% of the steel rebars with SMA bars significantly reduce the residual deformations of RC walls. In 2008, Youssef et

al. [35] tested RC beam- column joints with superelastic SMA bars in the plastic hinge area under reverse cyclic loading. SMA reinforced beam-column joints were able to recover most of their inelastic deformations. The location of the plastic hinge was also shifted from the face of the column by approximately half of the beam-depth.

Alam et al. [36] analytically evaluated the seismic performance of an eight-storey SMA RC frame using SMA bars at the plastic hinge areas of all beams. The SMA RC frame had reduced residual inter-storey drifts (RID) compared with a Steel-RC frame. Because of the relatively high cost of SMA bars, Youssef and Elfeki [37] analytically investigated the possibility of reducing the amount of SMA bars while keeping the benefit of reducing the RID. A six-storey steel-RC building was designed and exposed to incremental dynamic analyses. The frame was then redesigned using superelastic SMA bars at critical locations. The study concluded that using SMA bars at the critical beams as well as the beams intersecting with the critical columns lead to the best seismic performance in terms of maximum residual inter-storey drift (MRID) and damage scheme.

SMAAs are also used for retrofitting deficient RC structures. Dolce et al. [38] retrofitted an existing 2-storey RC frame using special braces incorporating superplastic NiTi SMA wires. Experimental tests were carried out to assess the cyclic behaviour of the retrofitted structure. The study revealed that using SMA braces provided the strong recentering capability and increased the safety against collapse. Cardone et al. [39] evaluated the effectiveness of SMA based bracing devices for seismic retrofitting of RC frames designed for gravity loads. A shaking table test was carried out on a 3D 1/4- scale RC frame model. The experimental results confirmed the great potential of using SMA based braces in RC frame structures because of their recentering capability compared to steel braces.

Several researchers have also investigated the seismic performance of bridges utilizing superelastic SMAs as dampers, base isolators, reinforcements, expansion joints, etc. [40-43]. Their studies highlighted the effectiveness of utilizing SMA to minimize the residual deformations of bridges.

1.2.5.2 Application of SMA in steel structures

Ocel et al. [44] first integrated smart shape memory alloy (SMA) into traditional steel connections. They tested innovative external beam-column connections using martensite SMA rods. The beam moment was transferred to the column by four large diameter NiTi SMA tendons connecting the beam flange to the column flange. Integrating SMAs had significantly enhanced the ductility and damping capacity of PR connections. In addition, the unique shape memory behavior provided the possibility of removing the residual deformations within the connection by heating the SMAs above their transformation temperature.

Ma et al. [45] investigated an extended SMA end-plate connection by using 3D finite element model. The results showed cyclic elongations of the SMA bolts in the connection, which were recoverable upon unloading. Moreover, the ductility of SMA connections was significantly influenced by the length of the SMA bolts. The inelastic inter-storey drift angle reached 0.035 rad, which indicated sufficient ductility. A quasi-static test of an extended SMA end-plate connection was also conducted by Ma and Yam [46]. The connection showed a high deformation capacity with maximum inter-storey drift angle reaching beyond 0.02 rad.

A PR connection using copper-based (CuAlBe) shape memory alloy (SMA) bars was tested by Sep'ulveda et al. [47]. The proposed connection showed self-centering behaviour, moderate energy dissipation capability, and no strength degradation under 3% drift ratio cycles. Speicher et al. [48] tested half-scale interior beam-column connection incorporating superelastic NiTi SMA to assess the feasibility of such a connection in a moment-resisting frame. This connection was compared to three other connections utilizing tendons made of steel, martensitic NiTi and superelastic NiTi paralleled with aluminum. The superelastic NiTi SMA connection showed significant recentering capability and recovered a large portion of the post-elastic drifts compared to other connections. Wang et al. [49] proposed an innovative connection that utilize superelastic SMA tendons along with steel tendons to connect an H shaped beam with a CHS column. The tested connection showed excellent recentering capability and moderate energy dissipation capacity up to 6% inter-storey drift angle. Fang et al. [50] conducted eight tests to investigate the cyclic performance of extended SMA end-plate connections. The connections showed excellent recentering capability, and moderate energy dissipation capacity. The same research group established a detailed finite element model of the connection and conducted parametric studies considering the effects of bolt layout, bolt length/diameter, beam to connection strength ratio, end plate thickness, column web panel deformation, and shear resistance [51]. Their recommendations to achieve reliable recentering connections include: 1) the maximum moment resistance of the connection should be less than the connecting members, 2) thick extended end plate is required to reduce the residual deformation of the connection and to result into uniform stress state in the SMA bolts, and 3) the column web panel should have sufficient shear resistance to avoid significant plastic deformation in the panel zone.

The global seismic performance of steel moment resisting frames with beam to column connections using SMA bars was studied by DesRoches et al. [25]. Two steel frames were selected for this purpose: low rise (three story) PR frame and medium rise (nine story) PR frame. The connections were considered as martensite SMA connections or austenite SMA connections. Nonlinear time history analyses were performed to determine the effect of SMA connections on peak and residual inter-storey drift demand. SMA connections were found to be most effective in controlling the structural response under high levels of seismic intensity. The study showed that superelastic austenite SMA connections were more suitable for controlling residual deformations while martensitic SMA connections were most effective in controlling peak deformations. Further probabilistic seismic demand assessment (PSDA) was also performed by Ellingwood et al. [52] to assess statically the efficiency of using SMA connections in steel moment resisting frames.

Researchers also investigated the seismic performance of steel braced frames using SMA in bracing members [53-56]. Auricchio et al. [53] analytically studied the seismic performance of three- and six-storey steel frame buildings equipped with traditional steel and superelastic SMA bracings. Incorporating SMA braces reduced the inter-storey drifts as well as residual inter-storey drifts, and, thus improved the seismic performance compared with those of steel braced frames. In 2007, McCormic et al. [54] assessed the performance of concentrically braced steel frames incorporating SMA braces. The results suggested that SMA braces are effective in limiting residual inter-storey drifts during an earthquake, due to the recentering capability of superelastic SMA. The seismic performance of steel braced frames equipped with superelastic SMA braces, considering different bracing configurations such as diagonal, split X, chevron (V and inverted V)

bracings, was investigated by Asgarian and Moradi [55]. The results highlighted the efficiency of SMA braces in reducing the residual roof displacements and peak inter-story drifts as compared to buckling restrained braced frames. Kari et al. [56] conducted a numerical study to investigate the benefits of using combination of buckling restrained braces and shape memory braces (dual bracing). Results revealed that, with the proper configuration, both minimum residual and inter-storey drifts can be attained.

Miller [57] experimentally investigated the seismic performance of self-centering buckling-restrained braces (SC-BRBs) that utilized the benefits of energy dissipation capacity of buckling restrained brace (BRB) components and recentering ability of superelastic NiTi SMA rods. The rods were attached to the BRB portion of the brace using a set of concentric tubes and free-floating anchorage plates in such a way that caused the SMA rods to elongate when the brace was in tension or compression. The braces exhibited stable and flag-shaped hysteretic response under cyclic loading. The study concluded that proper proportioning of the SMA pretension force and the BRB core yield force, influenced the full re-centering capacity of the bracing.

1.3 OBJECTIVES AND SCOPES

The primary aim of this thesis is to enhance the seismic performance of both regular and modular steel structures using certain amount of superelastic SMAs material. This was achieved by pursuing the following objectives:

- 1) Conduct a thorough literature review that summarizes the current seismic design philosophy of steel moment resisting frames, concentrically braced steel frames, modular steel braced frames, the characteristics of SMA material and its applications in civil engineering structures.
- 2) Develop and validate a simplified method based on pushover analysis to predict the location of seismic damage in steel moment resisting frames (SMRFs) considering both horizontal and vertical seismic components. Implement this method to identify the critical floors of a steel moment resisting frames.
- 3) Develop finite element model of SMA beam-column connection that can represent the hysteretic moment-rotation behavior of the connection accurately. Implement that model to study analytically the seismic performance of SMRFs.
- 4) Implement the simplified method proposed in step 2 as well as nonlinear dynamic analysis to determine the best locations of SMA connections to improve the seismic performance of SMRF at minimum cost.
- 5) Develop analytical model that can accurately predicts the seismic behavior of modular steel braced frames (MSBFs) equipped with buckling restrained SMA braces and implement this model to identify the locations of SMA braces to improve the seismic performance.
- 6) Assess seismic performance of modular steel braced frames connected vertically using SMA bolts.

1.4 ORGANIZATION AND OUTLINE

The dissertation comprises of six chapters. In the present chapter, a review of the current design philosophy of steel moment resisting frames, steel braced frames and modular steel buildings has been discussed. Properties of SMAs, their application in civil structures along with the scope and objectives of the research are then outlined. The following four chapters address the stated objectives. The thesis concludes by chapter six that briefly summarize the obtained conclusions, the major contributions and recommendations for future studies. Contents of chapter 2 to 5 are summarized below.

1.4.1 Prediction of local seismic damage in steel moment resisting frames

Steel moment resisting frames (SMRFs) are widely utilized as a lateral load resisting system. Their seismic performance is usually assessed by examining the maximum value of inter-storey drift (MID) of all floors. The accuracy of such assessment is debatable given the wide spread of values of MID at collapse that exist in the literature. In chapter 2, a simplified method to define the failure inter-storey drift for each floor of a SMRF is proposed. The method is validated with the experimental and analytical studies by other researchers. Three- and ten storey SMRFs are considered to further validate the proposed method. The effects of the vertical and/or horizontal seismic components of five different ground motions on the SMRFs are evaluated using incremental dynamic analysis.

1.4.2 Seismic performance of steel moment resisting frames utilizing superelastic shape memory alloys

Steel structures dissipate the seismic energy through steel yielding, which results in residual deformations. Although conventional earthquake-resisting structural systems provide adequate seismic safety, they experience significant structural damage when exposed to strong ground shaking. Therefore, systems that can minimize the seismic residual deformations are needed. Superelastic shape memory alloys (SMAs) have the ability to undergo large deformations and recover all plastic deformations upon unloading. Their utilization in steel structures can significantly reduce seismic residual deformations, which will facilitate post-seismic retrofitting. In chapter 3, the seismic performance of SMRFs equipped with superelastic SMA connection is investigated. The proposed simplified method developed in chapter 2 as well as incremental dynamic analysis is applied to identify the required locations of SMA connections in a typical SMRF to enhance its seismic performance in terms of maximum inter-storey drift, residual deformations, and damage scheme.

1.4.3 Seismic performance of modular steel frames equipped with shape memory alloy braces

The demand for modular steel buildings (MSBs) has increased because of the improved quality, fast on-site installation, and lower cost of construction. Steel braced frames are usually utilized to form the lateral load resisting system of MSBs. During earthquakes, the seismic energy is dissipated through yielding of the components of the braced frames, which results in residual drifts. The potential of using SMA braces to improve the seismic

performance of typical modular steel braced frames (MSBFs) is explored in chapter 4 utilizing incremental dynamic analysis.

1.4.4 Seismic performance of modular steel braced frames utilizing superelastic shape memory alloy bolts in the vertical module connections

In modular construction, the vertical connections can be achieved by welding or bolting the columns of stacked modules. The seismic performance of modular steel braced frames (MSBFs) connected vertically using superelastic shape memory alloy (SMA) bolts is investigated in chapter 5. The required locations of SMA connections in a typical MSBF are identified to optimize its seismic performance in terms of maximum inter-storey drift, maximum inter-storey residual drift, and damage scheme.

1.5 REFERENCES

- [1] CAN/CSA-S16-09, Design of Steel Structures, Canadian Standard Association, 2009.
- [2] FEMA 350, Recommended Seismic Design Criteria for New Steel Moment-Frame Buildings Federal Emergency Management Agency 2000.
- [3] AISC 341-10, Seismic Provisions for Structural Steel Buildings, American Institute of Steel Construction, 2002.
- [4] S.P. Schneider, C.W. Roeder, J.E. Carpenter, Seismic performance of weak-column strong-beam steel moment resisting frame, Final report, Department of Civil Engineering, University of Washington, Seattle, WA 1991.
- [5] J.C. Awkar, L. M. Lui, Seismic analysis and response of multistory semirigid frames, Eng. Struct. 21 (1999), 425–441
- [6] J.A. Swanson, R.T. Leon, Bolted steel connections: tests on T-stub components. J. Struct. Eng. 126(1) (2000) 50–56.
- [7] E.A. Sumner, T.M. Murray, Behavior of extended end-plate moment connections subject to cyclic loading, J. Struct. Eng. 128 (4) (2002) 501-508.
- [8] A.Wada, E. Saeki, T. Takeuch, A. Watanabe, Development of unbonded brace, Column technical publication no 115, Nippon steel, Japan 1989.
- [9] A. Watanabe, Y. Hitomoi, E. Saeki, A. Wada, M. Fujimoto, Properties of braced encased in buckling-restraining concrete and steel tube. In Proceedings of 9th World Conference on Earthquake Engineering, Tokyo-Kyoto, Japan, Vol. IV (1988) 719-724.
- [10] A. Watanabe, H. Nakamura, Study on the behavior of buildings using steel with low yield point, In Proceedings of 10th World Conference on Earthquake Engineering, Balkema, Rotterdam , The Netherlands , 1992, 4465-4468.
- [11] R. M. Lawson, J. Richards, Modular design for high-rise buildings, Proceedings of the Institution of Civil Engineers, Structures and Buildings, 163 (SB3) (2010)151–164.
- [12] R.M. Lawson, R. R.G. Ogden, R. Bergin, Application of modular construction in high-rise building, J. Archit. Eng. 18(2) (2012) 148-154.

- [13] C.D. Annan, M.A. Youssef, M.H. El Naggar, Experimental Evaluation of the Seismic Performance of Modular Steel-Braced Frames. *Eng. Struct.*, 31(7) (2009) 1435-1446.
- [14] C.D. Annan, M.A. Youssef, M.H. El Naggar, Seismic overstrength in braced frames of modular steel buildings, *J. Earthq. Eng.* 13(1) (2009)1-21.
- [15] C.D. Annan, M.A. Youssef, M.H. El Naggar, Seismic vulnerability assessment of modular steel building. *J. Earthq. Eng.* 13(8) (2009) 1065-1088.
- [16] A. Fathieh, O. Mercan, Seismic evaluation of modular steel building, *Eng. Struct.*, 122 (2016) 83-92.
- [17] NBCC 2005, National building code of Canada.
- [18] C. Ariyaratana, L.A. Fahnestock, Evaluation of buckling-restrained brace frame seismic performance considering reserve strength, *Eng. Struct.* 33 (2011) 77-89.
- [19] L.A. Fahnestock, R. Sause, J.M. Ricles, Seismic response and performance of buckling restrained braced frames, *J. Struct. Eng.* 133 (9) (2007)1195-1204.
- [20] R. Shabelli, S. Mahin, C. Chang, Seismic demand on steel braced frame buildings with buckling-restrained braces, *Eng. Struct.* 25(5) (2003) 655-666.
- [21] J.M. Ricles, R. Sause, M.M. Garlock, C. Zhao, Posttensioned seismic-resistant connections for steel frames, *J. Struct. Eng.* 127(2) (2001) 113-121.
- [22] M.M. Garlock, J. M. Ricles, R. Sause, Experimental studies of full-scale posttensioned steel connection, *J. Struct. Eng.* 131 (2005) 438–448.
- [23] C. Christopoulos, A. Filiatrault, C. Uang, B. Folz, Posttensioned energy dissipating connections for moment-resisting steel frames, *J. Struct. Eng.* 128 (2002) 1111–1120.
- [24] J. McCormick, J. Tyber, R. DesRoches, k. Gall, H. Maier, Structural engineering with NiTi Part II: Mechanical behavior and scaling, *J. Eng. Mech.* 133(9) (2007) 1019-1029.
- [25] R. DesRoches, B. Taftali, B.R. Ellingwood, Seismic performance assessment of steel frames with shape memory alloy connections, Part I- Analysis and seismic demands, *J. Earthq. Eng.* 14 (2010) 471-486.
- [26] F. Auricchio, J. Lubliner, Uniaxial model for shape-memory alloys. *Int. J. Solids. Struct.* 34 (1997) 3601-3618.

- [27] F. Auricchio, R.L. Taylor, J. Lubliner, Shape-memory alloys: macro modelling and numerical simulations of the superelastic behaviour. *Comput. Methods. Appl. Mech. Eng.* 146 (1997) 281-312.
- [28] F. Auricchio, R.L. Taylor, Shape memory alloy superelastic behavior: 3D finite element simulations. *Proceedings of SPIE - The International Society for Optical Engineering*, 2779 (1996) 487-492.
- [29] F. Auricchio, E. Sacco, Superelastic shape-memory-alloy beam model. *J. Intell. Mater. Syst. Struct.*, 8 (1997) 489-501.
- [30] H. Wang, A study of RC columns with shape memory alloy and engineered cementitious composites. M.Sc. Thesis, University of Nevada, Reno, USA, 2004.
- [31] A.H.M.M. Billah, M.S.Alam, Seismic performance of concrete columns reinforced with hybrid shape memory alloy (SMA) and fiber reinforced polymer (FRP) bars, *Construction and Building Materials* 28 (2012) 730-742
- [32] C. Ayoub, M. Saiidi, A. Itani, A, A Study of Shape-Memory-Alloy-Reinforced beams and Cubes, Center for Civil Engineering Earthquake Research, Report No. CCEER-03-7, Department of Civil Engineering, University of Nevada, Reno, Nevada, 2004.
- [33] A. Abdulridha, D. Palermo, S. Foo, F.J. Vecchio, Behavior and modeling of superelastic shape memory alloy reinforced concrete beams, *Eng. Struct.* 49 (2013) 893–904.
- [34] M. Ghassemieh, M. Mostafazadeh, M.S. Sadeh, Seismic control of concrete shear wall using shape memory alloys, *J. Intell. Mater. Syst. S*, 23(5) (2012) 535-543.
- [35] M.A. Youssef, M.S. Alam, M. Nehdi, Experimental investigation on the seismic behaviour of beam-column joints reinforced with superelastic shape memory alloys, *J. Earthq. Eng.* 12(7) (2008) 1205-1222.
- [36] M.S. Alam, M. Nehdi, M.A. Youssef, Seismic Performance of concrete frame structures reinforced with superelastic shape memory alloys, *Smart. Struct. Syst.* 5(5) (2009) 565-585.
- [37] M.A. Youssef, M.A. Elfeki, Seismic performance of concrete frames reinforced with superelastic shape memory alloys, *Smart. Struct. Syst.* 9(4) (2012) 313-333.

- [38] M. Dolce, D. Cardone, R. Marnetto, M. Mucciarelli, D. Nigro, F.C. Ponso, G. Santarsiero, Experimental static and dynamic response of a real R/C frame upgraded with SMA recentering and dissipating braces, 13th world conference on earthquake engineering, Vancouver, Canada, 2004, paper no. 2878.
- [39] D. Cardone, M. Dolce, F.C. Ponso, E. Coelho, Experimental behaviour of R/C frames retrofitted with dissipating and re-centering braces. *J. Earthq. Eng.* 8 (2004) 361-396.
- [40] R. DesRoches, M. Delemont, Design and analysis of innovative dampers for seismically isolated bridges in the United States, Proceedings of the 7th international seminar on seismic isolation, energy dissipation, and active control, Assisi, Italy, November, 2001 (2001)
- [41] O.E. Ozbulut, S. Hurlebaus Evaluation of the performance of a sliding-type base isolation system with a NiTi shape memory alloy device considering temperature effects, *Eng. Struct.* 32 (1) (2010), 238–249.
- [42] B. Andrawes, R. DesRoches Comparison between shape memory alloy seismic restrainers and other bridge retrofit devices, *J. Bridge. Eng.* 12 (6) (2007), 700–709.
- [43] E. McCarthy, T. Wright, J. Padgett, R. DesRoches, P. Bradford Mitigating seismic bridge damage through shape memory alloy enhanced modular bridge expansion joints, *Struct. Congr.* (2012) 708–717.
- [44] J. Ocel, R. DesRoches, R.T. Leon, W.G. Hess, R. Krumme, J.R. Hayes, S. Sweeney, Steel beam-column connections using shape memory alloys, *J. Struct. Eng.* 130 (2004) 732–740.
- [45] H. Ma, T. Wilkinson, C. Chongdu, Feasibility study on a self-centering beam-to-column connection by using the superelastic behavior of SMAs, *Smart. Mater. Struct.* 16 (2007) 1555–1563.
- [46] H. Ma, M. C. H. Yam, Experimental study on a beam-to-column connection using Shape Memory Alloy, *Adv. Mater. Res.* 374-377 (2012) 2176-2179.
- [47] J. Sepúlveda, R. Boroschek, R. Herrera, O. Moroni, M. Sarrazin, Steel beam-column connection using copper-based shape memory alloy dampers, *J. Constr. Steel. Res.* 64 (2008) 429-435.

- [48] M.S. Speicher, R. DesRoches, R.T Leon, Experimental results of a NiTi shape memory alloy (SMA)-based recentering beam-column connection. *Eng. Struct.* 33 (2011) 2448-2457.
- [49] W. Wang, T.M. Chan, H. Shao, Y. Chen, Cyclic behavior of connections equipped with NiTi shape memory alloy and steel tendons between H-shaped beam to CHS column, *Eng. Struct.* 88 (2015) 37–50
- [50] C. Fang, M.C.H. Yam, A.C.C. Lam, L. Xie, Cyclic performance of extended end-plate connections equipped with shape memory alloy bolts, *J. Constr. Steel. Res.* 94 (2014) 122–136.
- [51] M.C.H. Yam, C. Fang, A.C.C. Lam, Y. Zhang, Numerical study and practical design of beam-to-column connections with shape memory alloys, *J. Constr. Steel. Res.* 104 (2015) 177–192.
- [52] B.R. Ellingwood, B. Taftali, R. Desroches, Seismic performance assessment of steel frames with shape memory alloy connections, Part II- Probabilistic demand assessment, *J. Earthq. Eng.* 14 (2010) 631-645.
- [53] F. Auricchio, D. Fugazza, R. Desroches, Earthquake performance of steel frames with Nitinol braces, *J. Earthq. Eng.* 10 (1) (2006) 45–66.
- [54] J. McCormick, R. DesRoches, D. Fugazza, F. Auricchio, Seismic assesment of concentrically braced steel frames with shape memory alloy braces, *J. Struct. Eng.* 133 (2007) 862-870.
- [55] B. Asgarian, S. Moradi. Seismic response of steel braced frames with shape memory alloy braces, *J. Const. Steel. Res.* 67(1) (2011) 65-74.
- [56] A. Kari, M. Ghassemieh, S.A. Abolmaali, A new dual bracing system for improving the seismic behavior of steel structures, *Smart. Mater. Struct.* 20 (12) (2011) 125020.
- [57] D.J Miller, Development and experimental validation of self-centering buckling-restrained braces with shape memory alloy, M.Sc thesis, University of Illinois at Urbana-Champaign, USA, 2011.

CHAPTER 2

PREDICTION OF LOCAL SEISMIC DAMAGE IN STEEL MOMENT RESISTING FRAMES

2.1 INTRODUCTION

Steel moment resisting frames (SMRFs) are widely used as the lateral load resistance system for mid- to high-rise buildings. After 1994 Northridge earthquake, significant research was conducted to improve their global seismic performance. While damage of individual elements (beams, columns, and connections) can be based on their rotations, damage to the full frame is usually related to the maximum inter-storey drift (MID). Reported MID values at collapse have large variations in the literature. While FEMA 356 [1] limited the MID for steel structures to 5%, FEMA 350 [2] defined collapse of SMRFs in midrise buildings (4-12 storeys) to occur at 10% inter-storey drift. The New Zealand standard [3] limited the MID to 2.5%. UBC 1997 [4] specified MID values of 2.5% and 2.0% for structures with short and long period of vibrations, respectively. The actual MID depends on many factors including design assumptions, characteristics of the ground motion, and effect of higher modes of vibrations.

The damage due to the vertical component of a seismic excitation was observed to be very significant by many researchers [5-7]. The interior columns and interior beams of moment-resisting frames are significantly affected [5, 6]. The increase in the column axial forces caused by the vertical excitation of near-field and far-field earthquakes can reach 65% and 8%, respectively [7]. The fluctuation of column axial force can also increase the column's

rotational ductility demand, and, thus cause significant structural damage [8]. Several building codes account for the vertical seismic component by assuming that the vertical design response spectrum is 2/3 of the horizontal design spectrum [1, 4]. Eurocode 8 [9] and the National Earthquake Hazards Reduction Program [10] define the vertical spectrum independently from the horizontal spectrum.

The relationship between seismic damage and inter-storey drift (ID) was examined in this study to allow identification of the severely damaged storeys without the need for conducting nonlinear incremental dynamic analysis (IDA). The study proposes a simplified method that can identify the severely damaged floors of SMRFs when exposed to an earthquake while accounting for the vertical seismic component.

2.2 PROPOSED METHOD

Youssef and Elfeki [11] proposed a simplified method to predict the ID at collapse for reinforced concrete frames. The method does not account for the P- Δ effect, which might be appropriate for concrete structures. In this study, the method is further extended to account for P- Δ effect.

2.2.1 Lateral drift (Δ_m) based on P- Δ effect

The increase of fixed-end moments and shear forces of columns due to the P- Δ effect are shown in Figure 2.1 and can be calculated using equations (2.1) and (2.2).

$$M_f = \frac{6E_s I_c}{h_c^2} \Delta_m + \frac{P \Delta_m}{2} \quad (2.1)$$

$$V_f = \frac{12E_s I_c}{h_c^3} \Delta_m + \frac{P \Delta_m}{h_c} \quad (2.2)$$

Figure 2.2 shows an isolated column and the connecting beams. The figure assumes that: (1) joint rotations are equal for any two successive stories, (2) the stiffness of each beam is equally utilized by the columns above and below a specific floor (beams are split into hypothetical halves, each half possesses 50% of the stiffness of the original beam), and (3) Contra-flexure points are assumed to be at the mid-span of each beam and mid-height of each column [11-13]. The stiffness is presented in the figure by the ratio K where $K = I/L$.

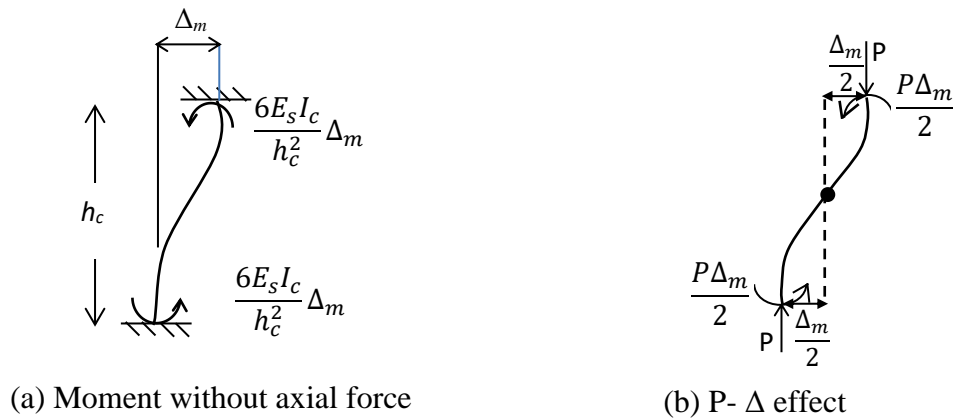


Figure 2. 1: Fixed-end moments induced by lateral displacement Δ_m

If a relative lateral displacement Δ_m is applied between the column ends, the column fixed-end moment can be obtained using equation (2.1). As the flexural stiffness of the top beams and the column are $3E_s K_1$, $3E_s K_2$ and $6E_s K_c$, the moment distribution factor d_{ct} can be calculated using equation (2.3). Applying the principal of moment distribution, the final moment at the column top (M_{ct}) can be obtained using equations (2.4).

$$d_{ct} = \frac{6K_c}{3K_1 + 3K_2 + 6K_c} = \frac{2}{K_t + 2} \quad (2.3)$$

Where $K_t = \frac{K_1 + K_2}{K_c}$.

$$M_{ct} = \left(\frac{6E_s I_c}{h_c^2} + \frac{P}{2} \right) \Delta_m \frac{K_t}{K_t + 2} \quad (2.4)$$

Similarly, the moment at the bottom end of the column (M_{cb}) can be calculated using equation (2.5).

$$M_{cb} = \left(\frac{6E_s I_c}{h_c^2} + \frac{P}{2} \right) \Delta_m \frac{K_b}{K_b + 2} \quad (2.5)$$

$$\text{Where } K_b = \frac{K_3 + K_4}{K_c}$$

The values of Δ_m that lead to instability failure for each of the floor columns can be estimated using equations 2.4 and 2.5.

2.2.2 Lateral drift (Δ_m) based on storey-pushover analysis

The calculation for Δ_m in this section is based on pushover analysis, and, thus accounts for nonlinearity of the beams as well as the columns. For each storey, the columns are first assumed to be fixed at their lower ends, i.e. the lower storeys are removed. Gravity loads are then applied to the remaining storeys. Displacement-controlled pushover analysis is carried out at the level of the considered storey. The evaluated drift at collapse is then magnified to account for the rotation of the storeys below the considered one, which was initially ignored. The magnification factor m was initially proposed by Muto [12] and later modified by Paulay and Priestley [13] and Youssef and Elfeki [11].

For equal inter-story drift, the shear force V_i of a partially restrained column is lower than that of fixed-end column by a factor α , equation (2.6). Replacing the values V_f , M_{ct} and M_{cb} in equation (2.6) by equations (2.2), (2.4), and (2.5), respectively, leads to equation (2.7). The drift magnification factor m that can correlate the deformation of fully and partially restrained column is equal to $1/\alpha$. Equation (2.8) was proposed by Youssef and Elfeki [11] to calculate average drift magnification factor (m_{av}) for each storey.

$$V_i = \alpha V_f = \frac{M_{ct} + M_{cb}}{h_c} \quad (2.6)$$

$$\alpha = \frac{1}{2} \left(\frac{K_t}{K_t + 2} + \frac{K_b}{K_b + 2} \right) \quad (2.7)$$

$$m_{av} = \frac{\sum \text{Stiffness of storey columns assuming fully fixed condition}}{\sum \text{Stiffness of storey columns assuming partially fixed condition}} \quad (2.8)$$

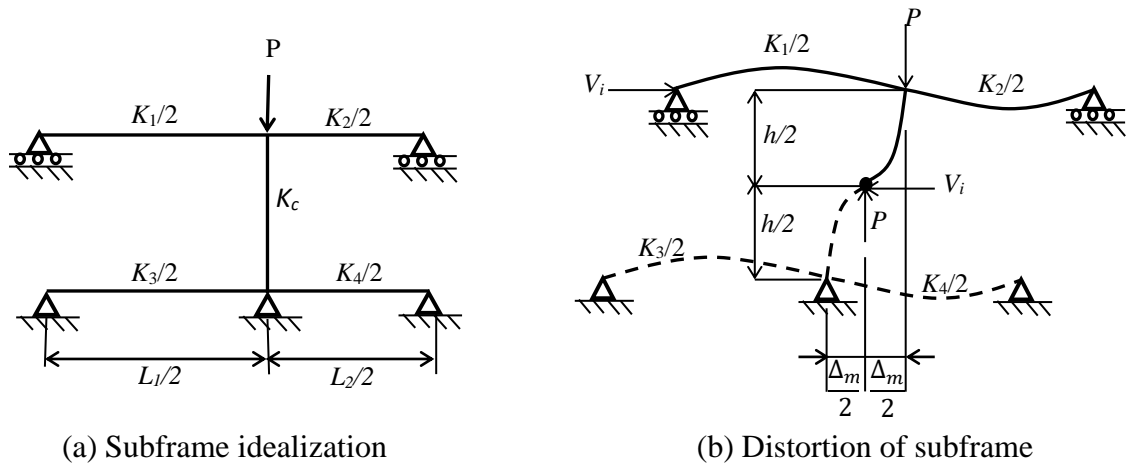


Figure 2. 2: Isolated column and restraining beams

2.2.3 Application of the proposed method

The minimum of the two limiting drift values evaluated in sections 2.1 and 2.2 represent the drift value leading to failure either due soft storey mechanism or instability. Figure 2.3 shows application of the proposed method to the second storey of a three storey building. The columns of the second floor are first assumed fixed at their lower ends. Gravity loads are then applied on the floors above the considered floor. Displacement controlled pushover analysis is carried out to calculate the ID values at collapse for the considered storey. Failure is assumed when any of the floor columns reaches its ultimate rotation. The

corresponding ID is magnified by the factor calculated using equation (2.8) to account for the rotation of the lower column ends. The drift leading to flexural failure of any of the storey's columns due to P- Δ effect is then calculated using equations (2.4) and (2.5). The minimum of the magnified drift and the drift evaluated based on the P- Δ effect is considered as the failure inter-storey drift (FID) for the considered storey. Inter-storey drift limit corresponding to yielding of columns (YDL) can also be evaluated using the same process.

2.2.4 Vertical seismic component

To account for the effect of the vertical seismic component, the FID is calculated while adding extra vertical loads on the considered storey and the stories above [14]. The extra vertical loads are estimated by multiplying the mass of each floor by the vertical design spectrum acceleration, which is assumed to be $2/3$ of the horizontal design spectrum acceleration [1, 4].

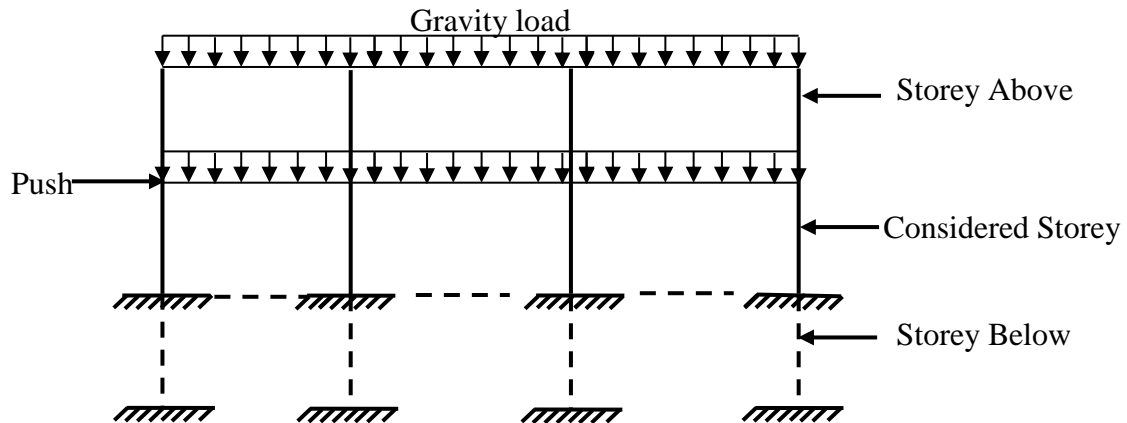


Figure 2. 3: Proposed method to estimate inter-storey drift limits for the second storey of a three storey building.

2.3 ASPECTS OF MODELING

Moment resisting frames were modeled in this paper using SeismoStruct [15]. Beams and columns were modelled using displacement-based inelastic-frame elements. The number of elements was decided upon using a sensitivity analysis. Sample of the obtained results for different number of elements was presented in section 2.6. The distributed dead and live loads were converted to equivalent point loads that are applied at the nodes of each element. For example: for a beam divided to 4 elements, the equivalent point loads were applied at 5 nodes. This modeling technique was justified as the main behaviour was linked to the seismic loads. The vertical loads only affected the stiffness and capacity of the columns. Such modeling technique was employed by other researchers [16]. The mass of the building was also converted into lumped masses and applied at the nodes of each beam element. Bilinear material behaviour with 3% strain hardening [1] was considered using the distributed plasticity approach. The analysis accounts for P- Δ effect.

2.3.1 Failure criteria

FEMA 356 [1] proposed moment rotation behaviour for nonlinear analysis of steel beams and columns is shown in Figure 2.4. The parameter “a” defines the plastic rotation at ultimate condition. Values for this parameter are given in Table 2.1. The yield rotation θ_y of beams and columns can be calculated using equations (2.9) and (2.10) [1]. The ultimate rotation (θ_u) can then be obtained by adding the plastic rotation to the yield rotation. Failure of a floor is defined when the rotation of any of its columns exceeds the ultimate rotation (θ_u).

$$\theta_y(\text{Beams}) = \frac{ZF_{ye} L_b}{6EI_b} \quad (2.9)$$

$$\theta_y(\text{Columns}) = \frac{ZF_{ye} L_c}{6EI_c} \left(1 - \frac{P}{P_{ye}}\right) \quad (2.10)$$

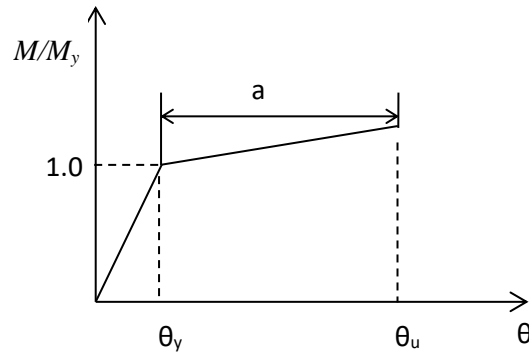


Figure 2. 4: Moment-rotation behaviour for steel elements

Table 2. 1: Modeling parameters for nonlinear procedures according to FEMA356 [1]

Component	Plastic rotation (radians) a
Beam	
a. $\frac{b_f}{2t_f} \leq \frac{52}{\sqrt{F_{ye}}} \text{ and } \frac{h}{t_w} \leq \frac{418}{\sqrt{F_{ye}}}$	$9\theta_y$
b. $\frac{b_f}{2t_f} \geq \frac{65}{\sqrt{F_{ye}}} \text{ or } \frac{h}{t_w} \geq \frac{640}{\sqrt{F_{ye}}}$	$4\theta_y$
Column	
For $P/P_{cl} < 0.2$	
a. $\frac{b_f}{2t_f} \leq \frac{52}{\sqrt{F_{ye}}} \text{ and } \frac{h}{t_w} \leq \frac{300}{\sqrt{F_{ye}}}$	$9\theta_y$
b. $\frac{b_f}{2t_f} \geq \frac{65}{\sqrt{F_{ye}}} \text{ or } \frac{h}{t_w} \geq \frac{460}{\sqrt{F_{ye}}}$	$4\theta_y$
Column	
For $0.2 \leq P/P_{cl} \leq 0.5$	
a. $\frac{b_f}{2t_f} \leq \frac{52}{\sqrt{F_{ye}}} \text{ and } \frac{h}{t_w} \leq \frac{260}{\sqrt{F_{ye}}}$	$11(1-1.7P/P_{CL})\theta_y$
b. $\frac{b_f}{2t_f} \geq \frac{65}{\sqrt{F_{ye}}} \text{ or } \frac{h}{t_w} \geq \frac{400}{\sqrt{F_{ye}}}$	$1\theta_y$

2.4 VALIDATION OF THE PROPOSED METHOD

Suita et al. [17] performed a shake table test on a full scale 4-storey steel building. The moment resisting frames were designed and constructed according to the Japanese design specification (2008). The building was subjected to 0.4, 0.6 and 1.0 of the JR Takatori station record of the 1995 Hyogoken-Nanbu earthquake. The building collapsed due to soft first-storey mechanism at 1 time Takatori record. The maximum storey shear was reached at an inter-storey drift of 4%. The proposed method was applied to estimate the FID and the location of the critical storey. Figure 2.5 compares the FID limits with the experimentally measured IDs at 1 times Takatori record. According to the proposed method the FID varied from 3.82% to 10.32% for the different stories. The FID of the 1st storey (3.82%) was almost equal to the experimental ID at collapse (4%). The experimental ID values for the remaining stories were much lower than the predicted FID. This explained the experimental observation that severe damage was only observed in the 1st storey.

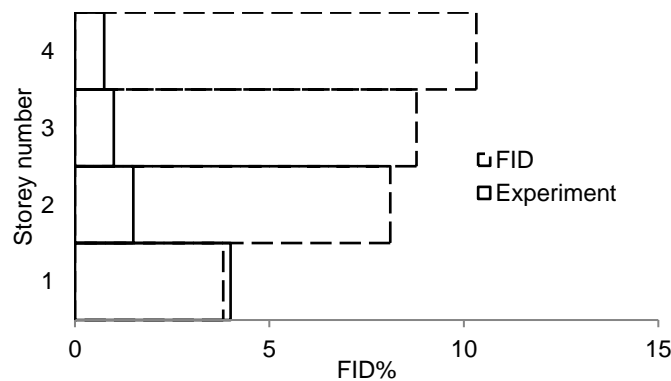


Figure 2. 5: Estimated FID at collapse compared with the IDs measured by Suita et al. [17]

Hajjar et al. [18] performed a computational investigation on the Borax corporate headquarters building, a four-storey steel-frame structure. During 1994 Northridge earthquake, the 1st and 2nd floors of the building were severely damaged. The maximum inter-storey displacement-ductility demands were estimated using 3-D dynamic analysis as 2.81, 2.84, 2.01, and 1.88 for the 1st, 2nd, 3rd and 4th storey, respectively. The proposed method was applied to the north-south moment frame to calculate the FID for each storey. The FID limits for the 1st, 2nd, 3rd, and 4th floors were 6.96%, 9.85%, 10.86% and 13.46%, respectively. The lowest value of FID indicated that failure was expected to occur at the first floor, which agreed with the observed damage distribution of the frame due to Northridge earthquake [18].

Kim et al. [19] experimentally investigated the inelastic nonlinear behaviour of a one-bay two-story steel frame subjected to Northridge and Loma Prieta earthquakes. The experimental ID for the 1st and 2nd stories were 2.22% and 1.85% due to Northridge earthquake, and 1.75% and 1.46% due to Loma Prieta earthquake. The measured strains revealed that the first storey columns yielded for both earthquakes. The yielding inter-storey drift (YDL) of each storey was calculated. The calculated YDL were 1.1% and 1.8% for the 1st and 2nd storey, respectively. Comparing the proposed YDL and the experimental ID showed that ID of the 1st storey exceeded the limit, and, thus yielding of columns occurred. The ratio of the experimental ID to the YDL for the 1st floor was 2.02 for the case of Northridge earthquake, which explained the severe plastic strains observed during the experiment.

2.5 CASE STUDY

A three-storey (Frame 3) and a ten-storey (Frame 10) SMRFs were selected to further validate the proposed method. The 3-storey building was designed by a consulting engineering firm [20]. Figure 2.6 shows the plan and elevation of the building. The solid lines indicate the locations of the moment frames. The design yield strengths of the beams and columns were 248 MPa and 345 MPa, respectively. The 10-storey building (Figure 2.7) was designed by Ozhendekci and Ozhendekci [21]. The design yield strength was 355 MPa. Sections for Frames 3 and Frame 10 are listed in Tables 2.2 and 2.3.

A 2D model of the SMRFs was developed using SeismoStruct. As the axial load of the columns was expected to be less than 50% of their capacity, displacement-based pushover analysis was performed to evaluate the FIDs for each storey. The drift magnification factors (m_{av}) to account for rotations of storeys below the considered storey are listed in Tables 2.4 and 2.5. The drifts at which the internal and external columns reached their ultimate moment capacity due to P- Δ effect were then calculated using equations (2.4) and (2.5) and are also listed in Tables 2.4 and 2.5. The FID for the upper storeys increased because of the rotation of the storeys below.

Table 2. 2: Section properties of Frame 3

Storey	Column		Beam
	Exterior	Interior	
1	W14×257	W14×311	W30×116
2	W14×257	W14×311	W30×116
3	W14×257	W14×311	W24×62

Table 2. 3: Section properties of Frame 10

Storey	Column	Beam
1	HEM550	IPE550
2	HEM550	IPE600
3	HEM550	IPE600
4	HEM550	IPE600
5	HEM500	IPE600
6	HEM500	IPE550
7	HEM500	IPE550
8	HEM400	IPE550
9	HEM400	IPE450
10	HEM400	IPE450

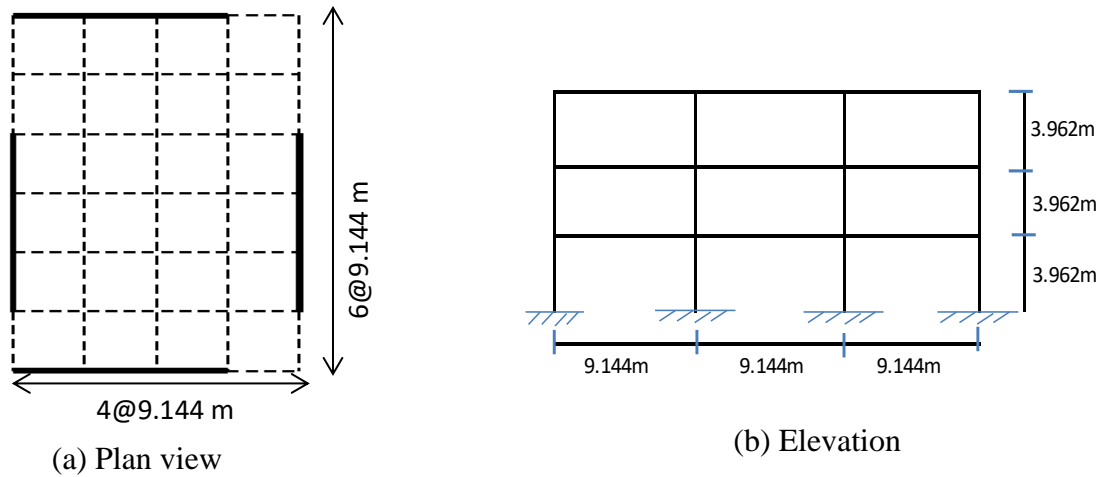


Figure 2. 6: Plan and elevation of selected 3-storey building [20]

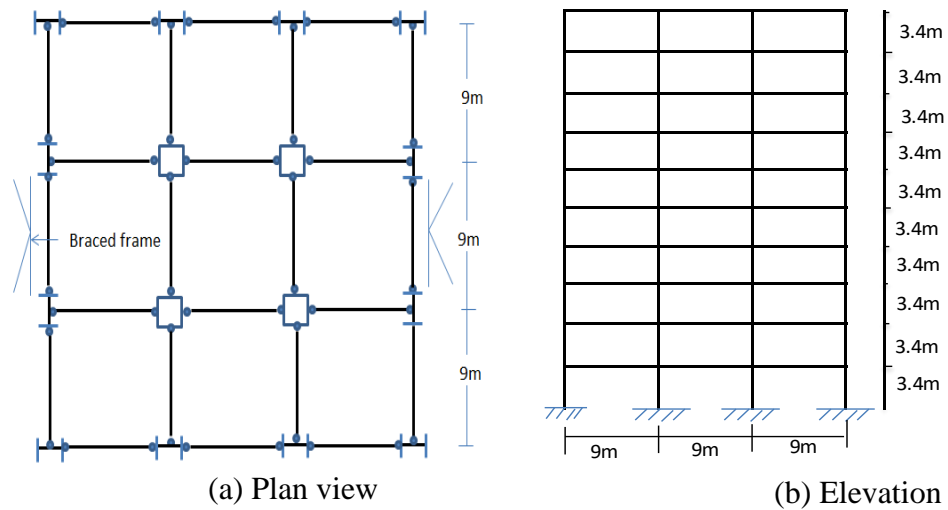


Figure 2. 7: Plan and elevation of selected 10-storey building [21]

Table 2. 4: Limiting FID (%) for different floors of 3 storey frame

Level	Drift magnification factor (m_{av})	Limiting ID% according to section 2.2	Limiting ID% based on section 2.1		Proposed FID (%)
			Interior column	Exterior column	
1	1	6.04	6.39	6.49	6.04
2	3.45	21.06	21.89	31.46	21.06
3	4.94	30.50	22.89	71.62	22.89

Table 2. 5: Limiting FID (%) for different floors of 10 storey frame

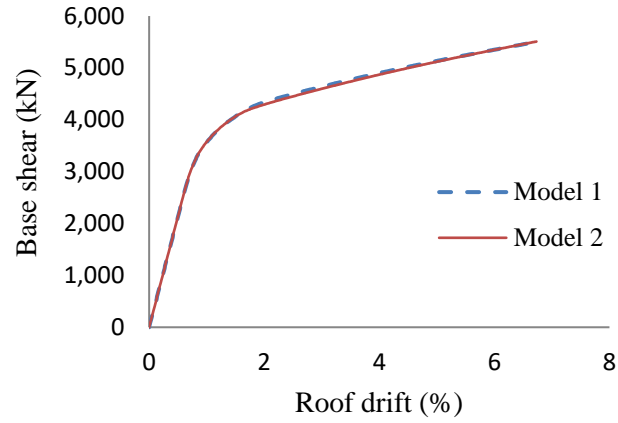
Storey	Drift magnification factor (m_{av})	Limiting ID % based on section 2.2	Limiting ID% based on section 2.1		Proposed FID (%)
			Interior column	Exterior column	
1	1	2.38	3.73	4.98	2.38
2	9.90	31.6	31.1	60.5	31.1
3	8.69	28.6	32.7	59.4	28.6
4	8.69	29.4	34.4	58.3	29.4
5	7.31	27.7	30.9	51.5	27.7
6	8.31	32.3	30.7	51.9	30.7
7	9.62	38.5	37.9	66.1	37.9
8	6.56	32.9	30.0	52.0	29.9
9	8.48	43.7	31.2	55.4	31.2
10	12.0	63.4	50.6	94.5	50.6

2.6 PUSHOVER ANALYSIS

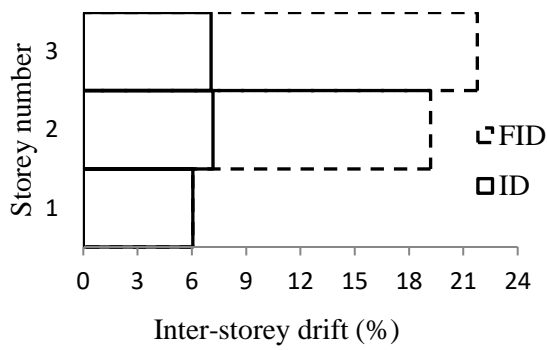
The lateral load distribution for the pushover analysis was assumed as the elastic base shear distribution. Different number of elements was considered in the analysis. Figure 2.8 shows results of pushover analysis for Frame 3 considering two mesh sizes, dividing beams and columns into 4 and 2 elements (Model 1) and dividing them into 6 and 4 elements (Model 2), respectively. The comparison of the base shear versus the roof drift curves for the two

models is shown in Figure 2.8 (a). It led to the conclusion that the number of elements in model 1 was adequate. For both models, the frame failed at a roof drift of 6.71% due to failure of a first floor column. Figure 2.8 (b) shows the comparison between the ID of different floors and the proposed FID. Although the maximum ID (7.17%) occurred at the 2nd floor, none of the floor columns failed. This agrees with the proposed method as the ID for this floor was lower than the FID. Figure 2.8(c) shows the damage distribution at failure. The four columns of the first floor exceeded the yield strain at their base. The exterior column reached its ultimate rotation. Yielding of beams was observed for all floors. Columns of the 2nd and 3rd storeys did not experience any yielding.

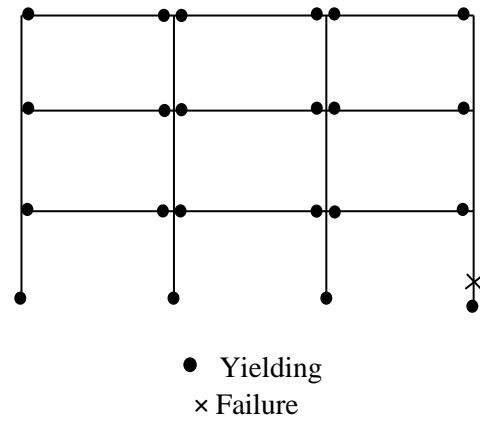
Figure 2.9 shows the results of pushover analysis for Frame 10. The frame failed at 2.98% roof drift. The lower ends of 1st floor columns and 2nd floor interior columns yielded. Two columns of the 1st first floor failed as shown in Figure 2.9 (c). Although the MID occurred at the third floor, its value was much lower than the predicted FID for that floor. The observed damage at collapse supported this fact as the 3rd floor columns did not experience any yielding. From the pushover analysis of both frames, it was observed that the storey experiencing the MID is not the critical storey and that the proposed method can accurately predict the drift limit for the critical storey.



(a)



(b)



(c)

Figure 2. 8 :Pushover analysis results for Frame 3 (a) Relationship between base shear and roof drift, (b) ID obtained from pushover analysis as compared with the proposed collapse ID limits (c) Observed damage at collapse

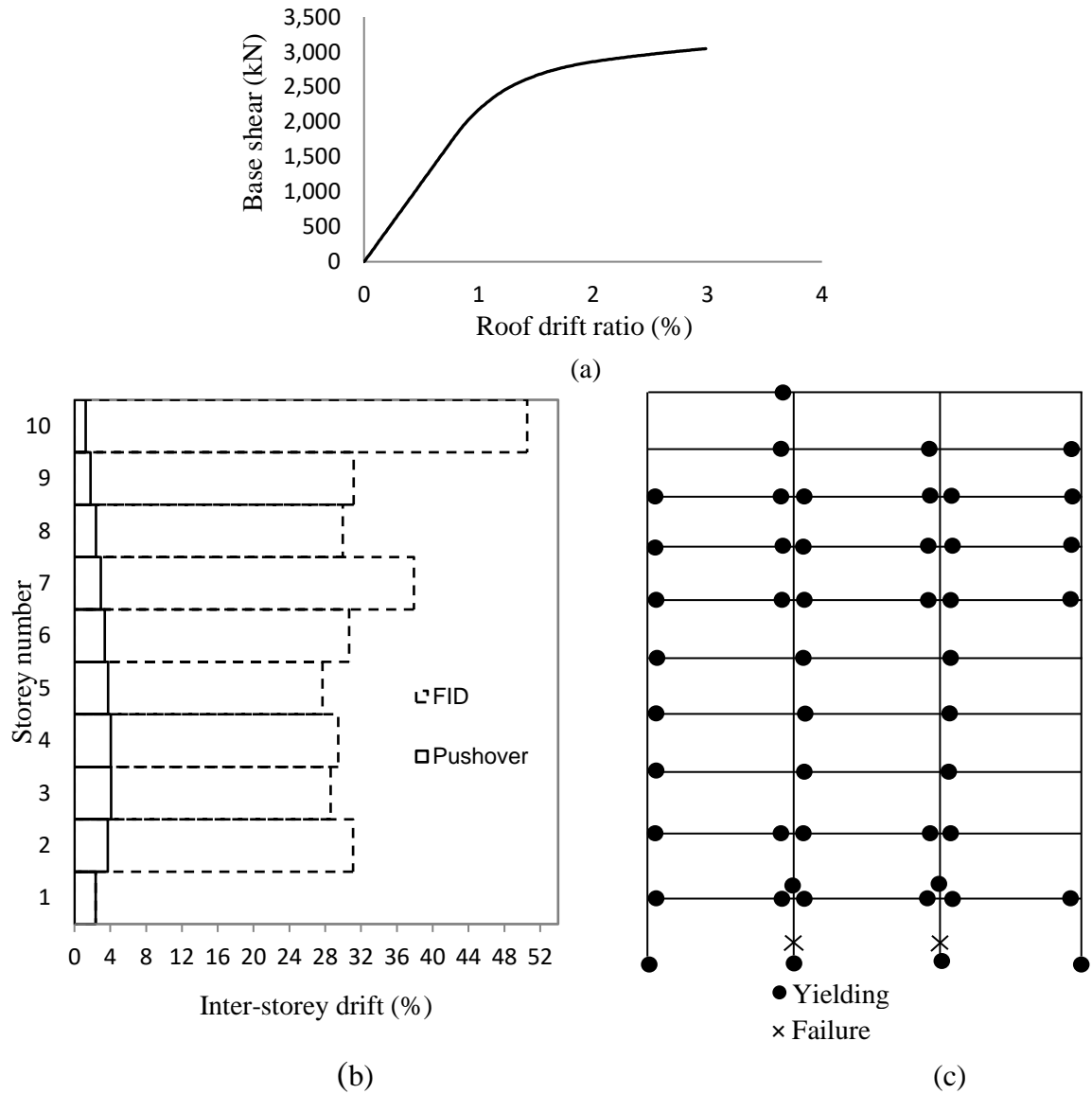


Figure 2. 9: Pushover analysis results for Frame 10 (a) Relationship between base shear and roof drift, (b) ID obtained from pushover analysis as compared with the proposed collapse ID limits (c) Observed damage at collapse

2.7 DYNAMIC ANALYSIS

The seismic performance of the considered frames depends on the seismic hazard parameters including frequency content, event duration and effective number of loading cycles. Five different ground motions were selected to conduct IDA analysis. They were

obtained from PEER ground motion database [22] and their characteristics are listed in Table 2.6. Figure 2.10 shows the elastic response spectra considering 5% damping for these selected ground motions.

Eigen value analysis was performed to determine the frequencies and mode shapes for the considered frames. The fundamental horizontal and vertical periods of vibration of Frame 3 are 0.338 sec. and 0.114 sec., respectively, and those for Frame 10 are equal to 2.385 sec. and 0.277 sec., respectively.

IDA was performed to further validate the proposed method. IDA was first performed considering the horizontal components of five ground motions. The analysis was then repeated while considering both the horizontal and vertical seismic components. The vertical components were scaled using the same scaling factor as the horizontal components to keep the V/H ratio constant. IDA analysis was terminated when the proposed FID limit was reached at any floor. The MIDs of both frames for the five different ground motions are listed in Table 2.7. It is observed that the MID does not necessary occur at the same storey for the different ground motions and that application of the vertical component can change the storey experiencing the MID.

Table 2. 6: Characteristics of ground motions

Earthquake	Date	M _s magnitude	Station	PGA(g)	
				Horizontal	Vertical
Northridge	January 17, 1994	6.7	Arleta-Nordhoff	0.344	0.438
Imperial Valley	October 15, 1979	6.9	El Centro Array #6	0.439	1.655
Loma Prieta	October 18, 1989	7.1	Capitola	0.451	0.5411
Tabas	September 16, 1978	6.9	Tabas	0.852	0.688
San Fernando	February 2, 1971	6.6	Pacoima dam	1.23	0.699

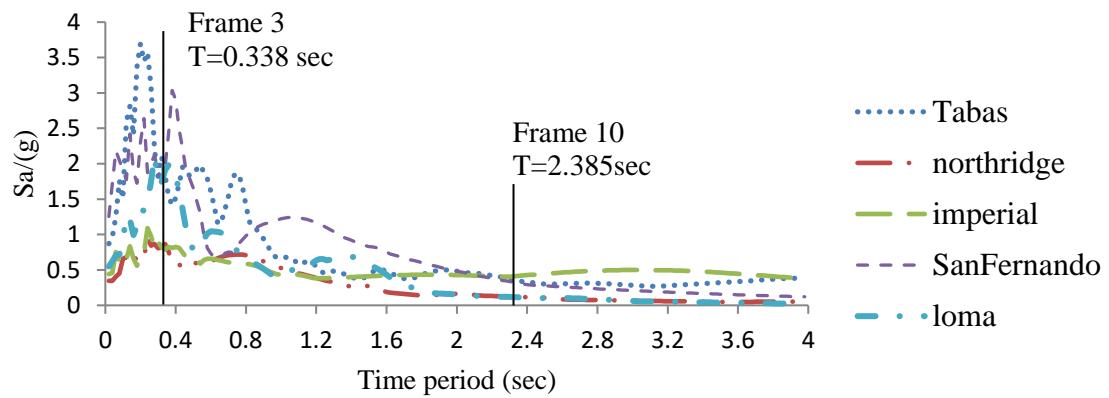


Figure 2. 10: Elastic response spectral acceleration for horizontal seismic component

Table 2. 7: MID at different ground motions

Ground motion	Frame 3		Frame 10	
	MID (Horizontal component)	MID (Horizontal and vertical component)	MID (Horizontal component)	MID (Horizontal and vertical component)
Imperial valley	7.13% (2 nd storey)	7.19% (3 rd storey)	3.46% (2 nd , 3 rd storey)	2.35% (4 th storey)
Northridge	6.45% (2 nd storey)	7.19% (3 rd storey)	3.57% (3 rd storey)	2.70% (8 th storey)
Tabas, Iran	6.94% (3 rd storey)	7.09% (3 rd storey)	3.51% (4 th storey)	2.38% (4 th storey)
San Fernando	7.47% (3 rd storey)	7.66% (3 rd storey)	2.99% (2 nd , 5 th storey)	2.53% (7 th storey)
Loma Prieta	8.33% (3 rd storey)	7.91% (3 rd storey)	5.42% (8 th storey)	3.63 % (8 th storey)

2.7.1 Building damage considering the horizontal components

The damage distribution of Frame 3 at failure considering the horizontal component of Imperial Valley earthquake [$Sa(T_1)=10.10g$] is shown in the Figure 2.11(a). It is observed that all beams yielded and three of the 1st floor columns reached the collapse rotation. The damage distribution clearly shows that the 1st storey was severely damaged as compared to

the other floors. Figure 2.11(b) shows the comparison between the ID of different storeys with the predicted FID limits. Although the IDs of the 2nd and 3rd stories were higher than that of the 1st storey, columns of those storeys did not experience any yielding. This agrees with the predicted limit as the ID for the 1st storey was equal to the predicted limit (6.04%) and the ID for the other storeys were much lower than the FIDs.

Figures 2.12-2.15 show the results of dynamic analysis of Frame 3 at failure considering the horizontal components of Loma [Sa (T1)= 32.71g], Northridge [Sa (T1)= 13.92g], San Fernando [Sa (T1)= 17.1g] and Tabas [Sa (T1)= 14.75g] earthquakes. All four columns of the 1st storey yielded and three of them failed. Columns of the 2nd and 3rd storeys experienced some yielding in the case of Loma and San Fernando records. However, they did not reach the failure state. Although, the damage distribution highlights that the 1st storey was the severely damaged storey, the MIDs occurred at a different storey considering the four records as shown in Figures 2.12(b) 2.13(b), 2.14(b) and 2.15(b). Reaching the FID limit of the 1st storey reflects that the storey was severely damaged, which agreed with the observed damage condition.

Results of the dynamic analysis at failure of Frame 10 are presented in Figures 2.16 to 2.20 considering the horizontal components of the ground motions. Figure 2.16(a) shows that all of the 1st floor columns and the interior columns of the 2nd floor yielded due to Imperial earthquake [Sa(T1) = 0.348g]. One interior column of the 1st storey failed. Although the MID was at the 2nd and 3rd storeys, failure did not occur at these levels. This agreed with the limits predicted using the proposed method as the ID of the first floor was almost equal to the predicted limit (2.38%) and the IDs for the 2nd or 3rd floor (3.46%) were much lower than the predicted limits.

Figures 2.17 to 2.20 show that three columns of the 1st floor failed due to the horizontal components of Northridge, Tabas and San Fernando earthquakes and one column failed in case of Loma earthquake. MID drift (5.42%) occurred at the 8th floor considering the horizontal component of Loma earthquake. Figure 2.20 (a) shows that this floor was not critical as none of its columns failed. Same observations can be made considering other records.

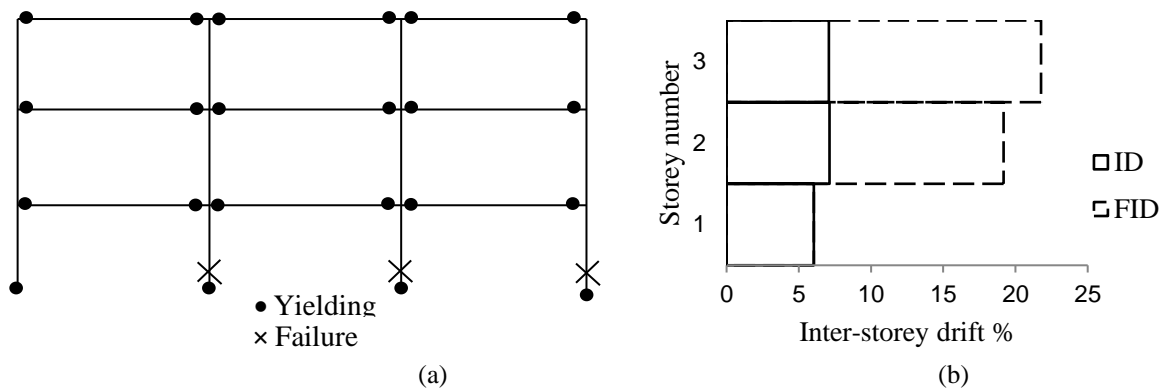


Figure 2. 11: Results of Frame 3 considering horizontal component of Imperial earthquake at $S_a(T1) = 10.10g$ (a) Distribution of yielding (b) ID compared with FID limits

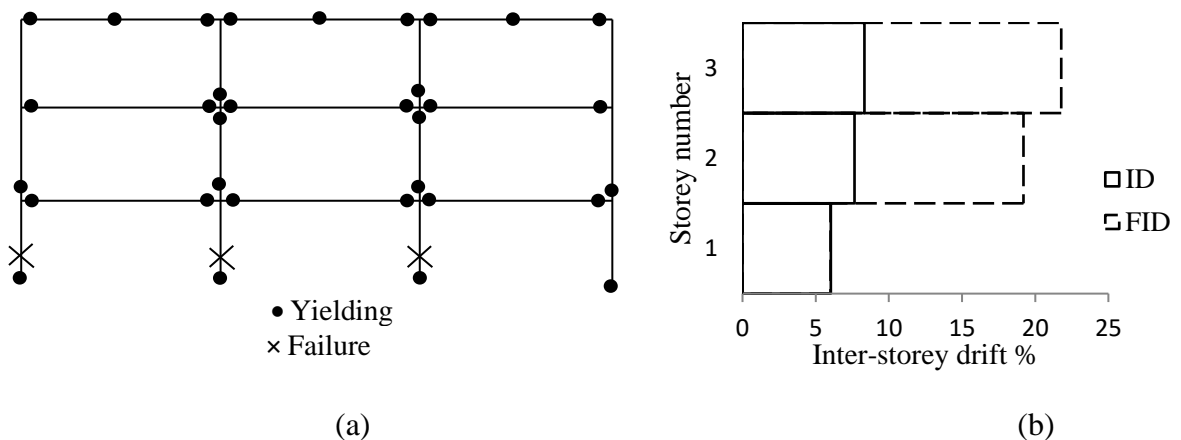


Figure 2. 12: Results of Frame 3 considering horizontal component of Loma earthquake at $S_a(T1) = 32.71g$ (a) Distribution of yielding (b) ID compared with FID limits.

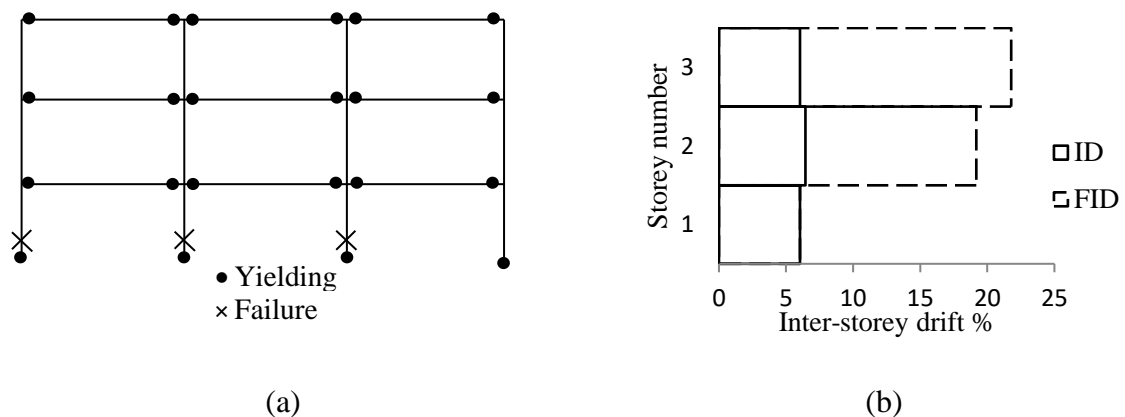


Figure 2. 13: Results of Frame 3 considering horizontal component of Northridge earthquake at $S_a(T1) = 13.92g$ (a) Distribution of yielding (b) ID compared with FID limits.

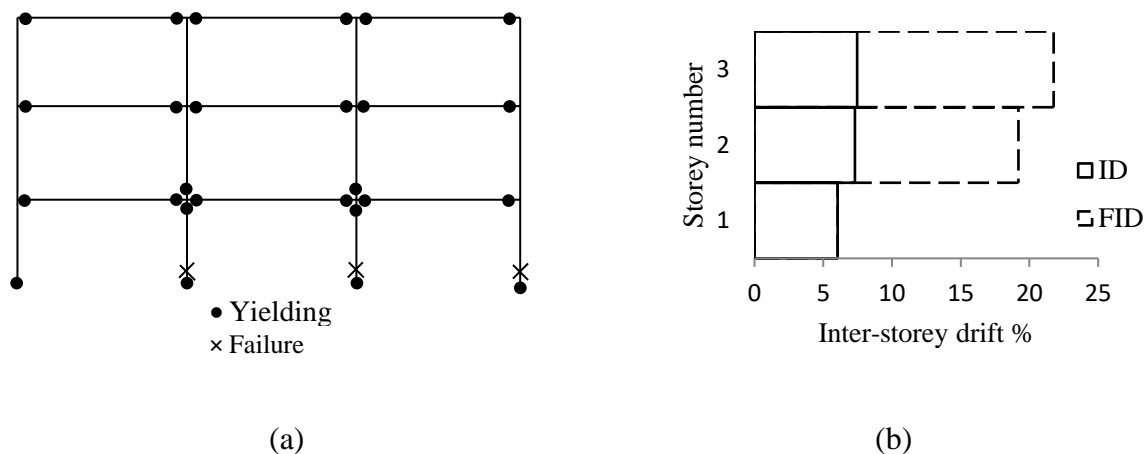


Figure 2. 14: Results of Frame-3 considering horizontal component of San Fernando earthquake at $S_a(T1) = 17.1g$ (a) Distribution of yielding (b) ID compared with FID limits.

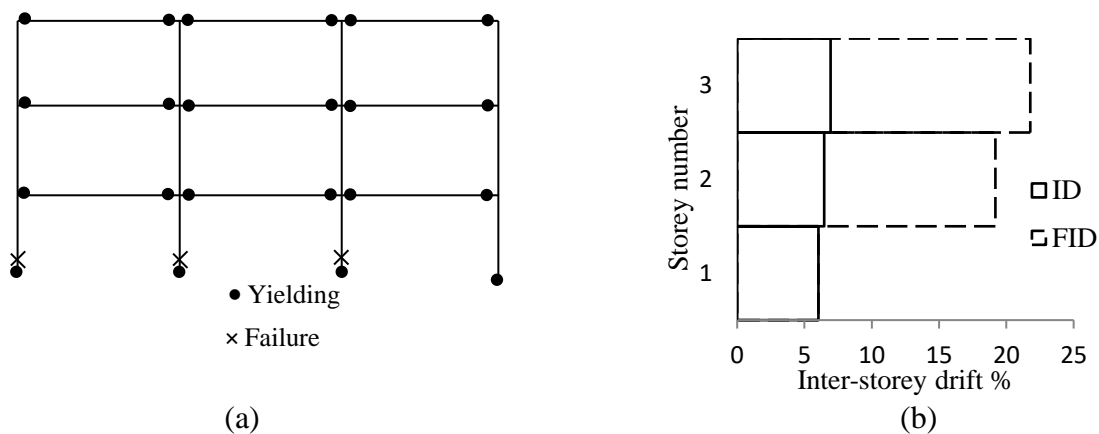


Figure 2. 15: Results of Frame 3 considering horizontal component of Tabas earthquake at $S_a(T1) = 14.75g$ (a) Distribution of yielding (b) ID compared with FID limits.

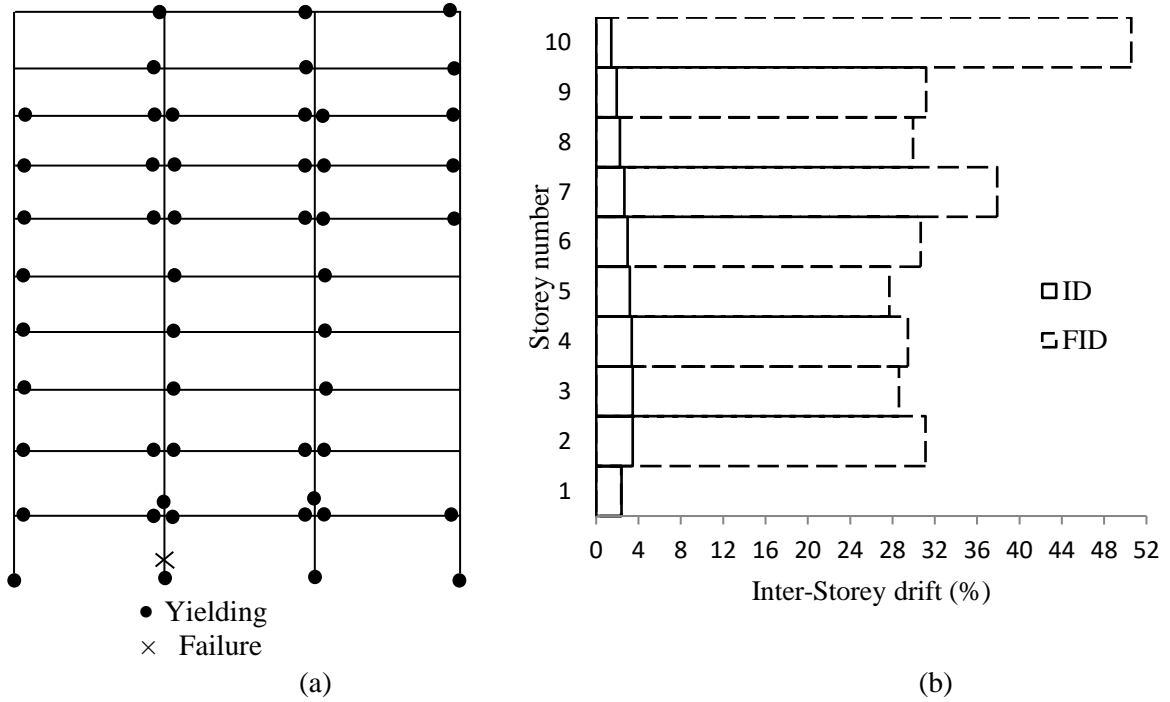


Figure 2. 16: Results of Frame 10 considering horizontal component of Imperial earthquake at $S_a(T_1) = 0.348g$ (a) Distribution of yielding (b) ID compared with FID limits.

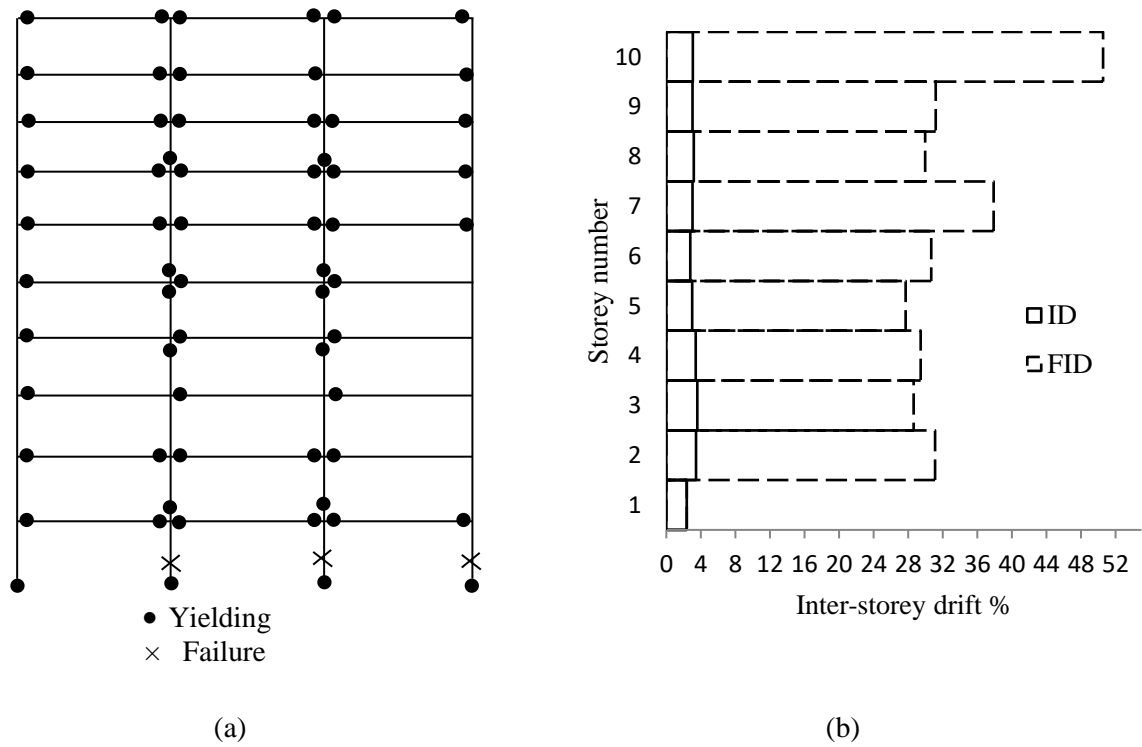


Figure 2. 17: Results of Frame 10 considering horizontal component Northridge earthquake at $S_a(T_1) = 0.424g$ (a) Distribution of yielding (b) ID compared with FID limits.

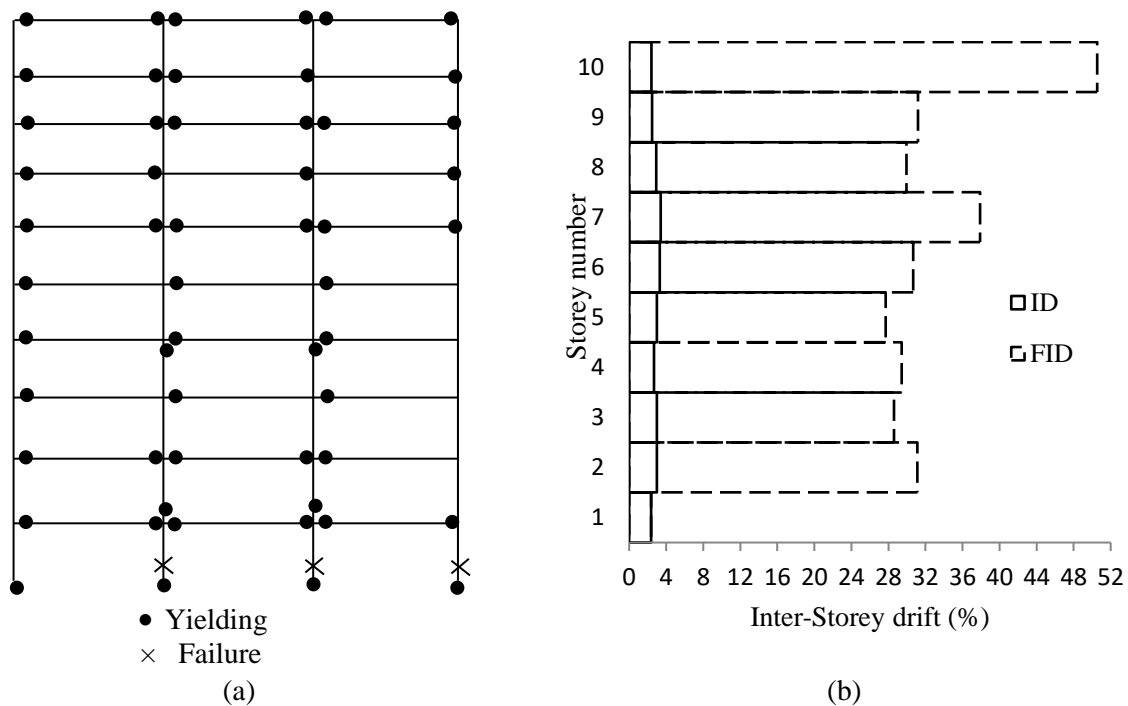


Figure 2. 18: Results of Frame 10 considering horizontal component of San Fernando Earthquake at $S_a(T_1) = 0.339g$ (a) Distribution of yielding (b) ID compared with FID limits.

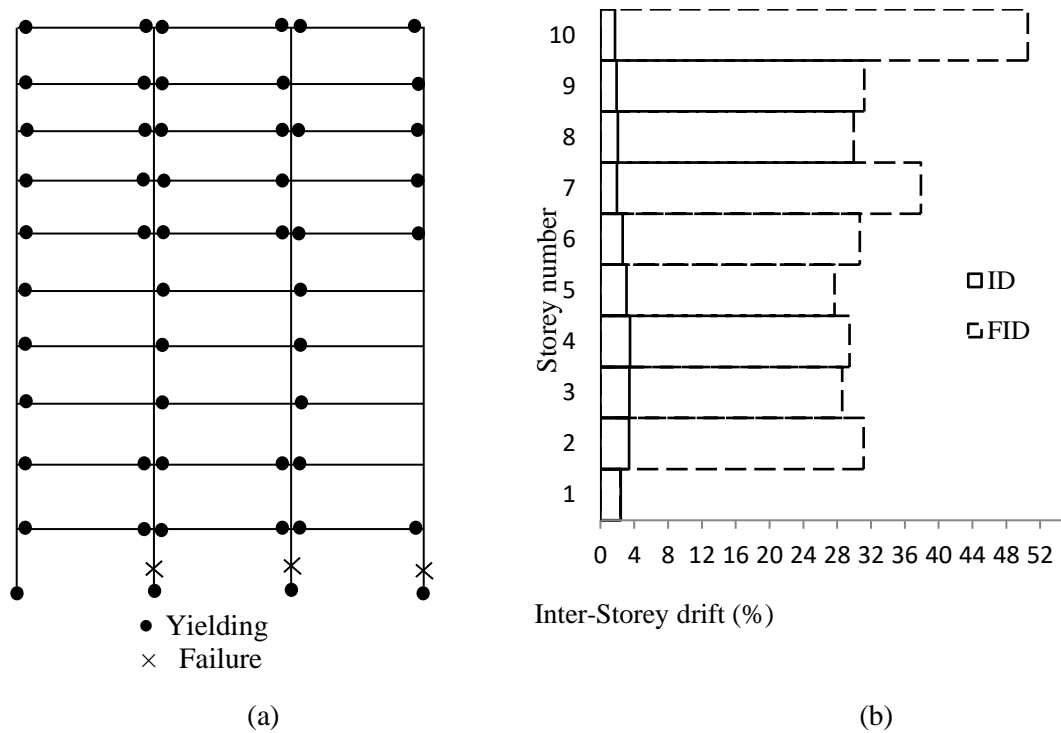


Figure 2. 19: Results of Frame 10 considering horizontal component of Tabas earthquake at $S_a(T_1) = 0.351g$ (a) Distribution of yielding (b) ID compared with FID limits.

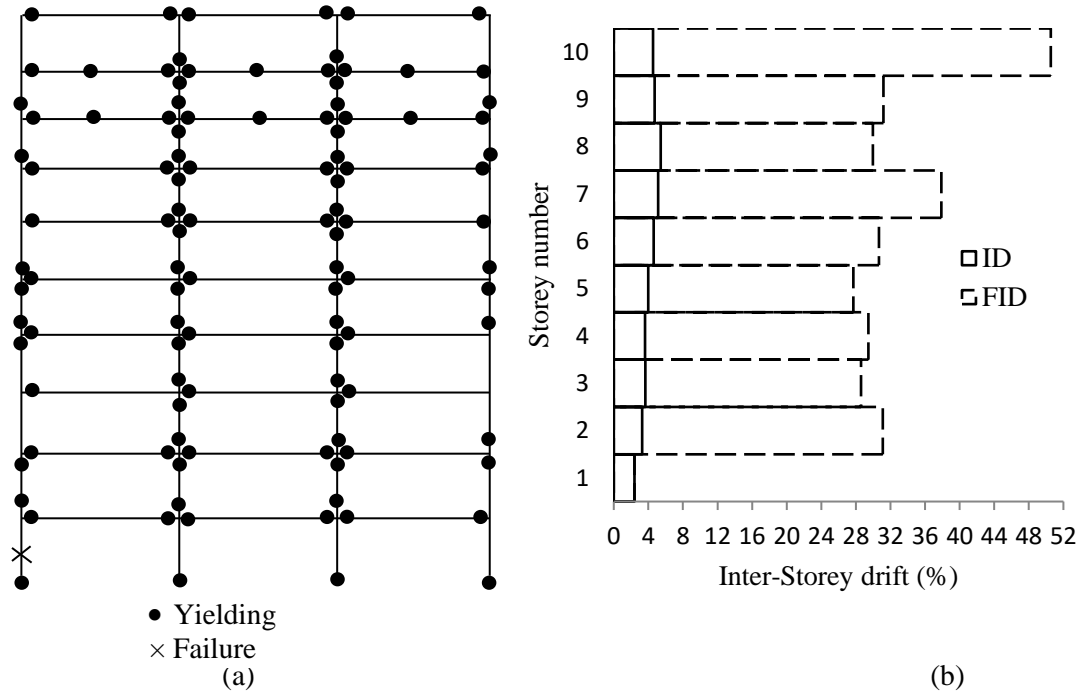


Figure 2. 20: Results of Frame 10 considering horizontal component of Loma earthquake at S_a (T_1) = 0.573g (a) Distribution of yielding (b) ID compared with FID limits.

2.7.2 Inter-storey drift limit at yield

As the first storey was the severely damaged storey for all of the considered frames, further validation of the proposed method was conducted considering Frame 10. For this purpose, the storey specific ID limits at yield (YDL) were calculated as shown in Figure 2.21.

For all five ground motions, the ID of the 1st storey exceeded the YDL which explained the yielding of all the columns of that storey (Figures 2.16 to 2.20). Northridge and Loma earthquakes were considered to further explain the yield distribution of Frame 10.

Due to Northridge earthquake, interior columns of the 2nd, 4th, 5th, 6th and 8th storey yielded (Figure 2.17). The YDL limits for these storeys were close to the experienced ID as shown in Figure 2.21(a). Although columns of the 3rd and 9th storeys did not yield, the strain of

the interior columns were 0.00174 and 0.00160, which were very close to the yield strain (0.00177).

The ID of the Frame 10 due to Loma earthquake was compared with the YDL limits, Figure 2.21(b). It was observed that the ID values exceed the YDL limits for the 1st, 5th, 6th, 8th and 9th storeys, which explained the yielding of all columns at these storeys, Figure 2.20. The ID of the 7th storey was almost equal to the YDL limit reflecting yielding of the interior columns. The strains of the exterior columns of this storey reached 0.0016, which was close to the yield strain (0.00177).

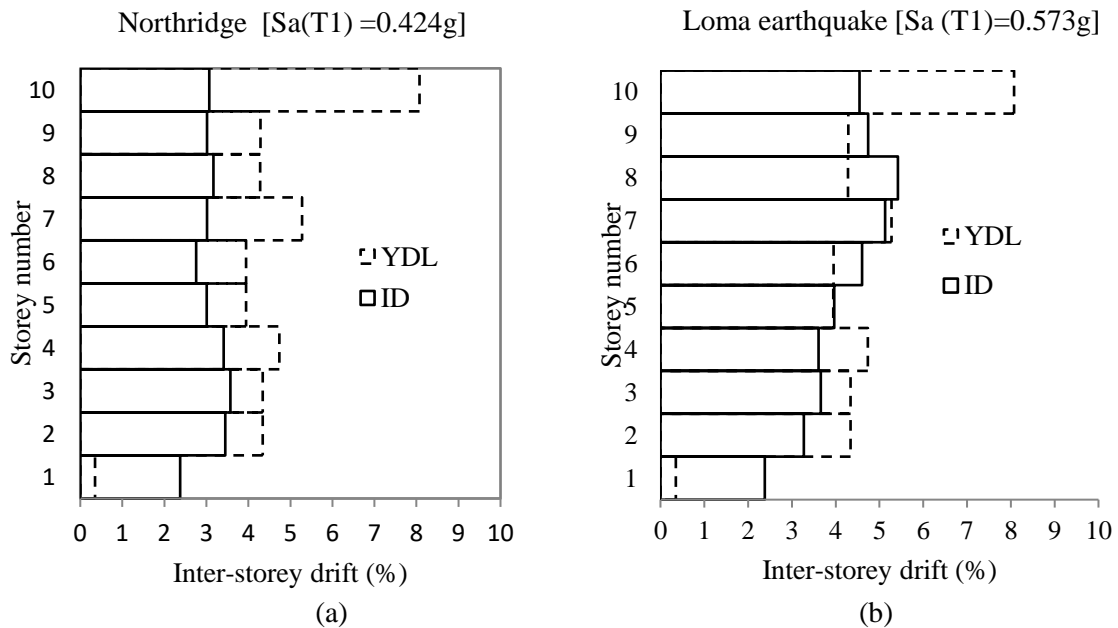


Figure 2. 21: Comparison of YDL and ID for horizontal component of Northridge [Sa (T1) = 0.424g] and Loma Earthquake [Sa (T1) = 0.573g]

2.7.3 Building damage considering the seismic vertical components

The FID limits were modified to account for the effect of vertical component of the ground motions. For the analyzed frames, the extra vertical loads reduced the ductility of the columns. Figure 2.22 shows the FIDs considering only the horizontal component and both the horizontal and vertical components. The effect of vertical component on the FID was not significant for Frame 3. For Frame 10, the assumed extra vertical forces resulted in up to 58% reduction in the FIDs.

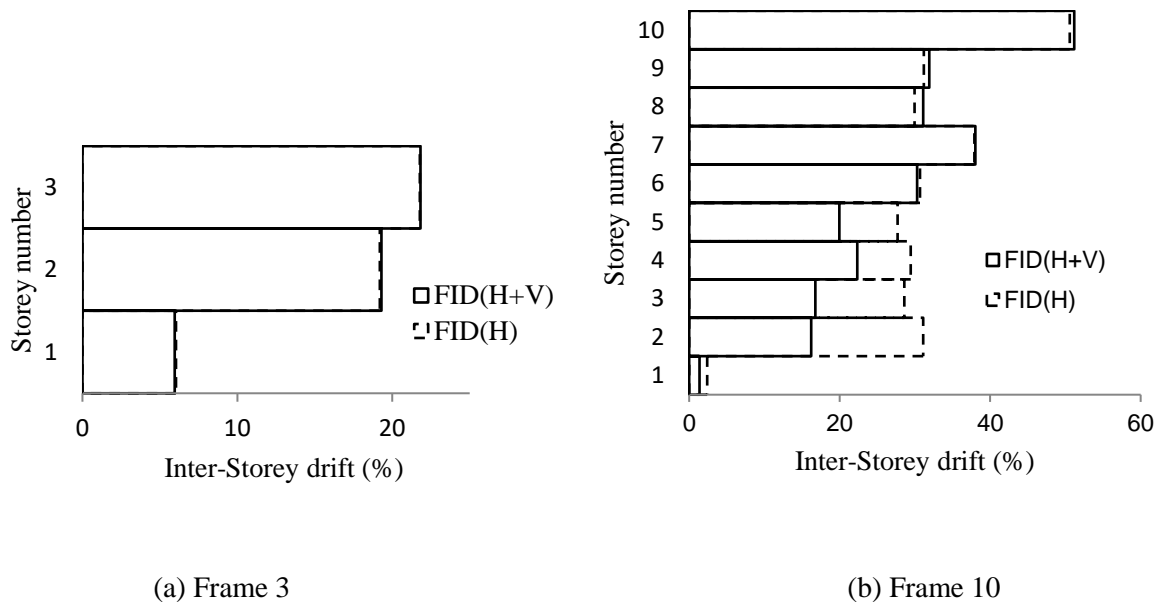


Figure 2. 22: Proposed Limiting FID considering horizontal and both horizontal and vertical components of ground motion.

Figures 2.23 to 2.32 show the results of the dynamic analysis considering both the horizontal and vertical seismic components. For Frame 3, the ends and mid-spans of all beams yielded. Three columns of the 1st floor failed due to Loma, Northridge and San Fernando earthquakes and two columns failed in the case of Imperial earthquake as shown in Figures 2.23(a), 2.24(a), 2.25(a) and 2.26(a), respectively. The ID of the floor was equal

to the predicted FID, which indicated that the first floor was the severely damaged floor. Considering Tabas earthquake, the first floor column yielded, however none of the columns failed, Figure 2.27(a). Thus, the proposed method was found to be conservative for Tabas earthquake due to the overestimation of the extra vertical loads that accounted for the effect of the vertical component.

Figures 2.28 to 2.32 show the results of the dynamic analysis of Frame 10 considering the horizontal and vertical seismic components. All of the first floor columns and the interior columns of the 2nd to 6th floors yielded due to Loma earthquake as shown in the Figure 2.28(a). Two interior columns of the 1st floor failed. For Imperial, Northridge, and Tabas earthquakes, all four columns of the 1st floor yielded (Figures 2.29 to 2.31). For San Fernando, the 1st storey columns and the interior columns of the 2nd storey yielded (Figure 2.32). However, none of the columns failed. The proposed FID limits were found to be either accurate or conservative.

2.7.4 Deflection of beams

The results obtained from the dynamic analysis considering the vertical component of the seismic motions showed that the vertical component caused the beams to have high vertical deflections. The mid-span deflections expressed as a ratio to the beam span were 3.12% for frame 3 at its top floor due to Imperial earthquake, and 1.28% for Frame 10 at its ninth storey due to Loma earthquake.

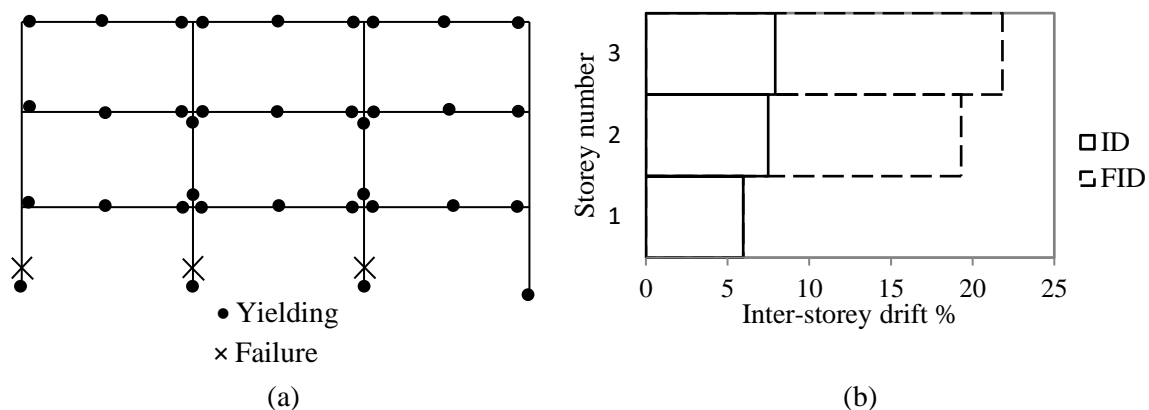


Figure 2. 23: Results of Frame 3 considering horizontal and vertical component of Loma earthquake at $Sa(T1) = 31.87g$ (a) Yielding distribution (b) ID compared with FID

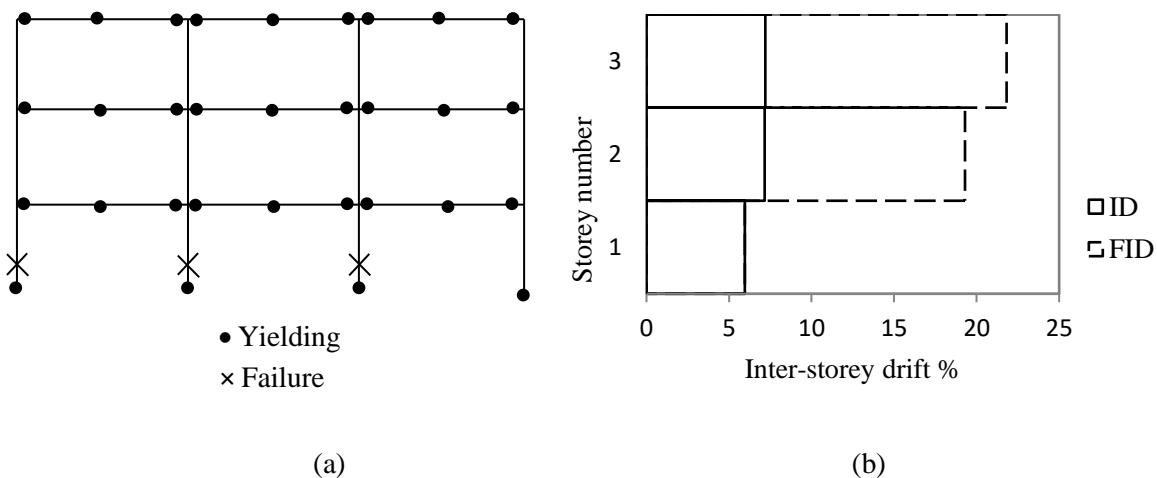


Figure 2. 24: Results of Frame 3 considering horizontal and vertical component of Northridge earthquake at $Sa(T1) = 13.67g$ (a) Yielding distribution (b) ID compared with FID

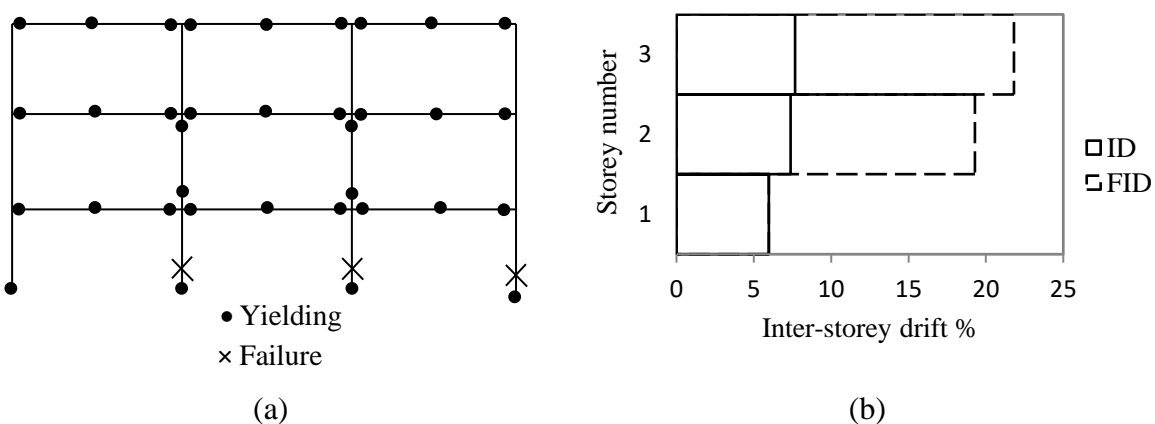


Figure 2. 25: Results of Frame 3 considering horizontal and vertical component of San Fernando earthquake at $Sa(T1) = 17.25g$ (a) Yielding distribution (b) ID compared with FID

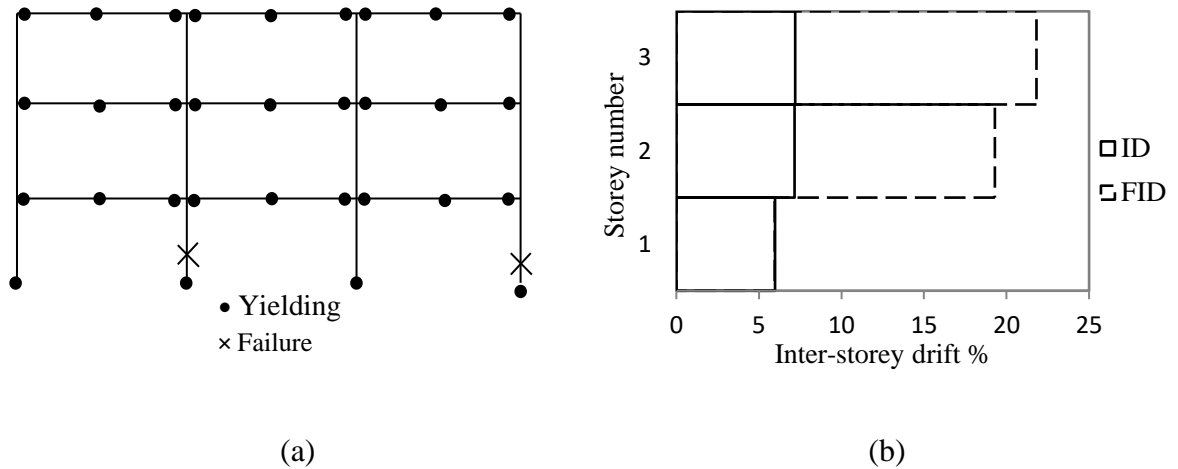


Figure 2. 26: Results of Frame 3 considering horizontal and vertical component of Imperial earthquake at $Sa(T1) = 10.14g$ (a) Yielding distribution (b) ID compared with FID

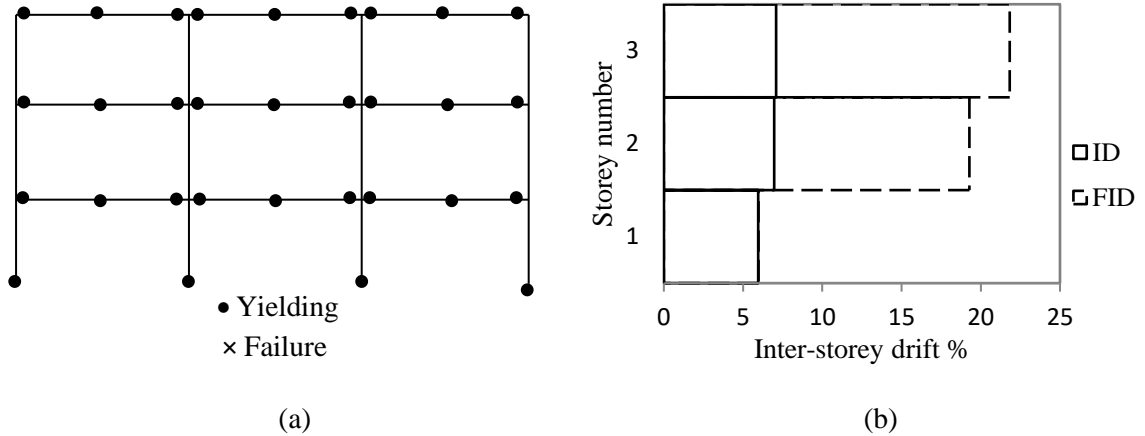


Figure 2. 27: Results of Frame 3 considering horizontal and vertical component of Tabas earthquake at $Sa(T1) = 15.07g$ (a) Yielding distribution (b) ID compared with FID

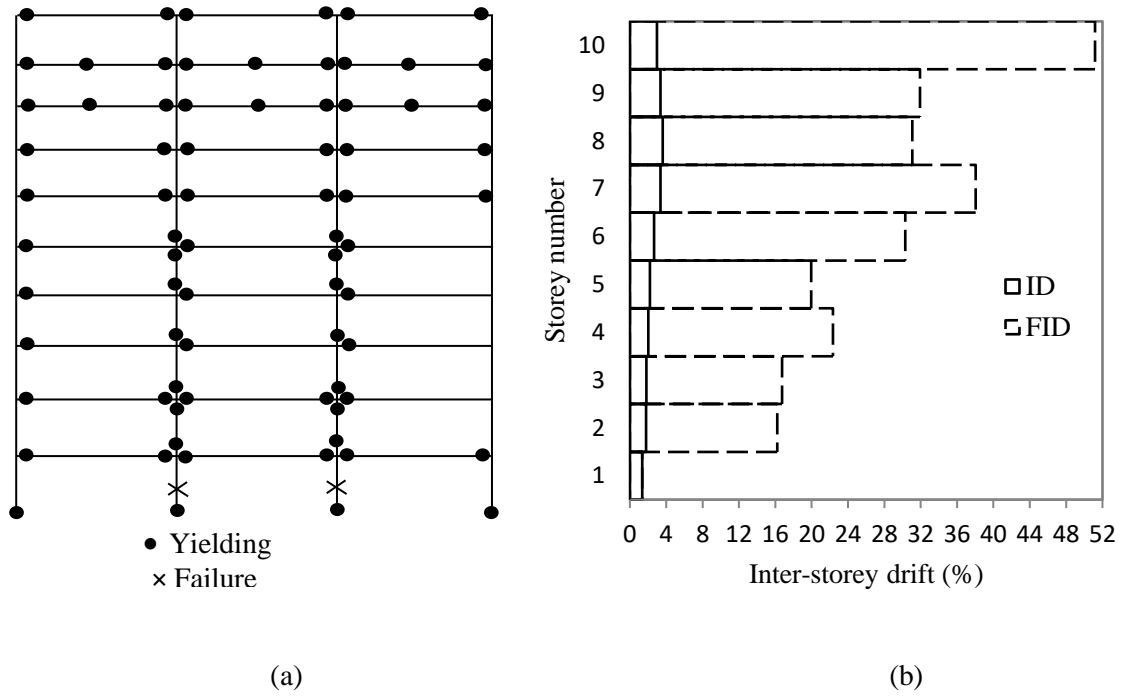


Figure 2. 28: Results of Frame 10 considering horizontal and vertical component of Loma earthquake at $Sa(T1) = 0.325g$ (a) Yielding distribution (b) ID compared with FID

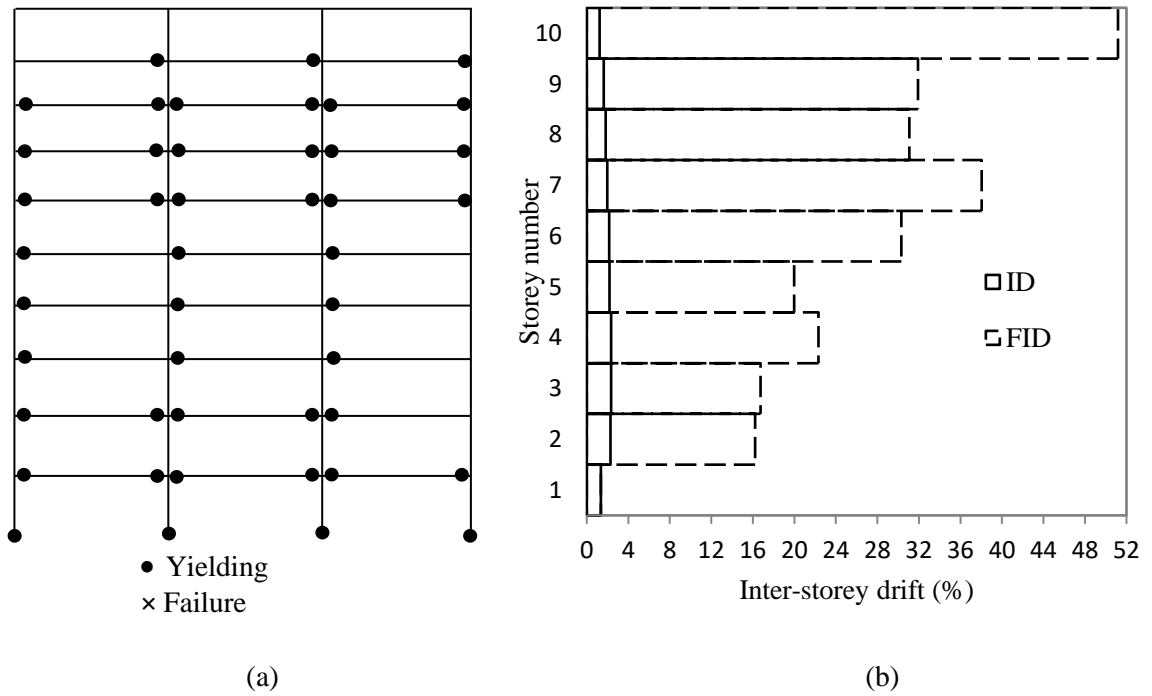


Figure 2. 29: Results of Frame 10 considering horizontal and vertical component of Imperial earthquake at $Sa(T1) = 0.271g$ (a) Distribution of yielding (b) ID compared with FID limit

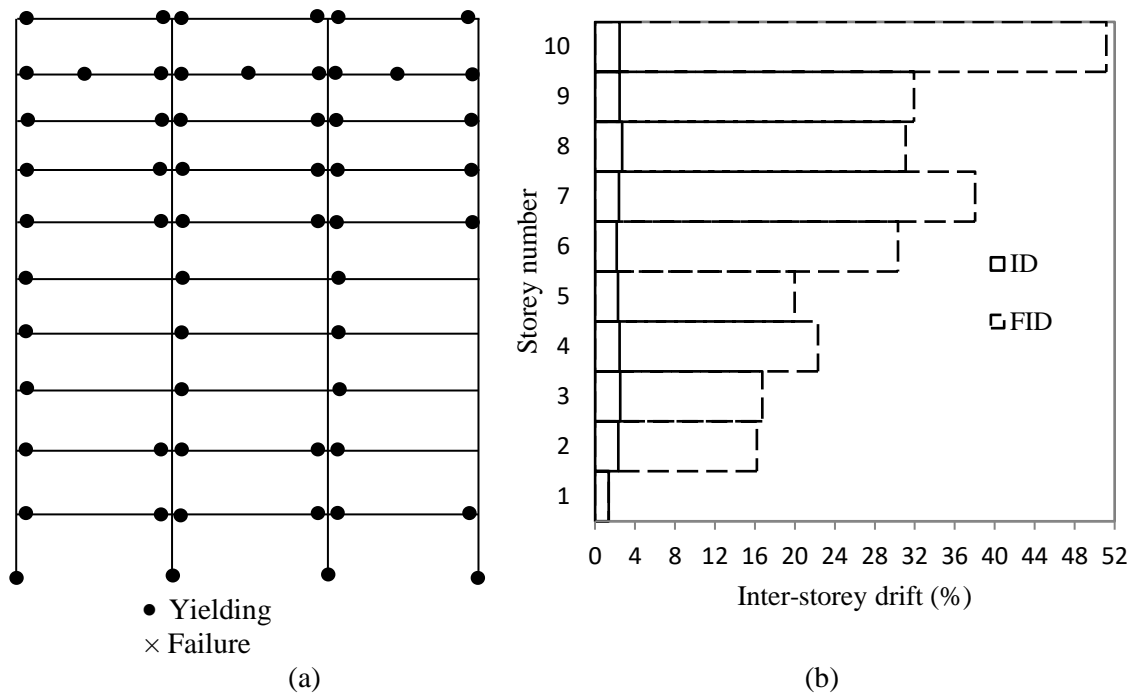


Figure 2. 30: Results of Frame 10 considering horizontal and vertical component of Northridge earthquake at $Sa(T1) = 0.313g$ (a) Distribution of yielding (b) ID compared with FID limit.

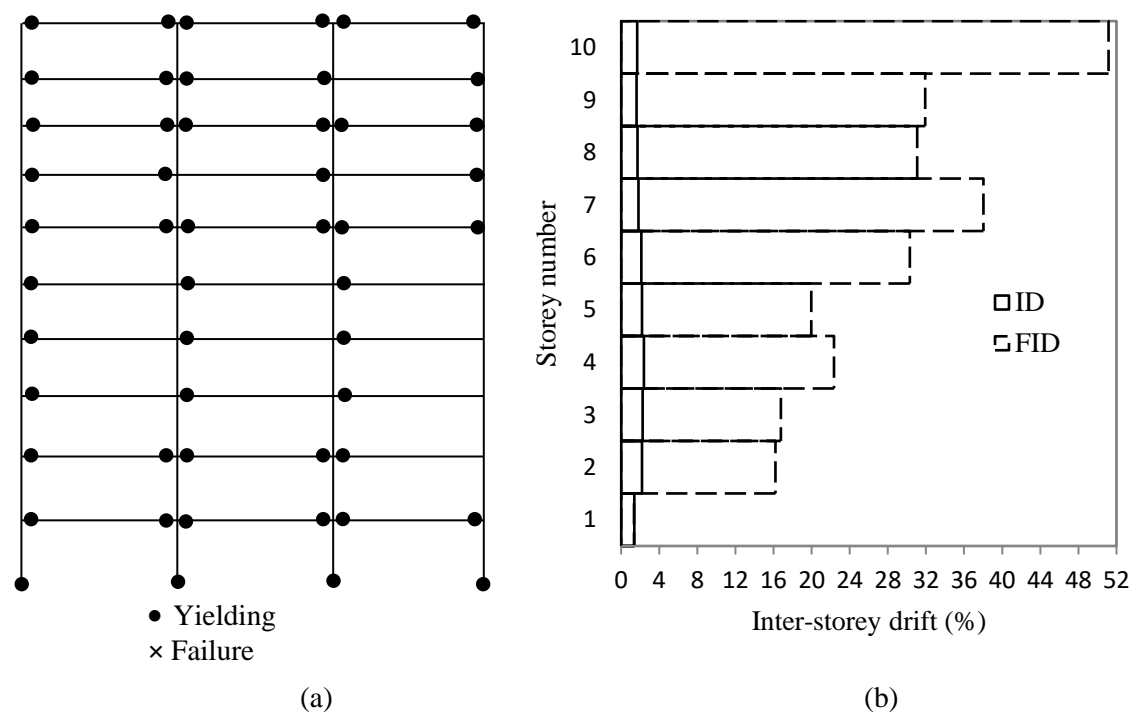


Figure 2. 31: Results of Frame 10 considering horizontal and vertical component of Tabas earthquake at $Sa(T1) = 0.27g$ (a) Distribution of yielding (b) ID compared with FID limit.

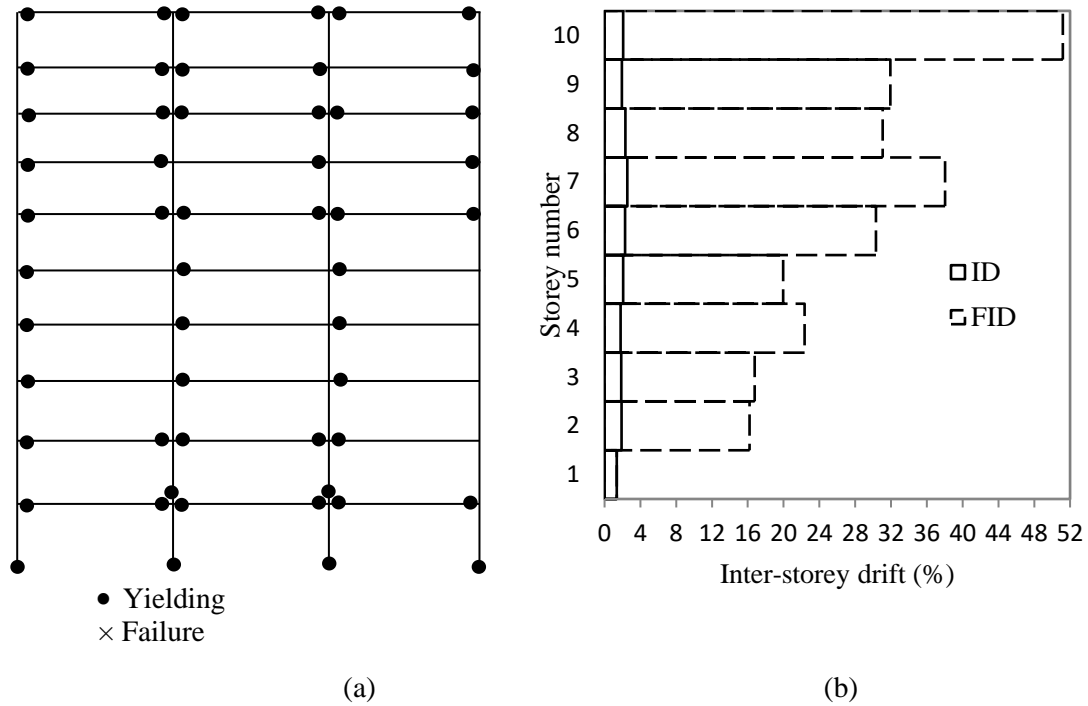


Figure 2. 32: Results of Frame 10 considering horizontal and vertical component of San Fernando earthquake at $Sa(T1) = 0.244g$ (a) Distribution of yielding (b) ID compared with FID limit.

2.8 SUMMARY AND CONCLUSIONS

Local damage of SMRFs cannot be identified using a single value of ID because the storey experiencing the MID is not necessary the severely damaged storey. A simplified method, which is based on pushover analysis, is proposed to calculate the failure inter-storey drifts (FIDs) of SMRFs corresponding to each storey. The method takes into account the rotation of the lower stories, P- Δ effect and the vertical seismic component. The effect of vertical seismic component on the FID limit is incorporated by adding extra vertical loads that can be estimated by multiplying the mass of each floor by the vertical design spectral acceleration. The proposed method was validated using experimental and analytical studies by other researchers. A three- storey and ten- storey SMRFs were considered as case studies

to further validate the method. The FIDs were calculated according to the proposed method while considering or ignoring the effect of the vertical seismic component. Both static and nonlinear dynamic analyses were performed considering five different ground motions. The static and dynamic analyses showed that the predicted limits accurately identified the critical stories of the frames. The proposed method needs to be extended to account for the three-dimensional behaviour of steel buildings.

2.9 REFERENCES

- [1] FEMA 356, Prestandard and commentary for the seismic rehabilitation of buildings, Federal Emergency Management Agency, 2000.
- [2] FEMA 350, Recommended seismic design criteria for new steel moment-frame buildings. Federal Emergency Management Agency, 2000.
- [3] NZS 1170-5, Structural Design Actions Part 5: Earthquake actions - New Zealand. 2004.
- [4] UBC 1997, Uniform Building Code. International Code Council, 1997.
- [5] B. Asgarian, A. Norouzi, P. Alanjari, M. Mirtaheri, Evaluation of seismic performance of moment resisting frames considering vertical component of ground motion, *Adv. Struct. Eng.* 15(8) (2012) 1439-1453.
- [6] G.A. Macrae, D. Fields, J. Mattheis, Ground motion characteristic effects on multistory steel frame response, *Proc. 12th World Conference on Earthquake Engineering*, Auckland, New Zealand, 2000, paper no 1056.
- [7] M.S.R. Labafzadeh, M. Tehranizadeh, Non-linear dynamic behavior of structures due to horizontal near field ground motions. *Proc. 8th U.S. National Conference on Earthquake Engineering*, San Francisco, California, USA, April 18-22, 2006, paper No. 714
- [8] K.H. Abdelkareem, A. Machida, Effects of vertical motion of failure mode and ductility of RC bridge piers, *Proc. 12th World Conference on Earthquake Engineering*, Auckland, New Zealand, 2000, paper no. 0463.
- [9] Eurocode 8. Design of structures for earthquake resistance, Part 1: General rules, seismic actions, and rules for buildings, European Committee for Standardization (CEN), 2004.
- [10] National Earthquake Hazards Reduction Program (NEHRP), Recommended seismic provisions for new buildings and other structures: Part 1, Washington D.C., 2009.
- [11] M.A. Youssef, M.A. Elfeki, Predicting local seismic damage of RC framed buildings considering the horizontal seismic component, *Mag. Concr. Res.* 65(23) (2013) 1411–1428.

- [12] K. Muto, A seismic design analysis of buildings. Maruzen Company Ltd, Tokyo, Japan, 1974.
- [13] T. Paulay, M.J.N. Priestley, Seismic design of reinforced concrete and masonry buildings, John Wiley & Sons, USA, 1992.
- [14] M.A. Elfeki, Seismic performance of steel and shape memory alloy reinforced concrete framed buildings, PhD thesis, Western University, London, Ontario, Canada, 2009.
- [15] SeismoStruct (version 6) - A computer program for static and dynamic nonlinear analysis of framed structures, available online from <http://www.seismosoft.com>
- [16] J. Wan Hu, Smart connection systems: design and seismic analysis, Taylor & Francis, 2015.
- [17] K. Suita, S. Yamada, M. Tada, K. Kasai, Y. Matsuoka, Y. Shimada, Collapse experiment on 4- story steel moment frame Part 2 detail of collapse behavior, 14th World Conference on Earthquake Engineering, Beijing, China; October 12-17, 2008.
- [18] J.F. Hajjar, C.B Gourley, D.P. O'Sullivan, R.T. Leon, Analysis of mid-rise steel frame damaged in Northridge earthquake, J. Perform. Constr. Facil. 12 (4) (1998) 221-231.
- [19] S.E. Kim, D.H. Lee, C. Ngo-Huu, Shaking table tests of a two story unbraced steel frame, J. Constr. Steel Res. 63 (2007) 412-421.
- [20] A. Gupta, H. Krawinkler, Seismic demands for performance evaluation of steel moment resisting frame structures, John A. Blume Earthquake Engineering Center, Department of Civil Engineering, Stanford University, USA, 1999, report No. 132.
- [21] D. Ozhendekci, N. Ozhendekci, Seismic performance of steel special moment resisting frames with different span arrangements. J. Constr. Steel Res. 72 (2012) 51-60.
- [22] PEER ground motion database, Pacific earthquake engineering research center, University of California, Berkeley, USA, 2013, <http://ngawest2.berkeley.edu/>.

CHAPTER 3

SEISMIC PERFORMANCE OF STEEL MOMENT RESISTING FRAMES UTILIZING SUPERELASTIC SHAPE MEMORY ALLOYS

3.1 INTRODUCTION

Structural steel is widely used in moment resisting frames of mid- and high-rise buildings. Modern code provisions categorize buildings according to their configurations, structural systems, materials and construction details [1-3]. A structure is assumed to behave in a ductile manner if it can experience large inelastic deformations without significant degradation in strength. Steel moment resisting frames are one of the popular seismic load resistance systems because of their ductility. During a seismic event, they are expected to experience large inelastic deformations, while maintaining the life safety level for the occupants. Plastic hinges are expected to form in the beams, which may exhibit large yielding deformations leading to localized damage in the floor slabs and columns. Those yielding deformations are not recovered after the seismic event, which results in permanent residual deformations.

Researchers are innovating to find design solutions that minimize the seismic residual deformations. Special post-tensioned partially restrained connections were designed to provide recentering capability after a seismic event [4-6]. Shape memory alloys (SMAs) had also widely attracted the attention of researchers in recent years because of their self-centering capability as well as energy dissipation features. Nickel Titanium (NiTi) SMAs

were the most researched [7]. The two fundamental and characteristic properties of SMA are: shape memory effect (SME) and superelasticity (SE). SME is the ability of the material to recover from large mechanically-induced strains via moderate increase in its temperature. SE is the ability of the material to support relatively high inelastic strains and return to its original shape upon load removal.

Ocel et al. [8] tested an external beam-column connection that utilized martensite SMA rods. The connection showed high energy dissipation, large ductility and no strength degradation up to 4% drift level. The connection was also able to recover 76% of the experienced drift when the SMA tendons were heated. Ma et al. [9] investigated the behaviour of extended end-plate connections consisting of long shank Nitinol superelastic SMA bolts, continuity plates, beam flange ribs and web stiffeners using a 3D finite element model. The connections experienced cyclic elongations of the SMA bolts, however the traditional beam local buckling was avoided. The deformations of the SMA bolts were recoverable upon unloading. Ma and Yam [10] conducted a quasi-static test of an extended end-plate connection utilizing long shank SMA bolts. The connection exhibited high deformation capacity with maximum inter-storey drift (MID) angle beyond 0.02 rad. Sepúlveda et al. [11] tested a connection that utilized 3 mm-diameter copper-based (CuAlBe) SMA bars. The proposed connection experienced self-centering behaviour, dissipated moderate amount of energy, and showed no strength degradation up to 3% drift ratio. Speicher et al. [12] tested four half-scale interior beam-column connections that utilized steel tendons, superelastic NiTi SMA tendons, martensitic NiTi SMA tendon, or combination of superelastic NiTi tendons and aluminum tendons. The superelastic NiTi SMA connection showed significant recentering capability, recovering a large portion of

the post-elastic drift compared to the other three connections. DesRoches et al. [13] studied the seismic performance of steel moment resisting frames with SMA bars at the beam to column connections. Two steel frames were selected: low rise (three-storey) frame and medium rise (nine-storey) frame. All the beam-column connections were assumed to utilize SMA bars. Nonlinear time history analyses showed that martensitic SMA connections are most effective in controlling MID demands whereas superelastic SMA connections are more effective in controlling maximum residual inter-storey drift (MRID) demands. Further, probabilistic seismic demand assessment (PSDA) was performed by Ellingwood et al. [14]. The hazard curves showed that the benefits of incorporating SMA connections depend on the seismic demand level. Researchers had also investigated the seismic performance of steel and RC frames equipped with SMA braces [15-17]. The conventional steel bracing system has limited ductility and energy dissipation due to buckling of the braces, and their asymmetric behavior [18]. McCormic et al. [17] assessed the performance of steel braced frames equipped with superelastic SMA braces. The MRID was limited following an earthquake due to the recentering capability of the braces. Kari et al. [19] conducted a numerical study to investigate the benefit of using combination of buckling restrained braces and SMA braces for new designs as well as retrofitting purposes. Results revealed that, with the proper configuration, residual and inter-storey drifts can be minimized. Antonio et al. [20] conducted shake table tests to assess the effectiveness of seven different passive and semi-active energy dissipating braces (EDBs). It was concluded that EDBs consisting of both SMA and visco-elastic damping material lead to recentering of the gravity load resisting system at the end of a seismic event with the added advantage of higher energy dissipation because of the visco-elastic material. Miller [21] investigated

the seismic behavior and performance of self-centering buckling-restrained braces (SC-BRBs) that utilized SMAs. The SC-BRBs consisted of a typical BRB component, which provides energy dissipation, and pre-tensioned superelastic NiTi SMA rods, which provide self-centering. The SMA rods were attached to the BRB portion of the brace using a set of concentric tubes and free-floating anchorage plates that caused the SMA rods to elongate when the brace is either in tension and compression. Two half-scale SC-BRB specimens were fabricated and subjected to quasi static cyclic loading. The specimens exhibited a stable, flag-shaped hysteretic response. The study concluded that proper SMA pretension force and BRB core yield force are imperative to achieve full self-centering of the bracing.

As SMAs are very expensive, studies are required to optimize their use in the steel frames. Although the literature provides few research data on using SMA in steel beam-column connections and bracing elements of steel frames, further research is necessary regarding their minimum use. This study examines the possibility of maintaining the benefit of reduced residual inter-storey drift (RID) using SMA connections at selected parts of the frame and, thus, reducing the associated costs. The objective of this paper is to identify the required locations of the SMA connections in a typical steel moment resisting frame to optimize its seismic performance in terms of inter-storey drift, residual deformations and damage scheme.

The paper starts by providing details about the examined steel frame and the modeling assumptions. The simplified method proposed by Sultana and Youssef [22] as well as incremental dynamic analysis (IDA) were then used to identify the floors that are expected to experience sever damage during seismic excitations. The frame was redesigned to incorporate SMA in the critical joints. Six different potential designs were examined using

nonlinear dynamic analyses. Their seismic performance as compared to the steel frame allowed selecting the frame that has the best seismic performance in terms of maximum inter-storey drift (MID), maximum residual inter-storey drift (MRID) and damage distribution.

3.2 STEEL MOMENT FRAME CHARACTERISTICS AND MODELING

A ten storey building is selected as a case study. The frame (Figure 3.1) is designed by Ozhendekci and Ozhendekci [23] according to Turkish standards, which is similar to AISC 316-89 [24]. As the structure is symmetric, a two-dimensional (2D) model of the steel moment resisting frame (SMRF) is developed using the software SeismoStruct [25]. This software is based on the fibre element approach. Beams and columns are divided into four and two displacement based inelastic frame elements, respectively. The distributed dead and live loads are converted to equivalent point loads and applied at the two end nodes of each beam element. The mass of the building is converted into lumped masses that are assumed to be located at the two ends of each beam element. The panel zone is modeled using rigid elements. Bilinear material behaviour with 3% strain hardening is considered using the distributed plasticity approach. The P- Δ effect is included in the analysis. Validation of this modeling technique was conducted by Sultana and Youssef [22]. Local failure of beams and columns are assumed to be associated with an ultimate chord rotation (θ_u) [26].

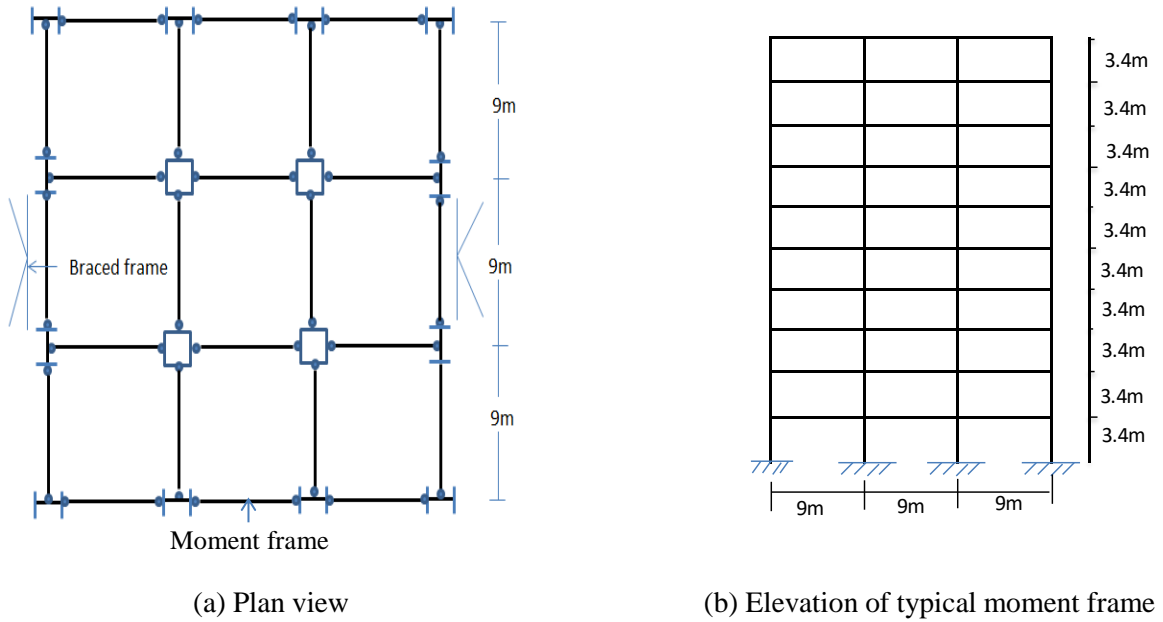


Figure 3. 1: 10-storey building [23]

3.3 PREDICTION OF THE SEVERELY DAMAGED FLOOR

Sultana and Youssef [22] proposed a simplified method to identify the critical storey of a SMRF based on pushover analysis. The method allows evaluating the failure inter-storey drift (FID) limits for each storey. These limits for the considered ten storey SMRF are given in the Table 3.1. The first storey is clearly the severely damaged storey as the limiting ID (2.38%) of this storey is the lowest followed by the 5th storey (27.7%).

Table 3. 1: Limiting FID (%) for different floors of the 10 storey frame

Storey	1	2	3	4	5	6	7	8	9	10
Proposed FID (%)	2.38	31.1	28.6	29.4	27.7	30.7	37.9	29.9	31.2	50.6

3.4 DYNAMIC ANALYSIS OF THE SMRF

Eigen value analysis was performed to determine the natural period of vibrations and mode shapes. The first and second fundamental horizontal periods of vibrations are 2.21 sec. and 0.78 sec., respectively. The behaviour of this frame was dominated mainly by the first mode with some sensitivity to higher modes.

Incremental dynamic analysis (IDA), developed by Luco and Cornell [27], was performed to assess the seismic performance of the frame, and, thus identify the location of the severely damaged beams and columns. This analysis requires a series of nonlinear dynamic analyses considering different intensity levels for the ground motion to cover the behaviour of the frame during the elastic, yielding, and collapse or dynamic instability stages. Five different ground motions, obtained from PEER ground motion database [28], were selected to conduct the IDA. Characteristics of the selected ground motions are listed in Table 3.2. Figure 3.2 shows the elastic response spectra for 5% damping of these selected ground motions. IDA analysis was terminated when one of the columns reaches the limiting rotation proposed by FEMA356.

Table 3.3 shows the 5% damped spectral acceleration at collapse at the structure's first mode period [$S_a(T1,5\%)$], MID and MRID of the steel frame considering the five ground motions. Values of the MID varied from 2.75% to 5.02% and the MRID varied from 0.29% to 1.21%. The damage schemes at collapse are shown in the Figure 3.3.

Table 3. 2: Characteristics of ground motions

Earthquake	Date m/d/yr	Ms magnitude	Station	PGA(g)
Northridge	01/17/1994	6.7	Arleta-Nordhoff	0.344
Imperial Valley	10/ 15/ 1979	6.9	El Centro Array #6	0.439
Loma Prieta	10/ 18/1989	7.1	Capitola	0.529
Tabas	09/16/1978	6.9	Tabas	0.852
San Fernando	02/02/1971	6.6	Pacoima dam	1.23

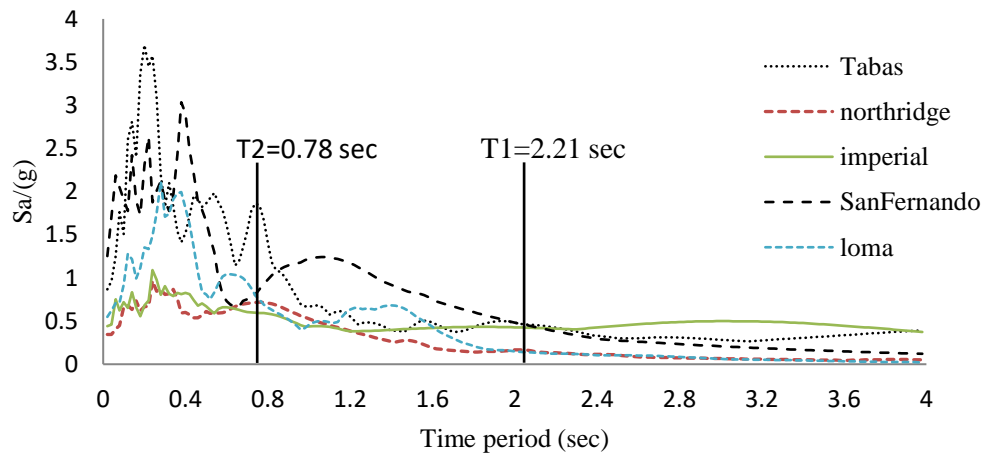


Figure 3. 2: Elastic response spectral acceleration for horizontal seismic component

Table 3. 3: MID and MRID of steel frame (Frame 1)

Ground motion	Sa(T1,5%) at collapse	Frame 1	
		MID (%)	MRID (%)
Imperial	(0.341g)	2.97 (2 nd storey)	0.67 (2 nd floor)
Northridge	(0.489g)	3.17 (3 rd storey)	0.41 (1 st floor)
Loma	(0.619g)	5.02 (7 th storey)	0.56 (8 th storey)
San Fernando	(0.476g)	3.48 (6 th storey)	1.21 (4 th storey)
Tabas	(0.445g)	2.75 (3 rd storey)	0.29 (2 nd storey)

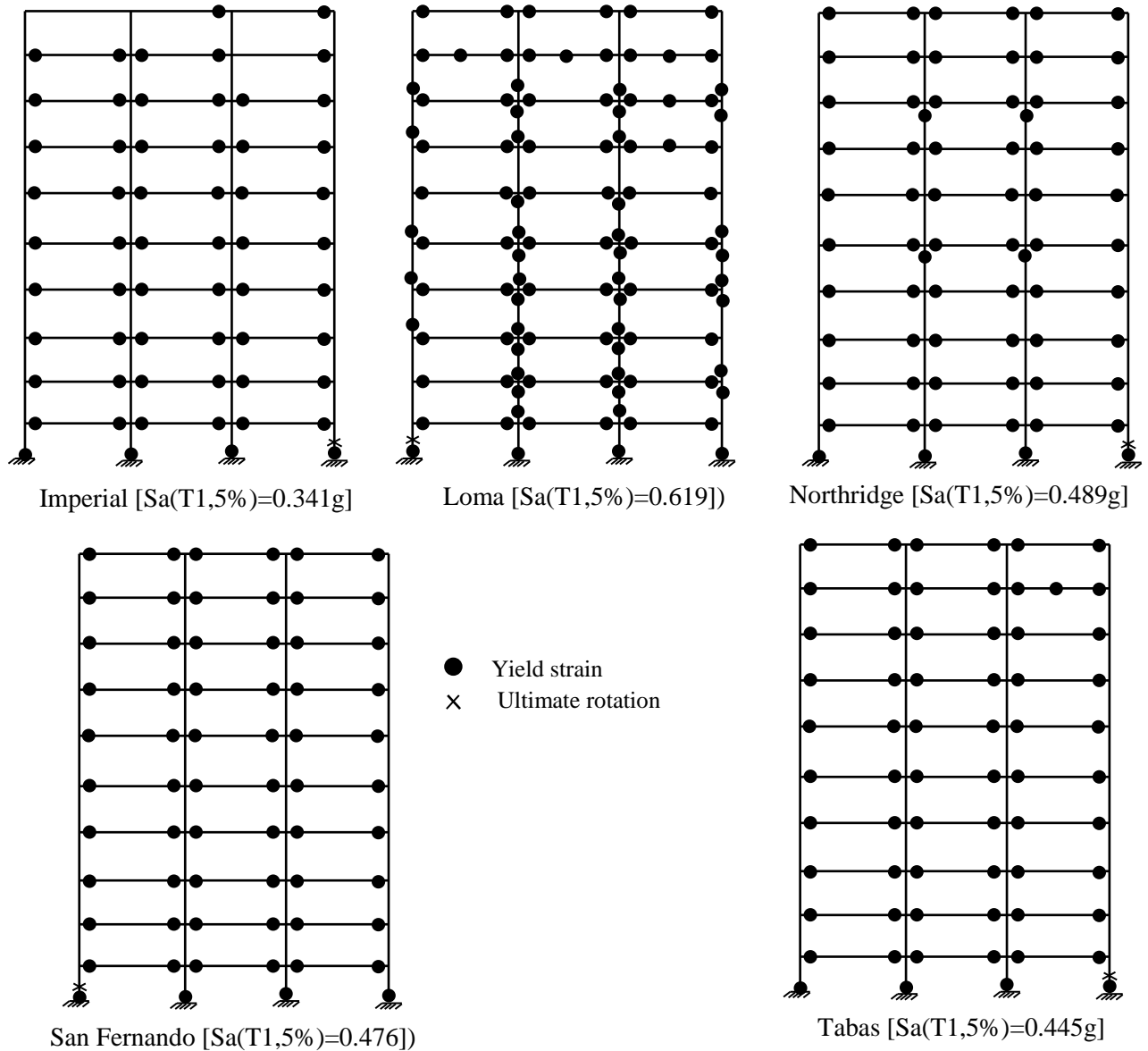


Figure 3. 3: Damage distribution of the steel frame (Frame 1)

The columns and majority of the beams of the first floor have yielded considering all ground motions. Loma earthquake has also resulted in yielding of the columns at other floors. Yielding can also be observed at mid-spans of the 7th, 8th, and 9th floor beams. For all of the considered seismic excitations, one of the first floor columns has reached the

ultimate rotation, which is considered as frame failure in this paper. The MID and MRID have not occurred at the first floor although it is the most damaged floor. The ID of the first floor varied from 1.90% to 2.17 % for the considered ground motions.

3.5 SMA- STEEL FRAME CHARACTERISTICS AND MODELING

The analyzed SMRF was redesigned using combination of rigid and SMA connections. According to the simplified method the columns of the 1st and the 5th storeys can be considered critical as the FID limits are the lowest, which suggests that potential locations for SMA joints are in the 1st, 4th, and 5th stories. The damage distributions obtained from dynamic analyses showed failure of a 1st storey column along with yielding of the columns in the 4th-6th and 8th-9th stories as well as severe yielding of the beams in the 9th storey. Based on the above observations, the six different designs, shown in Figure 3.4, were selected to capture potential locations for SMA connections. The SMA connections were assumed to have similar details as the joint tested by Speicher et al. [12]. In the design phase, the moment capacity of the SMA connections were set equal to 80% of the plastic moment capacity of the connecting beams to force inelastic deformations to occur in the SMA bars. The area of the SMA bars (A_{SMA}) is, thus, calculated using equation 3.1.

$$A_{SMA} = 0.8M_{pb}/dF_{Y(SMA)} \quad (3.1)$$

Where, M_{pb} is the plastic moment capacity of the connecting beam, d is the distance between the top and the bottom SMA bars, and $F_{Y(SMA)}$ is the stress at which SMA state changes from the austenite to stress-induced martensite.

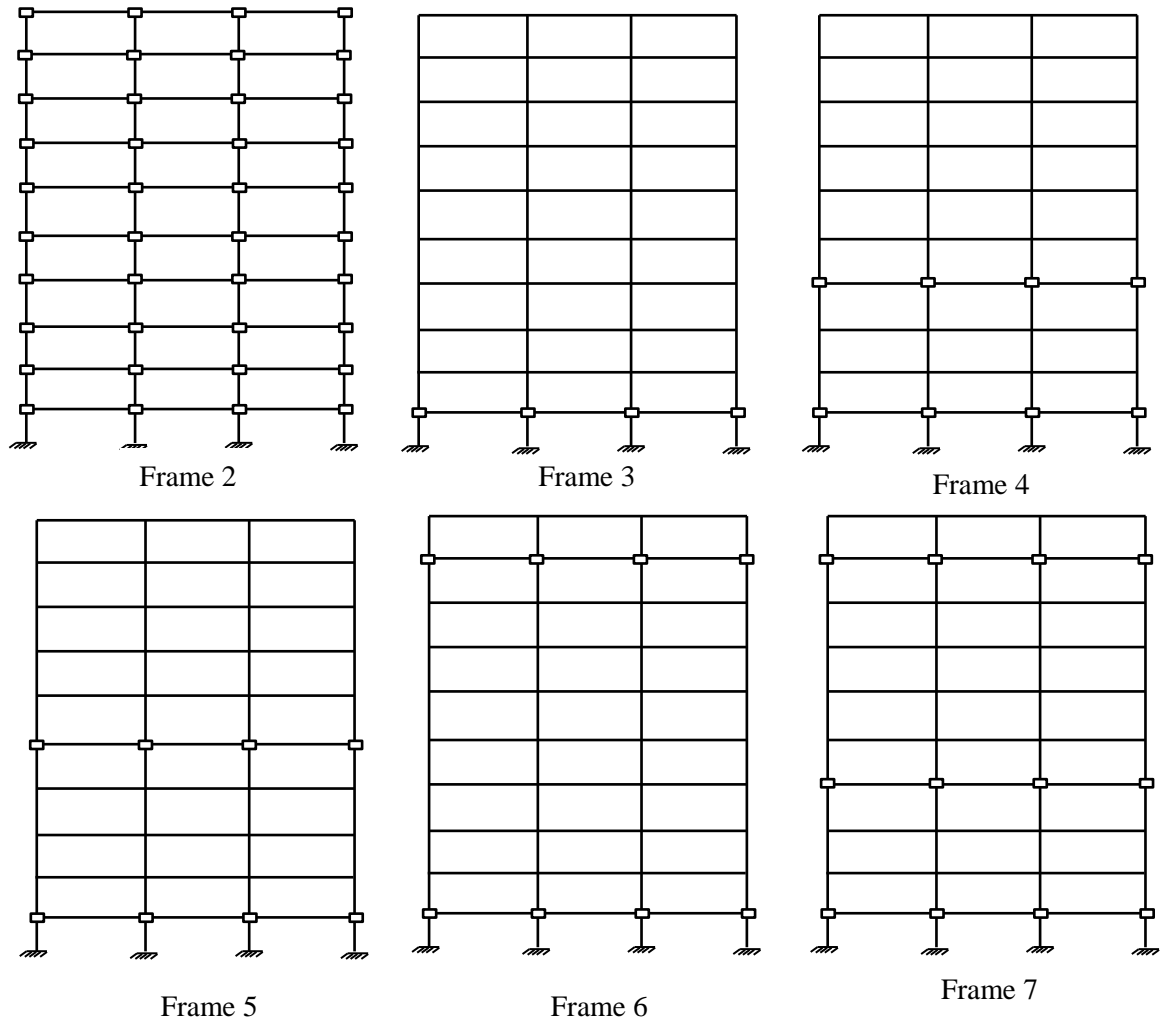


Figure 3. 4: Location of SMA connections

3.5.1 SMA connections

Two different SMA connections were modeled in SeismoStruct to validate the modeling technique. Figure 3.5 shows the FE model of the SMA connection that was tested by Speicher et al. [12]. The slotted shear tab allows for the relative rotation between the beam and the column. A special modeling technique was utilized to model this connection that involves: (1) modeling the SMA bars using inelastic truss elements, (2) capturing the

superelastic behaviour using the uniaxial material model that follows the constitutive relationship proposed by Auricchio and Sacco [29], (3) modeling the beams and columns using displacement based inelastic frame elements, and (4) allowing for relative rotation between the beam and column elements using hinges that were modelled using zero length link elements, as shown in the Figure 3.5(b). A martensite SMA connection, which was tested by Ocel et al. [8], was also modeled. A different modeling technique was utilized for this connection, where the SMA bars were modelled using zero length link elements as shown in Figure 3.6. The force-displacement response curves for those link elements were derived from the stress-strain behaviour of the SMA material. Good agreements between the experimental and simulated moment-rotation responses were achieved for both connections as shown in Figures 3.7 and 3.8. The proposed connection models were found to be capable of predicting the moment-rotation responses, energy dissipation, and residual deformations with adequate accuracy.

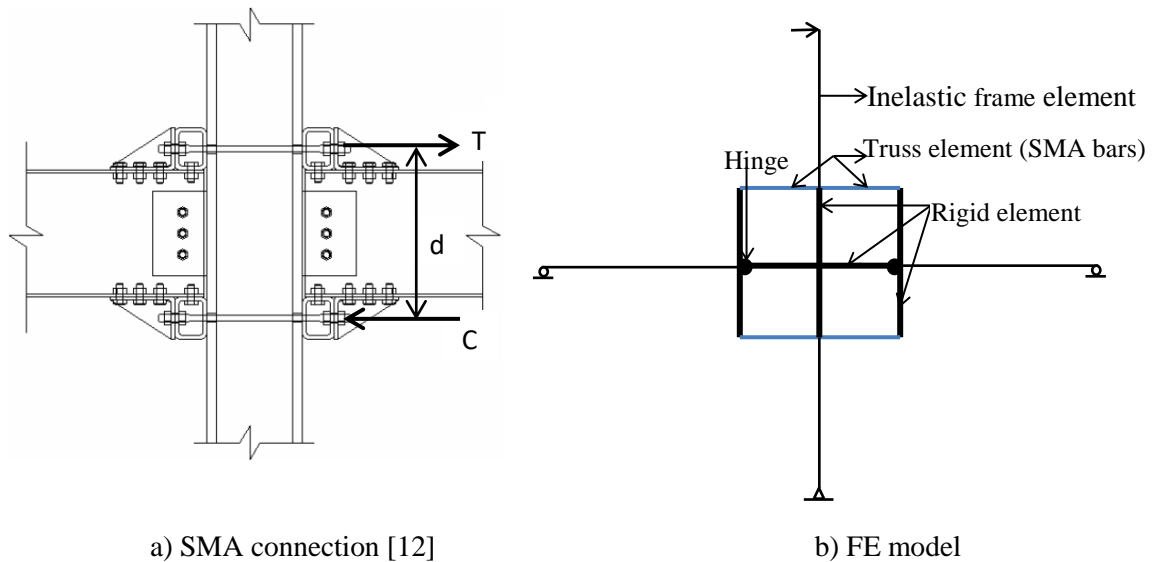
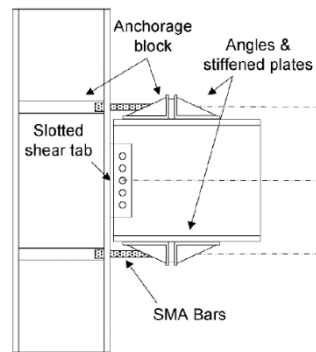
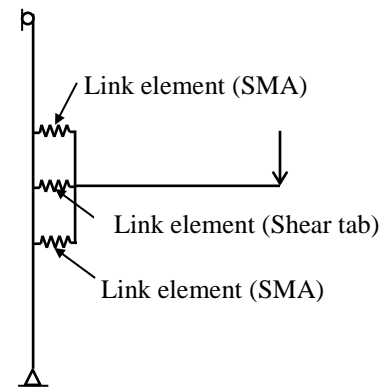


Figure 3. 5: Location of SMA connections

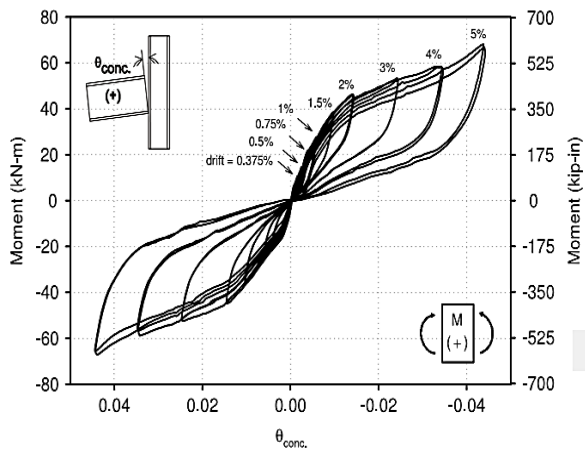


a) SMA connection [8]

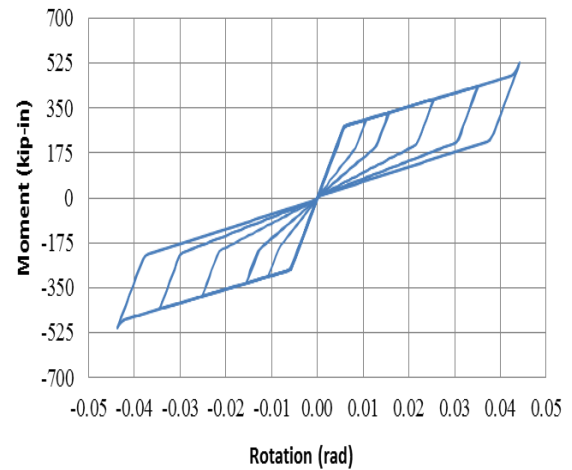


b) FE model

Figure 3. 6: Finite element model of martensite SMA connection



a) Experimental moment-rotation [12]



b) FE moment-rotation

Figure 3. 7: Experimental and simulated moment rotation behaviour of the superelastic SMA connection

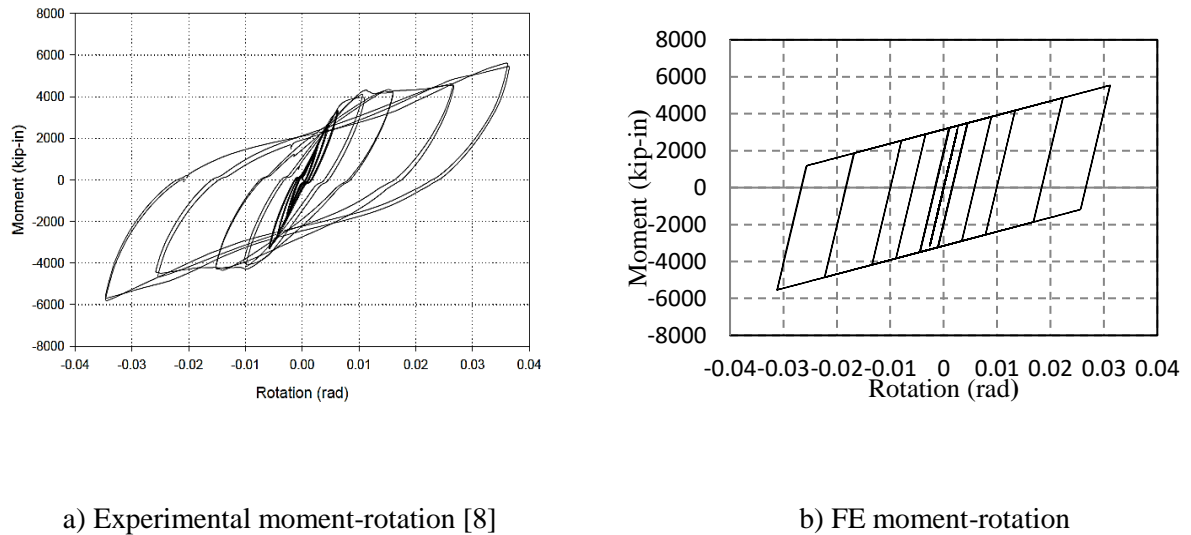


Figure 3. 8: Experimental and simulated moment rotation behaviour of martensite SMA connection

3.6 DYNAMIC ANALYSIS OF SMA-STEEL FRAMES

Eigen value analyses of the frames were first performed. Table 3.4 shows the natural periods of the frames. The location and number of SMA connections influenced the period. The first period of vibrations of the SMA frames increased by 1.8% to 26.2% as compared to the steel frame. Dynamic analyses of the SMA frames were then conducted considering the five selected earthquakes scaled to the intensity causing collapse of the steel frame (Frame 1).

The MIDs of the different frames are compared in Figure 3.9a. Frame 2 has the highest MID (3.48% to 6.48%). All of the other frames have relatively similar values (2.93% to 5.44%). Table 3.5 shows the percentage change of MID and MRID as compared with

Frame 1. The maximum increase in MID (reaching 110%), which was observed in Frame 2, signifies that using SMA in all of the frame connections is a solution that should be avoided. This increase in MID is related to the lower modulus of elasticity of the SMA as compared to steel. The minimum increase in MID was observed in Frame 6 (0.6%).

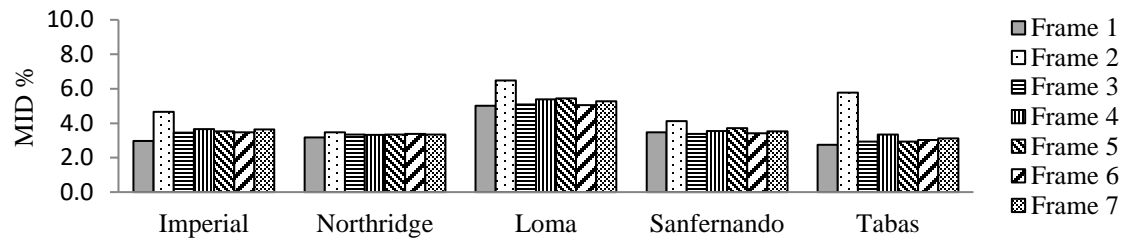
The MRID values of different frames are compared in Figure 3.9(b). The highest reduction of the MRID occurs in Frame 2 for four out of the five considered ground motions (up to 90%). For the fifth ground motion, the MRID increases as compared to Frame 1, which categorize the seismic behaviour of Frame 2 to below that of Frame 1. Although the same numbers of SMA connections were used in Frames 4, 5 and 6, Frame 4 shows better performance in terms of MRID as shown in the Table 3.5. The location of the SMA connections has significantly influenced the location of the storey experiencing the MID and MRID because the SMA connections have resulted in redistributing the seismic forces in the frame. The ID and RID distributions due to imperial earthquake (Figure 3.10) are discussed in the following paragraph. The remaining ID and RID distributions are given in Appendix A. The use of SMA connections has significantly reduced the RID for the first three floors of Frames 3 and 6. However, RID values for the remaining stories were not reduced. In case of Frames 4 and 5, the SMA connections have minimized the RID in all floors.

Table 3. 4: Natural time period of different frames (Seconds)

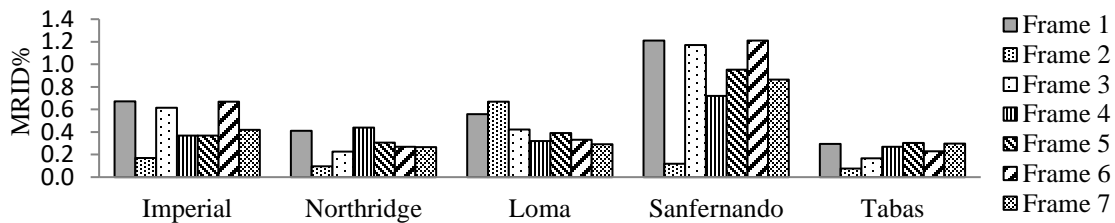
Time period	Frame 1	Frame 2	Frame 3	Frame 4	Frame 5	Frame 6	Frame 7
T1	2.21	2.79	2.25	2.34	2.32	2.27	2.33
T2	0.78	0.94	0.79	0.79	0.80	0.81	0.81

Table 3. 5: Percentage change of MID and MRID of SMA frames

	Imperial		Northridge		Loma		San Fernando		Tabas	
	MID % change	MRID % change	MID % change	MRID % change	MID % change	MRID % change	MID % change	MRID % change	MID % change	MRID % change
Frame 2	56.9	-74.7	9.78	-76.4	29.1	19.5	18.4	-90.3	110	-74.4
Frame 3	16.5	-8.77	5.27	-44.6	1.31	-24.7	-3.16	-3.31	6.55	-43.2
Frame 4	23.1	-45.3	4.73	7.07	7.17	-42.9	2.01	-40.50	21.8	-8.50
Frame 5	18.5	-45.3	5.14	-25.4	8.43	-30.2	6.90	-21.24	6.91	3.06
Frame 6	16.8	-0.590	6.62	-34.2	0.60	-40.7	-2.01	0.00	9.93	-21.8
Frame 7	22.2	-37.8	5.50	-35.1	4.96	-47.6	1.28	-28.52	13.7	1.61



a) MID of different frames



b) MRID of different frames

Figure 3. 9: Comparison of MID and MRID of different frames

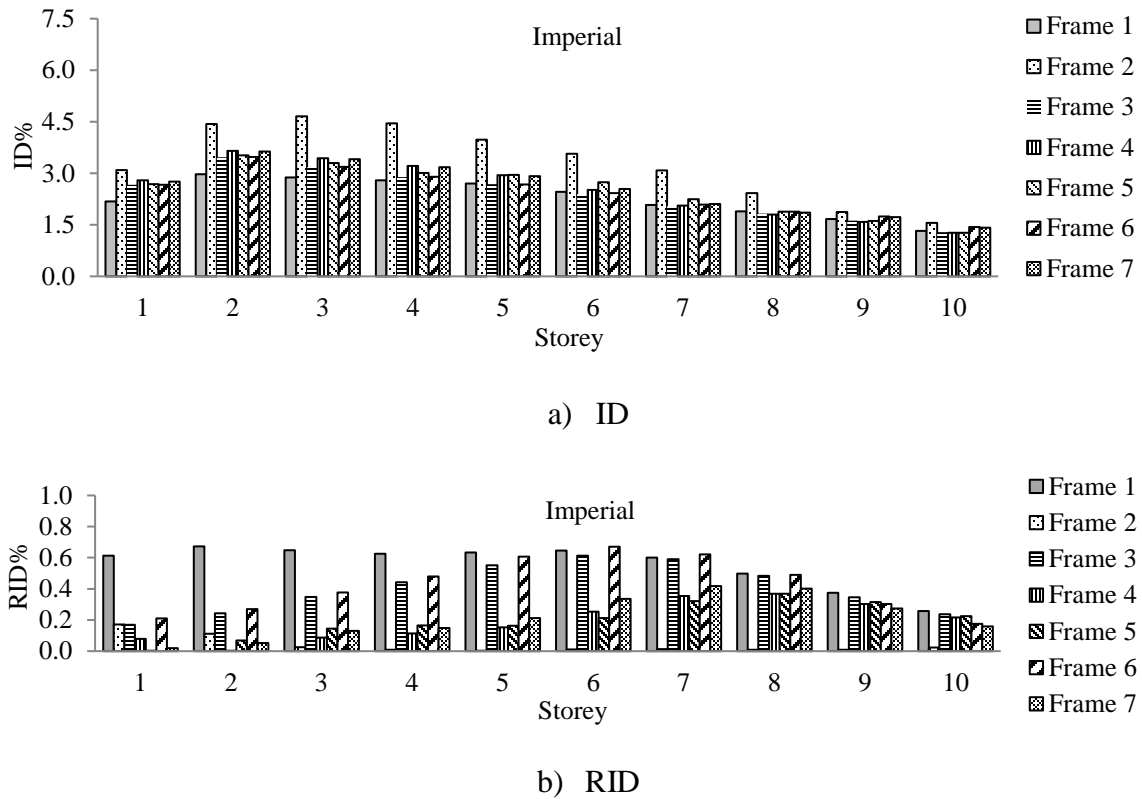


Figure 3. 10: Imperial earthquake [$S_a(T_{1,5\%})=0.341g$]

The damage schemes of the six SMA frames are presented in Figures 3.11 to 3.16. Yielding is observed at the ends of almost all of the beams for the selected records. Yielding also observed at the mid-span of the beams of top floors in case of Loma record.

The damage scheme of Frame 2 (Figure 3.11) shows that the first and the second storey columns yielded in cases of Imperial record, only the first storey columns yielded due to San Fernando records. Yielding of columns of other stories also observed due to Loma, Northridge and Tabas records. For Northridge and San Fernando records, Frame 2 has not reached failure. The worst damage distribution was observed due to Imperial, Loma and Tabas earthquakes as three or four columns failed, respectively.

In case of Frame 3, the first floor columns yielded due to Imperial, Northridge, San Fernando, and Tabas earthquakes (Figure 3.12). In case of Loma record, yielding of the columns was observed at multiple storeys and two of the 1st storey columns failed. Three columns of the 1st storey failed due to imperial record, two columns failed due to Northridge records, and one column failed due to San Fernando and Tabas records.

Using SMA connections at both the 1st and the 4th floor (Frame 4) reduces the yielding of the beams at these floors as shown in Figure 3.13. Yielding is only observed in the first floor columns due to imperial and Tabas earthquakes. Column yielding is also observed at 5th and 8th stories considering Northridge record, 8th storey considering San Fernando record and almost all storeys considering Loma record. Three and two columns of the 1st floor failed due to imperial and Loma records, respectively, whereas only one column failed due to Northridge, San Fernando and Tabas records.

The damage schemes for Frame 5 (Figure 3.14), using SMA connections at the 1st and 5th storey show that three columns of 1st floor failed due to Imperial and Northridge records whereas only one column failed due to Loma, San Fernando and Tabas records.

Although the same number of SMA connections is used in Frames 4, 5 and 6, Frame 6 is severely damaged compared with others as shown in the Figure 3.15. All columns of the first storey failed considering Loma earthquake, whereas three of the first storey columns failed due to imperial, Northridge, and San Fernando earthquakes.

The damage schemes of Frame 7 (Figure 3.16), using SMA connections at 1st, 4th and 9th storeys, shows that the first storey is severely damaged due to imperial and San Fernando records as three columns failed.

From the above discussions about drift values and damage schemes, it is clear that Frame 4 shows the best seismic performance as it has the best damage scheme, a minor increase in MID demands and high reduction of MRID compared with the other SMA-steel frames. The performance of Frame 4 as compared with the steel rigid frame (Frame 1) can be summarized in terms of MID and MRID. The average MID (3.85%) of Frame 4 increases by only 10.7%, whereas the average MRID (0.42%) decreases by 32%. The first storey of both frames was severely damaged.

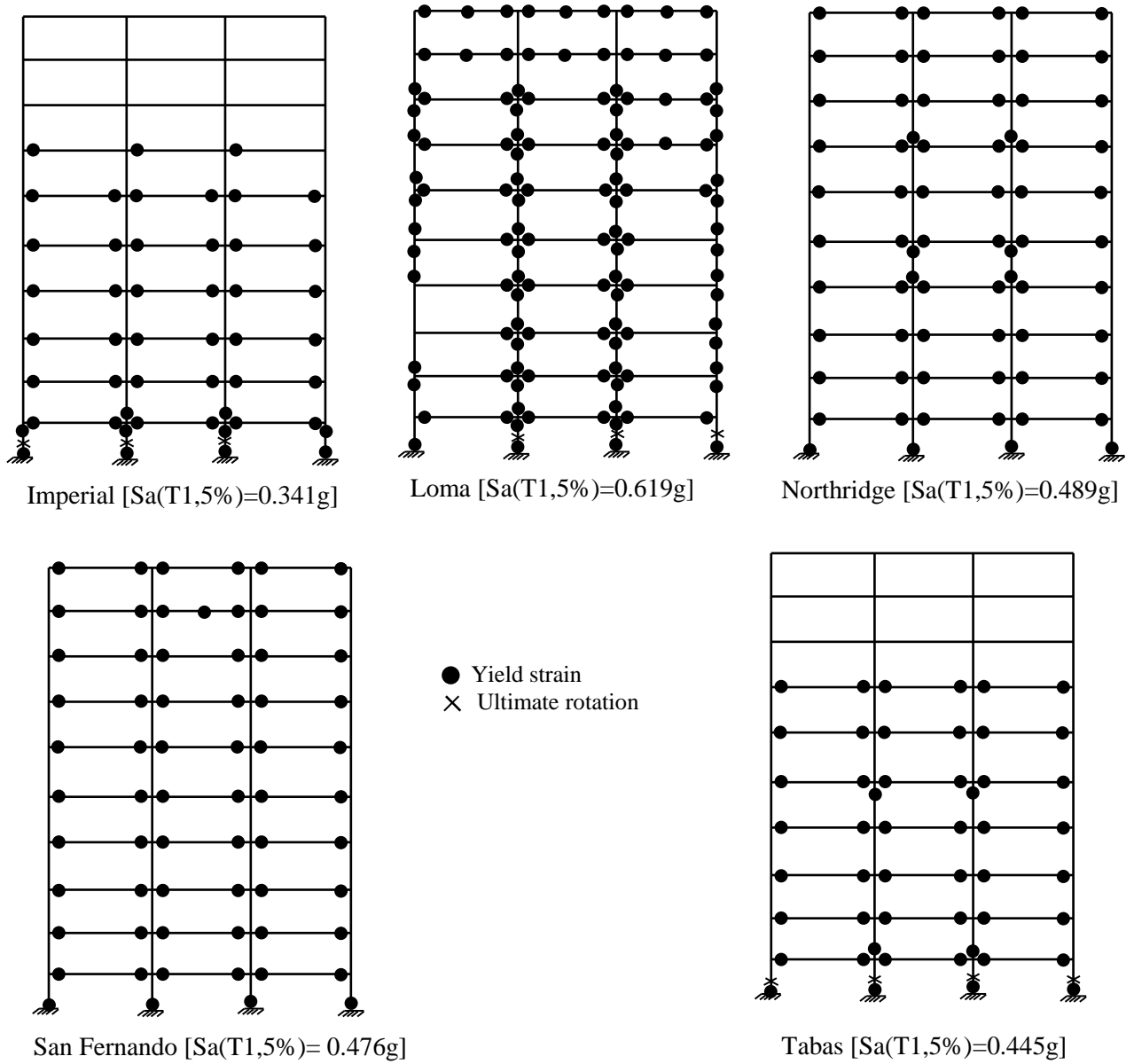


Figure 3. 11: Damage distribution of the Frame 2

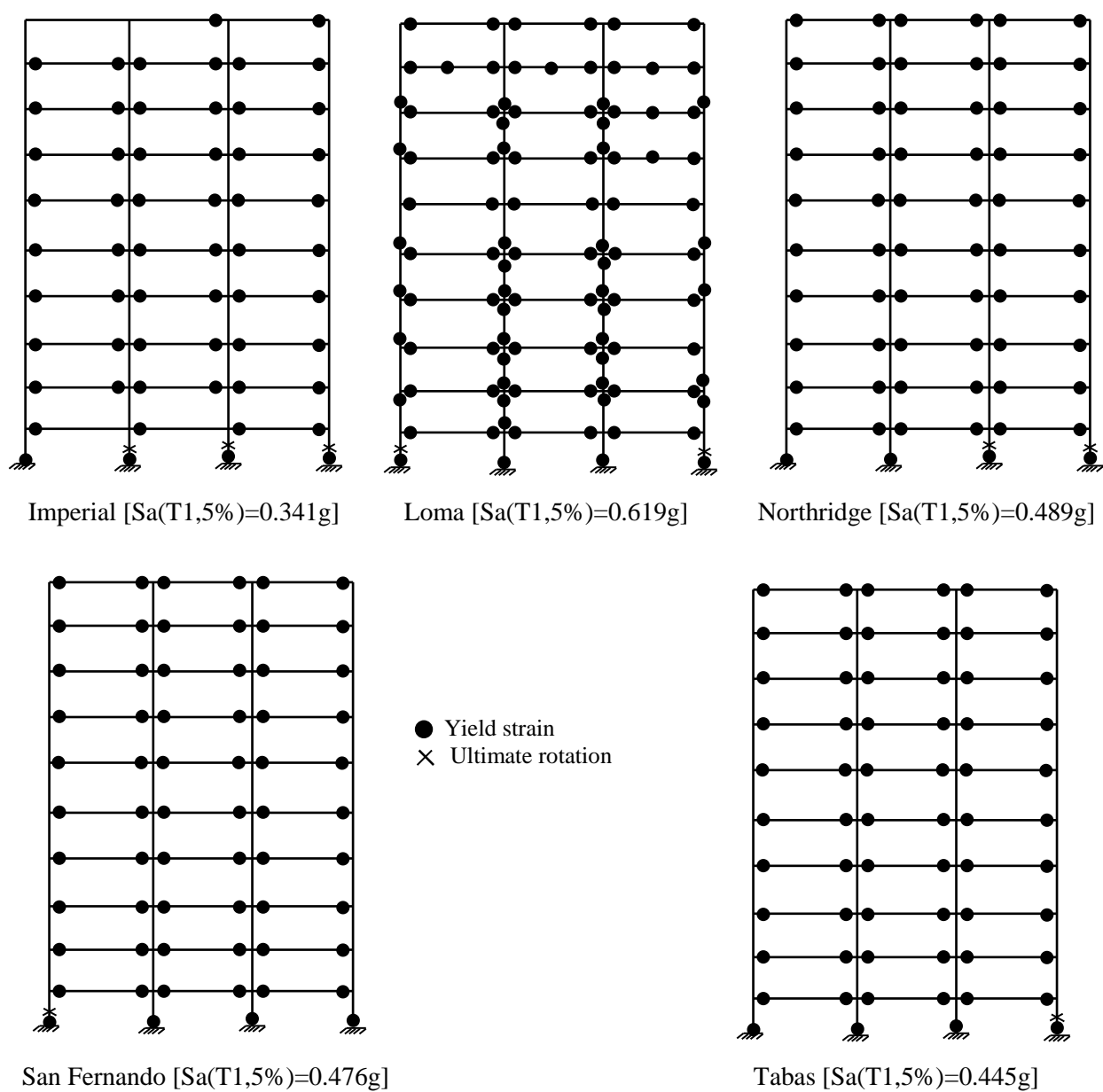


Figure 3. 12: Damage distribution of the Frame 3

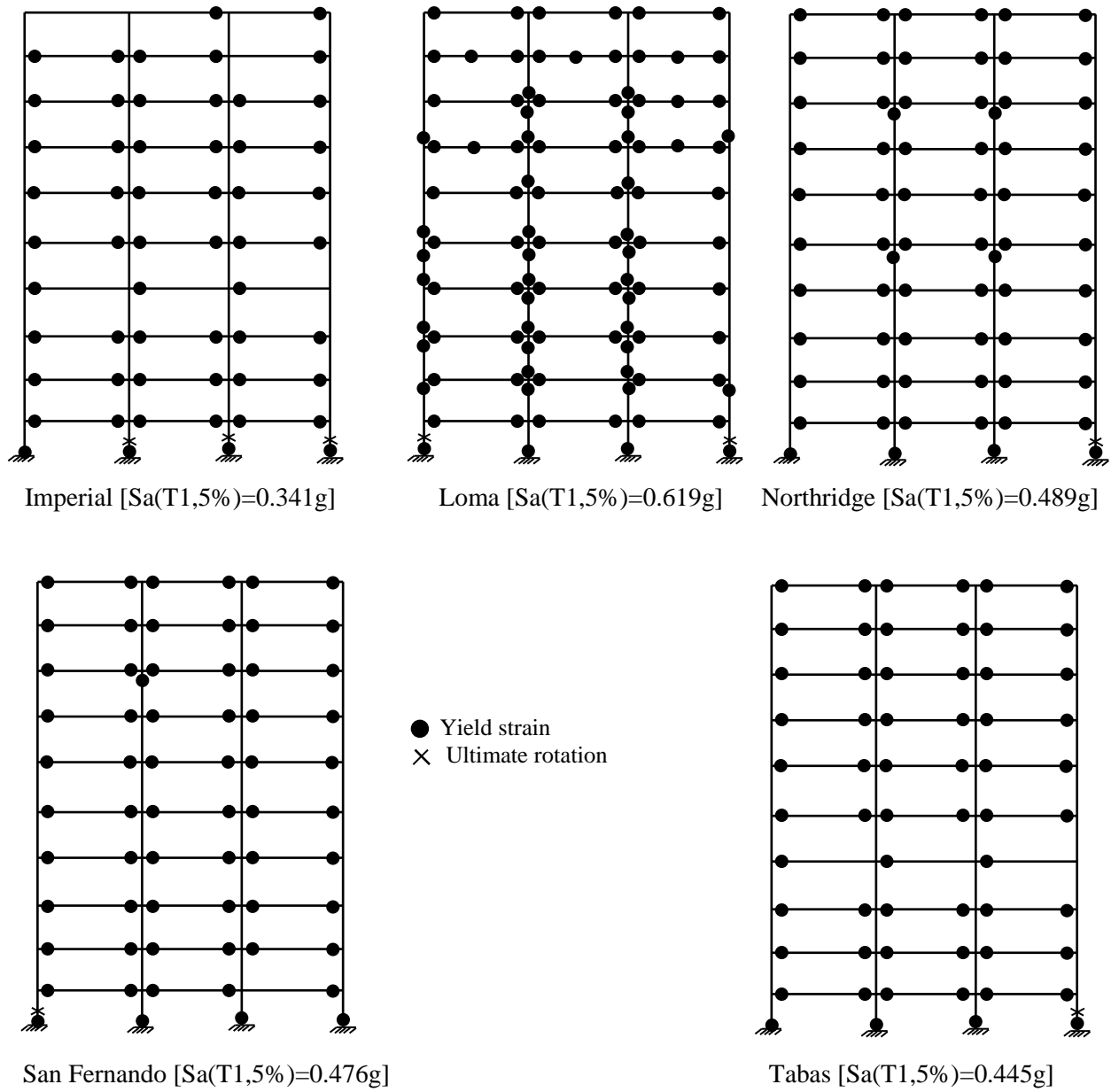


Figure 3. 13: Damage distribution of the Frame 4

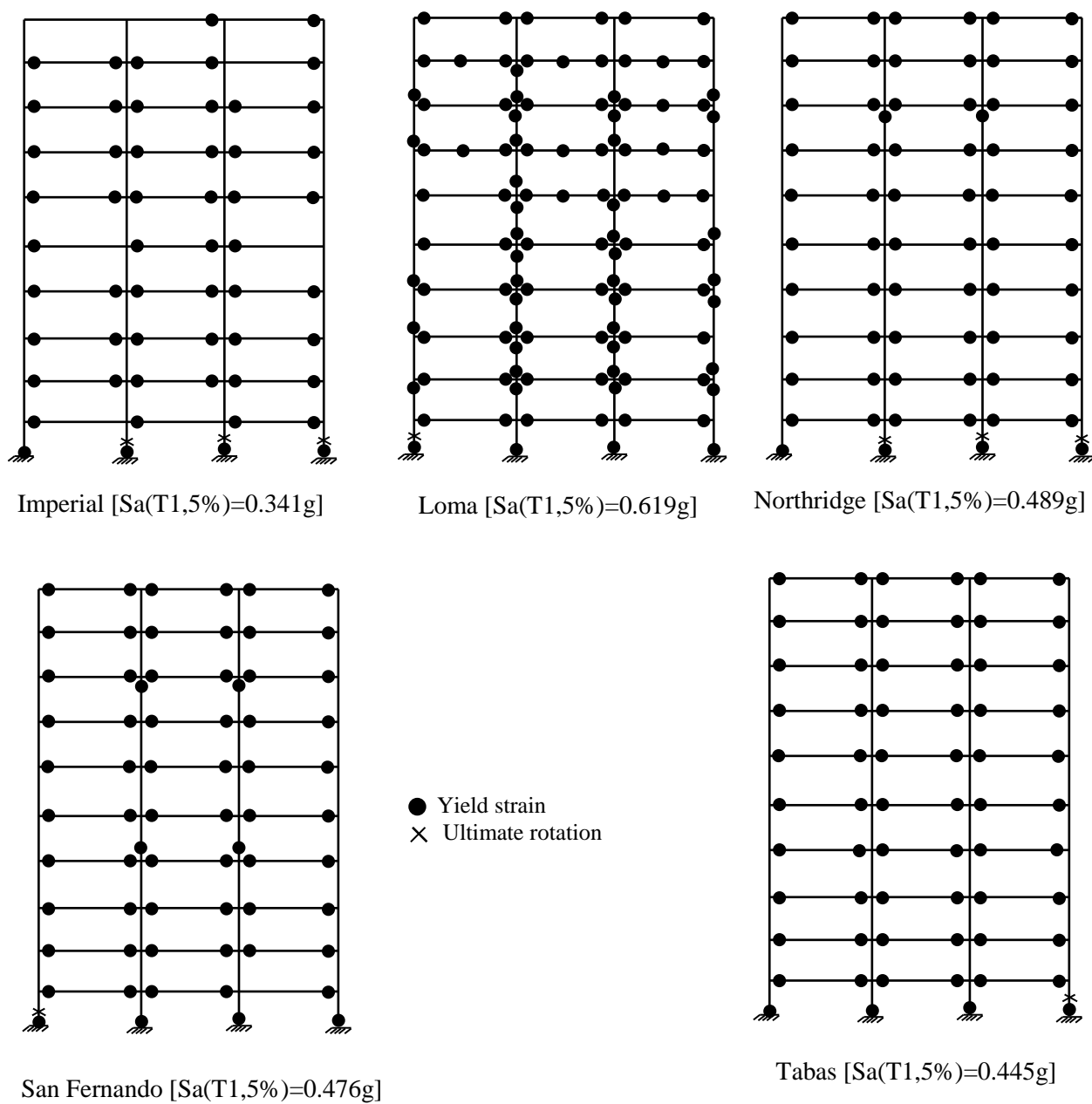


Figure 3. 14: Damage distribution of the Frame 5

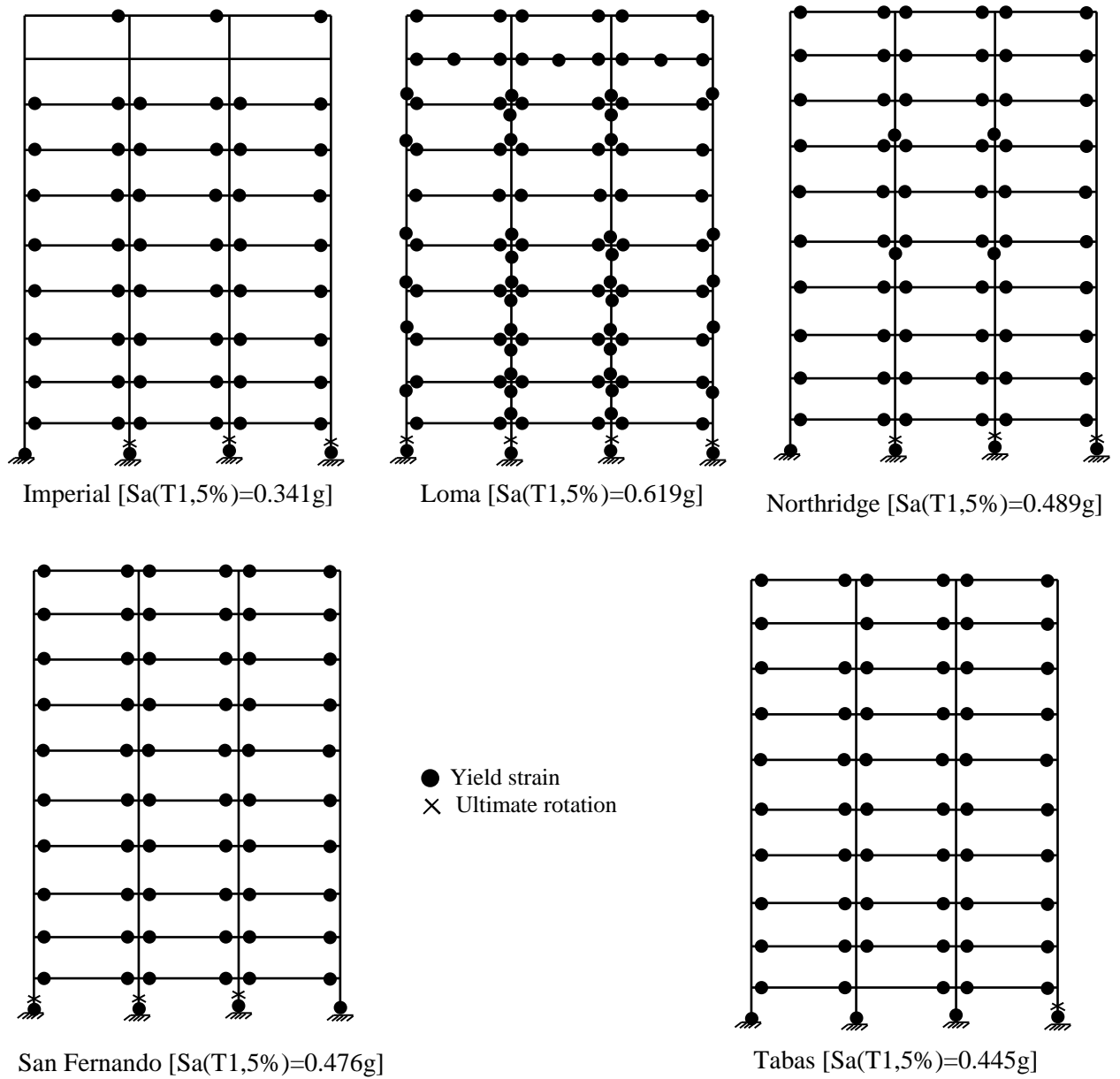


Figure 3. 15: Damage distribution of the Frame 6

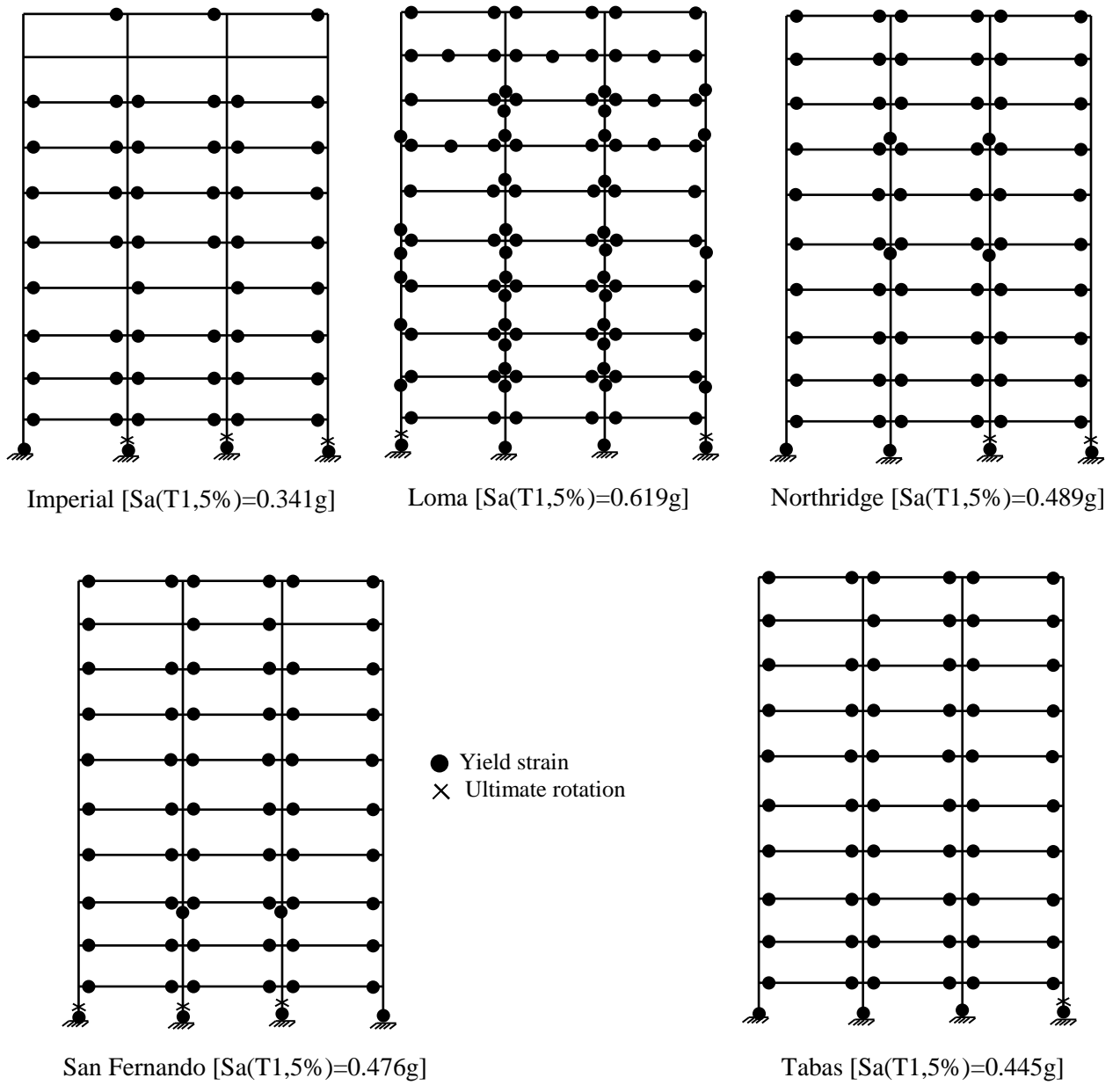


Figure 3. 16: Damage distribution of the Frame 7

3.7 CONCLUSION

The seismic performance of SMRFs using SMA connections at certain locations is investigated in this paper in terms of MID, MRID and damage scheme. The modeling technique of SMA connections is validated using the experimental results available in literature. A ten-storey building is considered as a case study. IDA analysis is conducted using five different ground motions scaled to different S_a levels up to collapse. After that rigid connections are replaced by the SMA connections. Nonlinear dynamic analyses of six different SMA frames are conducted using the same records scaled to the predefined S_a level that caused collapse of the steel frame. The seismic performance of the steel frame is compared with the SMA frames in terms of MID, MRID and damage schemes.

- The MID is influenced by the number of SMA connections used whereas the MRID is affected by the location of the SMA connections.
- Replacing all the rigid connections by SMA connections significantly increased MID (up to 110%), and, thus the frame was severely damaged for three records compared with the steel frame.
- Among all SMA frames, Frame 4 (using SMA connections at the critical first floor and fourth floor) showed very good seismic performance compared with the steel frames in terms of MID, MRID and damage schemes. The MID increased by 23% and the MRID reduced by 45%.
- Using SMA connections at the joints located at the top and/or bottom of the critical columns identified by the simplified method will lead to the best seismic performance.

- The seismic performance of the SMRFs can be improved by using SMA connections at chosen locations, which will lead to minor increase in MID, high reduction in MRID, and lower level of damage distribution.

3.8 REFERENCES

- [1] CAN/CSA-S16-09, Design of Steel Structures, Canadian Standard Association, 2009.
- [2] AISC 341-02, Seismic Provisions for Structural Steel Buildings, American Institute of Steel Construction, 2002.
- [3] FEMA 350, Recommended Seismic Design Criteria for New Steel Moment-Frame Buildings Federal Emergency Management Agency 2000.
- [4] J.M. Ricles, R. Sause, M.M. Garlock, C. Zhao, Posttensioned seismic-resistant connections for steel frames, *J. Struct. Eng.* 127(2) (2001) 113-121.
- [5] C. Christopoulos, A. Filiatrault, C. Uang, B. Folz, Posttensioned energy dissipating connections for moment-resisting steel frames, *J. Struct. Eng.* 128 (2002) 1111–1120.
- [6] M.M. Garlock, J. M. Ricles, R. Sause, Experimental studies of full-scale posttensioned steel connection, *J. Struct. Eng.* 131 (2005) 438–448.
- [7] J. McCormick, J. Tyber, R. DesRoches, k.Gall, H. Maier, Structural engineering with NiTi Part II: Mechanical behavior and scaling, *J. Eng. Mech.* 133(9) (2007) 1019-1029.
- [8] J. Ocel, R. DesRoches, R.T. Leon, W.G. Hess, R. Krumme, J.R. Hayes, S. Sweeney, Steel beam-column connections using shape memory alloys, *J. Struct. Eng.* 130 (2004) 732–740.
- [9] H. Ma, T. Wilkinson, C. Chongdu, Feasibility study on a self-centering beam-to-column connection by using the superelastic behavior of SMAs, *Smart. Mater. Struct.* 16 (2007) 1555–1563.
- [10] H. Ma, and M. C. H. Yam, Experimental study on a beam-to-column connection using Shape Memory Alloy, *Adv. Mater. Res.* 374-377 (2012) 2176-2179.
- [11] J. Sepúlveda, R. Boroschek, R. Herrera, O. Moroni, M. Sarrazin, Steel beam-column connection using copper-based shape memory alloy dampers, *J. Constr. Steel Res.* 64 (2008) 429-435.

- [12] M.S. Speicher, R. DesRoches, R.T Leon, Experimental results of a NiTi shape memory alloy (SMA)-based recentering beam-column connection. *Eng Struct.* 33 (2011) 2448-2457.
- [13] R. DesRoches, B. Taftali, B.R. Ellingwood, Seismic performance assessment of steel frames with shape memory alloy connections, Part I- Analysis and seismic demands, *J. Earthq. Eng.* 14 (2010) 471-486.
- [14] B.R. Ellingwood, B. Taftali, R. Desroches, Seismic performance assessment of steel frames with shape memory alloy connections, Part II- Probabilistic demand assessment, *J. Earthq. Eng.* 14 (2010) 631-645.
- [15] Y.L.Han, Q.S.Li, A.Q. Li, A.Y.T Leung, P.H. Lin, Structural vibration control by shape memory alloy damper, *Earthq Eng Struct D*, 32 (2003) 483-494.
- [16] M. Dolce, D.Cardone, R. Marnetto, M. Mucciarelli, D. Nigro, F.C. Ponzio, G. Santarsiero, Experimental static and dynamic response of a real R/C frame upgraded with SMA recentering and dissipating braces, *Proc. 13th World Conference on Earthquake Engineering, Vancouver, Canada, 2004*, (paper no. 2878).
- [17] J. McCormick, R. DesRoches, D. Fugazza, F. Auricchio, Seismic assesment of concentrically braced steel frames with shape memory alloy braces", *J. Struct. Eng.* 133 (2007) 862-870.
- [18] Shabelli, R., Mahin, S., and Chang, C. "Seismic demand on steel braced frame buildings with buckling-restrained braces", *Eng. Struct.* 25(5) (2003) 655-666.
- [19] A. Kari, M. Ghassemieh, S.A. Abolmaali, A new dual bracing system for improving the seismic behavior of steel structures, *Smart. Mater. Struct.* 20 (12) (2011) 125020.
- [20] A.D. Cesare, F.C. Ponzio, D. Nigro, M. Dolce, C. Moroni, Experimental and numerical behaviour of hysteretic and visco-recentering energy dissipating bracing systems, *Bull Earthquake Engineering*, 10(5) (2012) 1585–1607.
- [21] D.J Miller, Development and experimental validation of self-centering buckling-restrained braces with shape memory alloy, M.Sc thesis, University of Illinois at Urbana-Champaign, USA, 2011.

- [22] P. Sultana, M.A. Youssef, Prediction of local seismic damage in steel moment resisting frames, *J. Constr. Steel. Res.* 122 (2016) 122-137.
- [23] D. Ozhendekci, N. Ozhendekci, Seismic performance of steel special moment resisting frames with different span arrangements, *J. Constr. Steel Res.* 72 (2012) 51-60.
- [24] ANSI/AISC 361-89. Manual of Steel Construction: Allowable stress design, American Institute of Steel Construction, 1989.
- [25] SeismoStruct (version 6) - A computer program for static and dynamic nonlinear analysis of framed structures. Available online from <http://www.seismosoft.com>.
- [26] FEMA 356, Prestandard and Commentary for the Seismic Rehabilitation of Buildings, Federal Emergency Management Agency, 2000.
- [27] N. Luco, C.A. Cornell, Effects of random connection fractures on the demands and reliability for a three-storey pre-Northridge (SMRP) structure. Proc. of the Sixth US National Conf. on Earthquake Eng., Earthquake Engineering Research Institute, Oakland, California, USA.
- [28] PEER ground motion database, Pacific Earthquake Engineering Research Center, University of California, Berkeley, USA, 2013, <http://ngawest2.berkeley.edu/>.
- [29] F. Auricchio, E. Sacco, A one-dimensional model for superelastic shape-memory alloys with different elastic properties between austenite and martensite, *Int. J. Nonlin. Mech.* 32 (1997) 1101-1114.

CHAPTER 4

SEISMIC PERFORMANCE OF MODULAR STEEL FRAMES EQUIPPED WITH SHAPE MEMORY ALLOY BRACES

4.1 INTRODUCTION

Modular construction is the preferred choice, when repetitive units are required as can be found in schools, hospitals, hotels, etc. One to six storey modular steel buildings (MSBs) usually rely on bracing elements for lateral stability. Figure 4.1 shows a plan view of a typical MSB along with the horizontal and vertical connections between the modules [1]. Annan et al. [1-2] emphasized that the seismic performance of modular steel braced frames (MSBFs) is significantly different from regular steel braced frames. Such difference is attributed to the existence of ceiling beams, the eccentricity developed at the joints as the braces do not intersect at a single working point, and the semi-rigid connections between the columns of a module and the ones above or below it.

The design philosophy of regular steel braced frames ensures that plastic deformations occur only in the braces, leaving the beams, columns, and connections undamaged. As a result, steel braced frames are expected to survive strong earthquakes, and dissipate the seismic energy through ductile yielding of tension braces and buckling of the compression braces. The conventional steel bracing system has limited ductility and energy dissipation capacity due to buckling of braces and asymmetric behavior of the tension and compression braces.

Buckling restrained braced frames (BRBFs) offer an alternative to conventional braced frames and surpass their energy dissipation capacity. Each buckling restrained bracing (BRB) has two basic components: a steel core that supports the entire axial force, and an exterior element that prevents the core from buckling. Although, seismic damage to BRBFs is concentrated in the core, which can be easily repaired; they are still susceptible to residual drifts [3-5].

Superelastic shape memory alloys (SMAs) attracted the attention of researchers in recent years because of their ability to dissipate the seismic energy, while maintaining the self-centering ability. SMAs based on Nickel Titanium (NiTi) were found to be the most suitable for most commercial applications [6]. Researchers had investigated the seismic performance of steel and reinforced concrete frames equipped with SMA braces [7-17]. McCormic et al. [9] analytically studied the performance of steel frames equipped with SMA braces. Such braced frames were found to be effective in limiting inter-storey drifts (IDs) and residual inter-storey drifts (RIDs) following an earthquake. Kari et al. [10] investigated numerically the benefits of using a combination of buckling restrained braces and SMA braces in new designs as well as retrofitting. Results revealed that residual inter-storey drifts can be minimized using such a system. The seismic behavior and performance of self-centering buckling-restrained braces (SC-BRBs) that utilize SMAs were investigated experimentally by Miller [12]. The SC-BRB consisted of a typical BRB and pre-tensioned superelastic NiTi SMA rods. Recentering of the braces was achievable by using proper values for the SMA pretension force and the BRB core yield force. The application of these SC-BRBs in a real building was investigated by Eatherton et al. [13]. The study revealed that SC-BRBs are capable of reliably limiting residual drifts. The

seismic performance of SMA-braced frames with different bracing configurations was also studied [14-16]. Ghassemieh and Kargarmoakhar [17] assessed the seismic response of SMA braced frames in terms of overstrength and ductility and recommended using a value between 5.77 and 9.68 for the response modification factor, R .

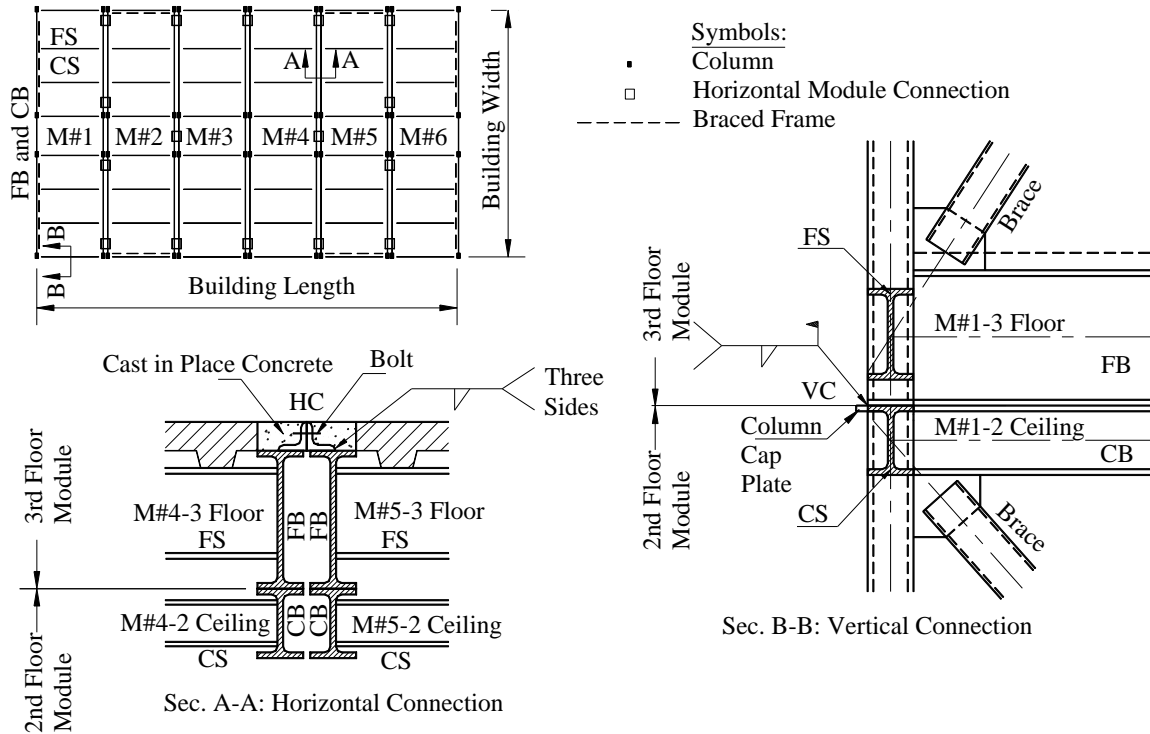


Figure 4. 1: A typical plan and section of a modular steel building [1]

Although few research data on using SMA in steel braced frames can be found in the literature, previous research did not address their use in MSBs. Sultana and Youssef [18] identified the required location of SMA connections in a typical steel moment resisting frame based on a simplified method [19] as well as incremental dynamic analysis. This study extends this research by exploring the seismic performance of MSBFs equipped with SMA braces. The finite element modeling technique, adopted in this study, was first

validated using available experimental studies. Incremental dynamic analysis of a MSBF that is equipped with steel braces, was performed considering five different ground motions. The steel braces were then replaced by superelastic SMA braces. Five different configurations of SMA braces were examined. The seismic performance of the analyzed frames was then compared in terms of MID, MRID, and damage distribution to identify the SMA brace configuration resulting in the best seismic performance.

4.2 MODULAR STEEL BRACED FRAME

The six-storey modular steel building (MSB) selected as a case study was designed by Annan et al. [1] according to the Canadian standard CSA-S16-01 [20] and the National Building Code of Canada [21]. Figure 4.2 shows a typical plan and an elevation of the MSBF. Each floor of the MSB consists of six modular units, which are connected horizontally. Lateral forces are resisted by external braced frames, as shown in Figure 4.2. The lateral response of the MSB in the N-S direction is considered in the study. Details about the design of the frames are given by Annan et al. [1]. Floor and ceiling beams were W250×33 and W100×19, respectively. Sections for the column and braces are given in Table 4.1.

Table 4. 1: section properties of the MSBF

Storey	Column Sections	Brace Sections
Storey 6	HS 102×102×6	HS 76×76×5
Storey 5	HS 178×178×6	HS 102×102×6
Storey 4	HS 203×203×10	HS 102×102×6
Storey 3	HS 305×305×10	HS 102×102×6
Storey 2	HS 305×305×13	HS 102×102×6
Storey 1	HS 305×305×13	HS 102×102×6

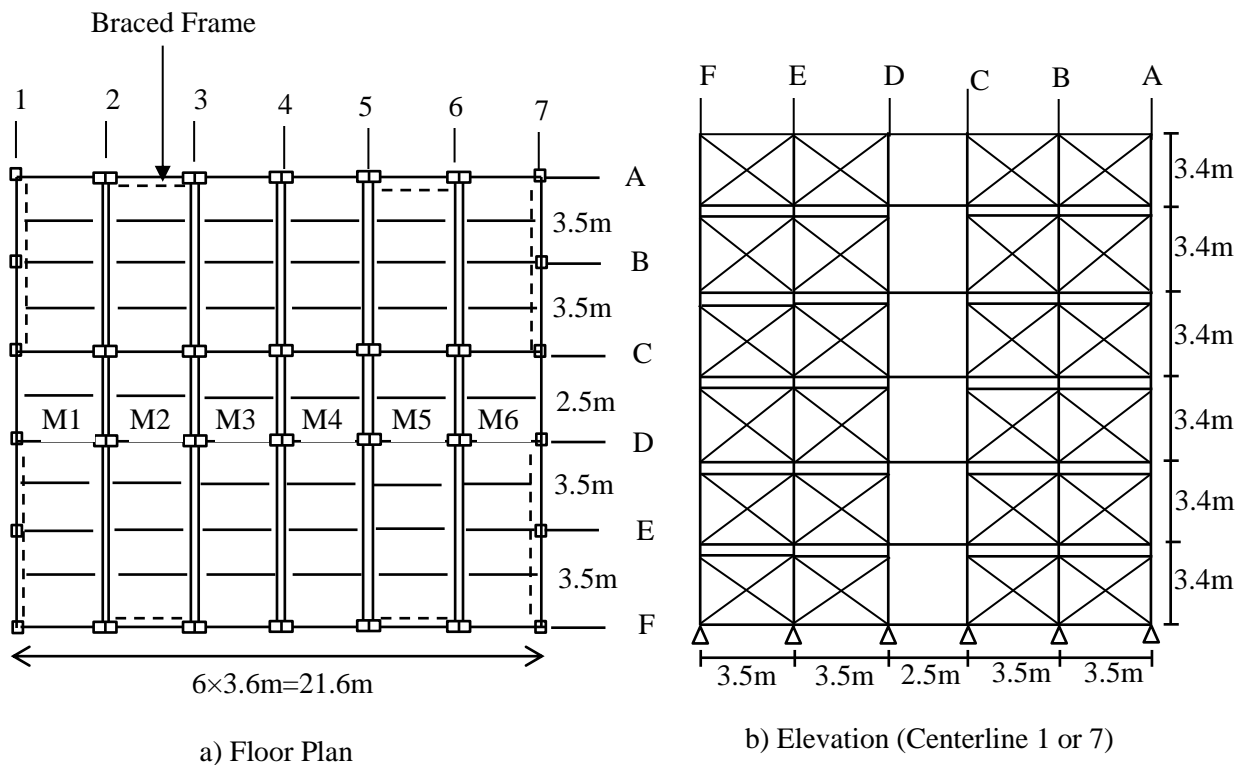


Figure 4. 2: Six-storey modular steel braced frames

4.3 FINITE ELEMENT MODELING OF MSBF

A nonlinear two-dimensional (2D) model was developed using the software SeismoStruct [22], which is based on the fibre element approach. The beams and columns were modelled using force-based (FB) inelastic frame elements. The distributed dead load and 25% of the live load were applied to the beams. The mass of each floor was converted into lumped masses at the joints. Careful attention was made to the unique detailing of the MSB. Specific modeling assumptions are given below:

- 1) As beams and columns were assumed to be connected by direct welding, rigid beam-to-column connections were utilized.
- 2) The modules were assumed to be connected vertically by field welding at the outer faces of the columns since the inner faces of the columns were not accessible. This connection allows independent rotations of the upper and lower modules. Thus, the vertical joint between the modules was simulated as a pin connection to account for this behaviour.
- 3) The steel braces and the SMA braces of the MSBF were modelled using inelastic truss elements. Buckling behaviour was not modelled as braces were assumed to be buckling restrained.

Menegotto-Pinto [23] hysteretic material model with a yield stress 350 N/mm^2 , an elastic modulus of 200 kN/mm^2 and 3% strain hardening is assumed for the steel elements. The SMA material model proposed by Aurichio and Sacco [24] and implemented by Fugaza [25] was adopted in this study. The model assumes a constant stiffness for both the fully austenitic and fully martensitic behavior. The SMA material properties, provided in Table 4.2, were adopted from the study conducted by DesRoches et al. [26]

Table 4. 2: Material properties of SMA

Modulus of elasticity, E	55000 MPa
Austenite –to-martensite starting stress	420 MPa
Austenite –to-martensite finishing stress	520 MPa
Martensite-to-austenite starting stress	310 MPa
Martensite-to-austenite finishing stress	240 MPa
Superelastic plateau strain length	6 %

4.3.1 Validation of FE modeling technique

A concentrically braced steel frame tested by Wakabayashi et al. [27] was modelled using the technique explained in the previous section. Braces were modelled using inelastic frame elements. Buckling of the braces was incorporated by assuming an initial geometric imperfection [28-29]. As the experimental cyclic load was not available, the cyclic load for numerical simulation was developed based on the experimental maximum storey displacement, shown in the Figure 4.3(a). The numerical and experimental results are shown in Figure 4.3. The FE model provided reasonable predictions of the frame behaviour in terms of maximum base shear, energy dissipation, and residual drift.

Annan et al. [2] experimentally assessed the hysteretic characteristics of a MSBF, Figure 4.4. The frame was modelled using the described modeling technique. Figure 4.5 shows details of the model. The rigid connections between beams and columns were modelled using rigid elements as presented with heavy lines. Member M1 represents the 150 mm vertical clearance required for fire proofing between any two storeys. The vertical joint, j5,

was simulated using a pin connection to allow independent rotation of upper and lower modules. Figure 4.6 compares the experimental and analytical results. The maximum base shear obtained from FE analysis is lower than that obtained experimentally by 6.67%. The model was also able to accurately capture the energy dissipation characteristics and the residual drift values.

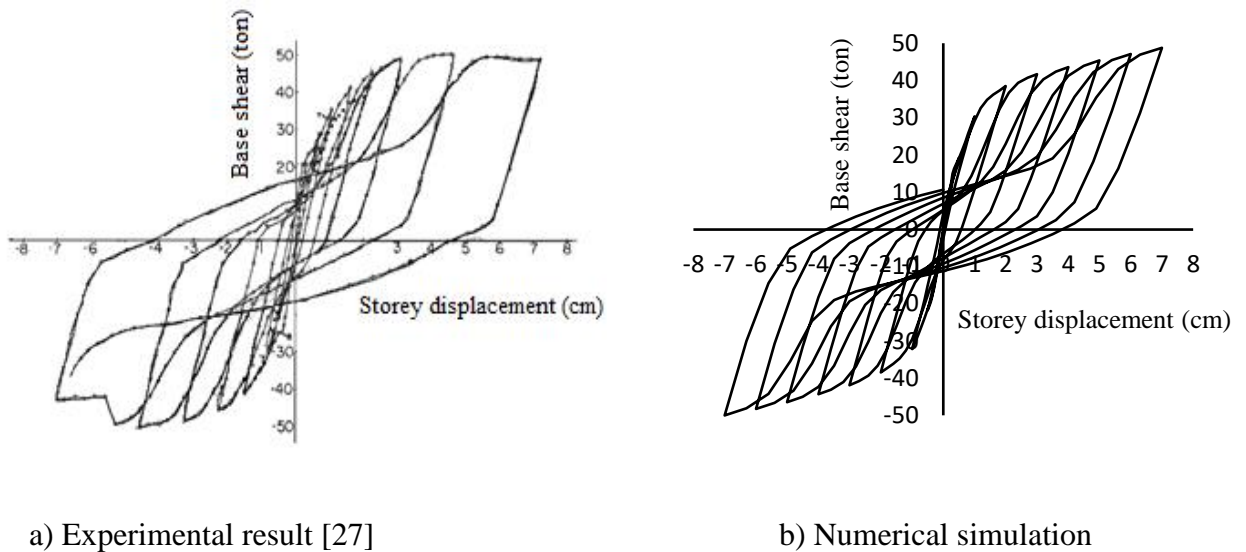


Figure 4. 3: Comparison of numerical and experimental responses

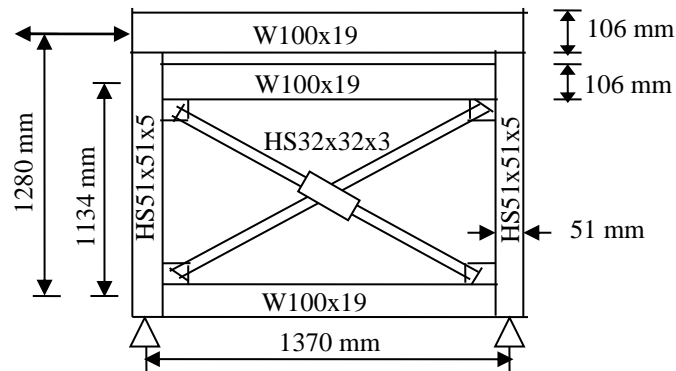


Figure 4. 4: Geometry of MSBF tested by Annan et al. [2]

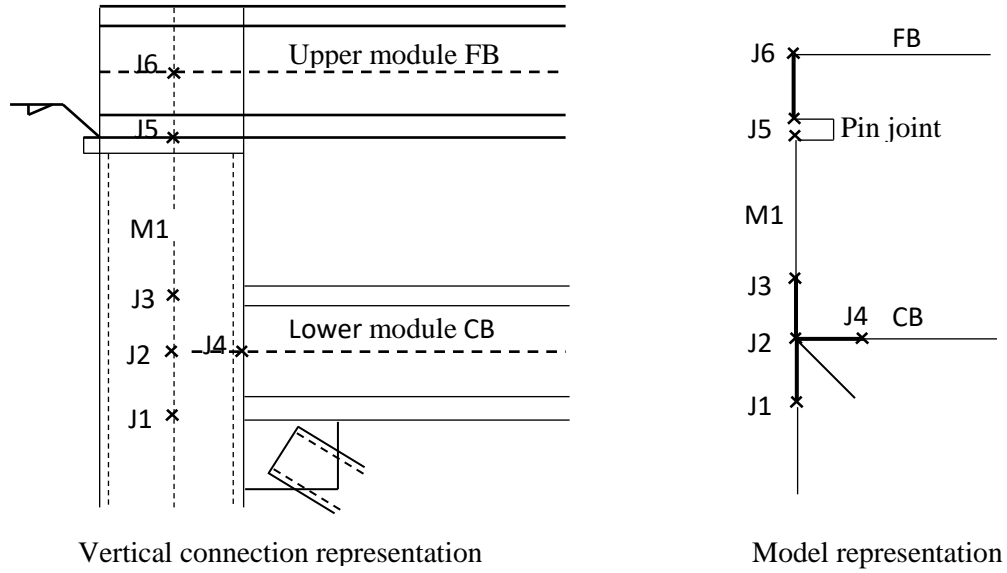


Figure 4. 5: Model of vertical connection of MSBF

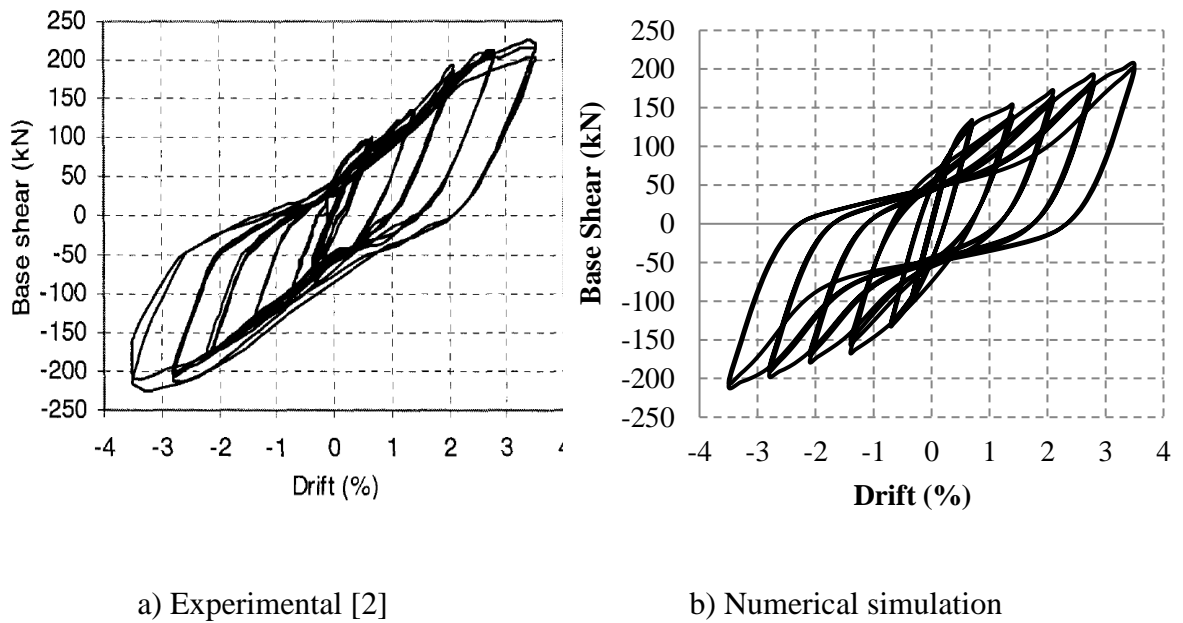


Figure 4. 6: Comparison of experimental and numerical results

4.4 DYNAMIC ANALYSIS OF STEEL-MSBF (FRAME 1)

The seismic performance of structures is highly influenced by the frequency content, duration and intensity of the ground motions. Five different ground motions that cover these variables were selected from PEER ground motion database [30]. Their characteristics are listed in Table 4.3. Figure 4.7 shows the elastic response spectra of the selected ground motions considering 5% damping.

Eigen value analysis was performed to determine the natural period of vibrations and mode shapes of the six-storey steel-MSBF (Frame 1). The first and second natural periods of vibrations were 0.54 seconds and 0.19 seconds, respectively. Incremental dynamic analysis (IDA) was then performed to assess the seismic performance of the frame considering the selected ground motions. The seismic intensity is expressed in term of the spectral acceleration at the first period of vibration [$S_a(T_1, 5\%)$]. MID and MRID were selected as global demand parameters of the selected frames.

Table 4. 3: Characteristics of the ground motions

Earthquake	Year	Ms magnitude	Station	PGA (g)
Imperial Valley	1979	6.9	El Centro Array #13	0.139
Northridge	1994	6.7	Arleta-Nordhoff	0.344
Superstition Hills-02	1987	6.54	Parachute Test Site	0.432
Loma Prieta	1989	7.1	Capitola	0.451
Tabas	1978	6.9	Tabas	0.852

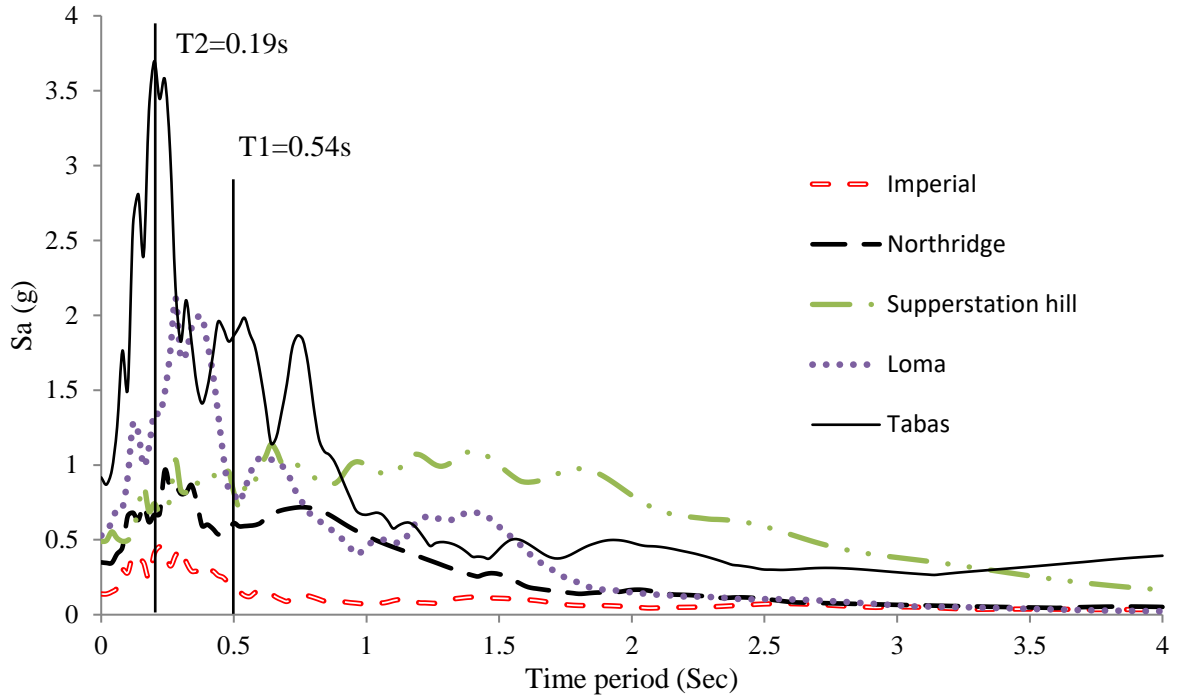


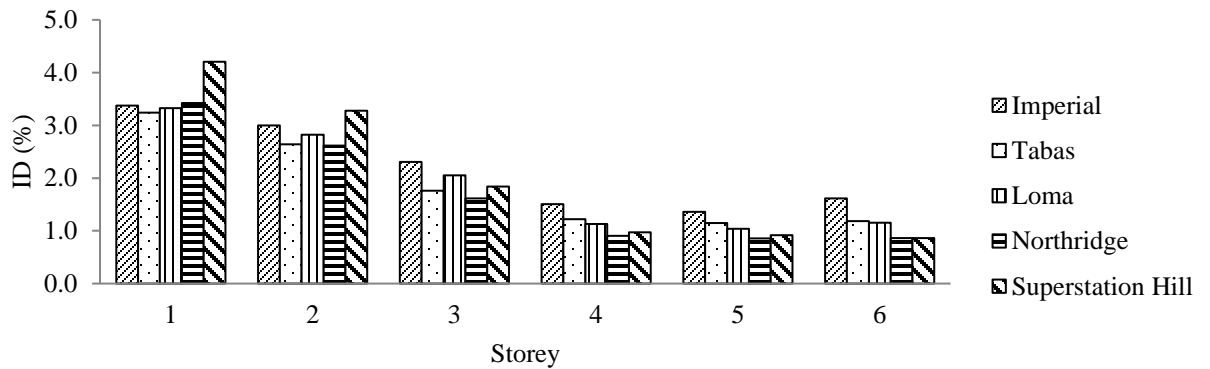
Figure 4. 7: Elastic response spectra

4.4.1 Results for Frame 1

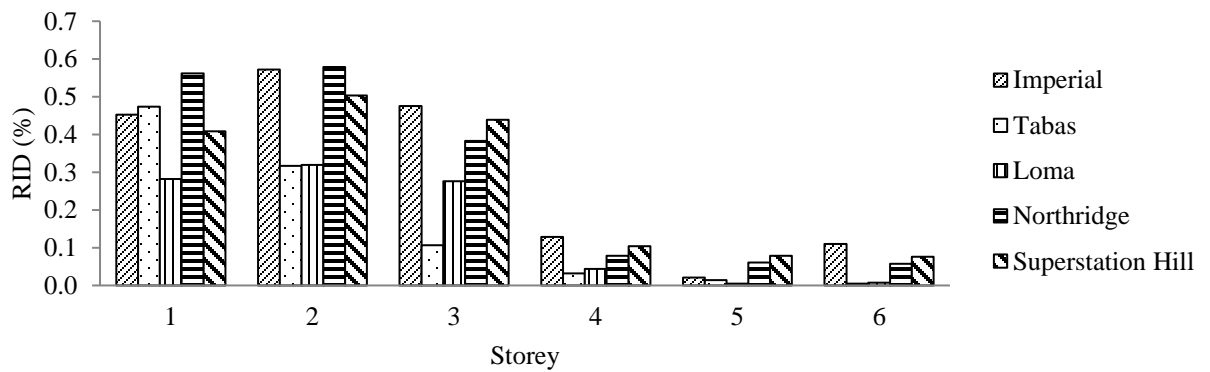
The intensity [$S_a(T1,5\%)$] at which Frame 1 failed as well as the corresponding MID and MRID are listed in Table 4.4. Values of the MID varied from 3.24% to 4.21% and occurred at the first storey. The MRID varied from 0.32% to 0.62%. The storey experiencing the MID was generally different than that experiencing the MRID with the exception of Tabas earthquake. Figure 4.8 shows the distribution of ID and RID along the building height at collapse. It is observed that first three storeys experienced higher IDs and RIDs as compared to the top three storeys.

Table 4. 4: MID and MRID of Frame 1 at collapse

Ground motion	Sa(T1,5%) at collapse	Frame 1	
		MID (%)	MRID (%)
Imperial	3.84g	3.37 (1 st storey)	0.57 (2 nd storey)
Northridge	2.81g	3.42 (1 st storey)	0.58 (2 nd storey)
Superstition Hill	3.36g	4.21(1 st storey)	0.62(3 rd storey)
Loma	3.95g	3.33 (1 st storey)	0.32 (2 nd storey)
Tabas	5.95g	3.24 (1 st storey)	0.47 (1 st storey)



a) ID



b) RID

Figure 4. 8: ID and RID distribution for Frame 1 at collapse

The seismic performance was evaluated according to FEMA 356 [31]. Failure of frame members is considered when they reach or exceed the acceptance criteria for “collapse prevention” performance level provided by FEMA 356. Figure 4.9 shows the damage distribution of Frame 1 at collapse. Yielding of columns and beams are presented by solid black dots and yielding of braces is represented by heavy lines. Beams in the unbraced bays as well as floor and ceiling beams of the 1st and 2nd storeys yielded considering all records. Yielding of ceiling beams at other stories was also observed. Braces of the bottom storeys were severely damaged whereas some braces of the top two storeys remained elastic. Yielding of columns is observed at different storeys. The exterior columns and the columns of the unbraced bays experienced more damage than the remaining columns. All of the interior columns of the unbraced bays failed during Imperial, Loma and Tabas earthquakes.

The ID and RID distributions along the frame height, shown in Figure 4.8, agree with the observed damage distribution. Also, the yielding of short columns between the modules that was observed agrees with the experimental results conducted by Annan et al. [2]. The yield distribution of the Frame 1 suggests good distribution of energy dissipation along the height and width of the modular braced frame.

4.5 SMA-MSBFS CHARACTERISTICS AND MODELING

Locations of the SMA braces were based on the damage distribution observed in Frame 1. Five different configurations for the SMA braces were selected as shown in Figure 4.10. The superelastic SMA braces were designed such that the natural period of vibration

remains unchanged. This was achieved by adjusting the area and length of SMA braces to have the same initial stiffness and yield forces as that of Frame 1. Similar design philosophy was used by other researchers [9, 15-17]. SMA braces were modelled using inelastic truss elements that were connected to rigid elements as shown in Figure 4.11. The same beam and column sizes of Frame 1 were maintained in the SMA-MSBF.

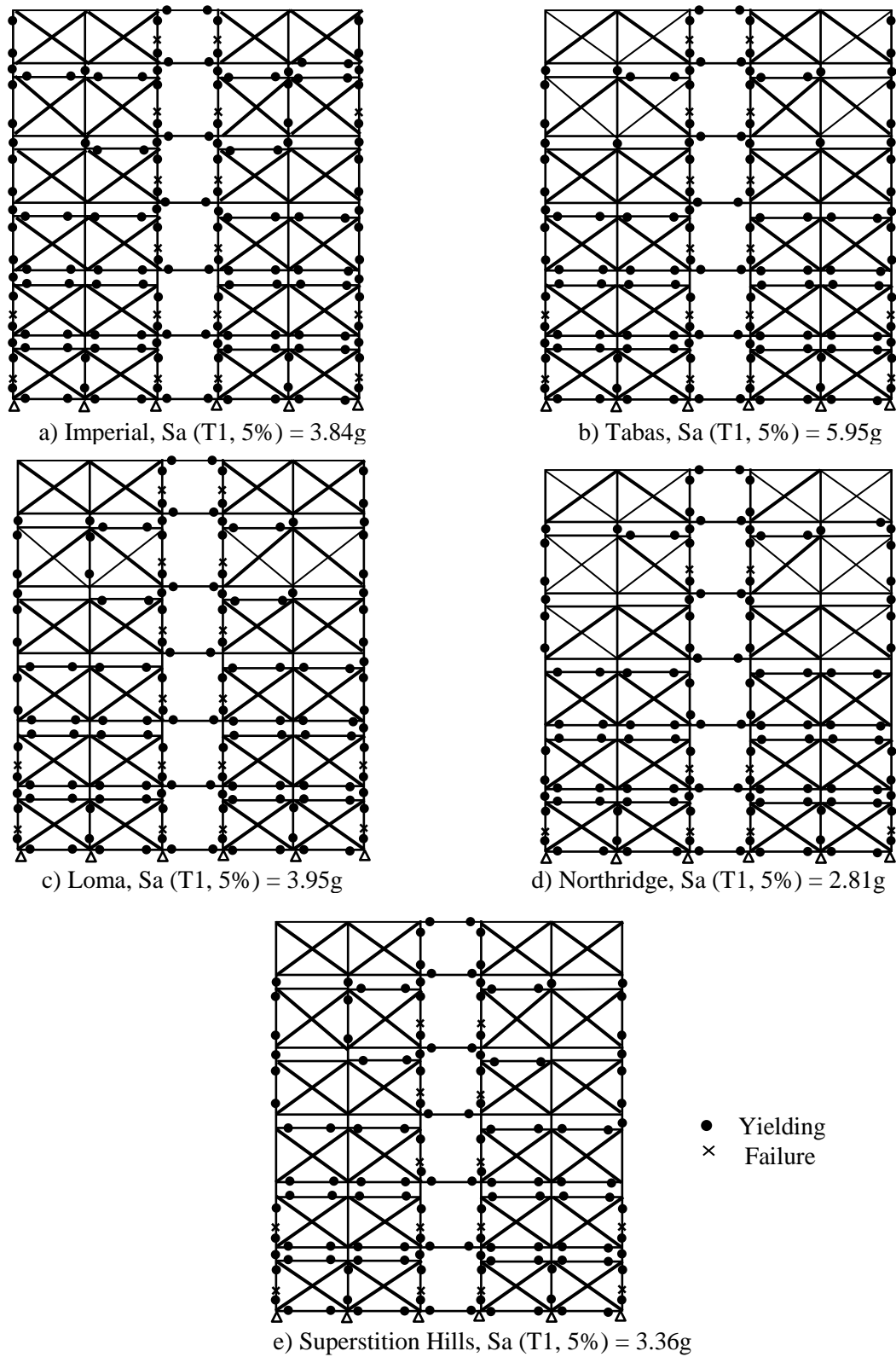
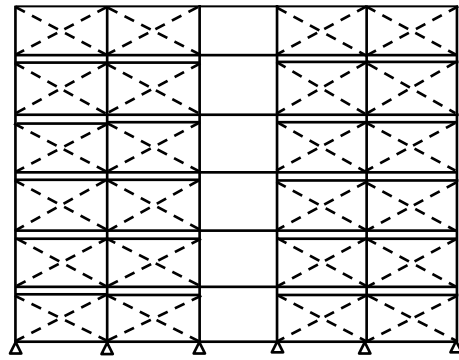
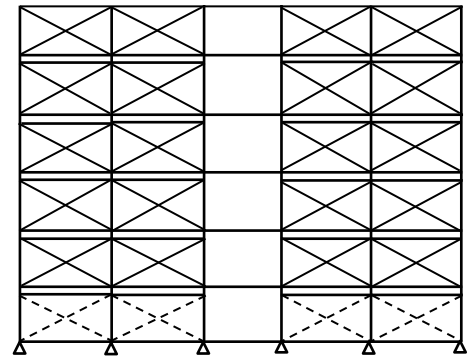


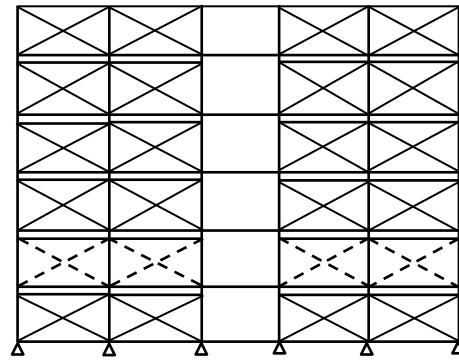
Figure 4. 9: Damage distribution of Frame 1 at collapse



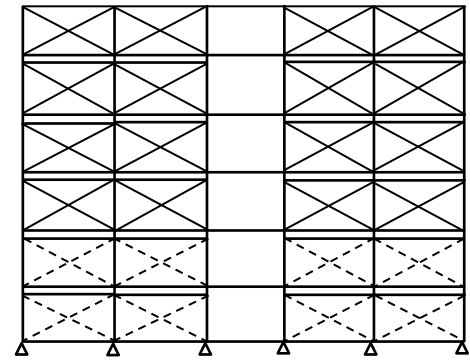
Frame 2



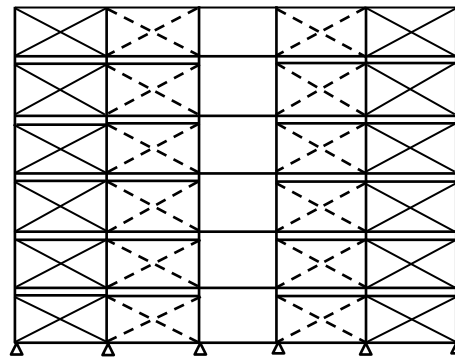
Frame 3



Frame 4



Frame 5



Frame 6

— Steel braces
 - - - SMA braces

Figure 4. 10: Different configurations for the SMA braces

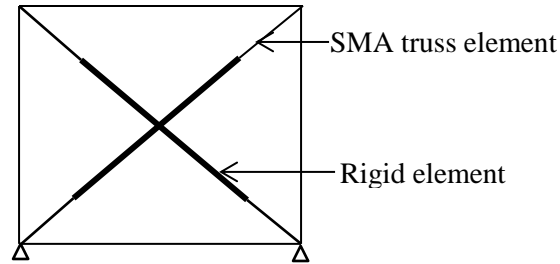


Figure 4. 11: Braced bay of SMA-MSBF

4.6 RESULTS FOR SMA-MSBFS

Dynamic analyses of the SMA-MSBFs were performed considering the same intensities at which Frame 1 collapsed. Figure 4.12 compares the MID and MRID distributions for the analyzed frames. It is observed that the MID and MRID of the SMA frames varied from 3.18% to 4.24% and 0.005% to 0.62 %, respectively. Table 4.5 shows the percentage change of MID and MRID as compared with Frame 1.

The MID depended on the locations of SMA braces and the characteristics of the considered ground motion. For example, replacing all braces by SMA braces (Frame 2) increased the MID considering imperial, Tabas, Loma and Northridge records up to 8.77% but reduced its value considering Superstition Hills record by 7.98%. Although the same numbers of SMA braces were used in Frames 3 and 4, the MID decreased in Frame 4 but increased in Frame 3 as compared to Frame 1 for Imperial, Loma and Northridge earthquakes. The slight increase or decrease in the MID values does not provide basis to choose a specific SMA configuration.

The highest reduction of the MRID occurred in Frame 2 reaching up to 98.6%. For Frame 3, the MRID increased in case of Superstition Hills record as compared to Frame 1, which clearly shows that using SMA at the wrong locations might worsen the seismic performance. For SMA frames 4 and 5, the percentage reduction of MRID varied from 4.31% to 40.2% and 18.71% to 87.9%, respectively. Frame 6 showed better seismic performance than Frames 3, 4 and 5 as its MID slightly increased (8.3%) but the frame regained 63.5% to 84.93% of its MRID.

Figures 4.13 to 4.17 compare the IDs and RIDs of the different frames. The IDs for Frames 2 to 6 were very similar. However, the RIDs were significantly different. The SMA braces resulted in redistributing the seismic forces in the frame, and, thus, had significantly influenced the location of the storey experiencing the MRID. It is observed that using SMA braces only in the first storey (Frame 3) had significantly reduced the residual drifts of that storey. This reduction was not pronounced in other storeys. The same observation can be made for Frames 4 and 5. The highest reduction of RIDs occurred in Frame 2 followed by Frame 6, which indicated the necessity of using SMA braces along the building height to minimize the RID.

Table 4. 5: Percentage change of MID and MRID of SMA frames

Frame type	Imperial		Tabas		Loma		Northridge		Superstition Hills	
	MID % change	MRID % change	MID % Change	MRID % change	MID % Change	MRID % change	MID % Change	MRID % change	MID % Change	MRID % change
Frame 2	8.77	-79.7	8.04	-86.5	1.63	-98.6	5.08	-88.1	-7.98	-81.1
Frame 3	2.89	-22.8	4.85	-13.7	0.83	-40.4	5.76	6.9	-8.42	7.8
Frame 4	-2.12	-24.4	0.34	-4.31	-4.45	-31.6	-0.08	-9.9	-8.42	-40.2
Frame 5	5.89	-30.9	4.17	-48.7	-1.53	-87.5	5.52	-54.5	0.76	-18.8
Frame 6	2.76	-74.7	8.30	-84.9	2.39	-81.6	5.79	-65.9	-9.74	-63.5

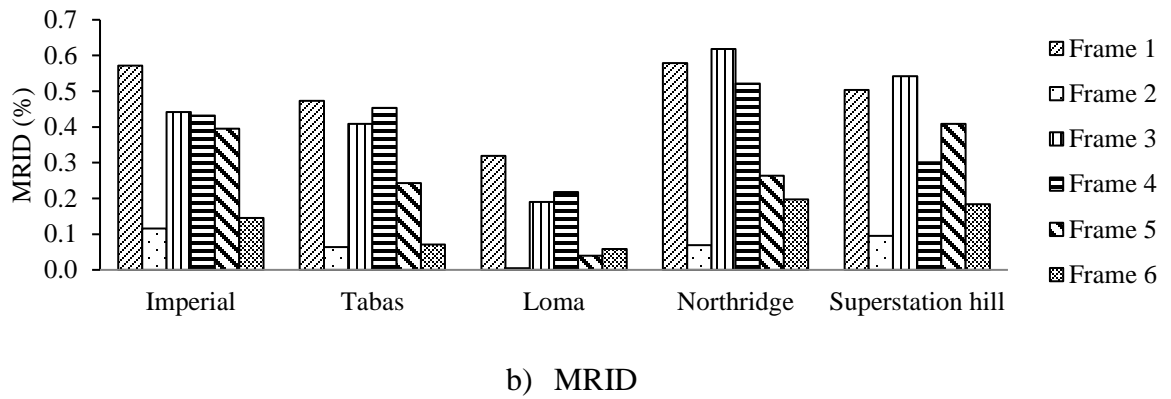
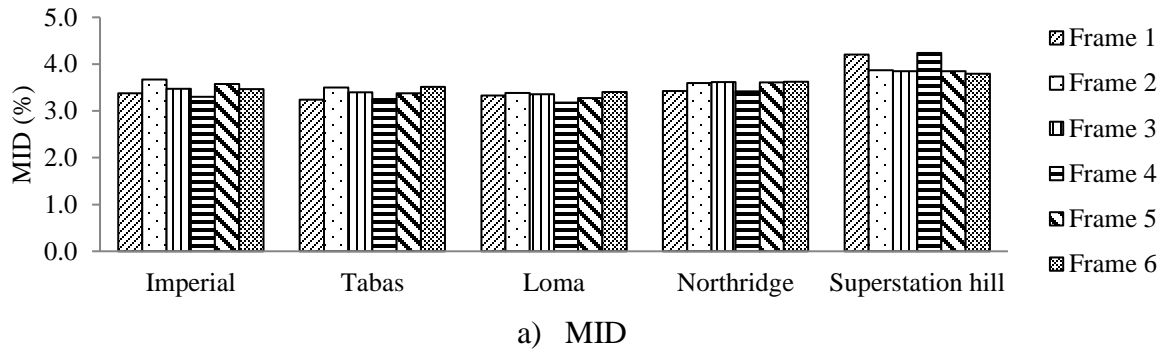


Figure 4. 12: Drift values at intensity causing collapse to Frame 1

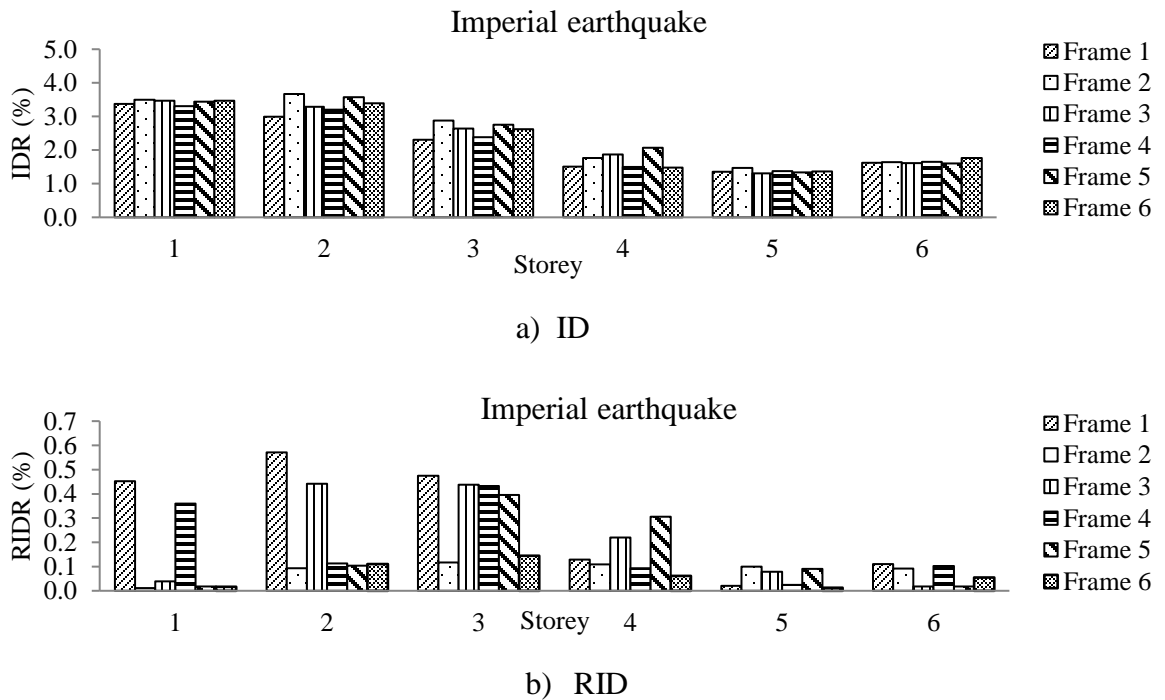


Figure 4. 13: Storey drifts for Imperial earthquake [$S_a(T1, 5\%)=3.84g$]

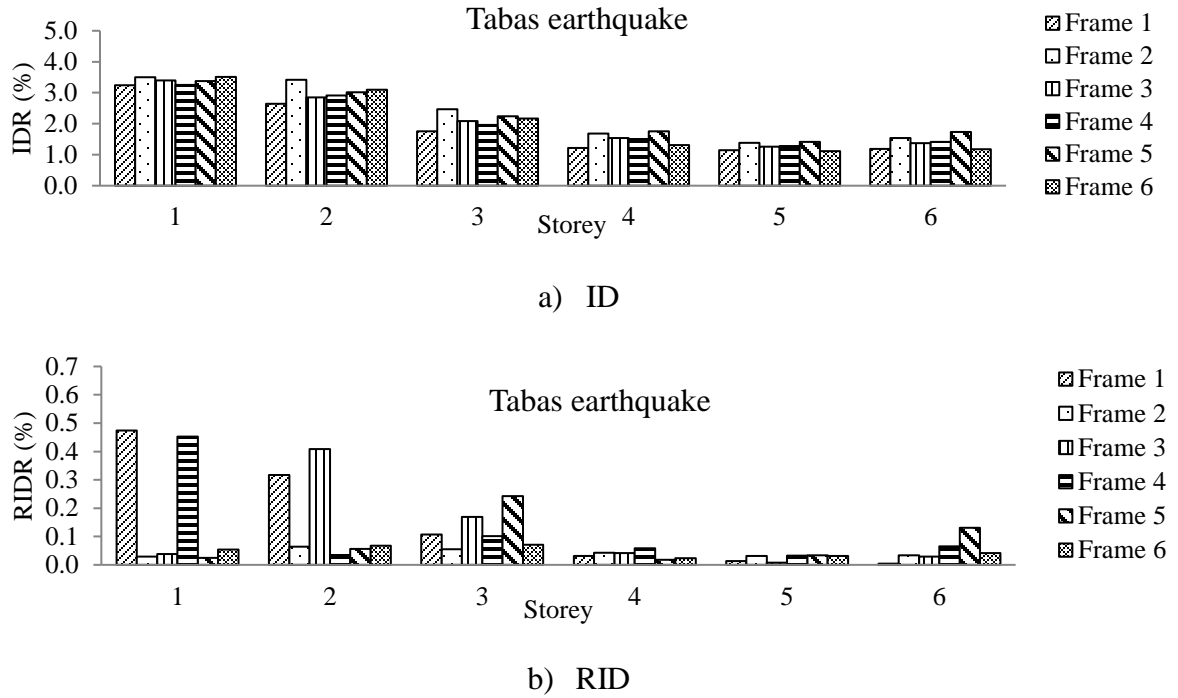


Figure 4. 14: Storey drifts for Tabas earthquake [Sa(T1, 5%)=5.95g]

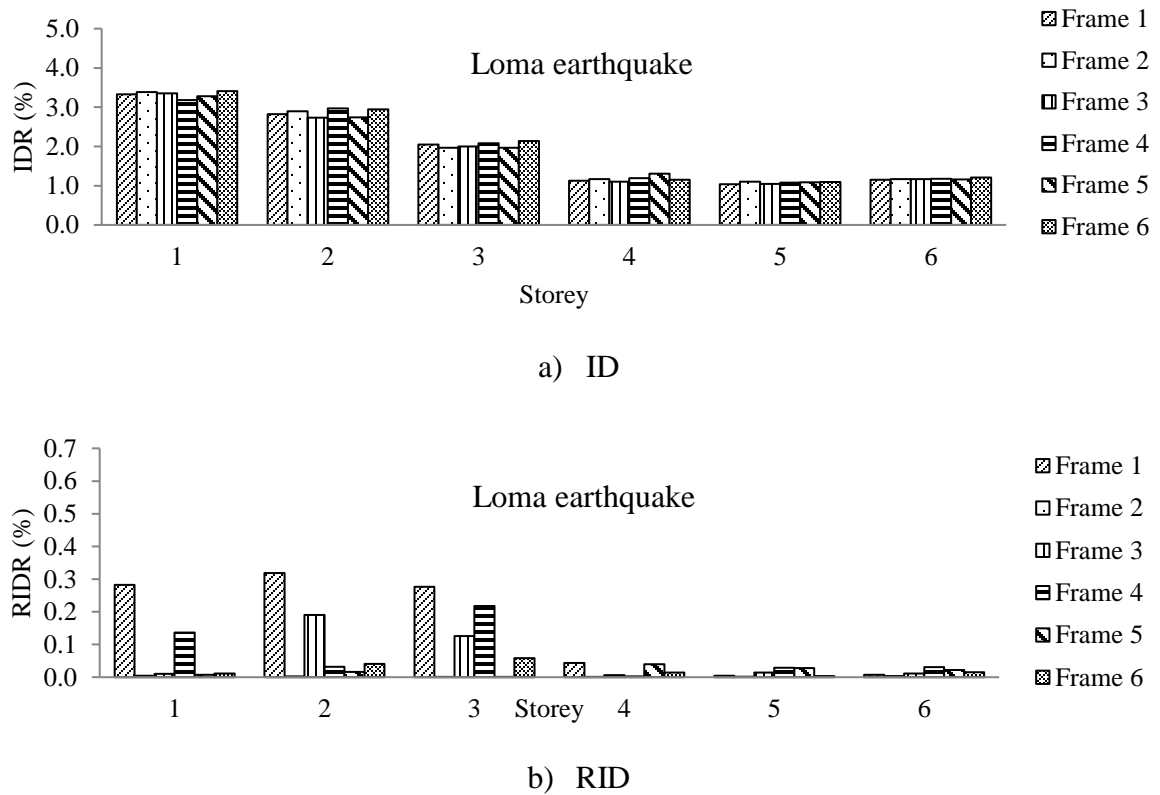


Figure 4. 15: Storey drifts for Loma earthquake [Sa (T1, 5%)=3.95g]

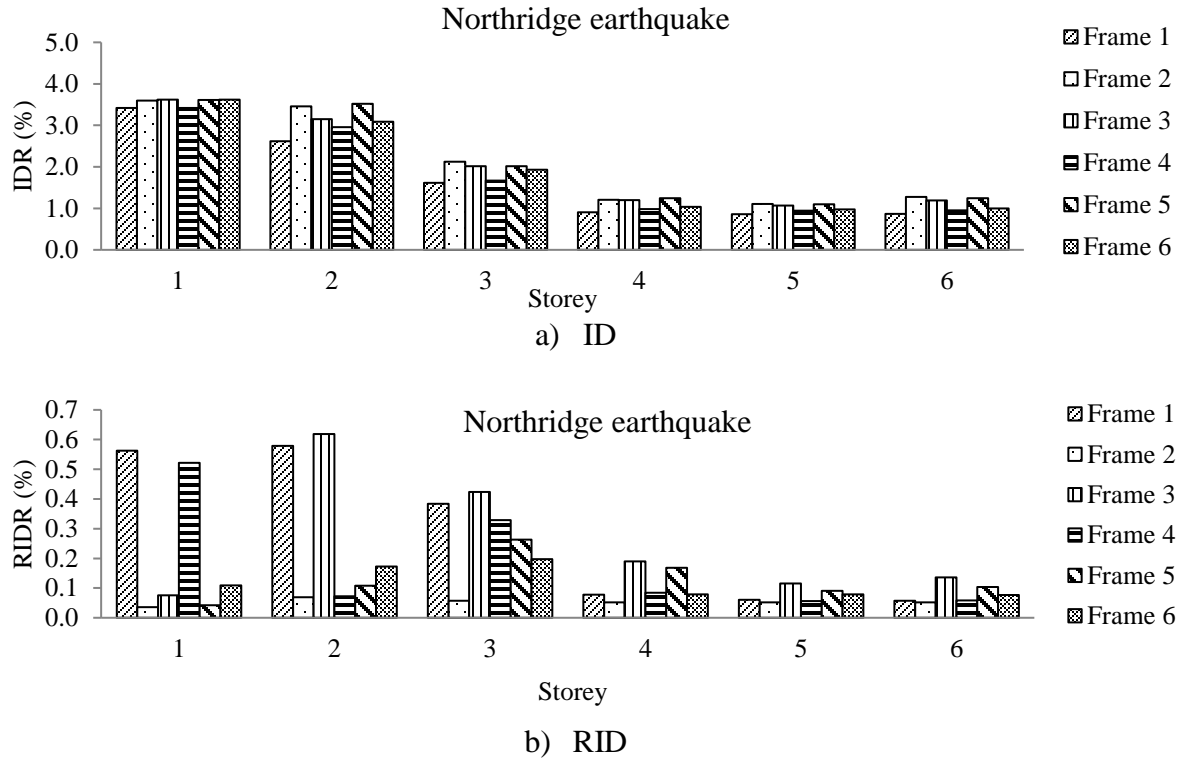


Figure 4. 16: Storey drifts for Northridge earthquake [$S_a(T1, 5\%)=2.81g$]

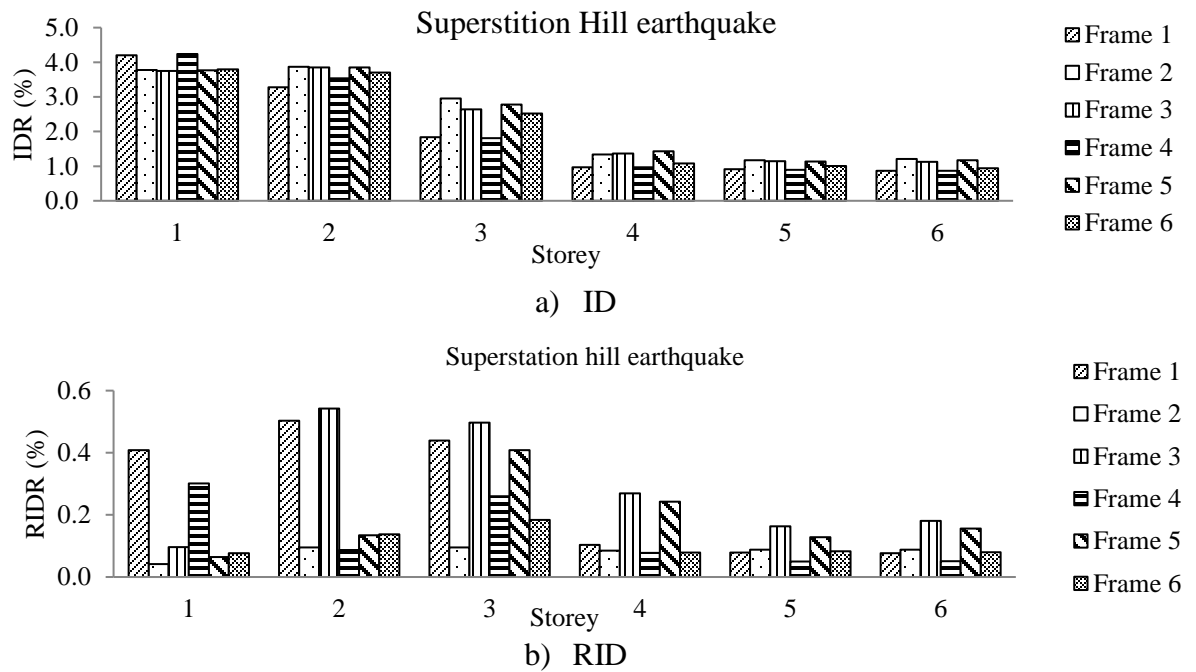


Figure 4. 17: Storey drifts for Superstition Hills earthquake [$S_a(T1, 5\%)=3.36g$]

The damage distributions of the SMA frames are shown in Figures 4.18 to 4.22. The distributions were generally similar to Frame 1. In case of Frame 2 (Figure 4.18), severe damage was observed up to the 4th storey due to Superstition Hills record, up to the 3rd storey for Imperial and Tabas records, and up to the 2nd storey for Loma and Northridge records. Using SMA in the first floor (Frame 3) caused failure of the four columns of the 1st to 3rd stories as well as the 5th storey considering Imperial record. It resulted in failure of the 1st, 2nd and 4th stories due to Superstition Hills record. Frame 4 showed better damage distribution (Figure 4.20) compared with Frame 3 (Figure 4.19) due to Imperial, Tabas, Northridge and Superstition Hills records. In case of Frame 5, severe damage occurred in the first 3 storeys while reduced damage was observed in the top three storeys as shown in Figure 4.21. Using SMA braces in the interior bays along the frame height (Frame 6) changed the force distribution keeping the 1st storey as the severely damaged storey. Extensive Damage is also observed in the first three stories for Imperial and Superstition Hills records and the first and second stories for Tabas, Loma, and Northridge earthquakes.

The damage distribution of Frame 2 (Figure 4.18) and Frame 6 (Figure 4.22) are further compared with that of Frame 1 (Figure 4.9). The comparison explains that both Frames 2 and 6 show almost similar damage distributions in terms of beam and column yielding for the considered earthquakes. The force deformation behaviour of a first storey steel brace of Frame 1 and SMA brace of Frame 2 subjected to Tabas earthquake are shown in Figures 4.23 and 4.24, respectively. The recentering capability of the SMA braces is clear in the figure. Considering the cost of SMA materials at one hand and the seismic performance in terms of MID, MRID and damage distribution on the other hand, Frame 6 can be judged as the most suitable solution.

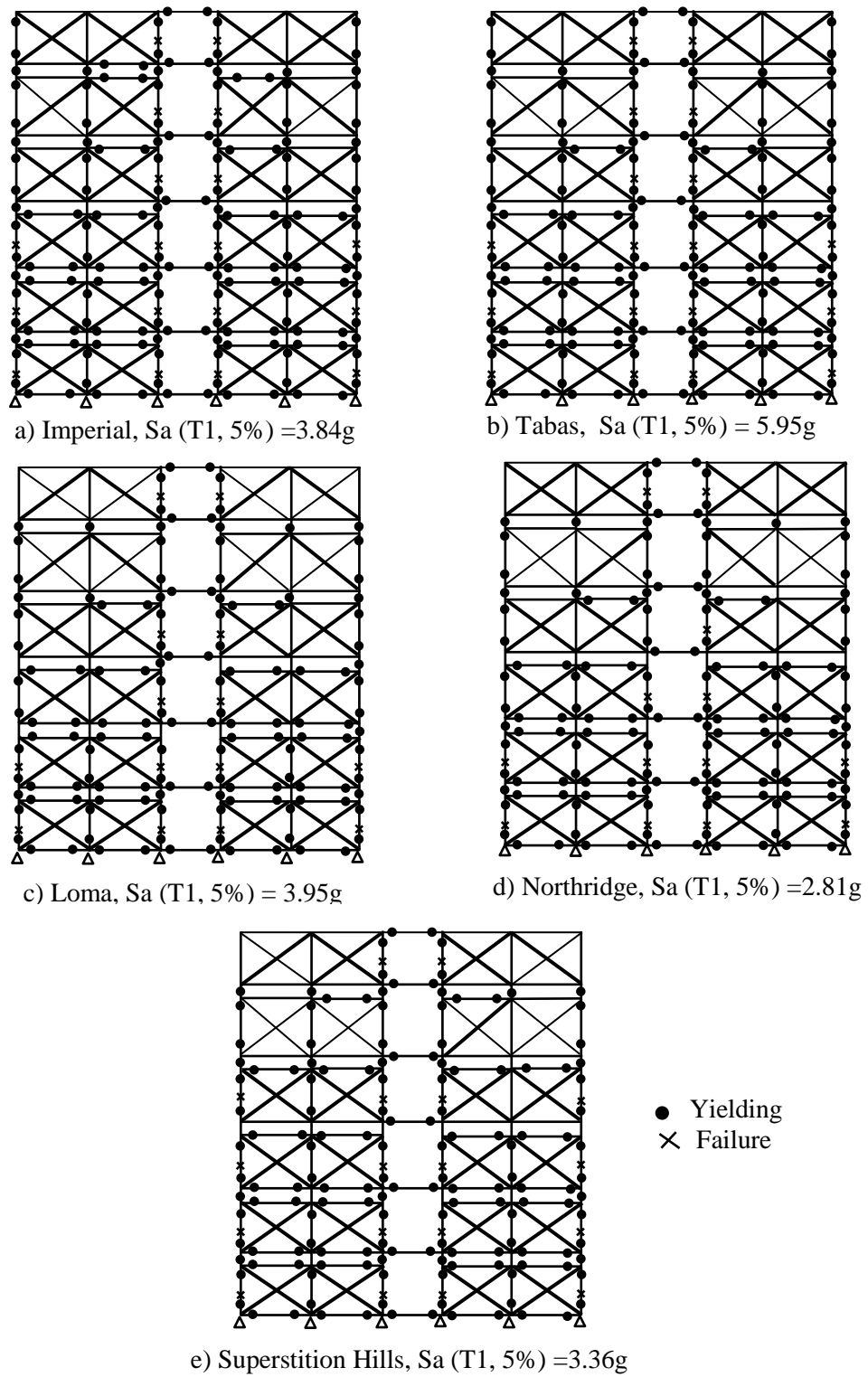


Figure 4. 18: Damage distribution of Frame 2

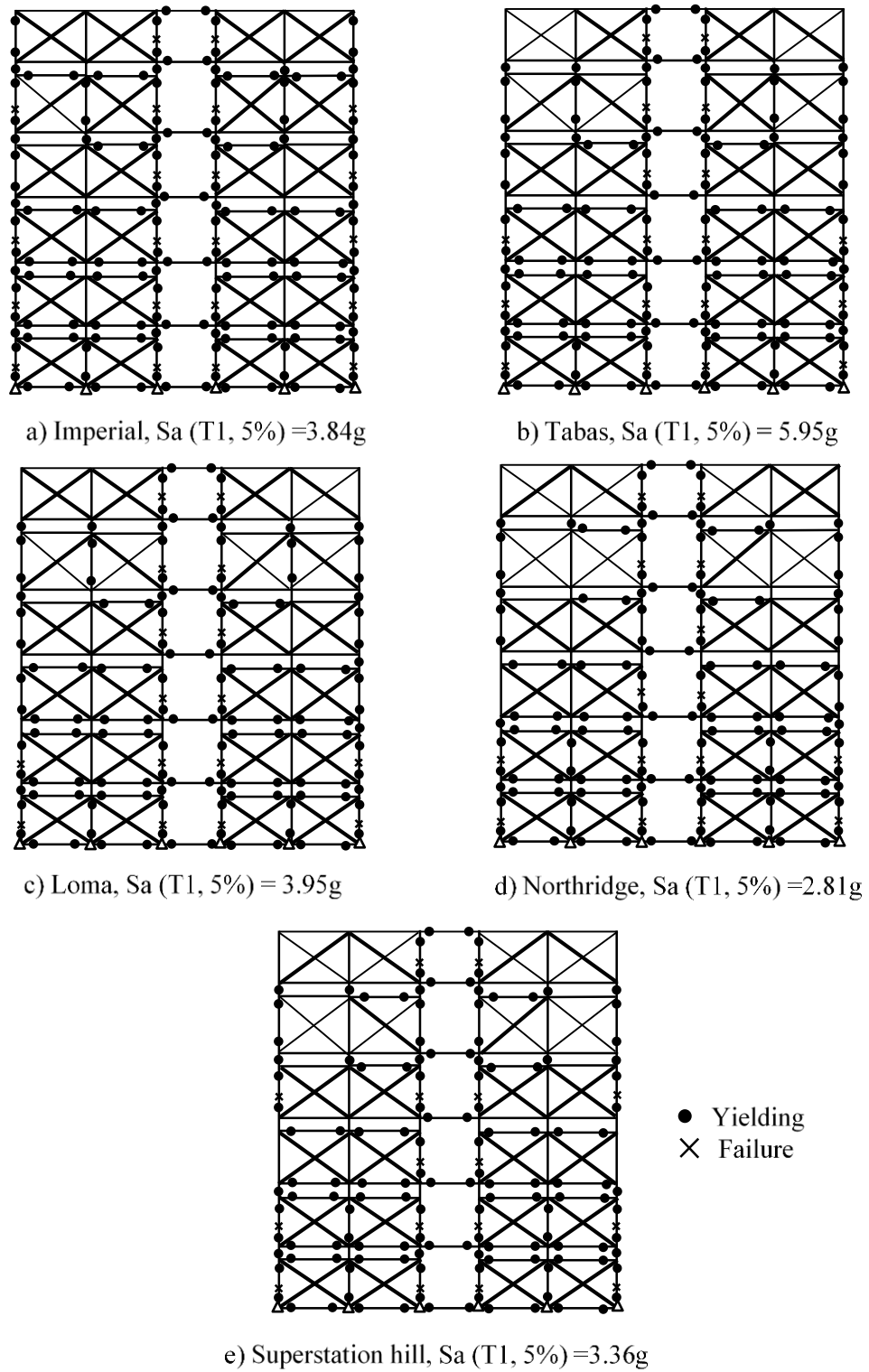
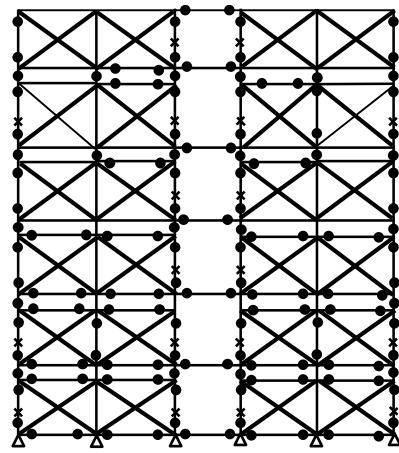
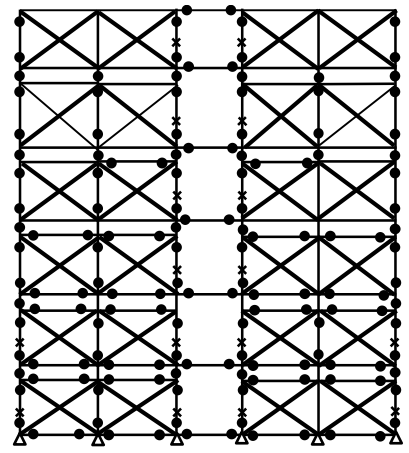
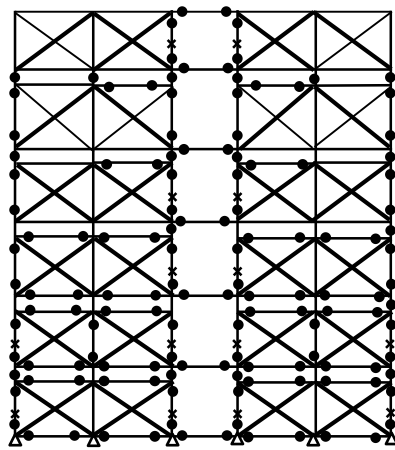
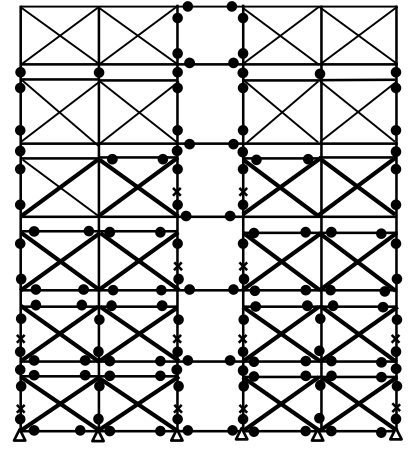
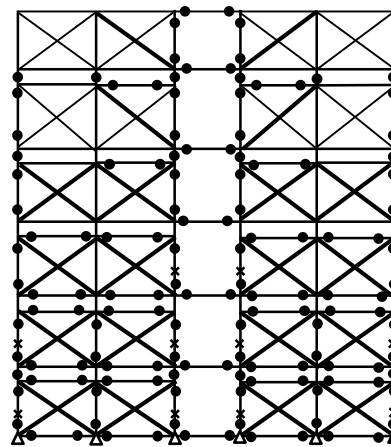


Figure 4. 19: Damage distribution of Frame 3

a) Imperial, $S_a(T1, 5\%) = 3.84g$ b) Tabas, $S_a(T1, 5\%) = 5.95g$ c) Loma, $S_a(T1, 5\%) = 3.95g$ d) Northridge, $S_a(T1, 5\%) = 2.81g$ e) Superstation hill, $S_a(T1, 5\%) = 3.36g$

● Yielding
× Failure

Figure 4. 20: Damage distribution of Frame 4

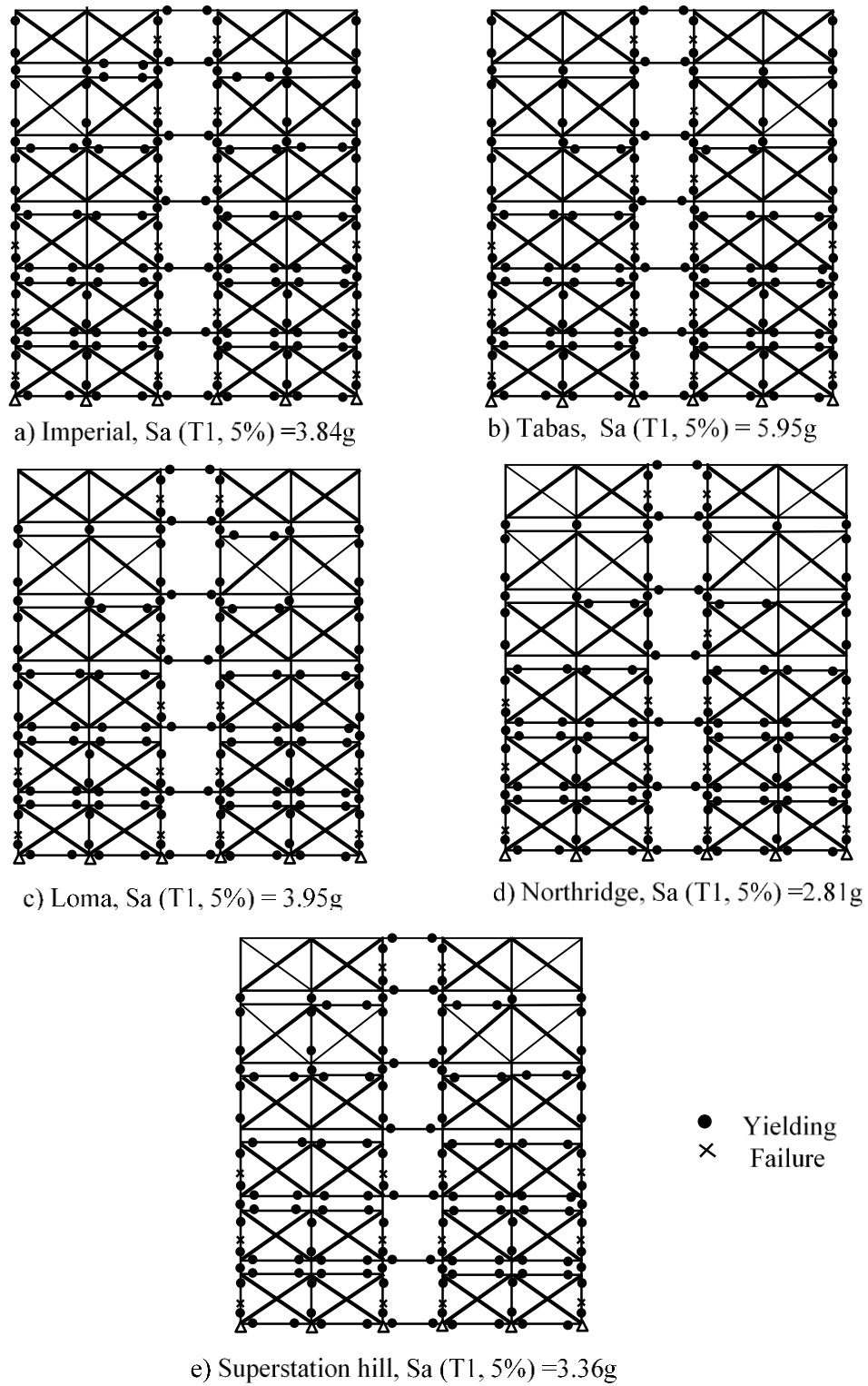


Figure 4.21: Damage distribution of Frame 5

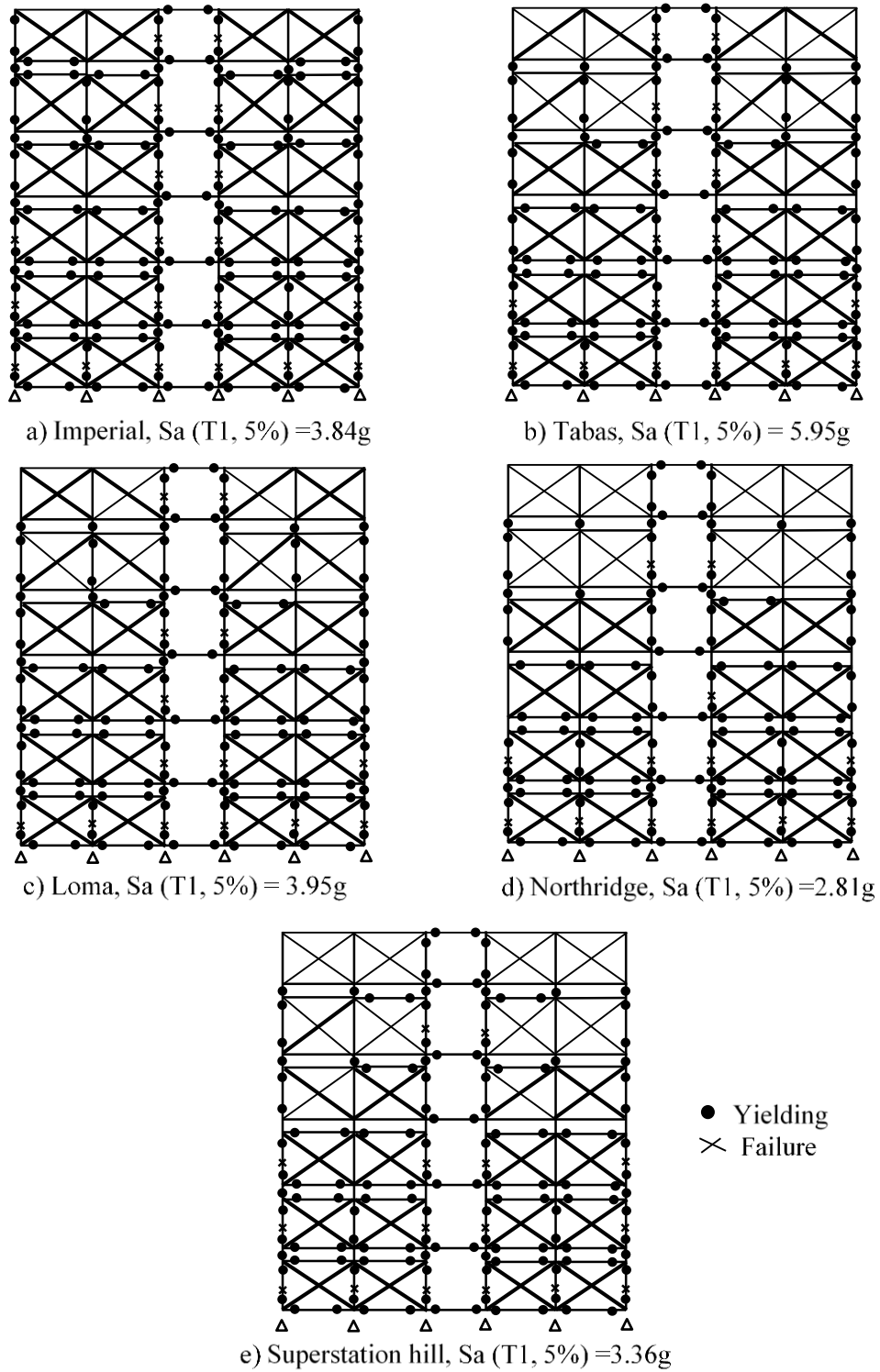


Figure 4. 22: Damage distribution of Frame 6

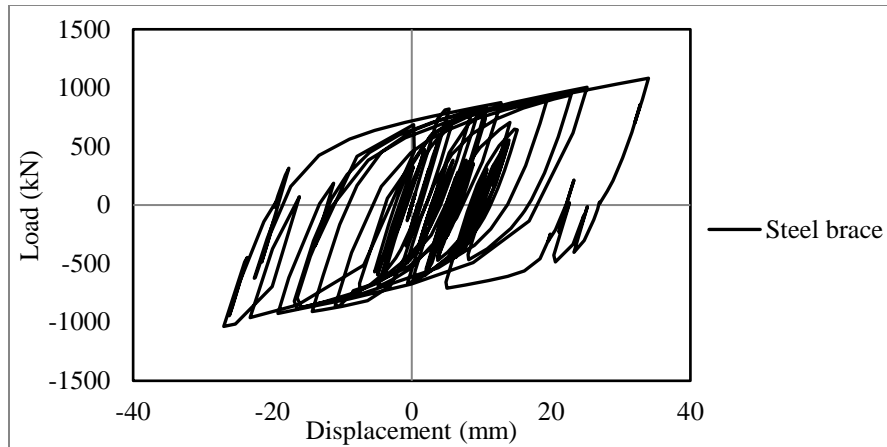


Figure 4.23 Load- deformation curve of a first storey steel brace (Frame 1) due to Tabas earthquake, $S_a(T1) = 5.95g$

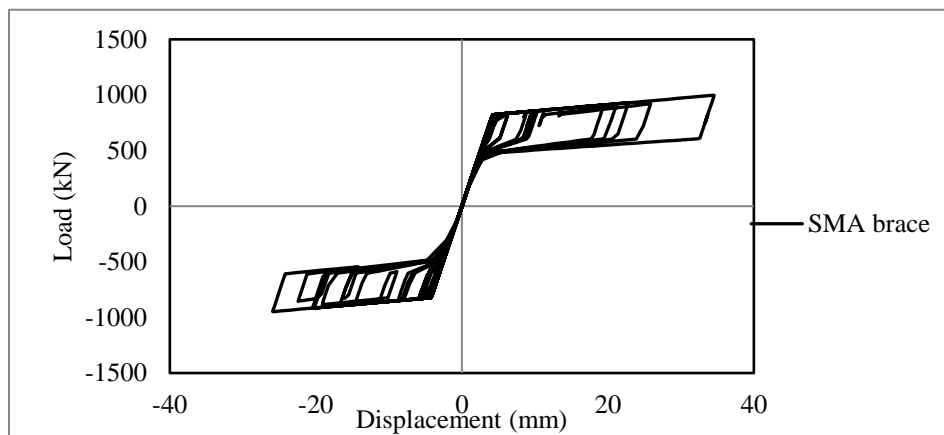


Figure 4.24 Load- deformation curve of a first storey SMA brace (Frame 2) due to Tabas earthquake, $S_a(T1) = 5.95g$

4.7 CONCLUSION

The seismic performance of MSBF equipped with superelastic SMA braces was investigated in this paper in terms of MID, MRID and damage scheme. The modeling

technique of MSBF was validated using the experimental results available in literature. A six-storey MSB was considered as a case study. IDA analysis was first conducted on a MSBF with steel braces using five different ground motions scaled to different intensities. Then, five different schemes of SMA braces were investigated. The SMA braces were designed such that the natural period of vibrations remained unchanged. Nonlinear dynamic analyses of the five different SMA frames were conducted using the same records scaled to the level that caused failure to the MSBF with steel braces. The seismic performance of the steel MSBF was compared with the SMA-MSBF frames in terms of MID, MRID and damage schemes. The specific conclusions drawn from the results of this study are summarised below:

- The MID of SMA frames are not affected significantly by the of SMA braces as compared to the steel counterpart. The increase in MID of the considered SMA frames varied from 0.34% to 8.77%.
- The MRID is highly affected by the location of the SMA braces. The study highlighted the need to use SMA braces at all floors. Replacing all the steel braces by SMA braces reduced the RID by 98.5%.
- The seismic performance of the MSBF can be improved by using SMA braces at the right locations. Among all SMA frames, the highest reduction of MRID occurred in Frame 2 where all braces were replaced by SMA braces (79.67% to 98.5%). Frame 6 where SMA braces were used in the interior bays along the building height had provided significant reduction in MRID (63.5% to 84.9%). Frame 6 was considered as a better economical solution based on cost, MID, MRID, and damage distribution compared to other frames.

- Beams and columns in the unbraced bays of MSBF were severely damaged considering all ground motions. Special care is required to design these members to facilitate the redistribution of forces after yielding of braces.

4.8 REFERENCES

- [1] C. D. Annan, M. A. Youssef, M.H. El Naggar, Seismic vulnerability assessment of modular steel building. *J. Earthq. Eng.* 13(8) (2009) 1065-1088.
- [2] C. D. Annan, M. A. Youssef, and M.H. El Naggar, Experimental evaluation of the seismic performance of modular steel-braced frames. *Eng. Struct.* 31:7(2009a) 1435-1446.
- [3] C. Ariyaratana, L.A. Fahnestock, Evaluation of buckling-restrained brace frame seismic performance considering reserve strength, *Eng. Struct.* 33 (2011), 77-89.
- [4] L.A. Fahnestock, R. Sause, J.M. Ricles, Seismic response and performance of buckling-restrained braced frames, *J. Struct. Eng.* 133 (9) (2007) 1195-1204.
- [5] R. Shabelli, S. Mahin, C. Chang, Seismic demand on steel braced frame buildings with buckling-restrained braces, *Eng. Struct.* 25(5) (2003), 655-666.
- [6] J. McCormick, J. Tyber, R. DesRoches, K. Gall, H. Maier, Structural engineering with NiTi part II: Mechanical behavior and scaling, *J. Eng. Mech.* 133(9) (2007) 1019-1029.
- [7] M. Meshally, M.A. Youssef, H.A. Elfath, Use of SMA bars to enhance the seismic performance of SMA braced RC frames, *Earthq. Struct.* 6(3) (2014) 267-280.
- [8] M. Dolce, D. Cardone, R. Marnetto, M. Mucciarelli, D. Nigro, F.C. Ponzo, G. Santarsiero, Experimental static and dynamic response of a real R/C frame upgraded with SMA recentering and dissipating braces, *Proc. 13th World Conference on Earthquake Engineering, Vancouver, Canada, 2004*, (paper no. 2878).
- [9] J. McCormick, R. DesRoches, D. Fugazza, F. Auricchio, Seismic assesment of concentrically braced steel frames with shape memory alloy braces, *J. Struct. Eng.* 133 (2007) 862-870.
- [10] A. Kari, M. Ghassemieh, S.A. Abolmaali, A new dual bracing system for improving the seismic behavior of steel structures, *Smart. Mater. Struct.* 20 (12) (2011) 125020.

- [11] A.D. Cesare, F.C. Ponzio, D. Nigro, M. Dolce, C. Moroni, Experimental and numerical behaviour of hysteretic and visco-recentring energy dissipating bracing systems, *Bull Earthquake Engineering*, 10(5) (2012) 1585–1607.
- [12] Miller, D.J., “Development and experimental validation of self-centering buckling-restrained braces with shape memory alloy”, M.Sc thesis, University of Illinois at Urbana-Champaign, 2011
- [13] M.R. Eatherton, A.L. Fahnestock, D.J. Miller, Computational study of self-centering buckling restrained braced frame seismic performance, *Earthquake Eng. Struct. Dyn.* 43 (2014) 1897-1914.
- [14] B. Asgarian, S. Moradi, Seismic performance of steel braced frames with shape memory alloy braces. *J. Constr. Steel Res.* 67 (2011), 65-64.
- [15] S. Moradi, M.S. Alam, B. Asgarian, Incremental dynamic analysis of steel frames equipped with NiTi shape memory alloy braces. *Struct. Des. Tall Special Build.* 23 (2014) 1406-1425.
- [16] J. Hu, E. Choi, Seismic design nonlinear analysis and performance evaluation of recentering buckling-restrained braced frames, *Int. J. Steel. Struct.* 14 (4) (2014) 683-695.
- [17] M. Ghassemieh, R. Kargarmoakhar, R. Response modification factor of steel frames utilizing shape memory alloys. *J. Intell. Mater. Syst. Struct.* 24(10) (2013) 1213-1225.
- [18] P. Sultana, M.A. Youssef, Seismic performance of steel moment resisting frames utilizing superelastic shape memory alloys, *J. Constr. Steel. Res.* 125 (2016) 239-251.
- [19] P. Sultana, M.A. Youssef, Prediction of local seismic damage in steel moment resisting frames, *J. Constr. Steel. Res.* 122 (2016) 122-137.
- [20] CAN/CSA-S16-01, Design of Steel Structures, Canadian Standard Association, 2001.
- [21] NBCC 2005 National building code of Canada.
- [22] SeismoStruct (version 6) - A computer program for static and dynamic nonlinear analysis of framed structures. available online from <http://www.seismosoft.com>.

- [23] M. Menegotto, P.E. Pinto, Method of analysis for cyclically loaded R.C. plane frames including changes in geometry and non-elastic behaviour of elements under combined normal force and bending. Symposium on the resistance and ultimate deformability of structures acted on by well defined repeated loads, International association for bridge and structural engineering, Zurich, Switzerland, (1973) 15-22.
- [24] F. Auricchio, E. Sacco, A one-dimensional model for superelastic shape-memory alloys with different elastic properties between austenite and martensite, *Int. J. Nonlin. Mech.* 32 (1997) 1101-1114.
- [25] D. Fugazza, Shape-memory alloy devices in earthquake engineering: mechanical properties, constitutive modelling and numerical simulations, Master's thesis, European school for advanced studies in reduction of seismic risk (ROSE School), Pavia, Italy. 2003.
- [26] R. DesRoches, J. McCormick, M. Delemont, Cyclic Properties of superelastic shape memory alloy wires and bars. *Journal of Structural Engineering*, 130(1) (2004) 38-46.
- [27] M. Wakabayashi, C. Matsui, K. Minami, I. Mitani, Inelastic behavior of Full-scale steel frames with and without bracings, *Bulletin of the disaster prevention research institute*, 24(1) (1974) 1-23.
- [28] J. Googins, S. Salawdeh, Validation of nonlinear time history analysis for single-storey concentrically-braced frames using full-scale shake table tests, *Earthq. Eng. Struct. Dyn.* 42(8) (2013) 1151-1170.
- [29] A. D'Aniello, G.L.M. Ambrosino, F. Portioli, R. Landolfo, Modelling aspects of the seismic response of steel concentric braced frames. *Steel. Compos. Struct.* 15(5) (2013) 539-566.
- [30] PEER ground motion database, Pacific earthquake engineering research center, University of California, Berkeley. USA, 2013, <http://ngawest2.berkeley.edu/>.
- [31] FEMA 356, Prestandard and commentary for the seismic rehabilitation of buildings, Federal emergency management agency, 2000.

CHAPTER 5

SEISMIC PERFORMANCE OF MODULAR STEEL BRACED FRAMES UTILIZING SUPERELASTIC SHAPE MEMORY ALLOY BOLTS IN THE VERTICAL MODULE CONNECTIONS

5.1 INTRODUCTION

Modular steel buildings (MSBs) are widely used for one-to-six storey buildings, where repetitive units are required, such as in schools, office buildings, hospitals, student residences, and military accommodations. The demand for MSBs is increasing because of their high quality, fast on-site installation, and lower cost of construction. They differ from regular steel construction in terms of detailing requirements and method of construction. Rectangular or square hollow steel sections (RHS/SHS) are commonly used as column sections in MSBs. The columns of stacked modules are connected vertically either by field welding or through a bolted connection, as shown in Figure 5.1. For a corner column, welding can only be achieved at the exterior faces. Considering bolted connections, access holes with a 50 mm diameter are needed to install the bolts [1].

Lawson and Richards [2] presented a review of modular technologies and proposed a design method for high-rise-modular buildings, which accounts for installation and construction tolerance. However, they did not discuss their seismic behaviour. Annan et al. [3-5] investigated the seismic performance of modular steel braced frames (MSBFs) that utilized field welding in their vertical connections. The seismic performance of MSBFs

was found to be significantly different from regular steel braced frames due to the existence of ceiling beams, the eccentricity developed at the joints as the braces do not intersect at a single working point, and allowed rotation at the semi-rigid welded connections between the columns of a module and the ones above or below them.

During 1994 Northridge and 1995 Kobe earthquakes, fracture of welded beam to column connections was widely observed due to changes in the base material properties, the use of weld filler metals with inherent low toughness, and the inability to detect hidden defects because of the basic connection geometry [6]. To eliminate this undesirable failure, bolted connections were recommended to replace welded connections [7-9]. Frames employing properly designed bolted connections are capable of undergoing an extensive inelastic response, with plastic hinges forming either in the connections or in the beams [6]. To force encouraging the inelastic behaviour to occur within the connection, their plastic moment should be set as a fraction of that of the connected framing elements [6].

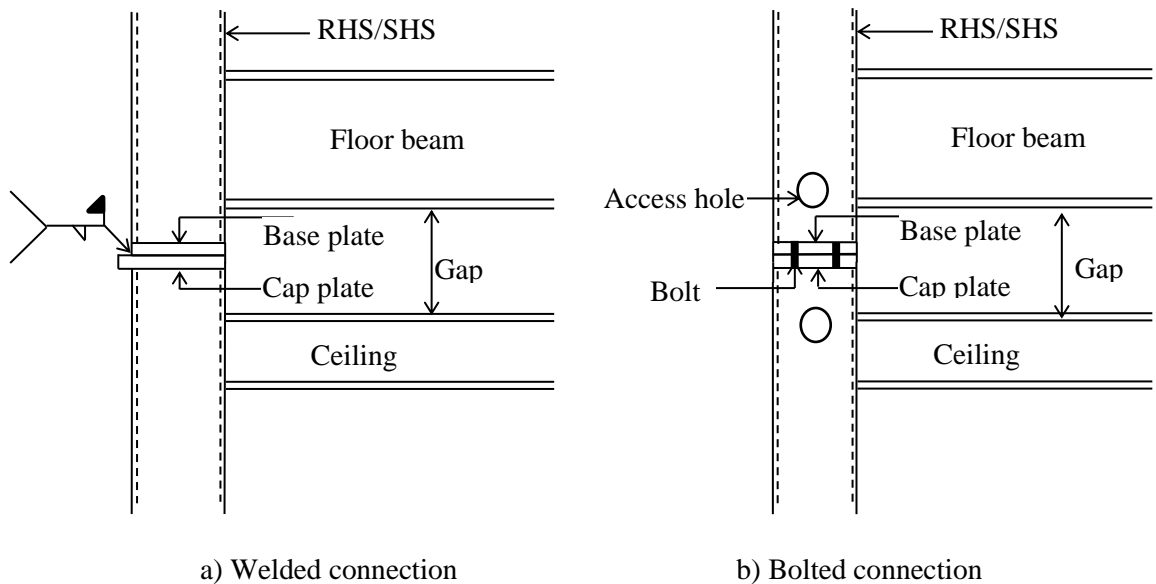


Figure 5. 1: Vertical connections between upper and lower modules

Residual drifts affect the decision to repair or demolish a seismically damaged structure [10]. Superelastic shape memory alloys (SMA) attracted the attention of researchers in recent years as a potential solution for this problem because of its self-centering capability as well as energy dissipation features. The most studied alloy is composed of Nickel and Titanium (NiTi) [11]. Superelasticity is the ability of the alloy to experience relatively high inelastic strains, and then recover its original shape when the load is removed. Researchers have investigated the seismic performance of bolted beam-to-column connections incorporating superelastic SMA material and found that they have excellent re-centering capability as well as moderate energy dissipation [12-16]. The global seismic performance of steel moment resisting frames (SMRFs) employing SMA connections was studied by DesRoches et al. [17] and Sultana and Youssef [18]. SMA connections improved the seismic performance in terms of maximum inter-storey drift, residual deformations, and damage scheme [18].

Although few research studies addressed the use of SMA bolts in SMRFs, previous research did not explore the use of superelastic SMA in the vertical connections of MSBs. This study investigates the seismic performance of MSBFs that utilize high strength steel and/or superelastic SMA bolts in their vertical connections. The possibility to use SMA connections at selected locations of the frame, and, thus reduce the associated costs is also investigated.

5.2 MODULAR STEEL BRACED FRAMES

The six-storey modular steel building selected as a case study was designed by Annan et al. [4] according to the Canadian standard CSA-S16-01 [19] and the National Building Code of Canada [20]. The plan and elevation of the MSB are shown in Figure 5.2. Each floor consists of six modular units, which are connected horizontally. Lateral forces are resisted by the external braced frames. The lateral response in the N-S direction was considered in this study. Details of the MSB design are given by Annan et al. [4]. Floor and ceiling beams were W250×33 and W100×19, respectively. Sections for the column and braces are given in Table 5.1. Braces were considered to be buckling restrained braces. The connections between beams and columns, and braces and gusset plates were achieved by welding. A clearance of 150 mm was allowed between floor beams and ceiling beams to install a fire protective layer. The welded vertical connections between the modules, which were designed by Annan et al. [4], were replaced by bolted connections. Frame 1 utilized 4-M30 high strength steel bolts in each vertical connection. The thickness of the base and cap plates was 20 mm, which ensured rigid plate behaviour.

Vertical connections of Frame 1 were redesigned by replacing the high strength steel bolts by the superelastic SMA bolts (M24) at selected locations. Five different frames were examined that had SMA vertical connections between: (1) all modules (Frame 2), (2) 1st and 2nd storey modules (Frame 3), (3) 1st and 2nd as well as 2nd and 3rd storey modules (Frame 4), (4) 1st and 2nd as well as 3rd and 4th storey modules (Frame 5), (5) 1st and 2nd as well as 4th and 5th storey modules (Frame 6). The locations of SMA connections are shown

in the Figure 5. 3. The SMA material properties used in this study are provided in Table 5.

2.

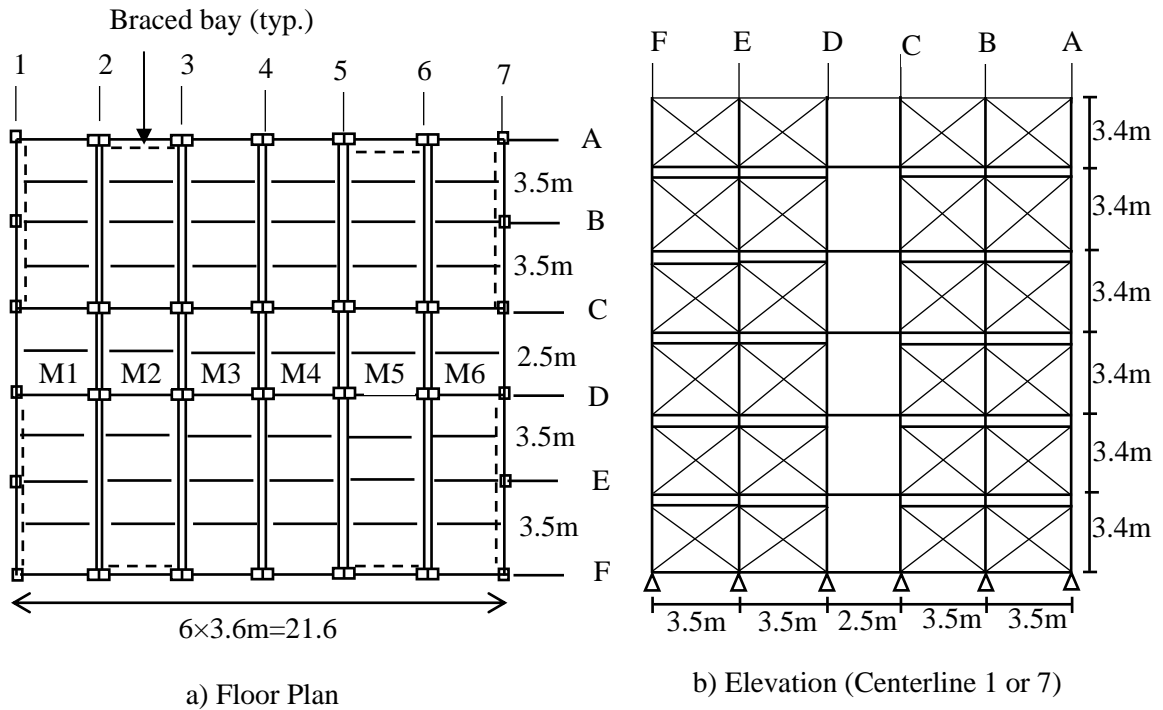


Figure 5. 2: Six-storey modular steel braced frames

Table 5. 1: Section properties of the MSBF

Storey	Column Sections	Brace Sections
Storey 6	HS 102×102×6	HS 76×76×5
Storey 5	HS 178×178×6	HS 102×102×6
Storey 4	HS 203×203×10	HS 102×102×6
Storey3	HS 305×305×10	HS 102×102×6
Storey 2	HS 305×305×13	HS 102×102×6
Storey 1	HS 305×305×13	HS 102×102×6

Table 5. 2: Material properties of SMA

Modulus of elasticity, E	40,000 MPa
Austenite –to-martensite starting stress	524 MPa
Austenite –to-martensite finishing stress	850 MPa
Martensite-to-austenite starting stress	450 MPa
Martensite-to-austenite finishing stress	200 MPa
Superelastic plateau strain length	6%

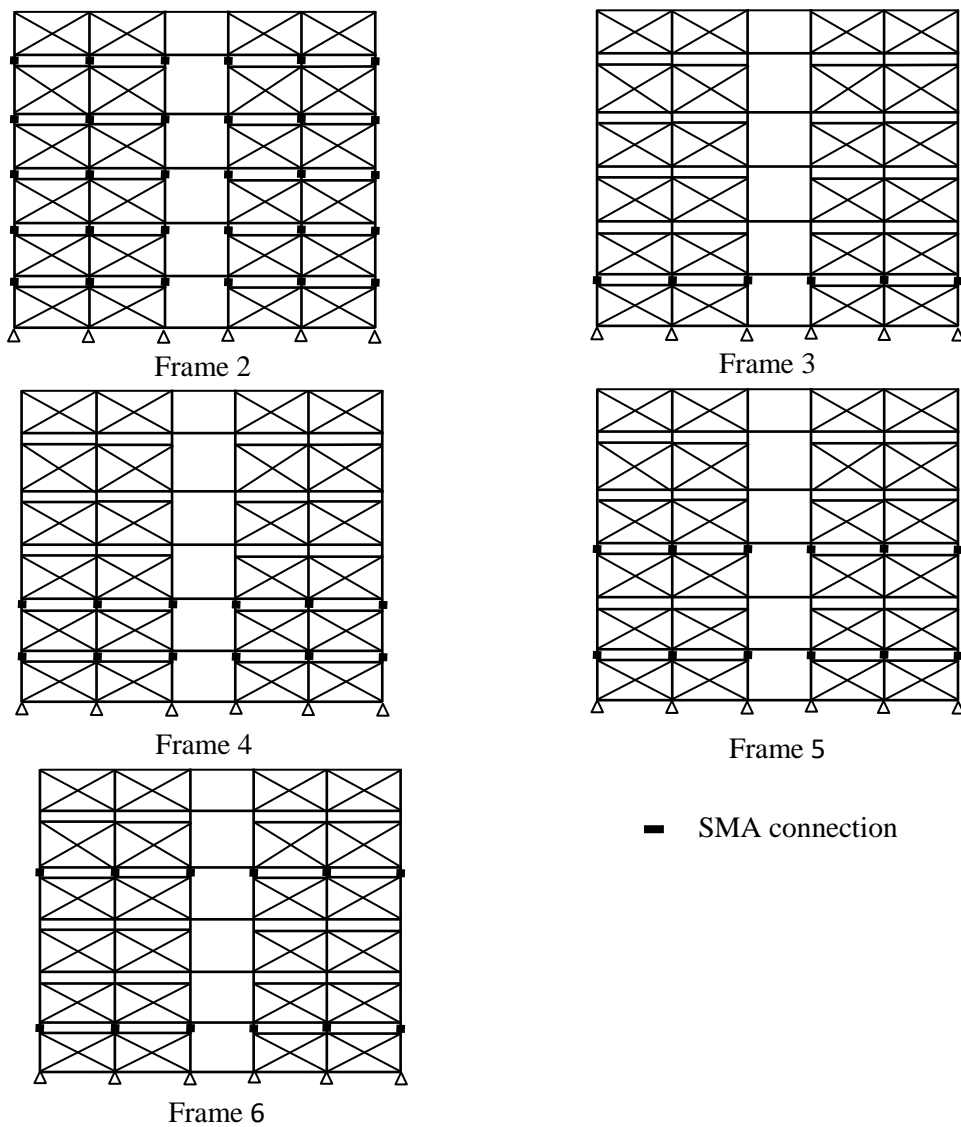


Figure 5. 3: Locations of SMA connections

5.3 FINITE ELEMENT MODELING OF MSBFS

A nonlinear two-dimensional model of the MSBF was developed using the software SeismoStruct [21]. The model was based on the fibre element approach where each fibre was assigned a uniaxial stress–strain relationship. The beams and columns were modelled using force-based inelastic frame elements. The distributed dead load and 25% of the live load were applied to the beams. The mass of each floor was converted into lumped masses at the joints. Careful attention was made to the unique detailing of the MSB. Specific modeling assumptions are given below.

- 1) As beams and columns were assumed to be connected by direct welding, rigid beam-to-column connections were utilized.
- 2) The steel and SMA braces of the MSBF were modelled using inelastic truss elements. Buckling behaviour was not modelled as braces were assumed to be buckling restrained.
- 3) Inelastic truss elements and compression only link elements were utilized to model the bolts and bearing behavior of the vertical connections, respectively.
- 4) The base and cap plates were modelled using rigid elements to simulate the rigid plate behaviour.
- 5) Rayleigh damping with a damping coefficient of 5% was assumed.

Figure 5.4 shows the finite element model of the vertical connections of the MSBFs. The $P-\Delta$ effect is included in the analysis. The material model parameters for the steel beams, columns and braces were as follows: yield stress of 350 N/mm^2 , elastic modulus of 200

kN/mm², and strain hardening of 1%. The yield strength of the steel bolts was assumed 780 MPa.

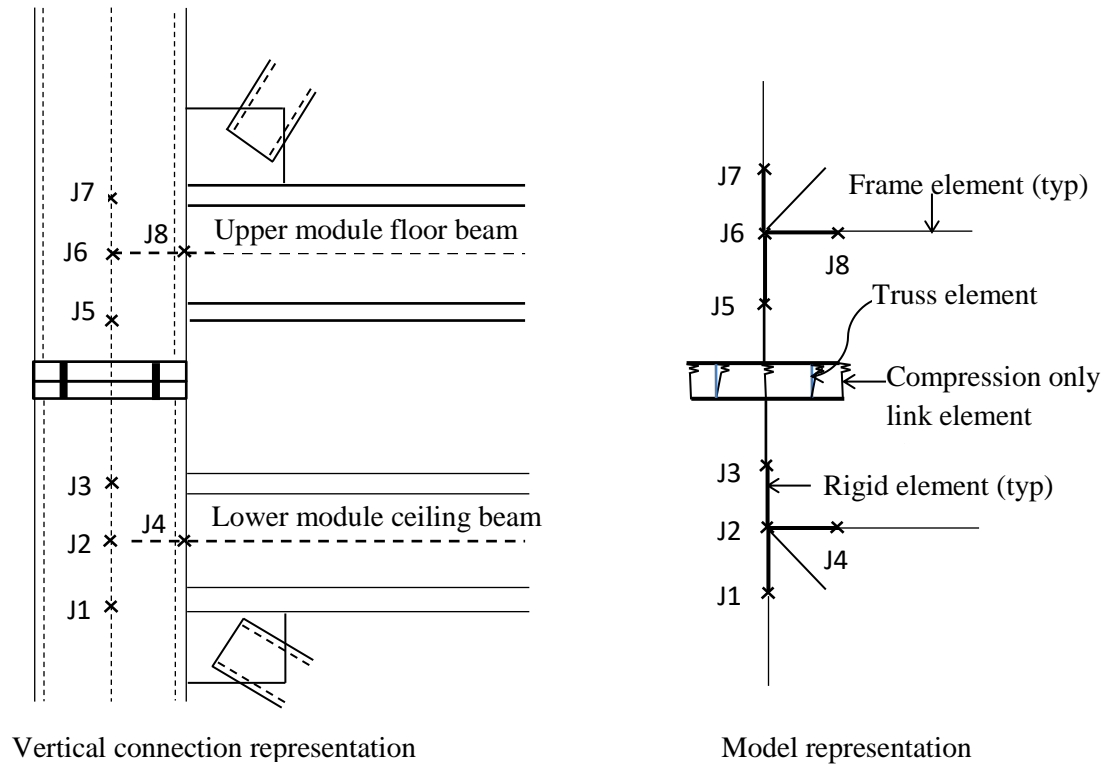


Figure 5. 4: Finite element model of MSBF

5.3.1 Validation of FE modeling technique

Three different finite element models were used to validated the modeling technique. They covered the modeling aspects that relate to (1) the unique details of MSBF, (2) the vertical bolted connections between the modules and (3) superelasticity and energy dissipation of SMA bolts. Details of these models are discussed in this section.

The one storey MSBF tested by Annan et al. [3] under cycling loading was modeled. Figures 5.5 and 5.6 show details of the frame and the FE model. Member M1 represents the 150 mm vertical clearance required for fire proofing between any two storeys. The modules were connected vertically by field welding at the outer faces of the columns. This connection allows independent rotations of the upper and lower modules. Thus, the vertical joint, j5, was simulated using a pin connection to allow this independent rotation. Figure 5.7 compares the experimental and analytical results. The maximum base shear obtained from FE analysis is lower than that obtained experimentally by 6.67%. The model was also able to accurately capture the energy dissipation characteristics and the residual drift values.

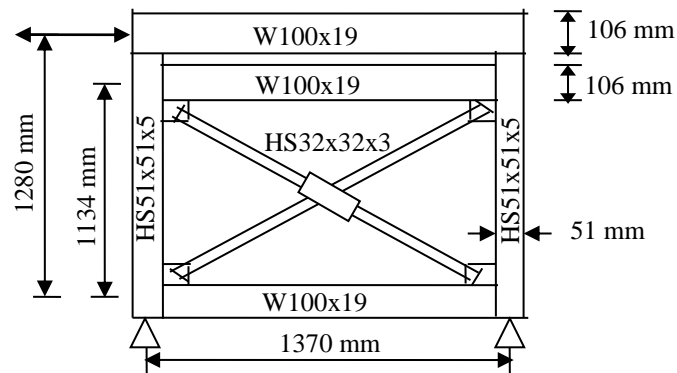


Figure 5. 5: Geometry of MSBF tested by Annan et al. [3]

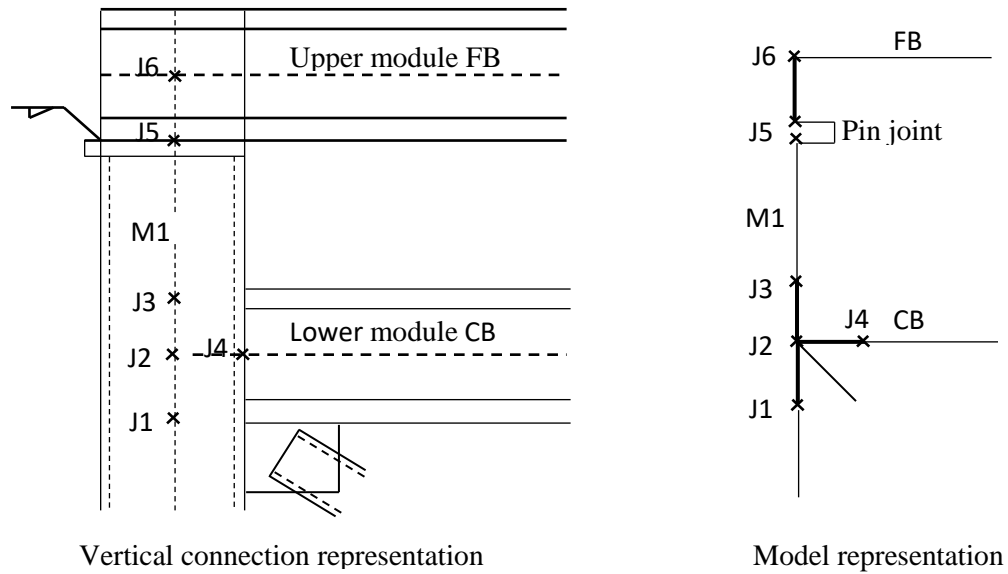


Figure 5. 6: Model of vertical connection of MSBF

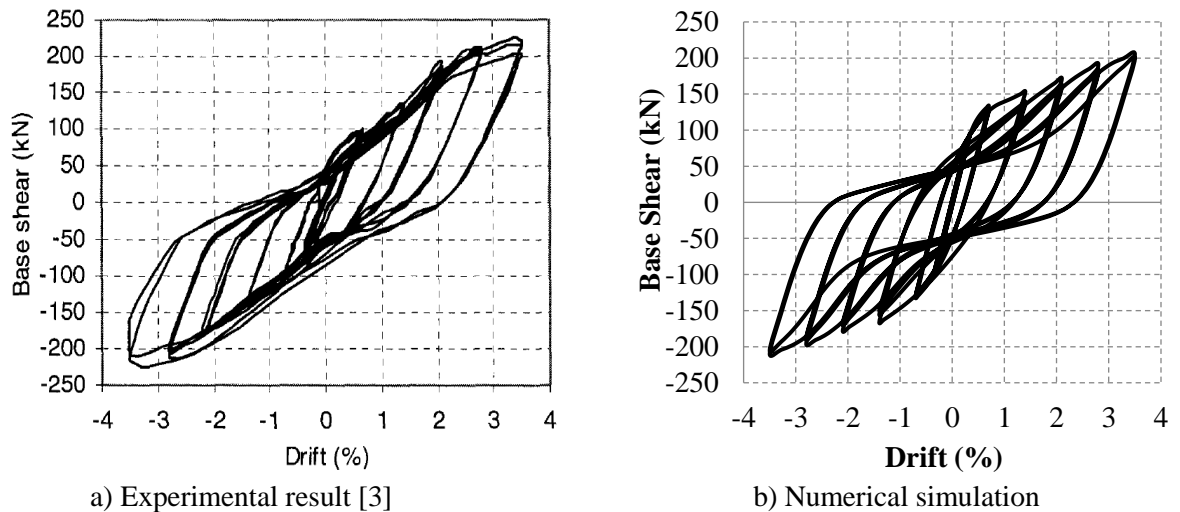


Figure 5. 7: Comparison of experimental and numerical results

Wheeler et al. [22] conducted an experimental program at the University of Sydney to investigate the moment capacity of end-plate connections in rectangular/square hollow sections (RHS/SHS). A simply supported beam spliced at mid-span section was subjected to a four-point bending test. The beam section was a square hollow section, SHS

150×150×9, and was spliced at mid-span using 4-M20 bolts, as shown in Figure 5.8. The end plates were modeled using frame elements that were rigid within the hollow section and represented the nonlinear plate stiffness outside the section. Inelastic truss elements modeled the steel bolts. Figure 5.9 shows a comparison of the numerical and experimental moment rotation behaviour of the connection and demonstrates the accuracy of the finite element model in capturing the connection behaviour. The numerical ultimate moment capacity of the connection is only 1.29% greater than the experimental value. Failure of the connection was due to tensile failure of the bolts, which agreed with the experimental results.

The interior beam-column connection that utilized superelastic SMA bars and tested by Speicher et al. [16] was modeled. Figure 5.10 shows the FE model of the SMA connection. The beams and columns were modeled using displacement based inelastic frame elements. Inelastic truss elements were used to model the SMA bars. The superelastic behaviour of SMA material was modeled using the uniaxial material model proposed by Auricchio and Sacco [23] and programmed by Fugazza [24]. Relative rotation between the beam and column elements were allowed by using hinges as shown in the Figure 5.10(b). The experimental and numerical moment-rotation responses of both connections are compared in Figures 5.11. The proposed connection model was found to be capable of predicting the moment-rotation response, energy dissipation, and residual deformations with adequate accuracy.

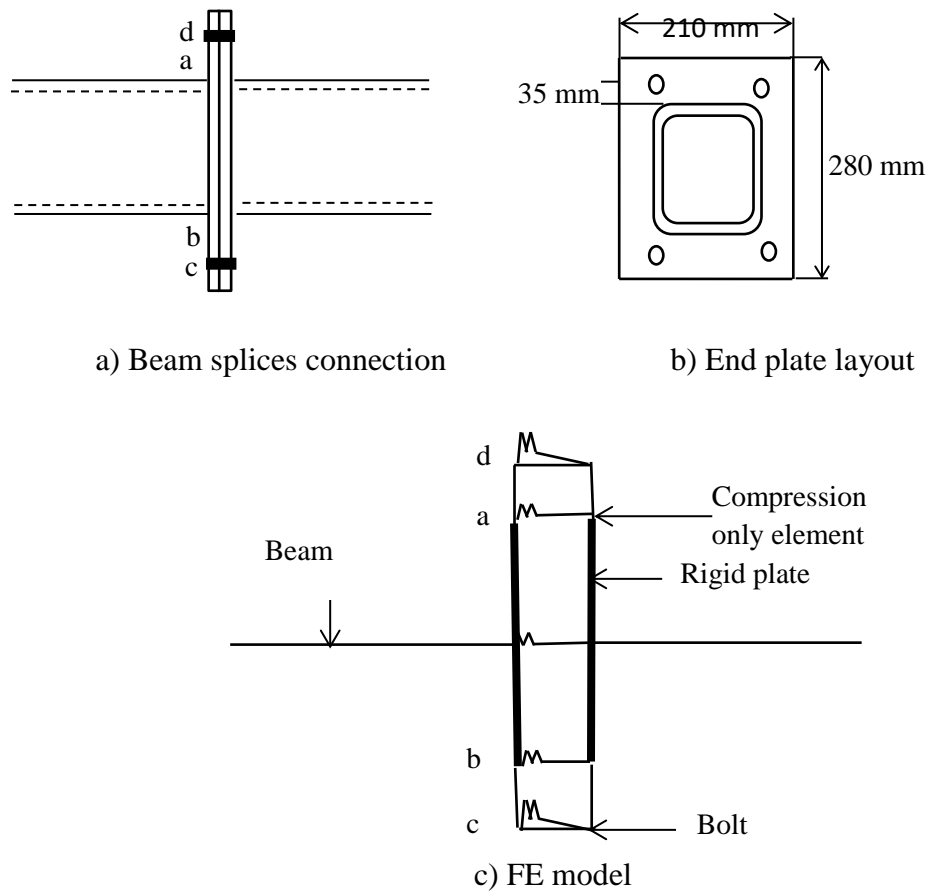


Figure 5. 8: Bolted end-plate connection

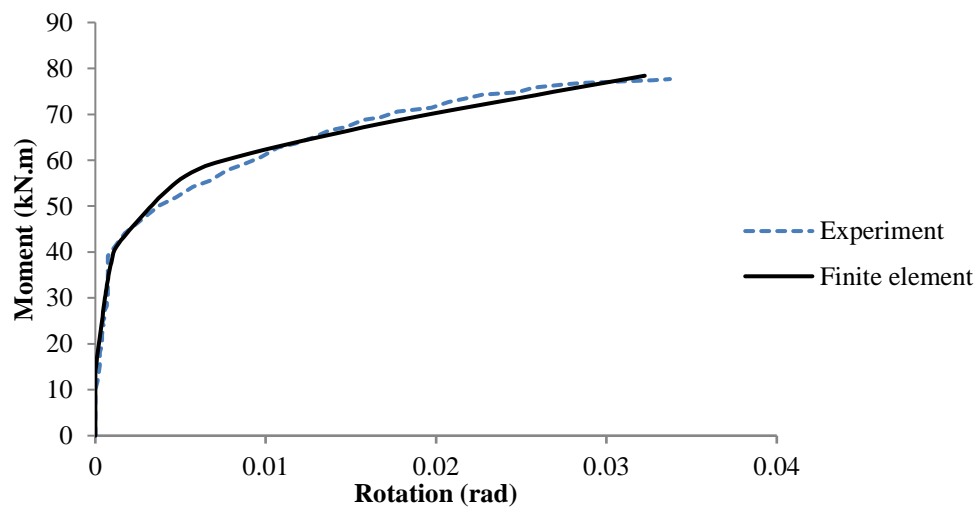


Figure 5. 9: Comparison of experimental and simulated moment rotation behaviour of bolted connection

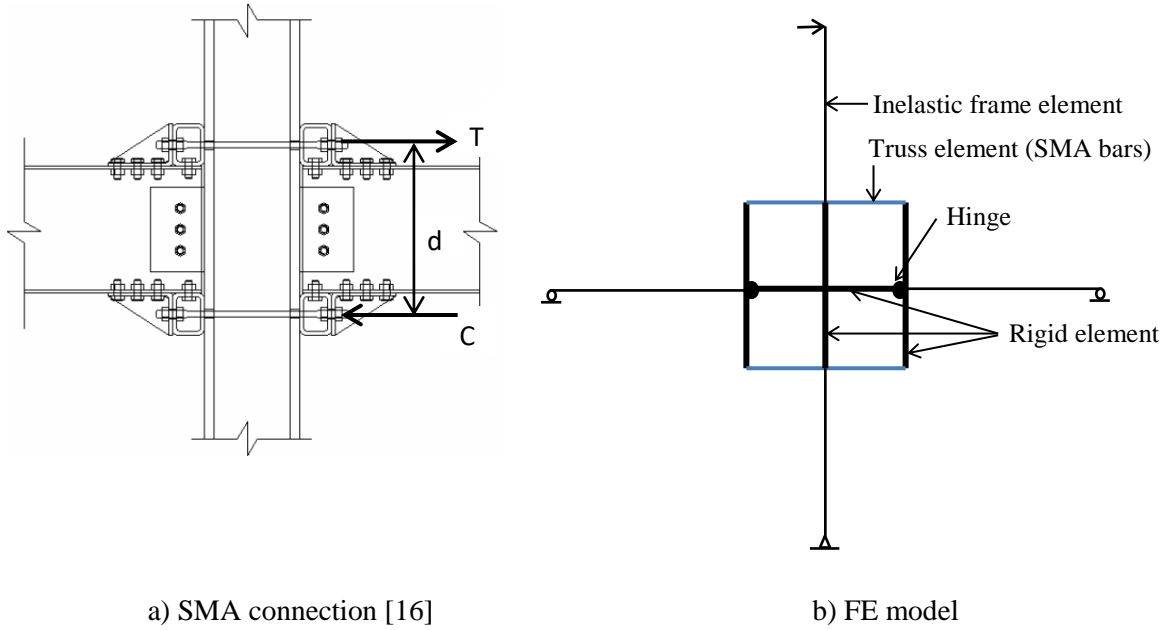


Figure 5. 10: Finite element model of superelastic SMA connection

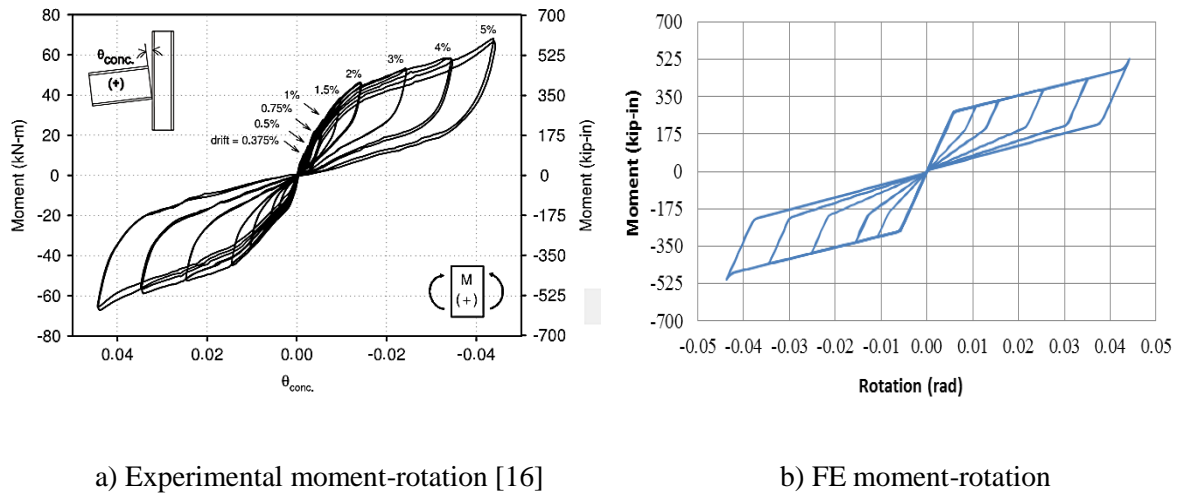


Figure 5. 11: Moment rotation behaviour of the superelastic SMA connection

5.4 MSBF WITH STEEL BOLTED VERTICAL CONNECTION

(FRAME 1)

A MSBF equipped with steel bolted connection (Frame 1) was modeled using the validated modelling technique. Eigen value analysis resulted in first and second natural periods of vibrations of 0.55 second and 0.19 second, respectively. Five different ground motions were then selected from PEER ground motion database [25], Table 5.3. The elastic response spectra of these unscaled ground motions considering 5% damping is shown in Figure 5.12. The seismic intensity is expressed in terms of the spectral acceleration at the first period of vibration [$S_a(T_1, 5\%)$]. Incremental dynamic analyses (IDA) were performed by scaling the ground motions to different intensities. IDA analyses were stopped at an earthquake intensity of 1.5g or failure of any of the steel elements. Failure of an element was assumed when its strain reaches the fracture strain (0.06). Results of the IDA at three different intensities are discussed in this section.

Table 5. 3: Characteristics of ground motions

Earthquake	Year	Ms magnitude	Station	PGA(g)
Northridge	1994	6.7	Arleta-Nordhoff	0.344
Superstition Hills-02	1987	6.5	Parachute Test Site	0.432
Loma Prieta	1989	7.1	Capitola	0.529
Tabas	1978	6.9	Tabas	0.852
San Fernando	1971	6.6	Pacoima dam	1.230

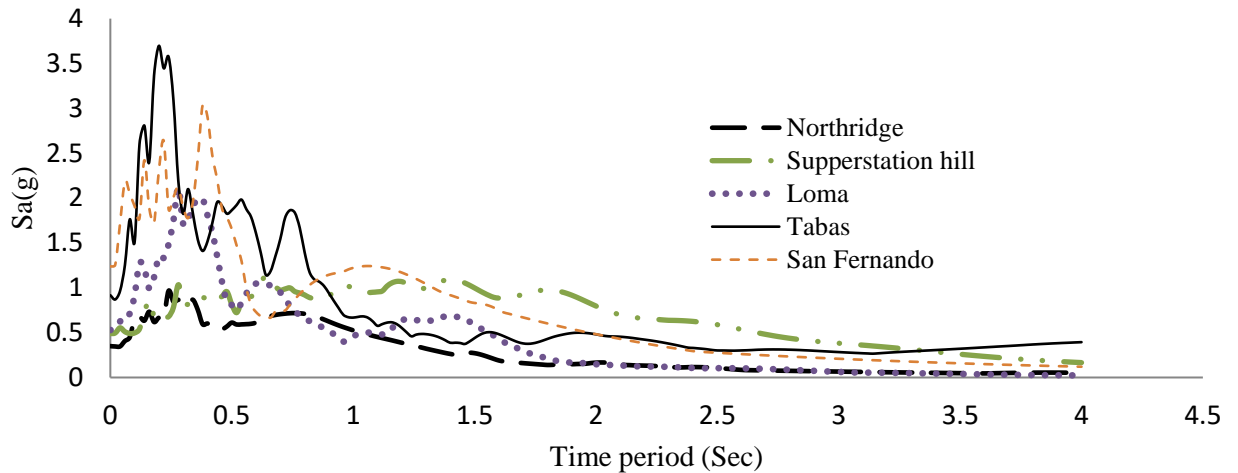


Figure 5. 12: Elastic response spectral acceleration

MID and MRID values of Frame 1 at different seismic intensities are given in Table 5.4. Their values reached 0.78% and 0.14%, respectively. MID occurred at the upper stories at seismic intensities lower than 1.2g. However, at higher seismic intensities, it occurred at the first storey leading to a soft first storey failure mechanism. The storey experiencing the MID was not always the storey experiencing the MRID. The 1st storey experienced the MRID for twelve of the conducted fifteen analyses. Figure 5.13 shows the damage distribution of Frame 1. The beams in the unbraced bays yielded in all cases. Yielding of the braces was observed in the first four stories due to Tabas (1.5g), Northridge (1.3g) and San Fernando (1.5g) earthquakes, and in the first three stories due to Loma (1.3g) and Superstition Hills (1.5g) earthquakes. Yielding of a 1st storey column was also observed in case of Tabas, Northridge, and Superstition Hills earthquakes. The first floor experienced more damage when compared to the remaining floors as was reflected in the large inelastic brace deformations as well as column yielding.

Table 5. 4: MID and MRID of Frame 1 at different intensity of ground motions

Earthquakes	Sa (T1,5%)	MID%	MRID%
Northridge	1.0g	0.54 (4 th storey)	0.01 (6 th storey)
	1.2g	0.62 (5 th storey)	0.03 (1 st storey)
	1.3g	0.67 (1 st storey)	0.10 (1 st storey)
Superstition Hills	1.0g	0.46 (4 th storey)	0.01(2 nd storey)
	1.2g	0.54 (4 th storey)	0.03 (1 st storey)
	1.5g	0.78 (1 st storey)	0.14 (1 st storey)
Loma	1.0g	0.45 (3 rd storey)	0.02 (1 st storey)
	1.2g	0.58 (1 st storey)	0.07 (1 st storey)
	1.3g	0.68 (1 st storey)	0.07 (1 st storey)
Tabas	1.0g	0.58 (6 th storey)	0.01 (6 th storey)
	1.2g	0.67 (6 th storey)	0.04 (1 st storey)
	1.5g	0.74 (6 th storey)	0.09 (1 st storey)
San Fernando	1.0g	0.51 (6 th storey)	0.01 (1 st storey)
	1.2g	0.58 (6 th storey)	0.03 (1 st storey)
	1.5g	0.69 (1 st storey)	0.02 (1 st storey)

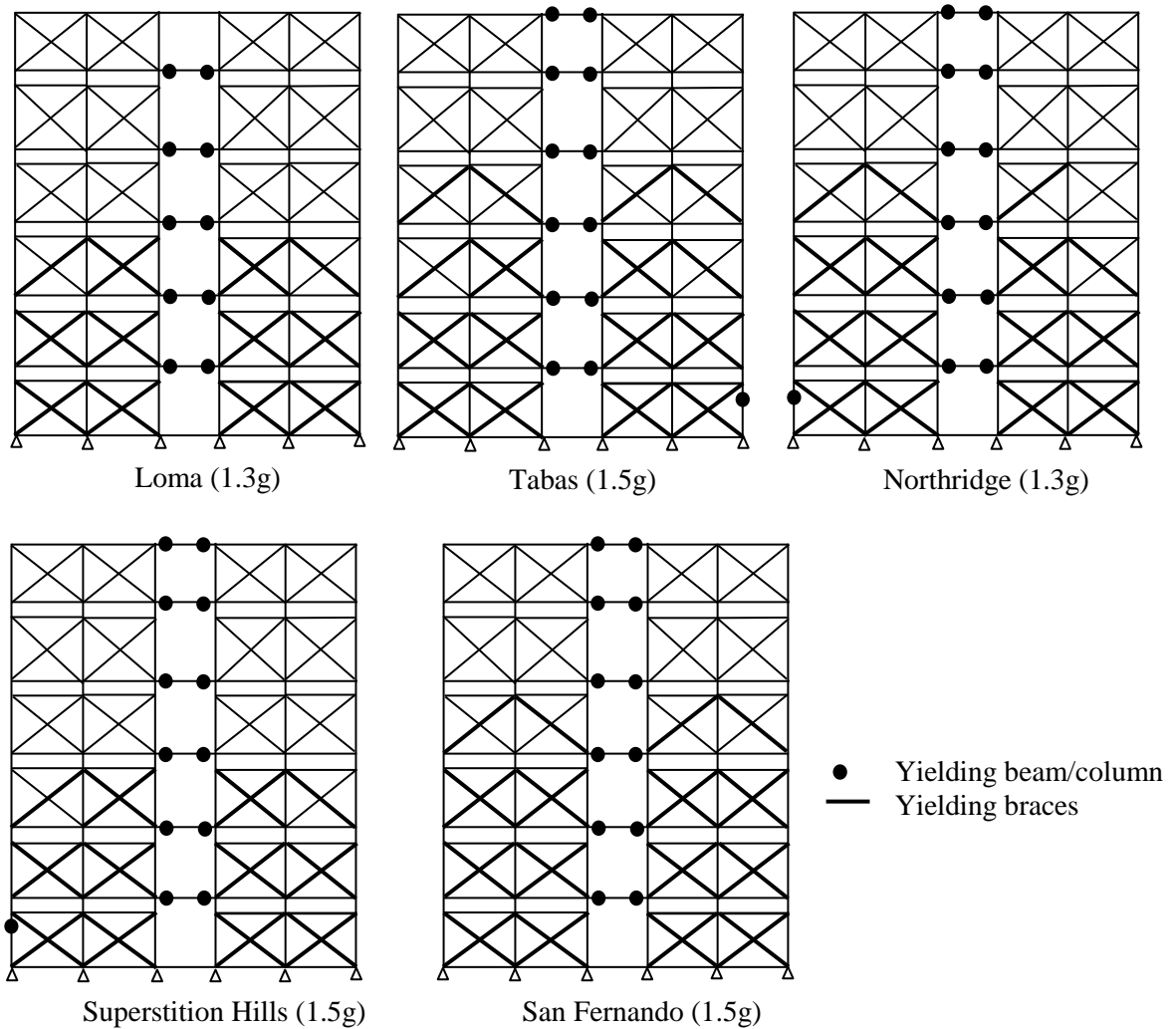


Figure 5.13: Damage distribution of Frame 1

5.5 MSBF EQUIPPED WITH SMA BOLTED VERTICAL CONNECTIONS

Nonlinear dynamic time history analysis was performed considering the same ground motions at the same intensities for Frame 1. The values of MID and MRID of the different frames considering different earthquake intensities are compared in Figures 5.14-5.18. Using SMA connections did not only change the values of MIDs and MRIDs, but also

changed the locations of stories experiencing these values. The maximum values of MID (0.87%) and MRID (0.11%) were observed in Frame 2. The percentage difference between the observed MID and MRID for Frames 2 to 6 as compared to Frame 1 are presented in Table 5.6. The use of SMA bolts in the vertical connections increased the MID considering Northridge and Tabas earthquakes and reduced it considering San Fernando earthquake. The seismic intensity influenced the MID values. For example, in case of Superstition Hills earthquake, the MID of the SMA frames increased with increasing the intensity from 1.0g to 1.2g and decreased at an intensity of 1.5g. The highest increase in MID (25.5%) occurred at Frame 2, whereas the highest reduction (15.47%) occurred in Frame 3. It is clear that the number of SMA connections, their locations, and the earthquake intensity affected the values of MIDs.

The MRIDs were significantly reduced by using SMA in vertical connections as shown in Figures 5.14 to 5.18. The reductions in MRID values were 91.5%, 82.9%, 87.1%, 85.6%, and 84.5% for Frames 2, 3, 4, 5 and 6, respectively. The reduction of MRID depends on the number and the locations of SMA connections as well as the ground motion and its intensity. The reduction in the MRID in Frame 2 increased from 30.0% to 91.5% when the intensity of Tabas earthquake increased from 1.0g to 1.5g.

The average values of the percentage changes of MID and MRID for the different SMA frames were also compared in Table 5.6. The influence of SMA bolts on reducing MRID is clear up to an earthquake intensity of 1.2g. The maximum average reduction (73.8%) occurred in Frame 4. At seismic intensity of 1.3g or more, the average reduction in MRID (46.06%) occurred in Frame 5.

Utilizing SMA at the carefully chosen locations plays a vital role in reducing the residual drifts. Using SMA bolts increased the MRID for the Frames 3 and 6 considering Northridge earthquake and Frames 2, 3, 5, and 6 considering Loma earthquake at an intensity 1.3g. This highlights that using SMA at the wrong locations might worsen the seismic performance. Frame 4 showed better seismic performance compared to other SMA frames as reduction in MRID occurred in all cases with an average of 57.36%.

ID and RID distributions along building height are shown in Figures 5.19 to 5.23. It was observed that the IDs for Frames 2 to 6 were very similar, however, the RIDs were significantly different. Utilizing SMA in the vertical connections redistributed the seismic forces in the frame, and, thus significantly reduced the residual drifts of the 1st storey. However, this reduction was not pronounced in other storeys of the SMA frames.

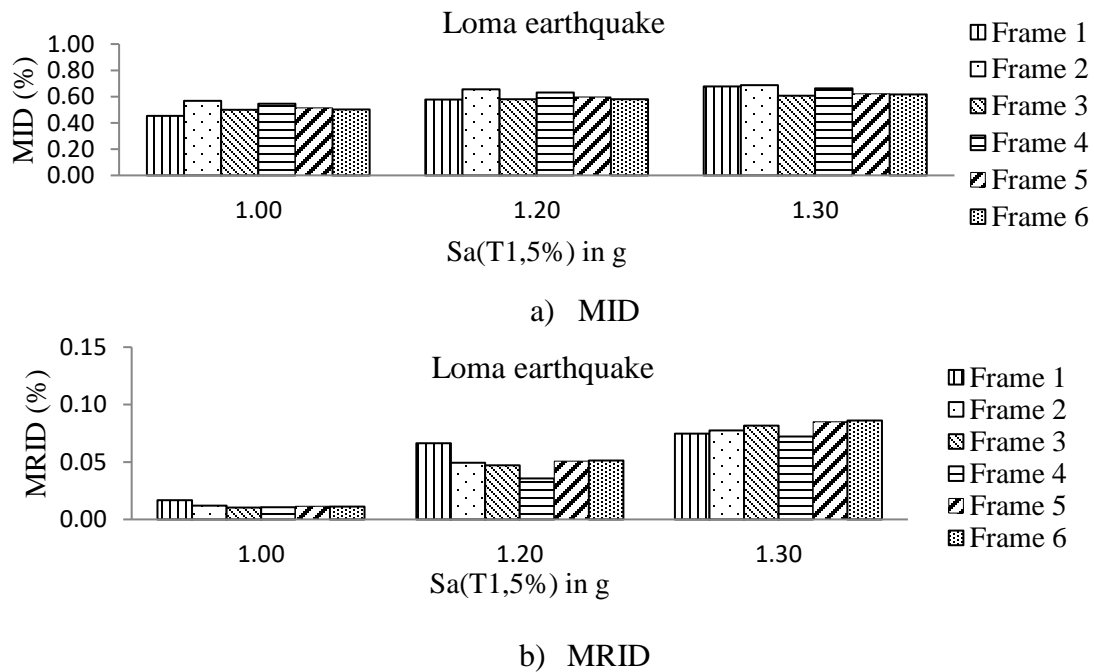


Figure 5. 14: Drifts considering Loma earthquake

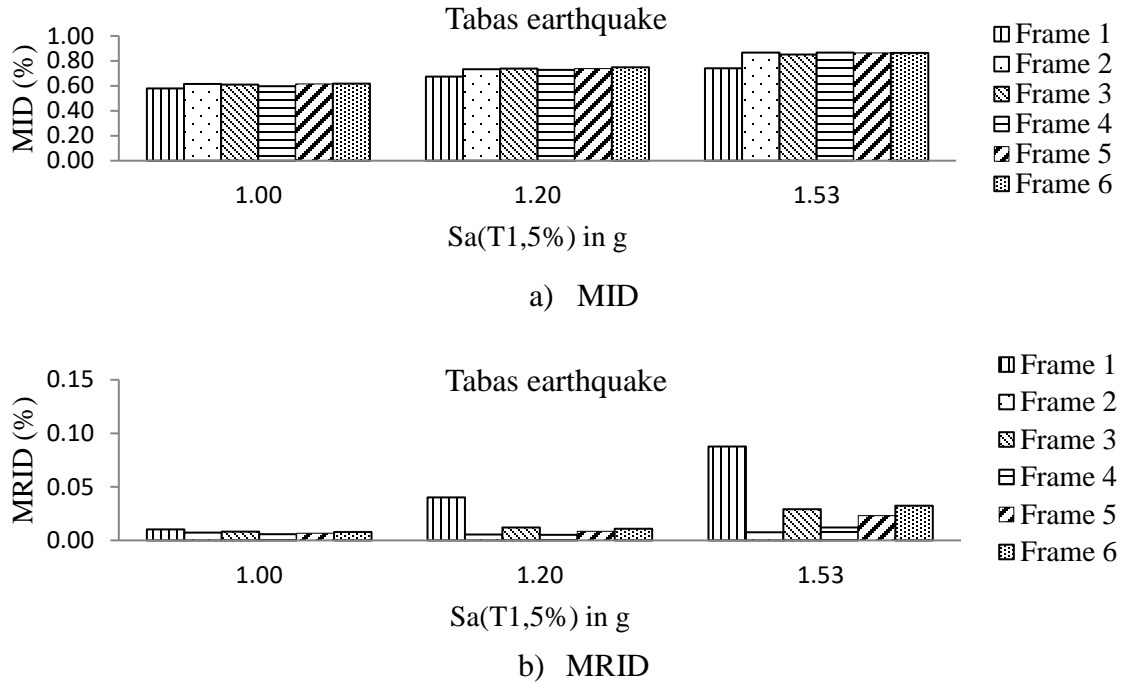


Figure 5. 15: Drift considering Tabas earthquake

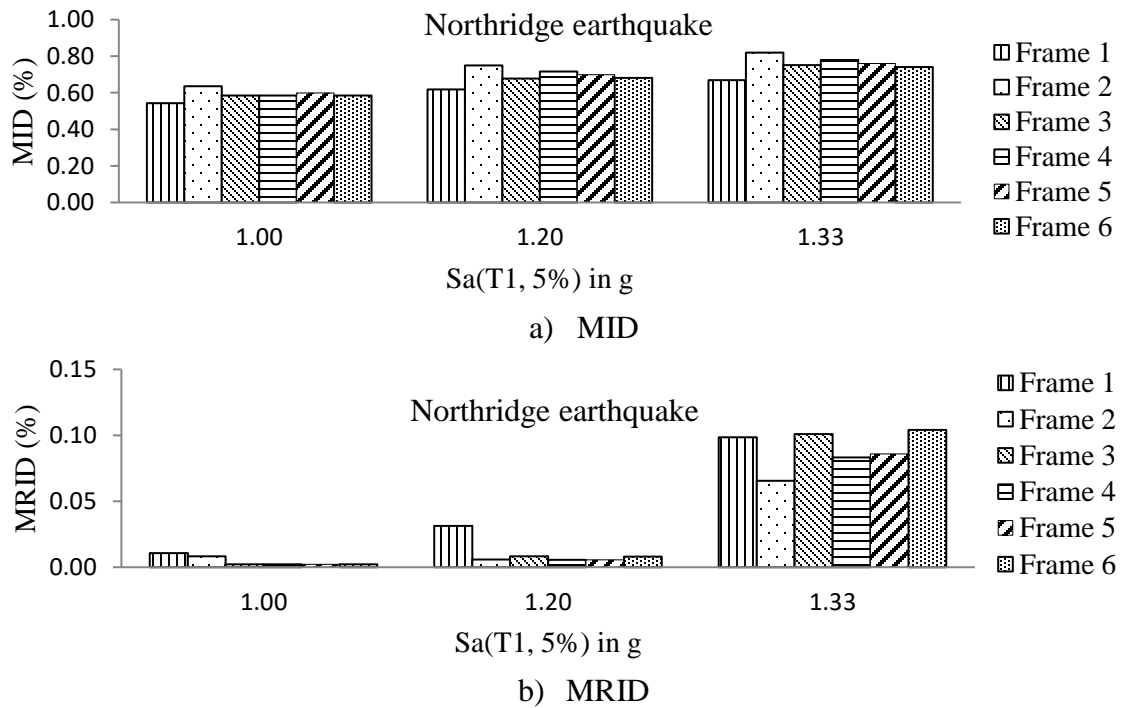


Figure 5. 16: Drifts considering Northridge earthquake

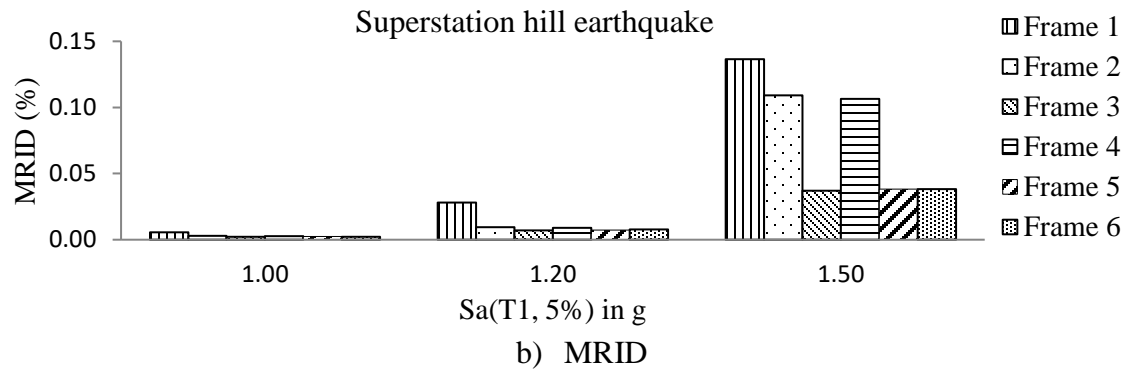
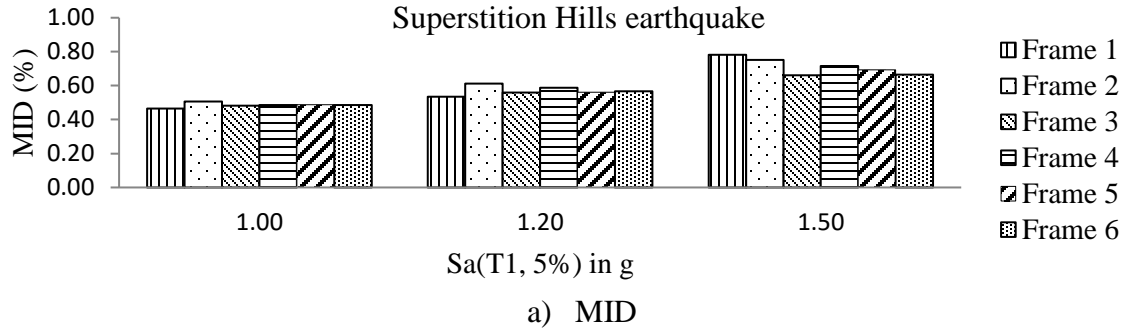


Figure 5. 17: Drifts considering Superstition Hills earthquake

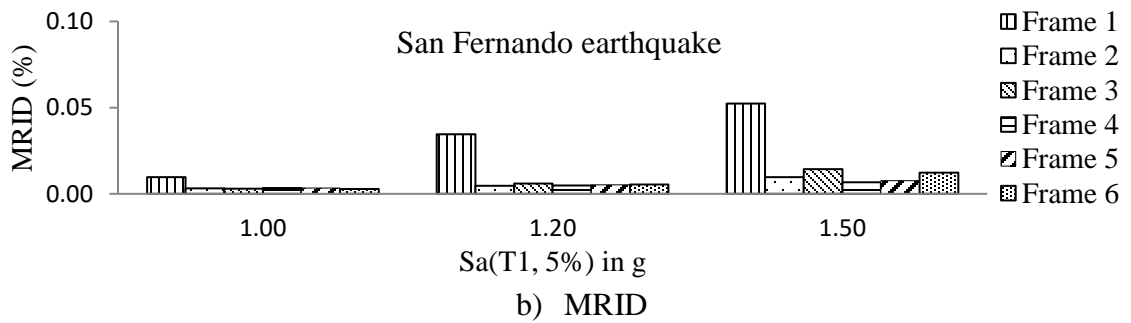
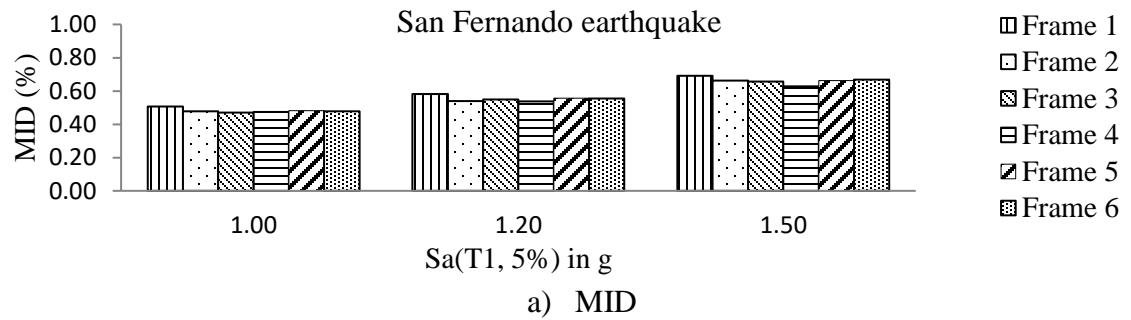


Figure 5. 18: Drifts considering San Fernando earthquake

Table 5. 5: Percentage change of MID and MRID of SMA frames

Ground motion	Intensity	Frame 2		Frame 3		Frame 4		Frame 5		Frame 6	
		Sa(T1,5%) in g	MID change (%)	MRID change (%)	MID change (%)	MRID change (%)	MID change (%)	MRID change (%)	MID change (%)	MRID change (%)	MID change (%)
Loma	1	25.5	-28.2	10.5	-39.1	20.3	-36.4	13.3	-32.7	11.0	-34.1
	1.2	13.9	-25.7	0.52	-29.2	9.3	-46.1	3.6	-23.6	0.7	-23.0
	1.3	1.4	3.4	-10.2	9.3	-1.9	-3.7	-7.9	13.8	-8.8	15.3
Tabas	1	6.3	-30.0	5.5	-21.7	3.0	-43.1	6.1	-36.3	6.7	-22.4
	1.2	9.1	-86.2	9.5	-69.9	8.1	-86.9	9.6	-78.9	11.2	-72.9
	1.53	17.1	-91.5	14.8	-66.7	16.8	-86.2	16.5	-73.7	16.7	-63.2
Northridge	1	17.0	-23.1	7.5	-79.3	7.5	-79.3	10.1	-79.8	7.7	-79.6
	1.2	21.2	-81.5	9.5	-73.4	15.7	-81.8	12.9	-81.9	10.1	-74.2
	1.33	22.5	-33.6	12.3	2.4	16.5	-15.5	13.8	-12.9	10.7	5.6
Superstation	1	8.9	-46.5	3.5	-63.0	4.6	-53.0	4.8	-58.2	4.5	-59.8
	1.2	14.4	-66.2	4.4	-75.3	9.9	-68.2	4.9	-74.2	5.9	-72.6
	1.5	-3.8	-19.9	-15.5	-72.9	-8.3	-21.9	-11.2	-71.9	-14.9	-71.9
San Fernando	1	-5.5	-66.8	-7.0	-69.8	-6.3	-65.4	-4.8	-65.9	-5.4	-70.2
	1.2	-7.2	-86.6	-5.8	-82.9	-7.8	-86.1	-4.3	-84.9	-4.8	-84.5
	1.5	-4.1	-81.5	-5.0	-72.6	-9.1	-87.1	-4.0	-85.6	-3.4	-76.4
Average	1.0g	10.4	-38.9	4.0	-54.6	5.8	-55.4	5.9	-54.6	4.9	-53.2
	1.2g	10.3	-69.3	3.6	-66.1	7.0	-73.8	5.4	-68.7	4.6	-65.4
	1.3g to 1.5g	6.6	-44.6	-0.7	-40.1	2.8	-42.9	1.4	-46.1	0.1	-38.1
	all	9.1	-50.9	2.3	-53.6	5.2	-57.4	4.2	-56.4	3.2	-52.3

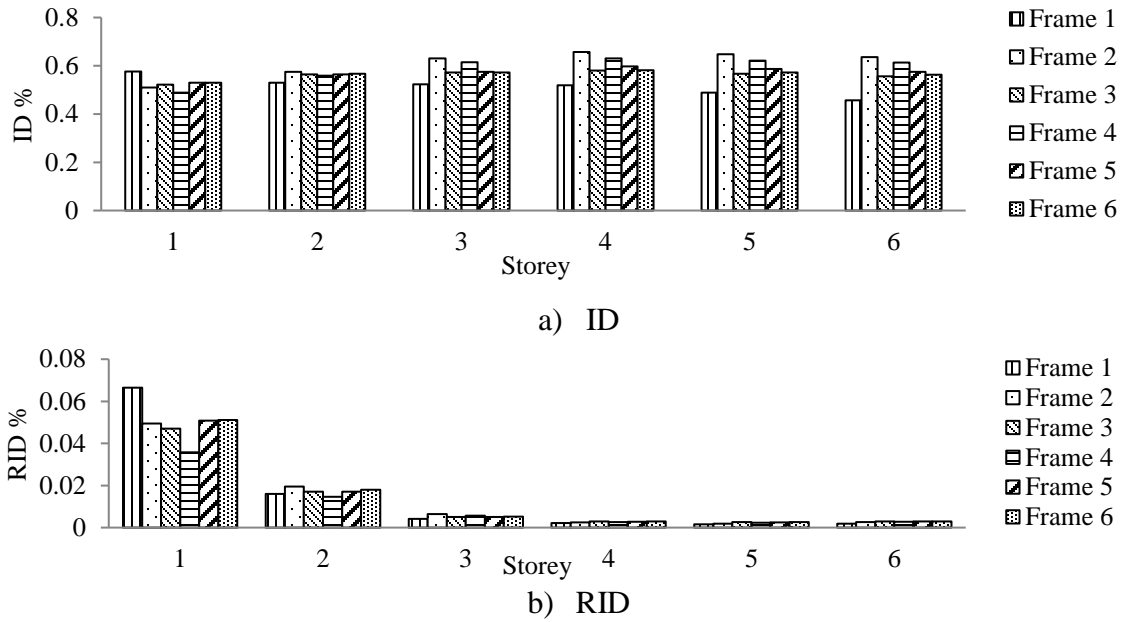


Figure 5. 19: ID and RID distribution considering Loma earthquake at $S_a(T_{1,5\%})=1.2g$

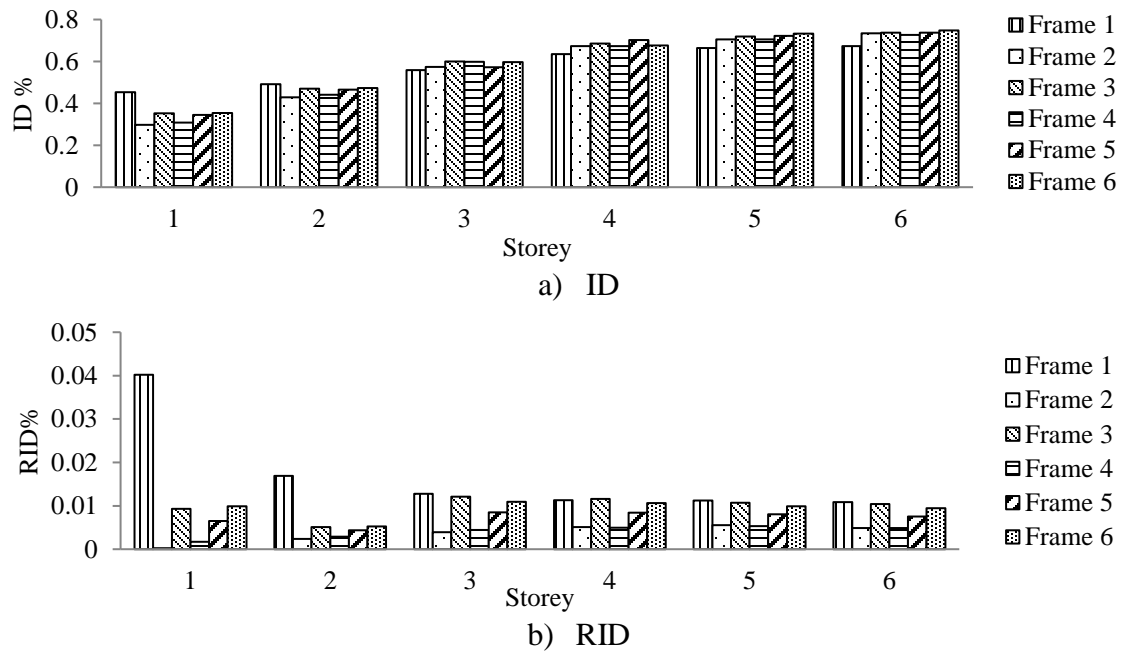


Figure 5. 20: ID and RID distribution due to Tabas earthquake at $S_a(T_{1,5\%})=1.2g$

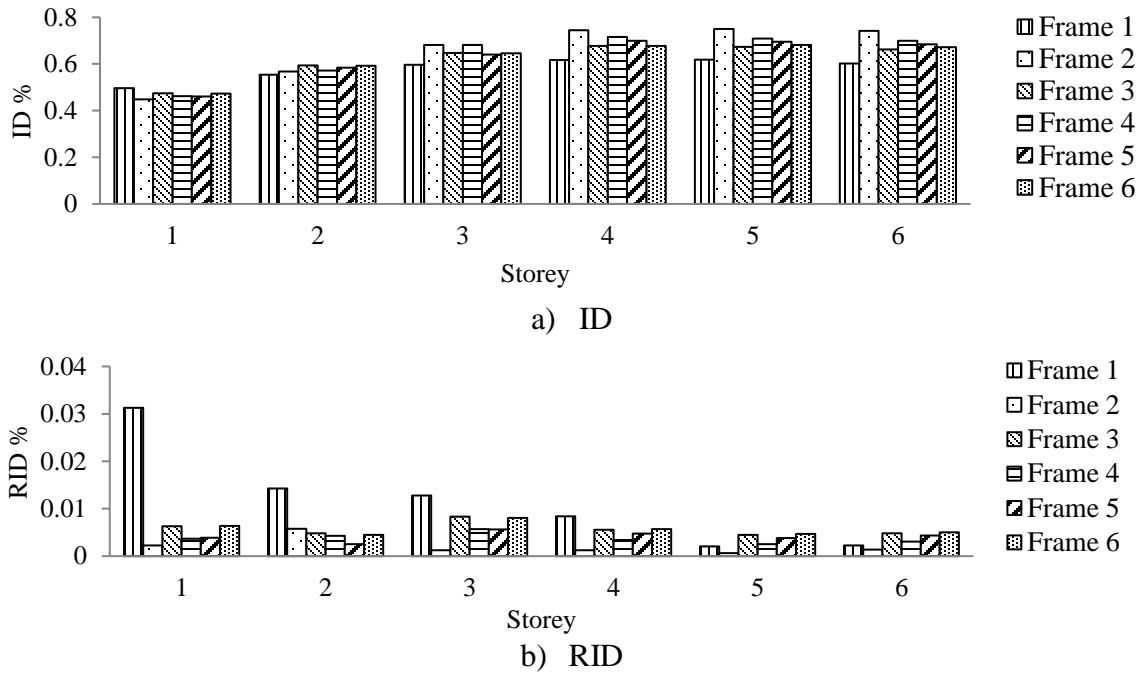


Figure 5. 21: ID and RID distribution due to Northridge earthquake at $S_a(T_{1,5\%})=1.2g$

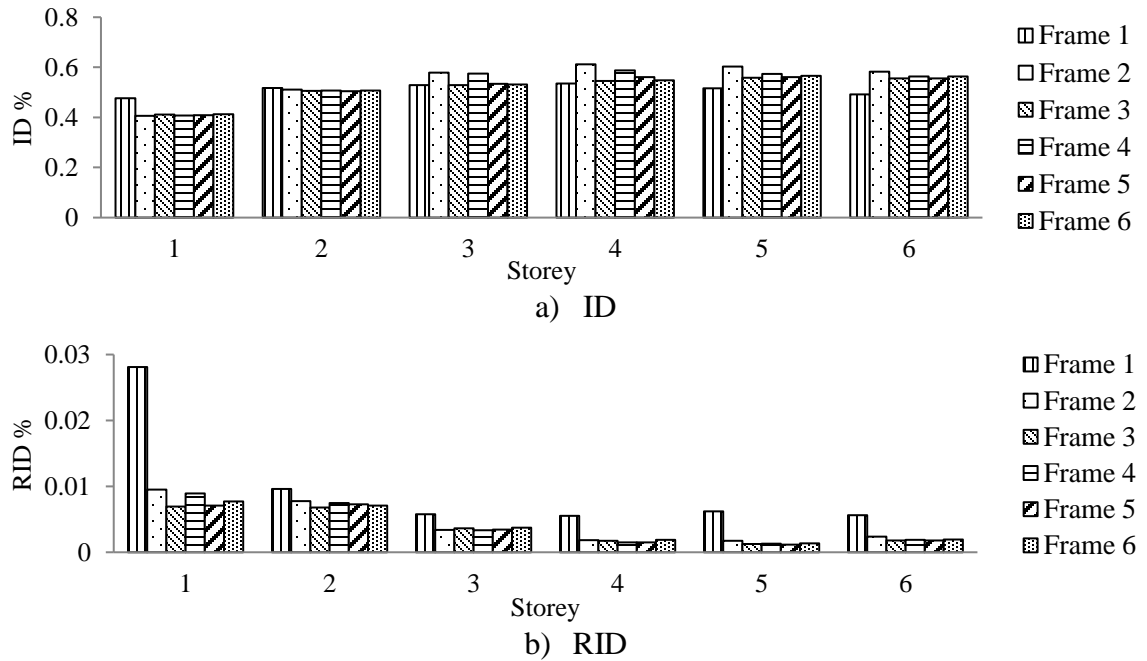


Figure 5. 22: ID and RID distribution due to Superstition Hills earthquake at $S_a(T_{1,5\%})=1.2g$

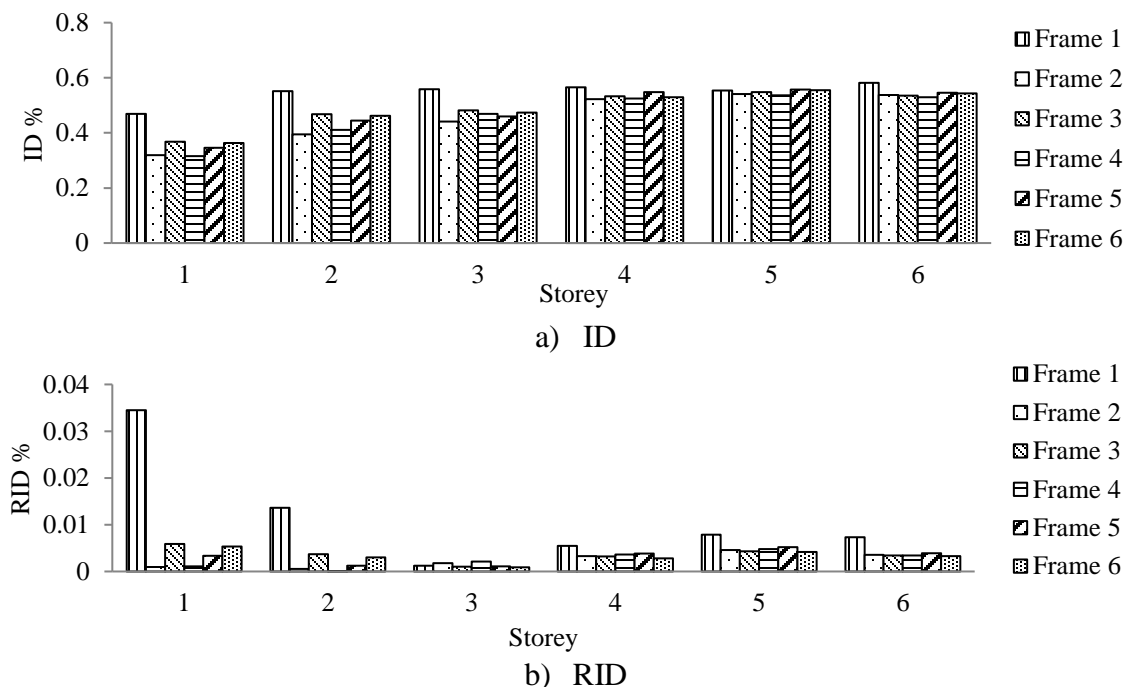


Figure 5. 23: ID and RID distribution due to San Fernando earthquake at $S_a(T_{1,5\%})=1.2g$

Figures 5.24 to 5.28 show the damage distribution of the five selected SMA frames. Yielding of the beams of the unbraced bays is observed for all records. All other beams remained elastic. Braces up to fourth stories were yielded while braces of the top two storeys remained elastic. The lowest numbers of yield braces were in Frame 2 due to Tabas and San Fernando records, in Frame 4 due to Loma and Superstition Hills records, and in Frame 5 due to Northridge record. Yielding of columns of SMA frames was observed for the considered earthquakes except San Fernando. A 1st storey column yielded in all frames due to Superstition Hills (1.5g) earthquake and in Frames 2 and 4 due to Loma earthquakes (1.3g). In case of Tabas earthquake (1.5g), yielding of column was observed in the 1st and 5th stories of Frames 3 and 6. Among all SMA frames, Frame 2 experienced less damage

due to Tabas, Northridge, and San Fernando, Frame 3 due to Loma, and Frame 4 due to Superstition Hills earthquakes.

Considering the cost of SMA materials at one hand and the seismic performance in terms of MID, MRID and damage distribution on the other hand, Frame 4 can be judged as the most suitable solution. Figure 5.29 compares the rotation of a critical vertical connection of the 1st floor of Frame 4 with that of Frame 1. It is observed that the SMA connections showed excellent recentering capability compared with the steel connections.

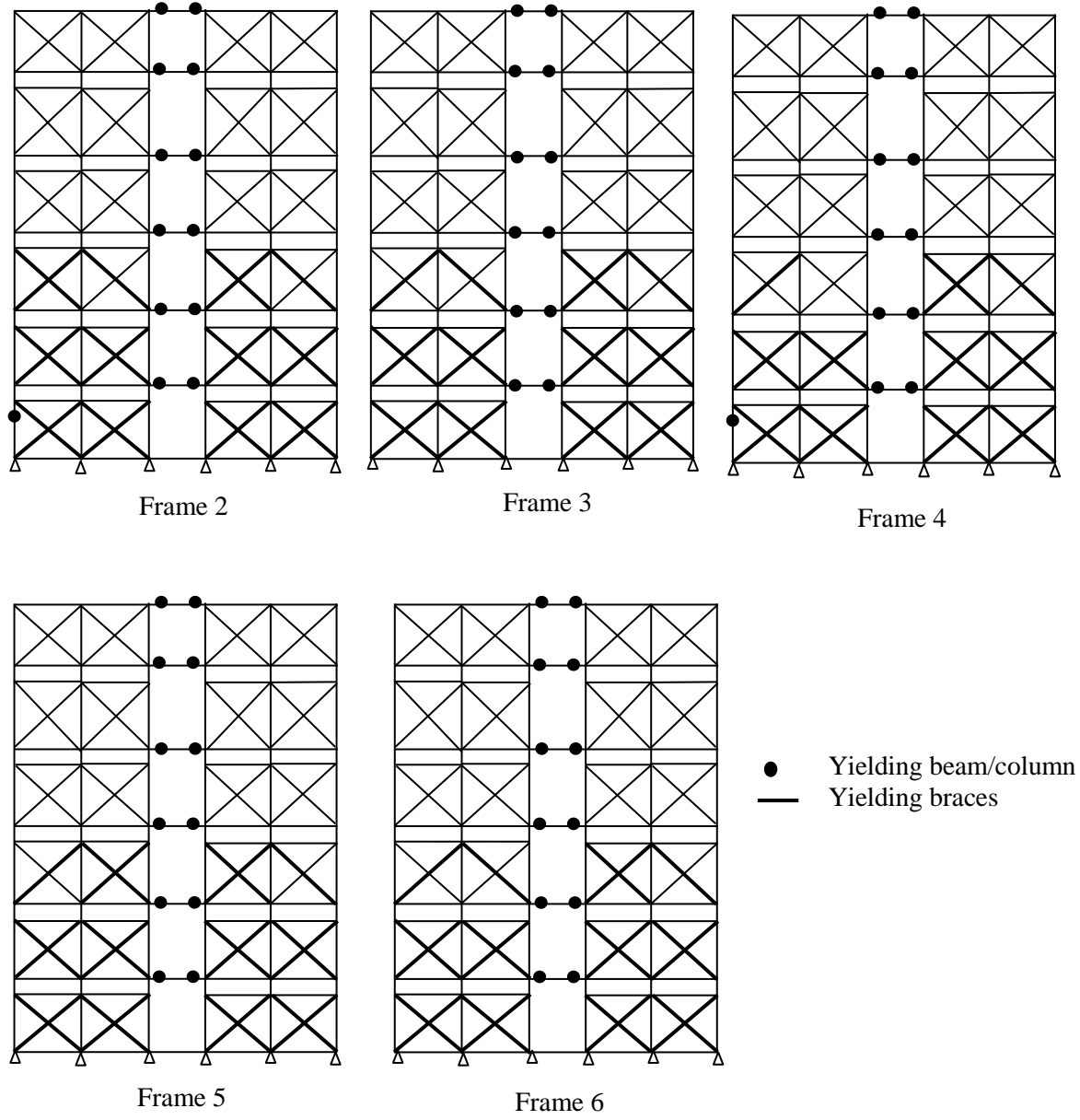


Figure 5. 24: Damage distribution due to Loma earthquake $S_a(T_{1,5\%})=1.3g$

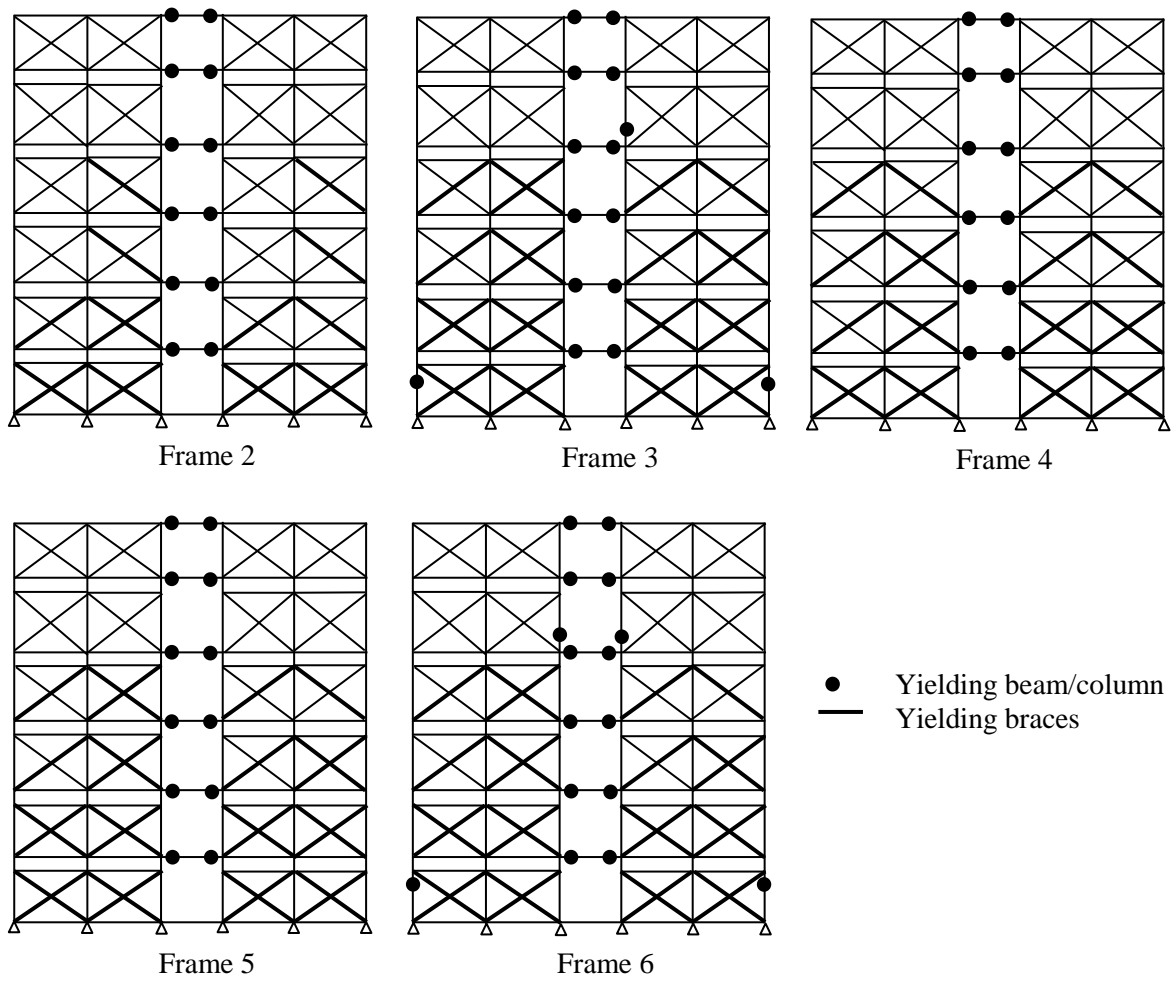


Figure 5. 25: Damage distribution due to Tabas earthquake $S_a(T1, 5\%) = 1.5g$

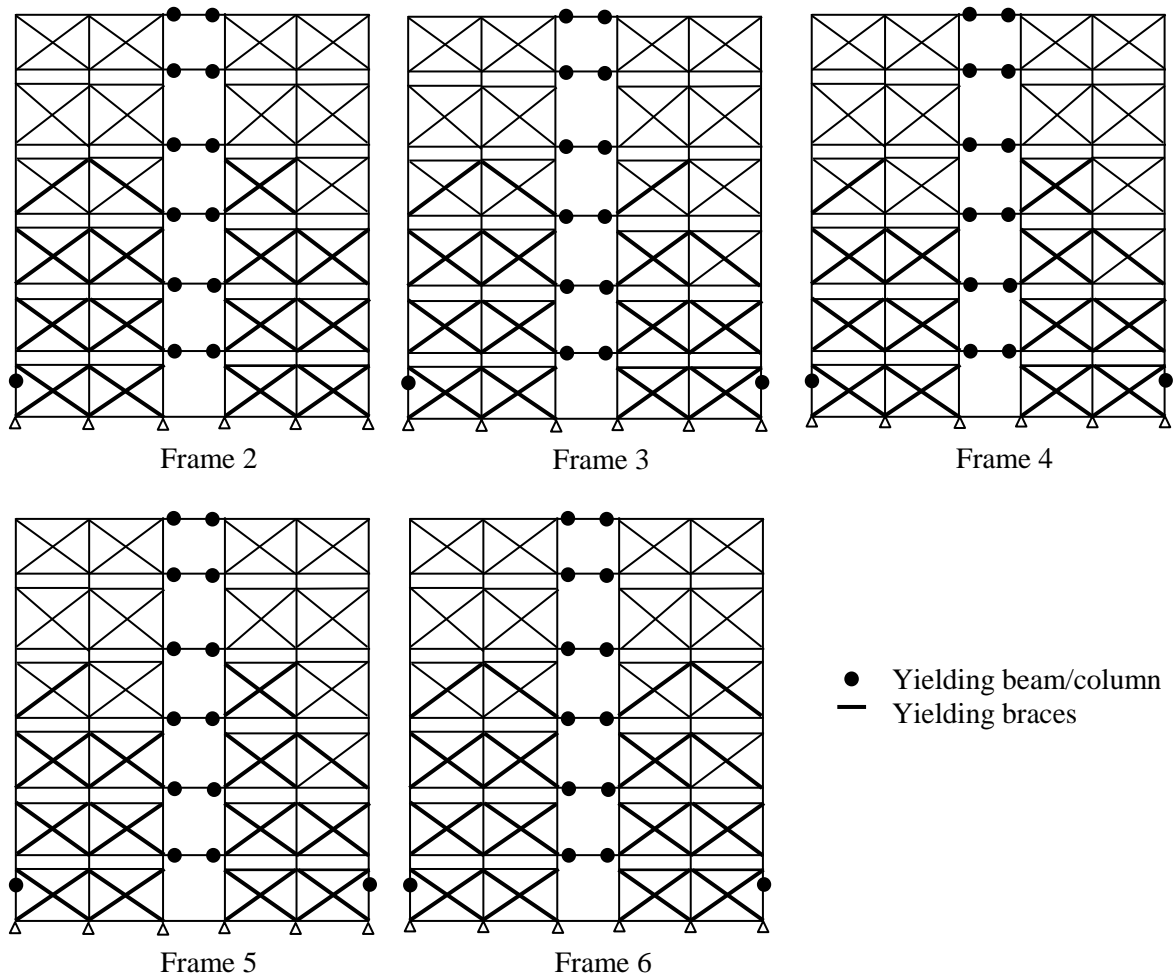


Figure 5. 26: Damage distribution due to Northridge earthquake $S_a(T_{1,5\%})=1.3g$

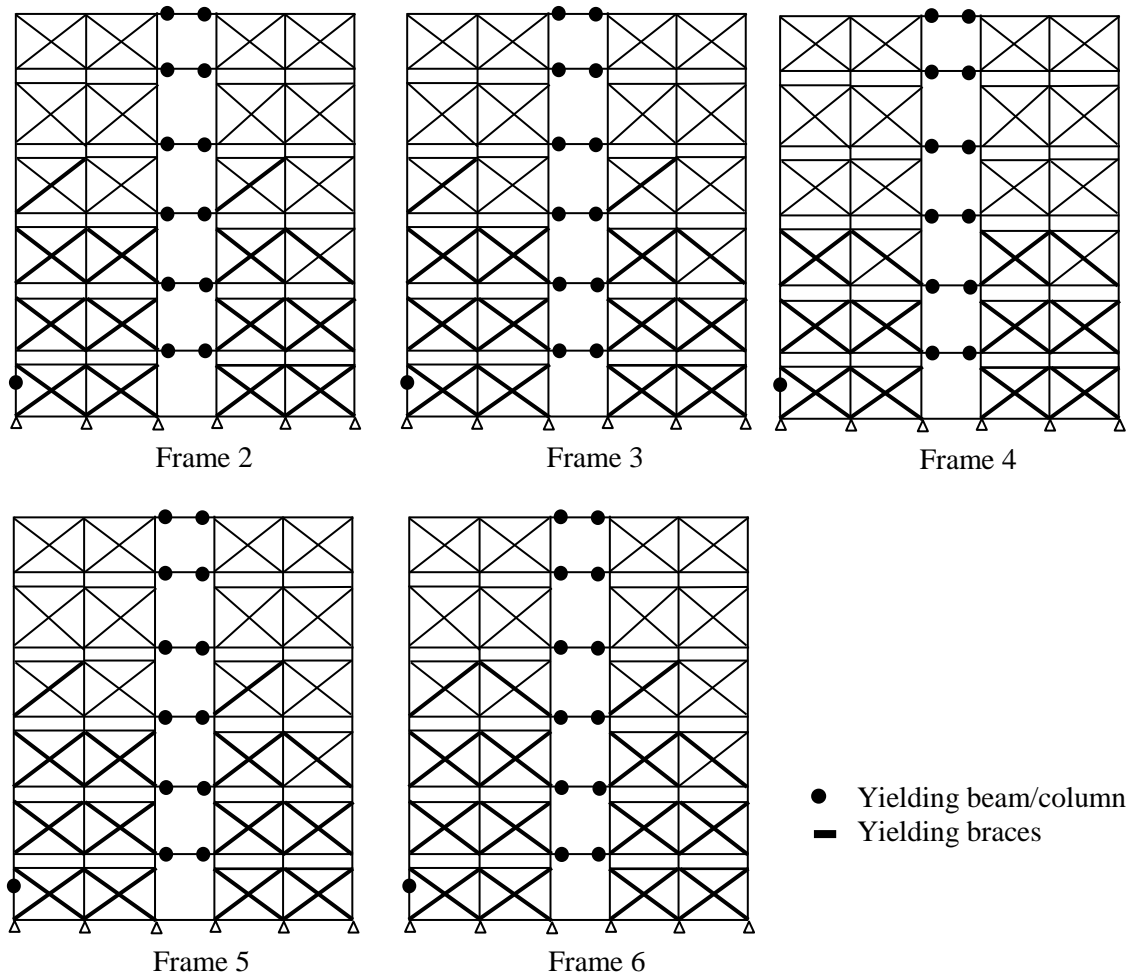


Figure 5. 27: Damage distribution due to Superstition Hills earthquake $S_a(T_{1,5\%}) = 1.5g$

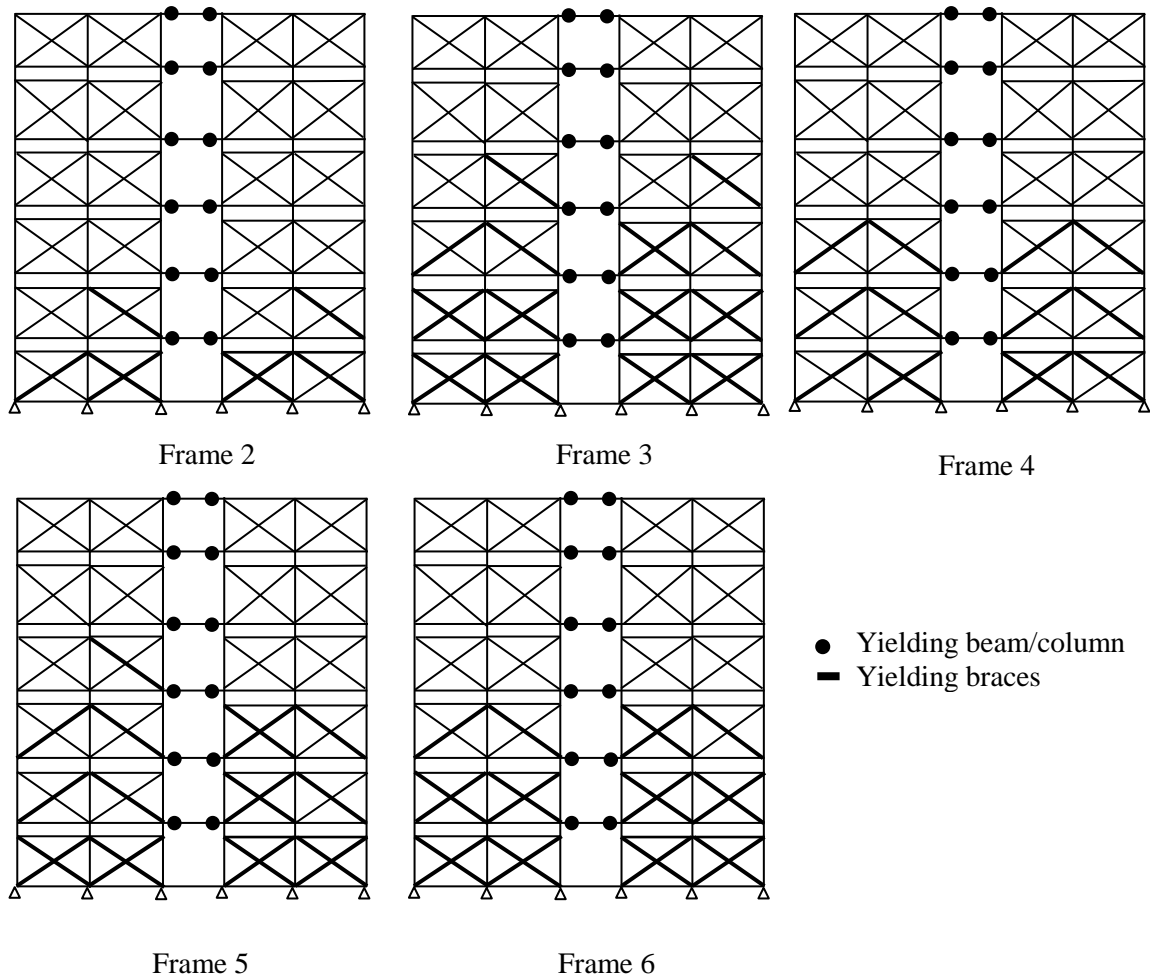


Figure 5. 28: Damage distribution due to San Fernando earthquake $S_a(T_{1,5\%}) = 1.5g$

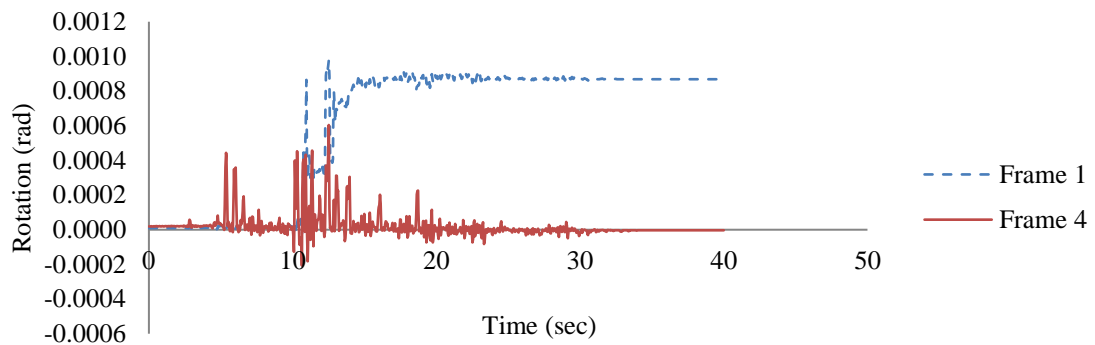


Figure 5. 29: Rotation of vertical connection at first floor due to Tabas earthquake
[$S_a(T_{1,5\%}) = 1.5g$]

5.6 CONCLUSIONS

The seismic performance of MSBF vertically connected using end plate bolted connections is investigated in this paper in terms of MID, MRID and damage scheme. The connections utilized either high strength steel bolts or superelastic SMA bolts. Finite element models of a MSBF, a bolted beam splice connection and a beam-column connection utilizing superelastic SMA bars were developed to validate the modeling technique. The modeling technique was then used to model the MSBF connected vertically using end-plate bolted connections. A six-storey building was considered as a case study. IDA of a MSBF vertically connected using high strength steel bolts were performed using five different ground motions scaled to different intensities. The steel bolts were then replaced by the superelastic SMA bolts. Five different frames with different SMA locations were selected. Nonlinear dynamic analyses of these frames were conducted using the same records scaled to the same intensities. Specific conclusions from this study are summarised below:

- MSBF connected vertically using end plate steel bolted connections showed good seismic performance in terms of MID, MRID and damage distribution.
- Using SMA connections at the vertical joints between the modules can reduce the residual drifts, and, thus improve the seismic performance of the frame as compared to steel counterpart.
- The values of MID and MRID of MSBFs are influenced by the number and location of the SMA connections, ground motion records and their intensities. Among the SMA frames, Frame 4, where SMA bolts were used in the vertical connections between 1st and 2nd as well as 2nd and 3rd storey modules, showed very good seismic performance compared with the steel frames in terms of MID, MRID and damage

schemes. The average MID was increased by 5.2% and the average MRID was reduced by 57.4%.

- The seismic performance of the MSBF can be improved by using SMA connections at right locations, which can lead to minor increase in the MID, high reduction in the MRID and better damage distribution.

5.7 REFERENCES

- [1] R M Lawson. Building design using modules. Steel Construction Institute (CSI), Publication number 348, UK.
- [2] R. M. Lawson, J. Richards, Modular design for high-rise buildings, Proceedings of the Institution of Civil Engineers, Structures and Buildings, 163 (SB3) (2010) 151–164.
- [3] C.D. Annan, M.A. Youssef, and M.H. El Naggar, Experimental evaluation of the seismic performance of modular steel-braced frames. *Eng. Struct.* 31:7(2009a) 1435-1446.
- [4] C.D. Annan, M.A. Youssef, M.H. El Naggar. Seismic overstrength in braced frames of modular steel buildings. *J. Earthq. Eng.* 13(1), (2009b) 1-21.
- [5] C.D. Annan, M.A. Youssef, M.H. El Naggar, Seismic vulnerability assessment of modular steel building. *J. Earthq. Eng.* 13(8) (2009): 1065-1088.
- [6] FEMA 350, Recommended seismic design criteria for new steel moment-frame buildings, Federal Emergency Management Agency, 2000.
- [7] J.C. Awkar, L. M. Lui, Seismic analysis and response of multistory semirigid frames, *Eng. Struct.* 21 (1999), 425–441.
- [8] E. A. Sumner, T. M. Murray, Behavior of extended end-plate moment connections subject to cyclic loading, *J. Struct. Eng.* 128:4(2002), 501-508.
- [9] J. A. Swanson, R. T. Leon, Bolted steel connections: tests on T-stub components. *J. Struct. Eng.* 126:1, (2000), 50–56.
- [10] J. McCormick, H. Aburano, M. Ikenaga, M. Nakashima. Permissible residual deformation levels for building structures considering both safety and human elements. Proceedings of 14th Conference on Earthquake Engineering, Beijing, China, October 2008.
- [11] J. McCormick, J. Tyber, R. DesRoches, k.Gall, H. Maier, Structural engineering with NiTi Part II: Mechanical behavior and scaling, *J. Eng. Mech.* 133(9) (2007) 1019-1029.

- [12] J. Ocel, R. DesRoches, R.T. Leon, W.G. Hess, R. Krumme, J.R. Hayes, S. Sweeney, Steel beam-column connections using shape memory alloys, *J. Struct. Eng.* 130 (2004) 732–740.
- [13] H. Ma, T. Wilkinson, C. Chongdu, Feasibility study on a self-centering beam-to-column connection by using the superelastic behavior of SMAs, *Smart. Mater. Struct.* 16 (2007) 1555–1563.
- [14] H. Ma, M.C.H. Yam, Experimental study on a beam-to-column connection using shape memory alloy, *Adv. Mater. Res.* 374-377 (2012) 2176-2179.
- [15] J. Sepúlveda, R. Boroschek, R. Herrera, O. Moroni, M. Sarrazin, Steel beam-column connection using copper-based shape memory alloy dampers, *J. Constr. Steel Res.* 64 (2008) 429-435.
- [16] M.S. Speicher, R. DesRoches, R.T Leon, Experimental results of a NiTi shape memory alloy (SMA)-based recentering beam-column connection. *Eng. Struct.* 33 (2011), 2448-2457.
- [17] R. DesRoches, B. Taftali, B.R. Ellingwood, Seismic performance assessment of steel frames with shape memory alloy connections, Part I- Analysis and seismic demands, *J. Earthq. Eng.* 14 (2010) 471-486.
- [18] P. Sultana, M.A. Youssef, Seismic performance of steel moment resisting frames utilizing superelastic shape memory alloys, *J. Constr. Steel. Res.* 125 (2016) 239-251.
- [19] CAN/CSA-S16-09, Design of Steel Structures, Canadian Standard Association, 2009.
- [20] NBCC 2005, National Building Code of Canada.
- [21] SeismoStruct (version 7) - A computer program for static and dynamic nonlinear analysis of framed structures. Available online from <http://www.seismosoft.com>.
- [22] A.T. Wheeler, M.J. Clarke, G.J. Hancock, Tests of bolted moment end plate connections in tubular members, Proceedings of 14th Australasian Conference on Mechanics of Structures and Materials, University of Tasmania, Hobart, Tasmania, Australia, 331-336, 1995.

- [23] E. Auricchio, A. Sacco, one-dimensional model for superelastic shape-memory alloys with different elastic properties between austenite and martensite, *Int. J. Nonlin. Mech.* 32 (1997) 1101-1114.
- [24] D. Fugazza, Shape-memory alloy devices in earthquake engineering: mechanical properties, constitutive modelling and numerical simulations, Master's thesis, European School for Advanced Studies in Reduction of Seismic Risk (ROSE School), Pavia, Italy. 2003.
- [25] PEER ground motion database, Pacific Earthquake Engineering Research Center, University of California, Berkeley, USA, 2013, <http://ngawest2.berkeley.edu/>.

CHAPTER 6

CONCLUSIONS AND RECOMMENDATIONS

6.1 SUMMARY

Superelastic SMA material has the ability to undergo large deformations and recover all plastic deformations upon unloading. Their utilization in steel structures can significantly reduce seismic residual deformations, which can facilitate post-seismic retrofitting. However, the high cost of this material is the main barrier for its implementation in the construction industry. Its low modulus of elasticity may also reduce the global lateral stiffness of a building resulting in excessive MID values during a seismic event. Although the existing literature provides few research data on using SMA in beam-column connections and bracing elements of steel frames, previous research did not address their minimum use. The use of SMA in modular steel structures was not examined. This study examines the potential use of SMAs in SMRFs and MSBFs. The study explores the possibility of using SMA material economically at specific locations to minimize the cost and improve the seismic performance. Appendix B shows the comparison of cost of regular steel structures and the steel structures utilizing superelastic SMAs. The following subsections briefly summarize the four major chapters (i.e. chapters two, three, four, and five).

6.1.1 Prediction of local seismic damage in steel moment resisting frames

In chapter 2, a simplified method, based on pushover analysis, was proposed to calculate the failure inter-storey drifts (FIDs) of SMRFs for each storey. The method compares the

maximum inter-storey drift demands with predefined FIDs to identify the damaged stories.

The method can be summarized in the following steps:

Step 1: Calculate the inter-storey drift limit of a storey based on P- Δ effect.

Step 2: Calculate the storey specific inter-storey drift limit based on pushover analysis assuming the column ends are fixed and ignoring the storeys below the considered one.

Step 3: Multiply the drift limit obtained in Step 2 by the drift magnification factor to account for the rotations of floors below.

Step 4: The smaller of the inter-storey drift limits obtained in Step 1 and Step 3 is the failure inter-storey drift limit of the considered storey.

The effect of the vertical seismic component on the FID limit is incorporated by adding extra vertical loads that can be evaluated by multiplying the mass of each floor by the vertical design spectral acceleration. The proposed method was validated using experimental and analytical studies by other researchers. A three-storey and a ten-storey SMRFs were considered as case studies to further validate the method. The FIDs were calculated according to the proposed method while considering or ignoring the effect of the vertical seismic component. Nonlinear dynamic analyses were performed considering five different ground motions. The predicted location of damage using the proposed method is compared to the results of the static pushover and nonlinear dynamic analyses. The proposed method accurately identified the critical stories of the frames. The study revealed that local damage of SMRFs cannot be identified using a single value of ID

because the storey experiencing the MID is not necessary the severely damaged storey. The findings of this study are limited to the building height up to 34m.

6.1.2 Seismic performance of steel moment resisting frames utilizing superelastic shape memory alloys

The seismic performance of SMRFs using SMA connections was investigated in chapter 3. The proposed simplified method developed in chapter two as well as incremental dynamic analysis was applied to identify the required locations of SMA connections in a typical SMRF to enhance its seismic performance in terms of MID, MRID, and damage scheme. The modeling technique of SMA connections was validated using the experimental results available in the literature. A ten-storey building was considered as a case study. IDA analysis was conducted using five different ground motions scaled to different S_a levels up to collapse. The rigid connections were then replaced by SMA connections. Nonlinear dynamic analyses of six different SMA frames were conducted using the same records scaled to the predefined S_a level that caused collapse of the steel frame. The seismic performance of the steel frame was compared with the SMA frames in terms of MID, MRID and damage schemes.

- The MID is influenced by the number of SMA connections, whereas the MRID is affected by the location of the SMA connections.
- Replacing all rigid connections by SMA connections significantly increased MID (up to 110%), and, thus the frame suffered severely damage when compared to the steel frame.

- Among all SMA frames, using SMA connections at the critical first and fourth floors showed very good seismic performance compared with the steel frames. The MID was increased by 23% and the MRID was reduced by 45%.
- Using SMA connections at the joints located at the top and/or bottom of the critical columns that can be identified by the proposed simplified method will lead to the best seismic performance.

6.1.3 Seismic performance of modular steel frames equipped with shape memory alloy braces

The seismic performance of MSBF equipped with superelastic SMA braces was investigated in chapter 4 in terms of MID, MRID and damage scheme. The modeling technique of MSBF was validated using the experimental results available in the literature. A six-storey MSB was considered as a case study. IDA analysis was first conducted on a MSBF with steel braces using five different ground motions scaled to different intensities. Then, five different schemes of SMA braces were investigated. The SMA braces were designed such that the natural period of vibration remained unchanged. Nonlinear dynamic analyses of the five different SMA frames were conducted using the same records scaled to the level that caused failure to the MSBF with steel braces. The seismic performance of the steel MSBF was compared with the SMA-MSBFs in terms of MID, MRID and damage schemes. Beams and columns in the unbraced bays of MSBF were severely damaged. Special care is required to design these members to facilitate the redistribution of forces after yielding of braces. Specific conclusions drawn from the results of this study are summarized below:

- The MID of SMA frames is not affected significantly. The increase in MID of the considered SMA frames varied from 0.34% to 8.77%.
- The seismic performance of the MSBF can be improved by using SMA braces at the right locations. The MRID is highly affected by the location of the SMA braces. The study highlighted the need to use SMA braces at all floors.
- Among all SMA frames, the highest reduction of MRID occurred in Frame 2 where all braces were replaced by SMA braces (79.67% to 98.5%). Frame 6 where SMA braces were used in the interior bays along the full building height had provided significant reduction in MRID (63.5% to 84.9%). Frame 6 was considered as a better economical solution based on cost, MID, MRID, and damage distribution compared to other frames.

6.1.4 Seismic performance of Modular steel braced frame using superelastic shape memory alloy bolts

The seismic performance of MSBF vertically connected using end plate bolted connections is investigated in chapter 5. The connections utilized either high strength steel bolts or superelastic SMA bolts. Finite element models of a MSBF, a bolted beam splice connection and a beam-column connection utilizing superelastic SMA bars were developed to validate the modeling technique. The modeling technique was then used to model the MSBF connected vertically using end-plate bolted connections. A six-storey building was considered as a case study. IDA of a MSBF vertically connected utilizing high strength steel bolts were performed using five different ground motions scaled to different intensities. The steel bolts were then replaced by superelastic SMA bolts. Five different frames with different SMA locations were selected. Nonlinear dynamic analyses of these

frames were conducted using the same records scaled to the same intensities. Specific conclusions from this study are summarized below:

- MSBF connected vertically using end plate steel bolted connections showed good seismic performance in terms of MID, MRID and damage distribution.
- Using SMA connections at the vertical joints between the modules can reduce the residual drifts, and, thus improve the seismic performance of the frame as compared to steel counterpart.
- The values of MID and MRID of MSBFs are influenced by the number and location of the SMA connections, ground motion record and seismic intensity. Among the SMA frames, the frame, where SMA bolts were used in the vertical connections between 1st and 2nd as well as 2nd and 3rd storey modules, showed very good seismic performance compared with the steel frames in terms of MID, MRID and damage schemes. The average MID was increased by 5.2% and the average MRID was reduced by 57.4%.

6.2 MAJOR RESEARCH CONTRIBUTIONS

The following is an outline of significant research contributions:

- 1) The research proposed an approximate method based on pushover analysis to predict the local seismic damage of SMRFs. The method is applicable considering both horizontal and vertical seismic components. It provides the designers with the tool to identify the critical storeys of SMRFs. It also allows identifying the best locations of SMA connections in SMRF.

- 2) The research, for the first time, has conducted a study on utilizing minimum amount of superelastic SMA material in SMRF. This study provides guidelines for the best locations of using SMA connections to improve the building seismic performance with minimum cost.
- 3) The study, for the first time, explored the benefits of utilizing superelastic SMA in modular steel braced frames. The research revealed that using SMA braces in modular steel braced frames can improve the seismic performance of modular steel buildings in-terms of residual drift and damage distribution. Instead of replacing all steel braces with SMA braces, the desired seismic performance can be achieved by using SMA braces along the frame height in interior bays.
- 4) The seismic performance of MSBFs connected vertically using end plate bolted connections is investigated. The seismic performance of the MSBF can be improved by using SMA connections at the right locations, which can lead to a minor increase in the MID, high reduction in the MRID and better damage distribution.
- 5) The research revealed that the seismic behaviour of SMRFs and MSBFs frames is very sensitive to the locations of the SMA bars. Improper use of SMA bars might result in downgrading the seismic performance of these frames.

6.3 RECOMMENDATIONS FOR FURTHER STUDIES

Excessive seismic residual deformations of structures may make the repair uneconomical or impossible. This study investigated the suitability of utilizing superelastic SMA material

in steel structures to reduce this seismic residual deformation. Thus, the repair cost can be substantially reduced and the structure may remain serviceable even after a severe earthquake. The following recommendations are made for further investigations:

1. The approximate method proposed in chapter two can be extended to account for the three-dimensional behaviour of steel buildings.
2. The proposed method to define local damage at collapse needs to be extended to be able to identify local damage of conventional as well as modular steel braced frames.
3. The behaviour of the horizontal connections of different modular units should be studied using three-dimensional analysis in order to ascertain their ability to transfer seismic forces within the floor to the lateral force resisting system.
4. Experimental investigation is required to further understand the seismic behaviour of end-plate vertical connections between modules. This study will confirm the results demonstrated in chapter five on the seismic performance of MSBFs.
5. Analytical studies should be conducted to study the application of the modular steel building technology to higher storey structures.

APPENDIX A

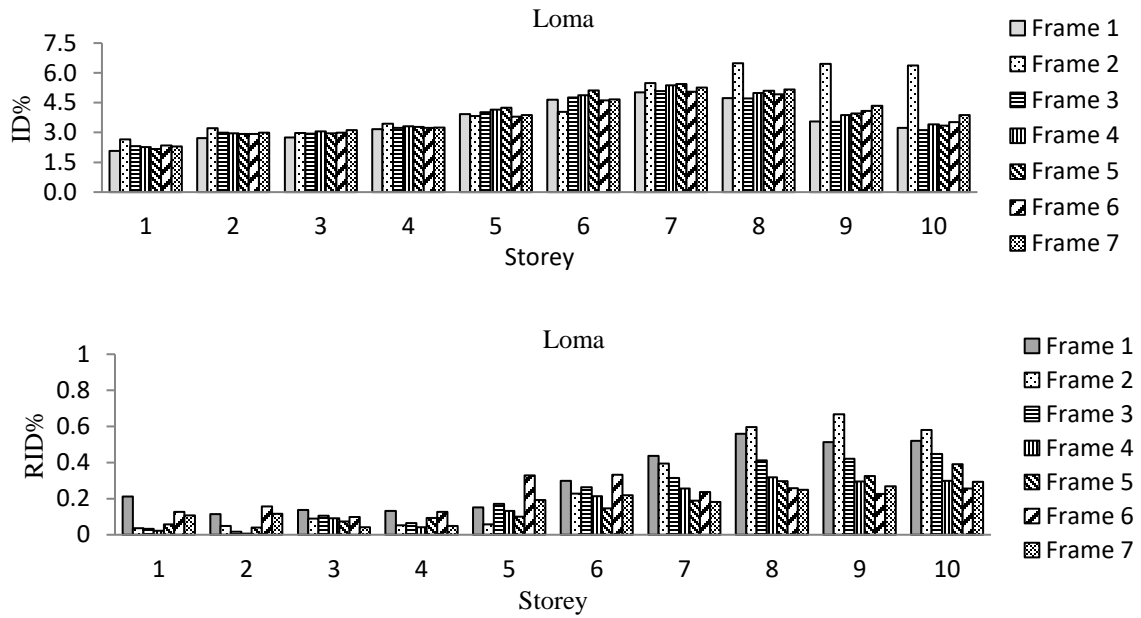


Figure A.1: Loma earthquake

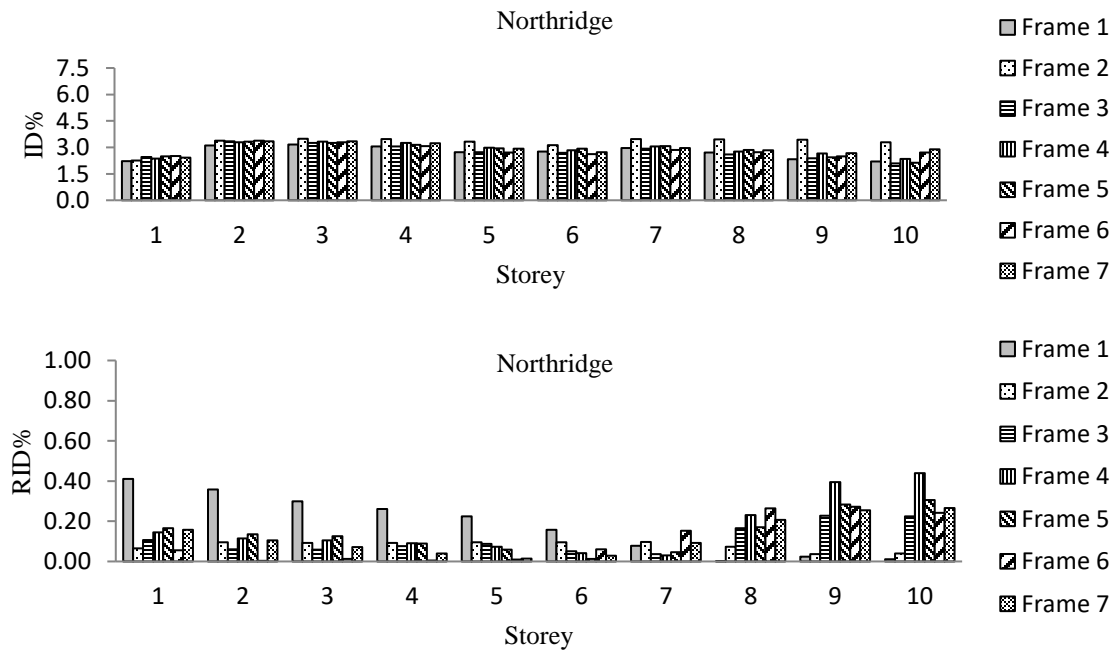


Figure A.2: Northridge earthquake

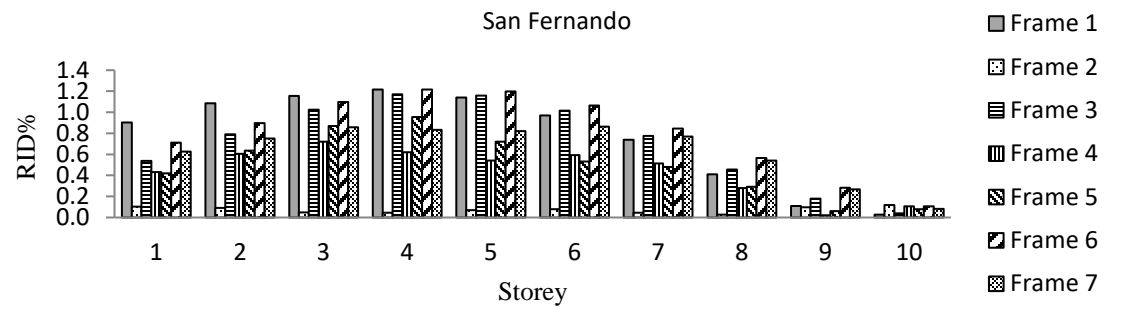
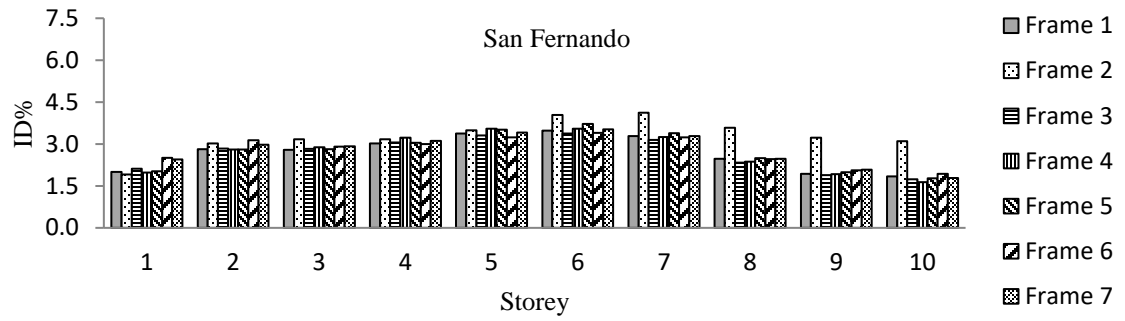


Figure A.3: San Fernando earthquake

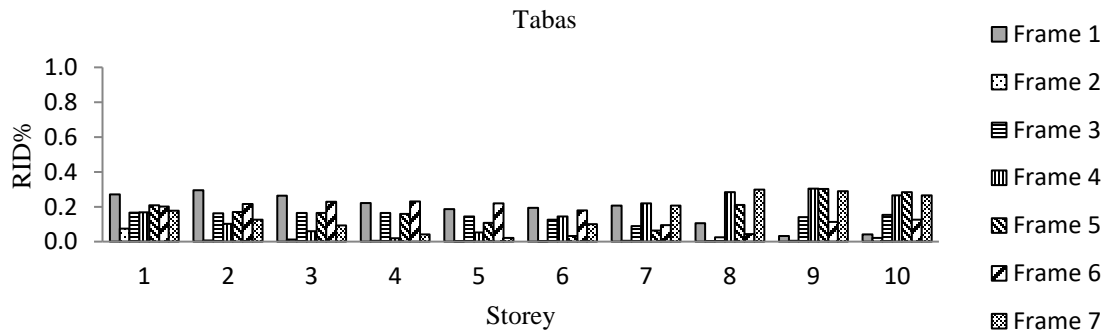
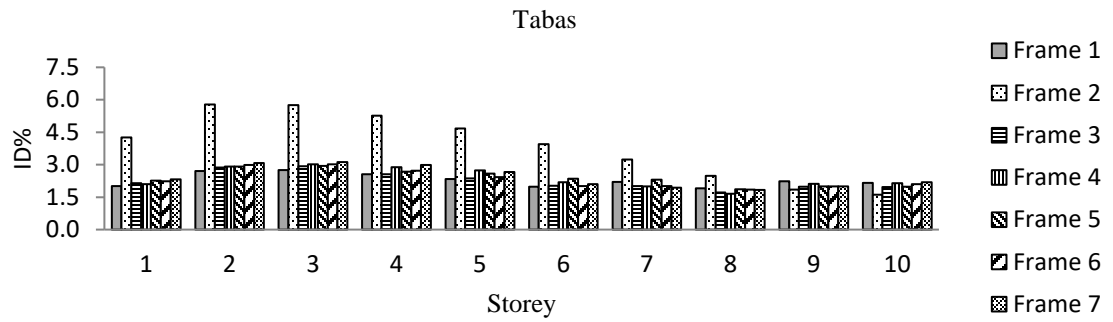


Figure A.4 Tabas earthquake

APPENDIX B

Table B.1 Comparison of material costs of utilizing superelastic SMA bars in SMRF
(Chapter 3)

Frames		diameter (mm)	Length/bar (m)	Cost/m	Total length (m)	Total cost
Frame 1	Steel bars	25	0.675	\$2.40	108	\$260
Frame 2	SMA bars	25	0.675	\$1200.0	108	\$155,520

Table B.2 Comparison of material costs of utilizing superelastic SMA braces in MSBFs
(Chapter 4)

Frames		Area of braces (mm ²)	Length of braces (m)	Total weight (kg)	Cost/kg	Total cost
Frame 1	Steel	2304	4.88	4340	\$0.95	\$4,123
Frame 2	SMA	1960	1.22	746	\$1024	\$763,959

Table B.3 Comparison of costs of utilizing superelastic SMA bolts in MSBFs (Chapter 5)

Frames	SMRF-Steel bolt	diameter (mm)	Cost/bolt	Total bolts	Total cost
Frame 1	Steel bolts	30	\$10.67	120	\$1,707
Frame 2	SMA bolts	24	\$116	120	\$13,920

CURRICULUM VITAE

- Name:** Papia Sultana
- Post-secondary Education and Degrees:** Bangladesh University of Engineering and Technology
Dhaka, Bangladesh
B.Sc in Civil Engineering.
- University of Waterloo
Waterloo, Ontario, Canada
M.A.Sc in Civil and Environmental Engineering
- The Western University
London, Ontario, Canada
Ph.D in Civil and Environmental Engineering (Expected)
- Honours and Awards:** Province of Ontario Graduate Scholarship
2013-2014, 2014-2015, 2015-2016
- Julie Lassonde Scholarship
Faculty of Engineering, UWO, 2016
- Canadian Government Commonwealth Scholarship
2005-2007
- Related Work Experience** Teaching Assistant
The Western University
2012-2016
Lecturer
Presidency University, Dhaka, Bangladesh, 2007-2012
- Publications:**
- P.Sultana**, M.A. Youssef, “Seismic performance of steel moment resisting frames utilizing superelastic shape memory alloys” , Journal of Constructional Steel Research, 2016, Vol.125, 2016 pp. 239–251
- P.Sultana**, M.A. Youssef, “Prediction of local seismic damage in steel moment resisting frames”, Journal of Constructional Steel Research, 2016, Vol.122, pp.122–137
- P.Sultana**, M.A. Youssef, “Seismic performance of modular steel frames equipped with shape memory alloy braces”, in review, Journal of Constructional Steel Research, 2016.

P.Sultana, M.A. Youssef, “Seismic performance of modular steel braced frames utilizing superelastic shape memory alloy bolts in the vertical module connections”, in review, Journal of Earthquake Engineering, 2016.

L. Xu, **P. Sultana**, X. Zhou, “Flexural strength of cold-formed steel built-up box sections”, 2009, Thin-Walled Structures, Vol. 47, Issues 6-7, pp.807-815.

Conference Proceedings

P.Sultana, M.A.Youssef, “ Seismic performance of modular steel frames equipped with shape memory alloy braces”, Proceedings of 5th International Structural Specialty Conference, CSCE, London, ON, 2016, paper no-834.

P. Sultana, M.A. Youssef, “Variations of maximum inter-storey drift for steel moment resisting frames considering the horizontal and vertical seismic components”, Proceedings of 5th International Conference on Performance, Protection and Strengthening of Structures under Extreme Loading, East Lansing, Michigan, USA, 2015, pp. 463-470.